AN INVESTIGATION OF THE REACTIONS OF CARBON DIOXIDE, CARBON MONOXIDE, METHANE, HYDROGEN, AND WATER OVER IRON, IRON CARBIDES, AND IRON OXIDES

by

Albert Sacco, Jr.

B.S., Northeastern University (1973)

Submitted in Partial Fulfillment

of the Requirements for the

Degree of Doctor of Philosophy

at the

Massachusetts Institute of Technology

July 1977

Signature of Author: _____
Department of Chemical Engineering

Certified by: _____
Thesis Supervisor

Accepted by: _____
Chairman, Departmental Committee on Graduate Theses

ARCHIVES
MASS. INST. TECH.
SEP 21 1977

ABSTRACT

Future long-duration manned space flights will require regenerative life-support systems. The Bosch process is one of several alternative regenerative life-support systems presently being evaluated by the National Aeronautics and Space Administration.

$$2H_2 + CO_2 = 2H_2O + C$$

Prototype Bosch units to reduce metabolic CO_2 to carbon have been constructed and operated successfully with large recycle ratios. The water obtained per pass was, however, far less than that predicted from equilibrium calculations.

An investigation was performed which determined this limitation to be due to oxide formation; the catalyst condition being controlled by P_{H_2}/P_{H_2O} and/or P_{CO}/P_{CO_2} ratios. Carbide formation was shown to be slow, having little effect on efficient Bosch operation. Conclusions were drawn and the optimal recycle configuration and operating conditions were specified.

In addition, a metallurgical investigation of morphological changes occurring during reaction was performed. Results indicate two distinct morphologies developed depending on temperature during the oxidation-reduction sequence. One is typical of a process controlled by solid state diffusion; the other by diffusion (gas)/interfacial reaction control. The effects of carbon fiber formation were shown along with the examination of individual carbon fibers.

ACKNOWLEDGMENTS

I would like to thank Mr. Phillip D. Quattrone and the National Aeronautics and Space Administration for their friendship and financial support in this investigation. Also, I appreciate the consultation of my peers while at MIT ("Massachusetts Institute for the Touched"). I thank the full-time staff, Drs. Dave M. Camp, Joe F. Cochetto, Terry M. Copeland, Anthony DiLeo, Hunter H. Ficke, Kevin O. Meyers, and Miss Alice Marie Sprouse (Charlie).

The friendship of Professors Mohr, Satterfield, Williams, and Vivian are gratefully acknowledged.

A special thanks to Mrs. Eleanor D. Kehoe for providing a warm heart in a sometimes rather cool environment.

To Professor Robert C. Reid (Bob), a man whom I respect and admire greatly, a heartfelt thanks.

To my entire family, Mr. and Mrs. Albert Sacco (Senior), Mr. and Mrs. Bernard A. Sacco, Mr. and Mrs. Patrick J. Sullivan, Mr. and Mrs. Thomas F. Courtney, Jr., Mr. and Mrs. Carl L. Gardner, and Nancy and Dana Gardner, I thank you for your support.

Finally, to my three lovely ladies, Miss Jennifer Lee Sacco, Miss Teran Lee Sacco, and most of all to my beautiful wife, Terri, for their love and support.

Oh yes, to He who gave me all those mentioned above; to Him I say, "thank You".

Department of Chemical Engineering
Massachusetts Institute of Technology
Cambridge, Massachusetts 02139
July 22, 1977

Professor Irving Kaplan
Secretary of the Faculty
Massachusetts Institute of Technology
Cambridge, Massachusetts 02139

Dear Professor Kaplan:

In accordance with the regulations of the faculty, I herewith submit a thesis, entitled "An Investigation of the Reactions of Carbon Dioxide, Carbon Monoxide, Methane, Hydrogen, and Water Over Iron, Iron Carbides, and Iron Oxides", in partial fulfillment of the requirements for the degree of Doctor of Philosophy in Chemical Engineering at the Massachusetts Institute of Technology.

Respectfully submitted,

Albert Sacco, Jr.

Table of Contents

Table of Contents (continued)

Table of Contents (continued)

Table of Contents (continued)

Table of Contents (continued)

Figures

Figures (continued)

Figures (continued)

Figures (continued)

TABLES

1. Summary

Future manned space vehicles will require full utilization of all metabolic waste products. In particular, regeneration of oxygen from all oxygen-bearing waste compounds will be essential in maintaining a closed, habitable ecological system. The Bosch process, of interest in this investigation, is one of several alternative regenerative life-support systems presently under consideration.

The Bosch process is the reaction of hydrogen with carbon dioxide to produce water and carbon.

$$2H_2 + CO_2 = 2H_2O + C \qquad (A)$$

The reaction is catalyzed by transition metals in the temperature range 800 to 1000 K.

Conceptually, water would be removed from the reactor effluent and electrolyzed. The hydrogen product would be recycled back to the reactor. The sum of these two processes would produce carbon and oxygen from metabolic carbon dioxide.

$$2H_2 + CO_2 = 2H_2O + C \qquad (A)$$

$$2H_2O = 2H_2 + O_2 \qquad (B)$$

$$CO_2 \rightarrow C + O_2 \qquad (C)$$

NASA has investigated several prototype Bosch recycle reactors utilizing an iron catalyst. Although moderately successful (if success is measured by carbon deposition), the effluent water concentration has been far below that expected from equilibrium considerations. Also, sizeable quantities of

carbon monoxide and methane have been found in the reactor effluent. This has resulted in recycle penalties (i.e., low energy utilization and high volume and weight requirements).

This investigation was undertaken to determine the limitation on water production; to ascertain the most efficient way to overcome and/or utilize this limitation and to specify optimal Bosch reactor operating conditions.

1.1 Pertinent Investigations

The stoichiometry indicated in reaction A is by no means representative of the reaction mechanism. The mechanism has been determined (Meissner and Reid {1972}, Manning {1976}) to consist of three major reaction systems: the carbon deposition reactions consisting of reaction D and/or reaction E

$$2CO = CO_2 + C \qquad (D)$$

$$H_2 + CO = H_2O + C \qquad (E)$$

the reverse water-gas shift reaction ,*

$$H_2 + CO_2 = H_2O + CO \qquad (F)$$

and the methane formation reactions

$$2H_2 + C = CH_4 \qquad (G)$$

$$2H_2 + Fe_xC = CH_4 + xFe \qquad (H)$$

1.1.1 Carbon Formation

Walker et al. (1959) performed an extensive study on carbon deposition from carbon monoxide-hydrogen mixtures over

* Note: Reaction F + D = E

a reduced iron catalyst. Typically, the carbon deposition versus time plots (Figure 1) were sigmoidal in shape showing a weak induction period followed by a period of constant carbon deposition; the carbon deposition rate gradually decreased to zero. This general behavior was similar to that observed by other investigators (Manning, 1976).

1.1.2 Carbide Inhibition

High intensity X-ray diffraction patterns for cementite (Fe_3C) were observed on the spent catalyst in Walker's investigation. Walker et al. felt that carbide formation caused the drop in carbon deposition rate shown in Figure 1.

Tsao (1974), investigating carbon deposition from carbon monoxide over alpha-iron, also found cementite detrimental to carbon formation. Utilizing Mossbauer Spectroscopy, Tsao observed that formation of Fe_3C (reaction I), caused a rapid drop off in carbon deposition from carbon monoxide

$$2CO + 3Fe = Fe_3C + CO_2 \qquad (I)$$

Podgurski et al. (1950), in support of the hypothesis of both Walker et al. and Tsao, found carbon monoxide would not adsorb on a carbided surface. Thus, carbides would not be expected to catalyze reactions requiring carbon monoxide adsorption.

1.1.3 Oxide Inhibition

Manning (1976) determined that iron oxide inhibits carbon deposition from binary gas mixtures of carbon monoxide-carbon

dioxide at 823 K. Figure 7 indicates, when the CO/CO_2 ratio was such as to favor magnetite formation, reaction J-A, no carbon deposition occurred even though it was thermodynamically favorable.

$$4CO_2 + 3Fe = Fe_3O_4 + 4CO \qquad (J-A)$$

$$2CO = CO_2 + C \qquad (D)$$

If the P_{CO}/P_{CO_2} ratio favored α-iron formation (i.e., $P_{CO}/P_{CO_2} = 1.76$), rapid weight gain was observed.

Additional evidence suggesting iron oxide may not be catalytic for carbon deposition was provided by Everett (1967). Everett, while investigating the effects of trace quantities of water, hydrogen, carbon monoxide, and carbon dioxide over an iron wire catalyst, observed carbon deposition to cease when the P_{H_2}/P_{H_2O} ratio approached 10. This occurred in the temperature range 548-848 K and was attributed to iron oxide formation.

1.1.4 Reverse Water-Gas Shift Reaction

The reverse water-gas shift reaction is perhaps the most widely studied reaction in the Bosch sequence.

Kusner (1962) performed a detailed investigation of the reverse water-gas shift reaction in a packed bed.

$$CO_2 + H_2 = CO + H_2O \qquad (F)$$

His results indicated reaction F will go to completion, at 922 K, over both an iron and/or iron oxide ($Fe_{1-y}O$) catalyst.

Barkley et al. (1952), while investigating the shift reaction as a possible means of adjusting the H_2/CO ratio in

synthesis gas, determined an iron oxide-copper catalyst will catalyze reaction F at 811 K. Again, the reaction went to completion in a packed bed reactor.

1.1.5 Methane Formation

Manning (1976) studied methane formation in binary gas mixtures of hydrogen-methane at 823 K. The iron catalyst was preconditioned prior to introduction of the reactant gases. Figure 14 indicates at high hydrogen contents (i.e., 75-100%), carbon rapidly reacts; in 25-40% hydrogen mixtures, both reactions G and H should proceed to the left. However, no weight change was noticed suggesting carbide inhibits carbon deposition from methane.

Virtually no data are available on methane formation in five component gas mixtures. However, the equilibrium investigations of Browning et al. (1950, 1951) indicate reaction G was a problem in measuring the equilibrium for reaction H above 930 K. This implies that reaction G becomes kinetically more favorable at high temperature (i.e., $\geq$ 930 K).

Although nothing definitive can be said concerning methane formation, the inhibiting effects of iron oxide and iron carbide are clearly suggested in the literature. By simultaneously adjusting the gas phase composition to favor both carbon deposition and the solid phase of interest, the catalytic effects of that phase can be determined.

1.2 Equipment and Procedure

The experimental apparatus consisted of three integrated sections: the feed-gas delivery section, the reactor section, and the analytical equipment section.

In the feed-gas delivery system, chemically pure gases were individually metered, mixed, and fed dry or saturated with water to the reactor section.

In the reactor (Figure 32), the feed gases were preheated and passed into the bottom of a 28 mm vertical quartz tube. A thermocouple well allowed two thermocouples to be positioned under the catalyst bed; one was used with a proportional controller to maintain a preset temperature; the other provided a continuous reading of the reactor temperature. The catalyst assembly was positioned midway up the vertical quartz reactor tube. Clean steel wool was employed as the catalyst and, normally, 500 mg were charged. During a run, the reacting gases were forced to pass through the catalyst. At intervals of 10 to 20 minutes, the feed-gas flow was diverted and the catalyst carrier weighed *in situ* with an analytical balance. Weight changes within ± 1 mg could be detected.

The inlet and outlet streams were sampled and analyzed using an on-line gas chromatograph. An external standard was used in conjunction with the method of Dal Nogare and Juvet (1962) to obtain all gas compositions except hydrogen; hydrogen being determined from an empirical calibration curve following the method of Purcell and Ettre (1965).

1.3 Results and Conclusions

1.3.1 Effect of Preconditioning

Clean #2 steel wool catalyst was preconditioned by oxidizing with a carbon dioxide-water mixture followed by reduction with hydrogen. Two distinct surface morphologies were observed depending on conditioning temperature.

At 800 K, Figure 54 shows a thin, dense layer characteristic of oxidation-reduction processes controlled by solid state diffusion (Landler and Komarek, 1970).

Preconditioning at 900 K showed a highly porous, sponge-like shell surrounding a dense core. The shell region (Figure 39) is seen to consist of two distinct layers, and thus indicates the possibility of multiple oxide formation.

Spitzer et al. (1966) has shown multiple oxidation morphology occurs when the catalyst behaves as a porous body under diffusion (gas) or mixed diffusion-interfacial reaction control. Multiple oxide formation poses some interesting kinetic problems. Depending on the past history of the oxygen activity, changes in P_{H_2}/P_{H_2O} and/or P_{CO}/P_{CO_2} ratio (i.e., oxygen activity) will elicit a different response from the system. This indicates a system response time is to be expected and this response time may vary.

Also of interest is the fact that the effective catalyst area is increased by 500% after preconditioning at 900 K.

1.3.2 Carbon Inhibition by Fe_3O_4 (Magnetite)

The Bosch reaction systems and the various solid phases which may form during reaction can be conveniently represented on triangular phase diagrams.

Figure 55 illustrates the system behavior for six runs at 800 K for three different O/H ratios over a preconditioned, pre-carboned* steel wool catalyst. At each individual O/H ratio, two different experiments were run; one approached the α-iron/Fe_3O_4 phase boundary from the reduced side; the other approached the boundary from the oxide side. The phase field of interest was investigated by adjusting the P_{H_2}/P_{H_2O} ratio of the 5-component gas mixture, at a fixed O/H value, to a value thermodynamically favoring formation of that phase. Then, by observing if and when carbon deposition would start or stop, the catalytic activity of that phase for carbon deposition would be determined and the position of the phase boundary of interest established.

Figure 55 indicates the excellent agreement between the experimentally determined phase boundary and the theoretical phase boundary. The effluent concentration in all runs indicated methane remained constant; the weight gain during carbon deposition coming from carbon monoxide conversion. Due to the errors involved in experimentation, data acquisition and reduction; no definitive statements on the carbon

---

*After preconditioning, a 50% H_2- 50% CO mixture was used to deposit a carbon bed on the catalyst.

deposition mechanism could be made.

1.3.3 Carbon Inhibition by $Fe_{1-y}O$ (Wustite)

Figure 46 represents several experimental runs at various O/H ratios at 900 K. With the one exception of O/H equal to 0.17, all these data concur with the data obtained at 800 K. That is, iron oxide, in this case $Fe_{1-y}O$, inhibits carbon deposition. Again, the experimentally determined α-iron/$Fe_{1-y}O$ phase boundary is seen to be in agreement with that predicted by theory. The runs at O/H ratios equal to 0.17 are to be viewed with caution due to equipment limitations imposed by the high water concentrations necessary to obtain these O/H ratios.

Some scatter was associated with the various run conditions. That is, carbon deposition did not always start or stop where expected. Most of these "errors" were within 10% of the expected equilibrium P_{H_2}/P_{H_2O} ratio. A propagation of error analysis indicates the maximum error in P_{H_2}/P_{H_2O} can be as large as 11%. Undoubtedly part of this scatter comes, therefore, from normal inherent error associated with the experimental procedure, data collection, and data analysis methods.

It was felt, however, that some of the scatter may reflect another process(es) which affect the rate of both carbon deposition and oxide formation. An intriguing possibility is the formation and reduction of multiple oxide phases.

The catalyst from run A-43 is shown in Figure 49. Experiment A-43 was performed at high water concentration (i.e., O/H ratio equal to 0.17) with a reactor set temperature of 900 K. The run was prematurely terminated due to equipment malfunction. Figure 49 is a series of scanning electron micrographs of catalyst morphology found. Shown clearly in Figure 49 is the double layer structure indicative of multiple oxide formation. In this case the local oxygen potential was apparently higher than the bulk composition; which should not have supported multiple oxide formation. This high localized oxygen potential is believed to be caused by product poisoning; product poisoning has been reported by Everett (1967) and Wilson (1971) under similar conditions.

Since the rate of reduction or oxidation in a system capable of multiple oxides varies (Spitzer et al., 1966), the scatter in these data at 900 K was not unexpected.

1.3.4 The Effect of Carbides on Carbon Deposition

The role of carbides during carbon deposition is still unclear. The problem lies in the fact that carbides are difficult to identify and can form not only during reaction but, as the reaction goes through wide temperature fluctuations such as in hot spot formation or during the reactor cooling-down sequence.

In an attempt to determine the effect of carbides on carbon deposition, runs A-58 and A-59 were performed at fixed C/H values of 0.2 and 0.35, respectively. The catalyst was

preconditioned using the standard procedure and a carbon bed laid down.

Figure 51 indicates that a weight gain was observed in the region where cementite (Fe_3C) would be expected to be the stable solid phase. However, the effluent in both runs A-58 and A-59 indicate no change in methane concentration; the observed weight gain resulted from carbon monoxide conversion.

There are two possible reactions which could account for the weight gain observed, reaction I and/or reaction D.

$$2CO + 3Fe = Fe_3C + CO_2 \qquad (I)$$

$$2CO = CO_2 + C \qquad (D)$$

From stoichiometric considerations it is impossible to determine which reaction accounts for the observed weight gain. The fact that 3.5 times as much weight gain is observed as needed for complete carbiding (35 mg) and, considering the work of Podgurski et al. (1950) and Walker et al. (1959) suggesting carbiding with carbon monoxide is very slow, indicates that the weight gain is probably due to carbon deposition.

Although the data are inconclusive in determining if carbides inhibit or catalyze carbon deposition, from an operational standpoint, it appears that oxide formation is the most immediate problem in efficient Bosch reactor operation.

1.3.5 Structural Changes During Reaction

Varying oxygen potential in the system to control carbon

deposition will cause structural changes depending on initial morphology and temperature. In addition, carbon deposition has been shown to alter the catalyst structure through the formation of carbon fibers (Walker et al., 1959, Ruston et al., 1969). In an attempt to illustrate the morphological changes occurring on a Bosch catalyst, a metallographic examination was performed.

The catalyst from run A-18 was examined using a scanning electron microscope. In run A-18 the P_{H_2}/P_{H_2O} ratio was varied between (∞) (i.e., no water and rapid carbon deposition) to a value of 1 (little or no observable weight gain). The reactor set temperature was 900 K and the total pressure 1.01×10^5 N/m^2.

Micrograph (a) illustrates the shell and core type morphology which results from the oxidation-reduction sequence used in A-18. Carbon-bearing gases diffuse through the porous-iron shell and deposit carbon. This deposition results in a brittle external shell that breaks easily from the more structurally solid core. In micrograph (b), carbon fibers are seen to form in bundles or nodules. Transmission electron micrographs indicate these nodules are electron-dense material, presumably iron or iron compounds.

Micrographs (c), (d), and (e) represent a small section of the exterior shell. Here, the nodule-like fiber bundles are clearly seen; micrograph (e) reveals carbon fibers having both tubular and circular shape.

Figure 43 is a transmission electron micrograph of a typical carbon fiber formed in the external shell region of a catalyst fiber from run A-18.

The "camel" shaped fiber was suspended securely from the main catalyst surface by carbon fibers. This is indicative of the type of shell structure developed during carbon deposition following catalyst pretreatment. The shell region appears to consist of an intricate network of interwoven fibers connected securely by fiber bundles or nodal points. These nodal points consist of iron and/or iron compounds.

The shaft region is seen to be hollow, with some electron dense material along the outside. Most fibers appeared to have an electron dense tip.

These results are in agreement with the fiber structures noticed by Walker et al. (1959) and Ruston et al. (1969).

Fiber formation is fascinating, but little can be said concerning the growth mechanism from this investigation. However, these micrographs clearly indicate an increase in total as well as effective (metallic) surface area. Also, they suggest possible diffusion limitations as reaction proceeds. A detailed knowledge of structural changes as a function of time is necessary, however, before a definitive statement can be made.

1.4 Recommendations

The conclusions suggested from this investigation lead to the following recommendations.

First, if it is desirable to use steel wool as a catalyst, there is an optimum system design. This optimum design utilizes the knowledge that carbide formation is slow and will not influence process operation. However, care must be taken to avoid and/or utilize oxide formation to maximum advantage; second, if other transition metal catalysts are investigated, care must be taken to evaluate the effects and amount of water and/or carbon dioxide necessary for oxide formation. Also, the effects and rate of carbide formation should be evaluated.

1.4.1 Optimal Reaction Conditions

It can be shown that the maximum water concentration occurs at the intersection of the graphite-gas/iron-iron oxide phase boundaries. The optimal O/H ratio (i.e., the intersection point) will increase with temperature. Ideally, one would like to operate at this point; however, if running a Bosch reactor alone or in combination with a reverse water-gas shift prereactor, having fixed the total moles in the system at the inlet H_2/CO_2 ratio of 2.0; the O/H ratio throughout the system is constrained by material balance to be 0.5. The optimal operating conditions would be determined by the intersection of an operating line drawn from the carbon apex to the point where the O/H ratio equals 0.5 (i.e., position of H_2O) with the phase boundary intersection point where the O/H ratio equals 0.5. This has been shown by Manning (1976) to occur at 915 K with a corresponding recycle ratio of 10.0 total moles recycled per mole CO_2

processed.

This limitation can be overcome, however, if one allows for the addition or removal of hydrogen to the system on start-up. A balance can then be made which equates the product of the recycle rate from the Bosch reactor times the water concentration (at the optimum O/H ratio desired) to the rate at which oxygen, hydrogen, and carbon are being fed to the reactor. This type of design is optimal using a shift reactor to initially take out some of the water. A conceptual reactor design is shown in Figure 57. An actual reaction gas flow path is shown in Figure 56 as envisioned on a triangular phase diagram at 875 K.

Initially, 2 moles of hydrogen are mixed with 1 mole of CO_2 and fed to the shift reactor. Point 1 represents the position of the mixture which must fall on the intersection between the O/H operating line for the shift reactor (i.e., 0.5) and a line drawn from the position of carbon dioxide to the position of hydrogen as represented on the phase diagram. Removing the water formed in the shift reactor, the gas mixture moves along the O/H operating line to point 2. The gas mixture at point 2 is mixed with a gas mixture at point 3 to give point 4. The mixture at point 3 was composed of the Bosch reactor effluent at an O/H ratio of 0.204 minus the water formed. At this time , it should be again pointed out hydrogen was added on start-up to initially get this optimum O/H ratio. The gas composition at point 4, having an O/H

ratio of 0.204, proceeds down the Bosch reactor operating line to the intersection point, at point 5.

Evaluation of this process indicates a minimum recycle ratio of 9.2 at a reactor temperature of 875 K for both the shift and the Bosch reactors.

The effect of hydrogen recycle in the shift reactor (i.e., decreased O/H ratio) is to increase the total moles to be recycled per mole of CO_2 processed. Increasing the O/H ratio in the shift reactor (i.e., decreasing the inlet H_2/CO_2 ratio), again, increases the minimum recycle rate. The minimum recycle rate can be decreased by increasing the shift reactor temperature but this decrease is small being only 3% for every 100 degree increase in shift temperature.

In conclusion, therefore, the optimum operating conditions are the shift reactor-Bosch reactor configuration with both reactors operating at 875 K; the minimum recycle rate in the Bosch reactor being set at 9.2 total moles recycled per mole CO_2 processed.

1.4.2 The Use of Nickel and Cobalt as Catalysts

The iron system has been shown to be restrictive due to oxide formation. Other transition metals such as nickel and cobalt are believed to catalyze all the reaction systems involved in the Bosch sequence but,no determination as to the behavior of their oxides is known. Garmirian and Reid (1977) have shown that oxide formation may not be a problem for these systems. That is, the nickel/nickel oxide and cobalt/cobalt

oxide systems have equilibrium water concentrations well above that expected for the Bosch system (i.e., the graphite-gas equilibrium). Thus, these two metals show promise as efficient catalysts for the Bosch process.

In all metallic catalytic systems, the various phases which form during reaction should be carefully evaluated. A tractable way to accomplish this is the phase diagram type of analysis used in this investigation.

2. Critical Literature Review

The Bosch process consists of a complex set of reactions thought to occur in both parallel and series combinations. Some of these reactions are catalyzed by transition metals and/or their oxides and carbides; others are involved in solid gas reactions that change the catalyst structure and phase during reaction. It is believed a clear understanding of these processes is necessary to understand the experimental methods and results obtained in this investigation.

2.1 Gas Phase Reaction Systems of Interest

2.1.1 Carbon Formation

Walker et al. (1959) performed one of the more extensive studies on carbon formation from carbon monoxide-hydrogen mixtures. This investigation was conducted in a reactor consisting of a Vycor tube into which the catalyst was placed. The catalyst itself was in a porcelain combustion boat. The cumulative weight of carbon formed during reaction was determined from the volume of gas measured before and after the reactor, assuming reactions D and B were the only reactions of significance.

$$2CO \rightleftharpoons CO_2 + C \qquad (D)$$

$$H_2 + CO \rightleftharpoons H_2O + C \qquad (B)$$

Most runs were conducted with a carbon monoxide-rich gas (carbon monoxide-hydrogen ratios were normally between 99.2/0.8 to 80.8/19.2). The temperature range covered was between

723-973 K. The flowrate was varied and a number of reduced iron powders tried. Baker analyzed reagent grade powder, 100 μm, reduced in hydrogen was found to be the most active.

A typical plot of carbon deposition versus time is shown in Figure 1. The curves were generally sigmoidal in shape showing a weak induction period followed by a period of constant carbon deposition. Finally, after a period of decreasing rate, carbon deposition stopped entirely.

Walker et al. studied the effects of hydrogen addition on carbon deposition rates at a variety of different temperatures. Figure 2 was typical of the behavior found.

As the hydrogen content was increased, the temperature at which the maximum rate of carbon deposition occurred generally increased. Also, the amount of carbon deposited per gram of catalyst increased. At temperatures below 801 K, the change in gas composition had little effect on carbon deposition. Above 849 K, Walker observed, the maximum rate of carbon deposition increased with hydrogen content to a point and then decreased.

2.1.1.1 Carbide Inhibition

Walker et al. noted that x-ray diffraction analysis on deactivated* catalyst indicated predominantly cementite (Fe_3C) and carbon peaks. No diffraction patterns were reported for Fe_3O_4, Fe_2O_3, or α-Fe. They speculated that cementite was not a catalyst for carbon deposition; i.e., carbon deposition ceased when the fraction of available α-Fe became negligible.

* After no more carbon would deposit.

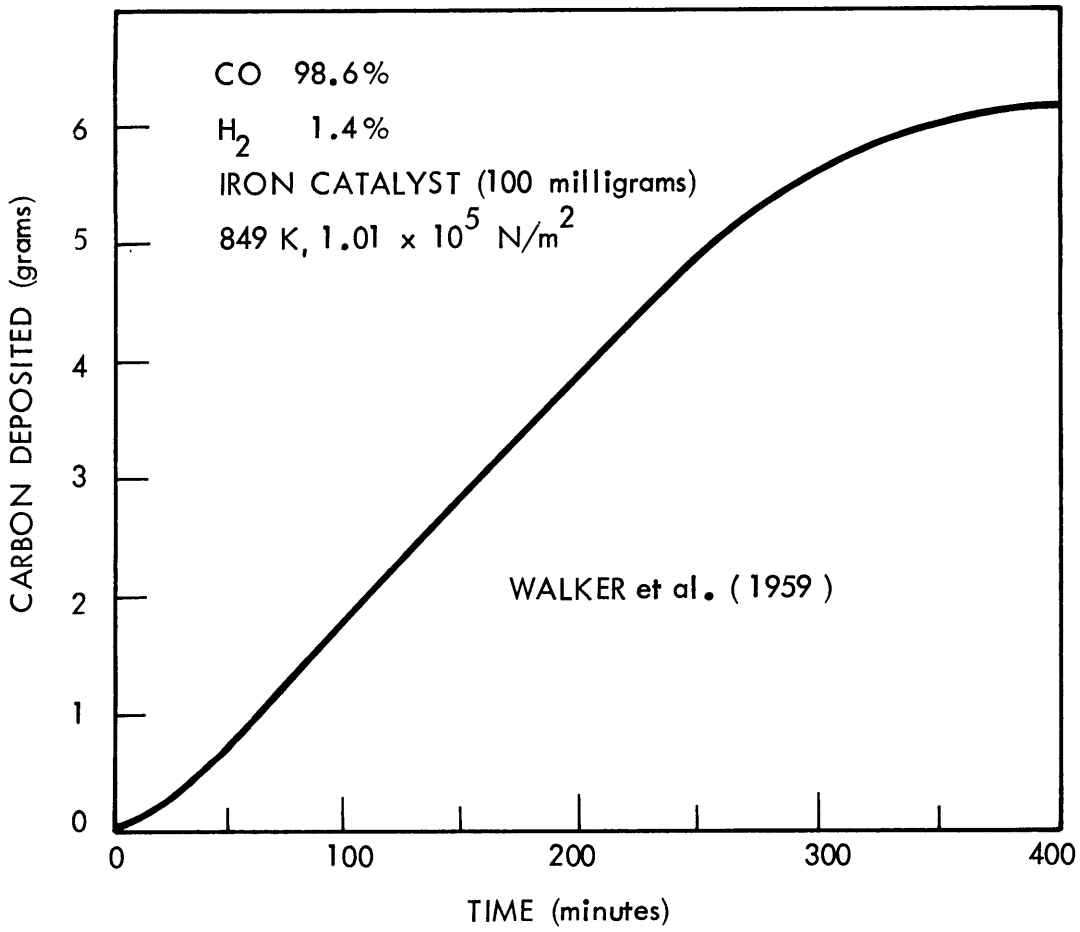

FIGURE 1

CARBON DEPOSITION VERSUS TIME, GENERAL SYSTEM RESPONSE

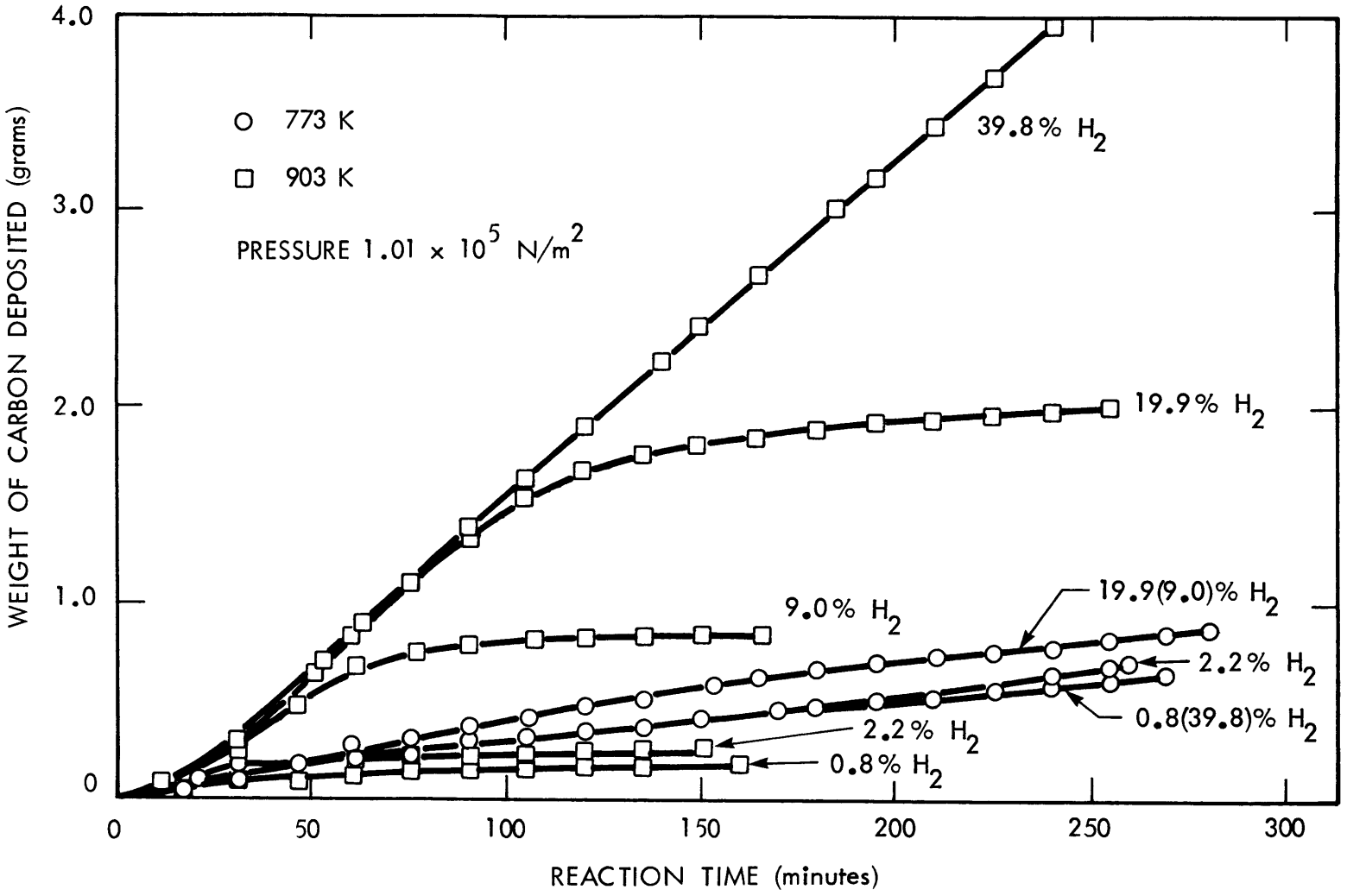

FIGURE 2 EFFECT OF HYDROGEN ADDITION ON CARBON DEPOSITION FROM CARBON MONOXIDE AT 773 K AND 903 K (WALKER et al.,1959)

The rather confusing behavior observed with hydrogen addition was qualitatively explained using this hypothesis.

At low temperatures carbide formation occurred at a very slow rate. The addition of hydrogen to the system would not be expected, therefore, to have a substantial effect on the fraction of α-Fe available for reaction. At high temperatures, however, carbide formation is rapid and the high hydrogen contents are necessary to keep a sufficient fraction of the catalyst in the reduced form. The odd behavior of carbon deposition first increasing then decreasing with increased hydrogen content at high temperatures, could be explained through the influence of reaction G but, no qualitative state-

$$2H_2 + C \rightleftarrows CH_4 \qquad (G)$$

ment was made. This proposed mechanism of carbide inhibition agrees with that suggested by Tsao (1974).

Tsao studied the dissociation of carbon monoxide over reduced, porous iron disks. The disks were suspended from a Ni-span C spring balance into a vertical alumina reaction tube housed in a resistance furnace. Operating temperatures were between 903-1027 K and a flowrate of 0.3 ℓ/min (STP) was normally used.

Figure 3 illustrates the behavior Tsao observed. Three distinct regions were found: initially, the rate of carbon deposition was constant; then, it suddenly dropped off; this was followed by a slow increase in reaction rate (the one exception being at 903 K).

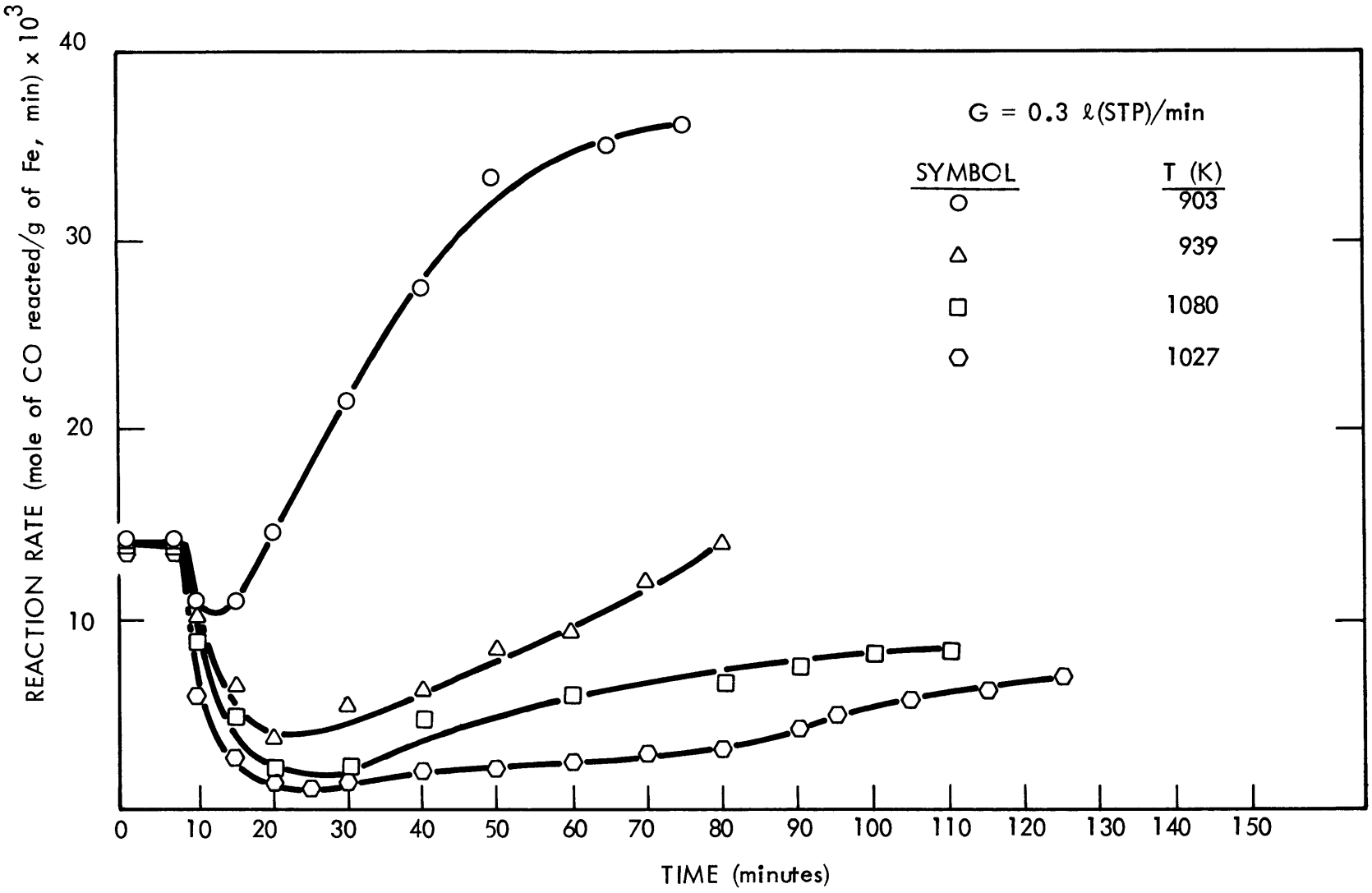

FIGURE 3 REACTION RATE VERSUS TIME (TSAO, 1974)

Tsao explained this behavior based on competition between reactions D and I.

$$2CO \rightleftarrows CO_2 + C \qquad (D)$$

$$3Fe + 2CO \rightleftarrows Fe_3C + CO_2 \qquad (I)$$

The data for Figure 4 were obtained by Mossbauer analysis of the iron-bearing compounds on the surface of the disks. As shown, cementite appeared to have formed at a faster rate initially than did "free" carbon. Tsao concluded that the observed drop in carbon deposition rate was due to the formation of carbide. The slow increase in deposition rate noted after complete carbiding was attributed to the increase in "free" carbon surface area; which, he measured.

Tsao's proposed mechanism agrees in principle with Walker and co-workers. Unfortunately the results at low temperature (i.e., 903-939 K), in the range Walker studied, could be interpreted as Fe_3C being a more active catalyst than α-Fe, as well as the way it was interpreted.

The question of carbides being promotors or inhibitors is a complex one. The problem lies in the nature of analysis, as well as the age-old question: Does one have on completion of reaction what one had during reaction? Most data indicate that carbides should not be catalysts for carbon deposition from carbon monoxide (Podgurski et al., 1950). However, the question of the catalytic effects of carbides is still open to interpretation.

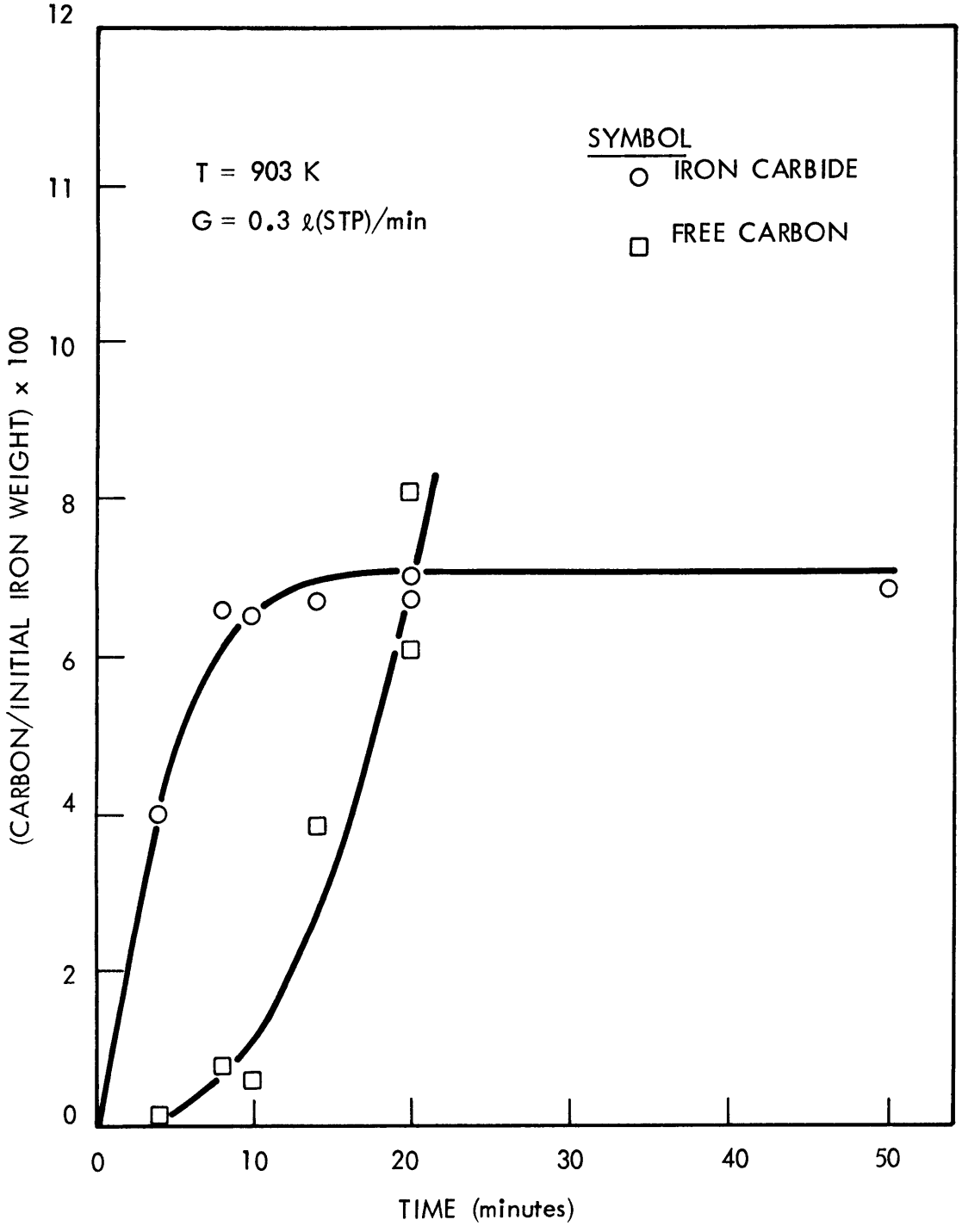

FIGURE 4

CARBON ANALYSIS OF THE DISKS REACTED AT 903 K (TSAO, 1974)

2.1.1.2 Recent Research at MIT

Manning (1976) studied the formation of carbon from various hydrogen-carbon monoxide mixtures at 823 K. The catalyst used was a commercial grade steel wool. A detailed description of the apparatus used is given in the Apparatus and Procedure Section.

Figure 5 is a plot of weight of carbon deposition versus time for a typical run. In this particular experiment, a 1:1 mole ratio of hydrogen to carbon monoxide was passed over 250 mg of steel wool catalyst. As shown, carbon deposition was initially a linear function of time; this period corresponds with the Walker et al. (1959) induction period. However, after a short period (120 minutes) the carbon deposition rate increased. This change occurred in the same time frame as Walker's region of increased rate and is believed similar.

During the initial linear period, Manning found trace amounts of carbon dioxide and water. These corresponded, at the given flowrate {19.8 cm^3/s (STP)}, to a conversion of less than 1% for both hydrogen and carbon monoxide.

The reactions by which carbon forms from CO are not clear. There are several proposed routes by which carbon may be produced. One is the carbon monoxide disproportionation reaction (reaction D).

$$2CO \rightleftarrows CO_2 + C \qquad (D)$$

Alternately, carbon may be formed by reaction B coupled with

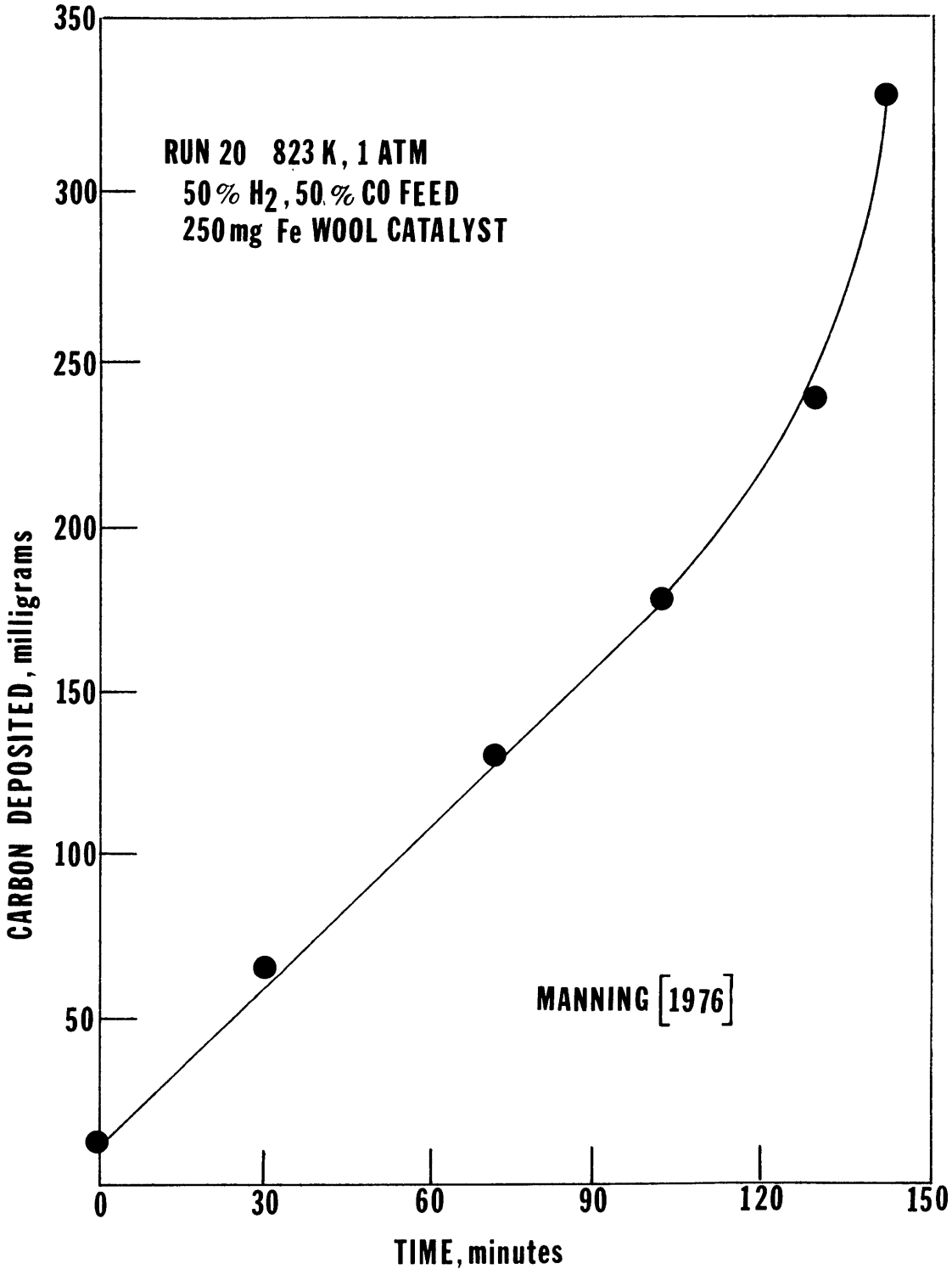

Figure 5 Carbon Deposition During Start-Up With CO-H_2 Feed

reaction F giving the observed effluent.

$$CO + H_2 \rightleftarrows H_2O + C \qquad (B)$$

$$H_2O + CO \rightleftarrows CO_2 + H_2 \qquad (F)^*$$

Also possible, as Walker et al. (1959) suggested, reaction D may occur in parallel with reaction B.

Manning's data, obtained at low conversion, were unable to ascertain the mechanism for carbon deposition. However, several interesting results were noted. Using a least square analysis, Manning obtained the following statistically significant correlation:

$$\text{rate (g mole carbon/cm}^2\text{-s)} = 4.3 \times 10^{-8}(P_{CO}P_{H_2})^{0.42\pm0.10} \qquad (1)$$

The carbon monoxide and hydrogen dependence was similar to that found by Everett (1967) for high content hydrogen-carbon monoxide mixtures.

Also, Manning determined the incipient reaction rate for carbon deposition could be increased significantly by pre-oxidation of the catalyst. Initially, 250 mg of steel wool catalyst were oxidized in CO_2 for several hours. A 75% H_2—25% CO reducing gas mixture was then fed to the reactor. Figure 6 illustrates the observed effect. It was speculated that reduction of the surface occurred rapidly, providing a highly reactive, high area α-Fe surface.

The effects of an oxidized surface were further investi-

*Note reaction D = reaction B + reaction F

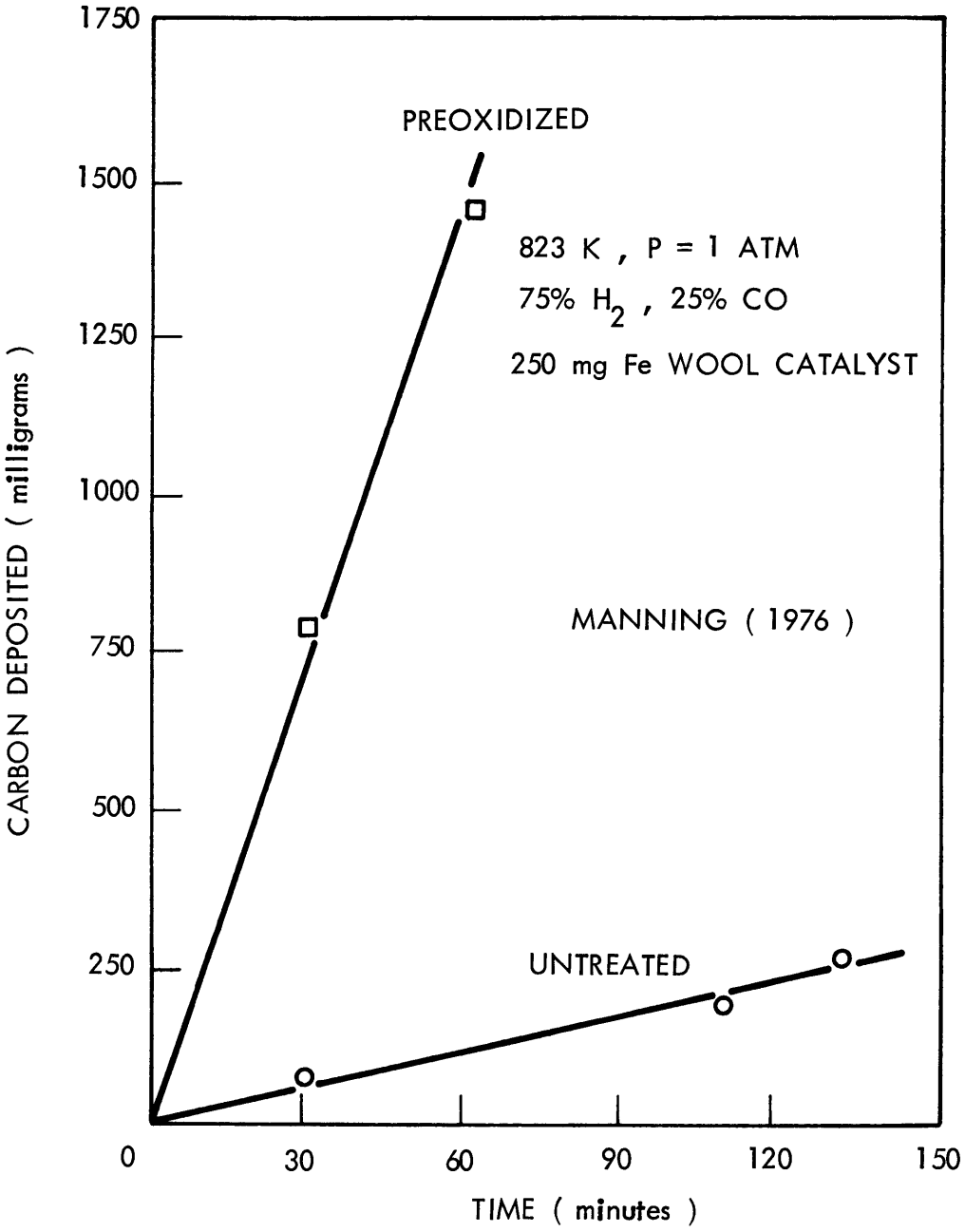

FIGURE 6

COMPARISON OF START-UP BETWEEN AN OXIDIZED AND AN UNTREATED BOSCH CATALYST

gated by studying the effect of binary gas mixtures of carbon monoxide-carbon dioxide over a pre-carbonized catalyst, Figure 7. When carbon monoxide-carbon dioxide ratios of 1-1.3 were passed over the catalyst, no significant weight loss or gain was noted. Increasing the carbon monoxide-carbon dioxide ratio to 1.5, produced erratic weight loss and weight gain; and, a ratio of 1.94 produced rapid weight gain.

Analysis of Figure 7 indicates the formation of Fe_3O_4 (reaction J-A) inhibits reaction D from depositing carbon.

$$4CO_2 + 3Fe \rightleftarrows Fe_3O_4 + 4CO \qquad \text{(J-A)}$$

$$2CO \rightleftarrows CO_2 + C \qquad \text{(D)}$$

This conclusion is based on thermodynamic considerations.

All the binary carbon monoxide-carbon dioxide gas mixtures fed exceeded the equilibrium carbon monoxide partial pressure (i.e., 13%) for reaction D. Thus, thermodynamically, reaction D should have proceeded to the right depositing carbon. However, when the carbon monoxide-carbon dioxide ratios were such as to favor the formation of Fe_3O_4 rather than Fe (i.e., $CO/CO_2 \leq 1.13$), no carbon deposition occurred. Further, when the carbon monoxide-carbon dioxide ratio favored α-Fe formation (i.e., 66% CO, 34% CO_2), rapid weight gain was observed, the implication being that iron oxide (Fe_3O_4) is not a catalyst for carbon deposition.

2.1.1.3 Oxide Inhibition

The idea of oxides of iron inhibiting carbon deposition from carbon monoxide was developed in an investigation per-

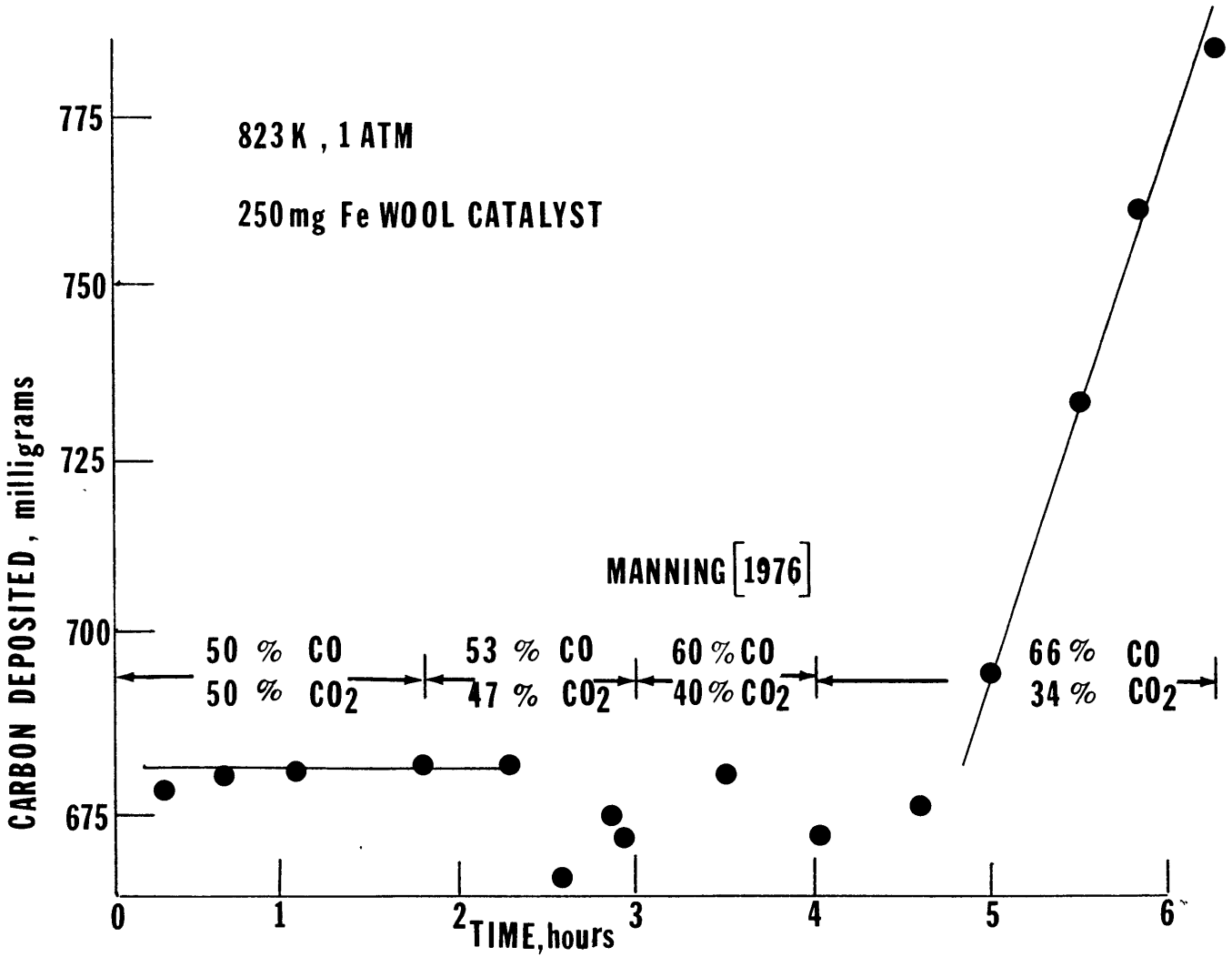

Figure 7 Carbon Deposition From $CO-CO_2$ Mixtures

formed by Everett (1967).

Everett studied the kinetics of carbon deposition reactions in high temperature gas-cooled nuclear reactors. This investigation was undertaken to ascertain the likelihood of metal fatigue caused by trace quantities of water, carbon dioxide, carbon monoxide and hydrogen.

The experimental apparatus consisted of a furnace housing a silica reaction tube and a set of steel samples. The temperature could be varied between 548-848 K. A high temperature graphite furnace for partial reconversion of the water and carbon dioxide products back to hydrogen and carbon monoxide was used to maintain a steady hydrogen-carbon monoxide feed. The entire system was connected in a closed loop; if desired, reaction gases could be recirculated until equilibrium was obtained.

Everett ran helium containing carbon monoxide and hydrogen over identical iron specimens. He observed that the rate of carbon deposition was highest for specimens at the entrance to the reactor. The rate of reaction decreased to zero in the direction of flow. This type of behavior is typical of reactions which are inhibited by their products (in this case, carbon dioxide and water).

Everett noticed if he shut down the graphite reconversion furnace, the hydrogen-to-water ratio decreased to a constant value of 10 and carbon deposition ceased. He proposed that the metal catalyst was in the oxide state and as such no

longer acted as a catalyst for carbon deposition.

In an effort to verify his hypothesis, Everett constructed phase diagrams based on the following reaction systems:

$$Fe + H_2O \rightleftarrows FeO + H_2 \qquad \text{(N-A)}$$

$$3/4Fe + H_2O \rightleftarrows 1/4Fe_3O_4 + H_2 \qquad K_1 = \frac{P_{H_2}}{P_{H_2O}} \qquad \text{(N-B)}$$

$$Fe + CO_2 \rightleftarrows FeO + CO \qquad \text{(J-B)}$$

$$3/4Fe + CO_2 \rightleftarrows 1/4Fe_3O_4 + CO \qquad K_2 = \frac{P_{CO}}{P_{CO_2}} \qquad \text{(J-A)}$$

$$C + H_2O \rightleftarrows CO + H_2 \qquad K_3 = \frac{P_{H_2} P_{CO}}{P_{H_2O}} \qquad \text{(E)}$$

$$CO + H_2O \rightleftarrows CO_2 + H_2 \qquad K_4 = \frac{P_{H_2} P_{CO_2}}{P_{H_2O} P_{CO}} \qquad \text{(F)}$$

Everett assumed carbide and methane formation could be ignored and constructed several phase diagrams. An example of which is shown in Figure 8. Diagrams using both the P_{H_2}/P_{H_2O} and P_{CO}/P_{CO_2} ratios were constructed.

In Figure 8 the line labelled K_1 represents the change in equilibrium P_{H_2}/P_{H_2O} ratio as a function of temperature for reaction N. Above K_1, metallic iron (Fe) is the stable solid iron phase. Below K_1, iron oxide (Fe_3O_4 or FeO) is the stable solid iron phase. The sharply sloped solid lines represent the equilibrium for reaction E and F at a fixed CO/H_2 ratio of 1.0 and at a fixed total pressure. To the right of these solid lines carbon deposition is favored, while

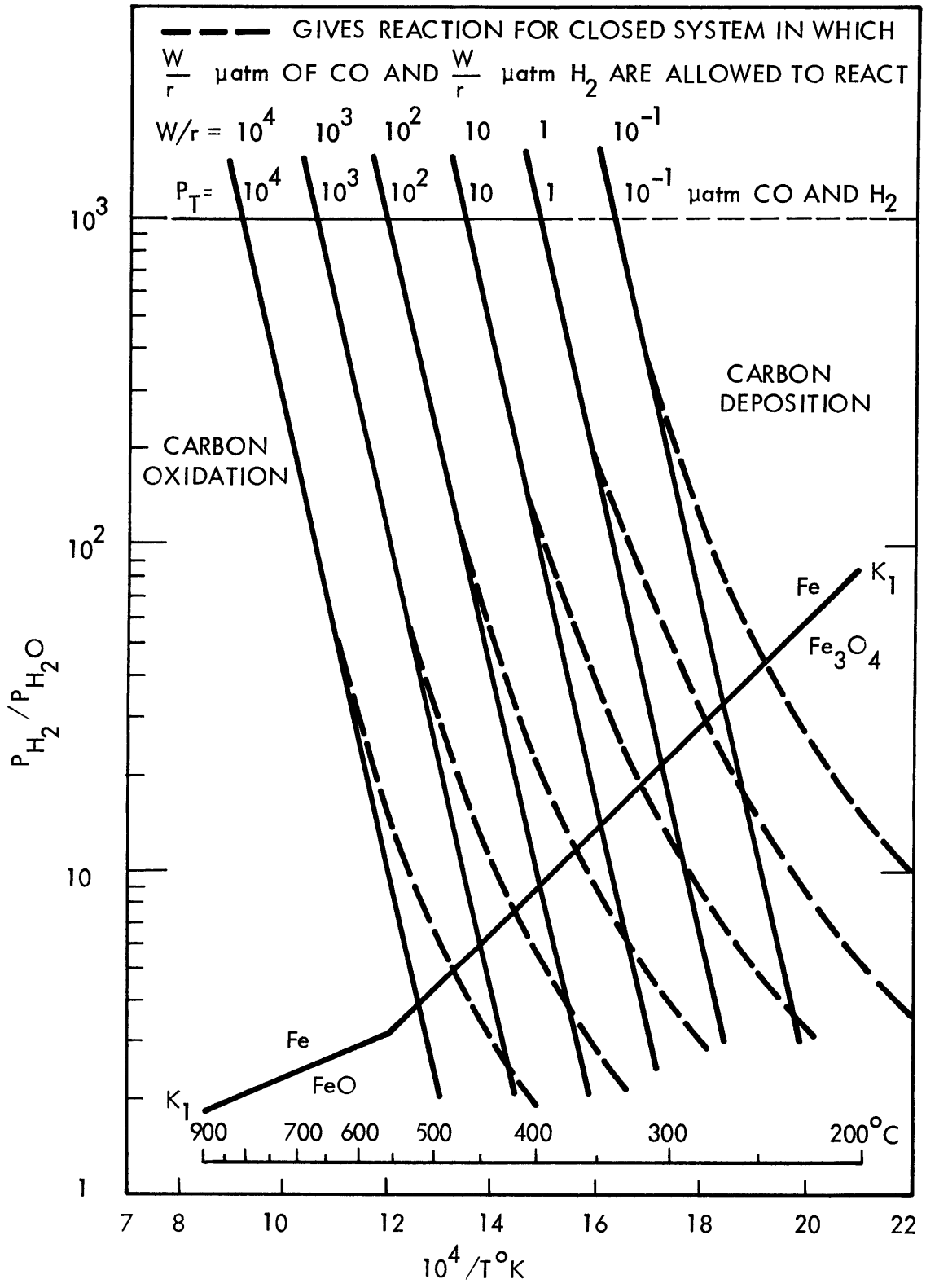

FIGURE 8

P_{H_2} / P_{H_2O} VERSUS 1/T K, FOR SYSTEM WHERE H_2/CO RATIO EQUALS 1 (EVERETT, 1967)

to the left carbon should react (oxidize). If a 1:1 molar mixture of carbon monoxide-hydrogen are initially fed, and the pressure is allowed to vary, then the reaction path for the P_{H_2}/P_{H_2O} ratio is represented by the dashed line.

Everett used these diagrams to analyze his data. He found good agreement with regard to the prediction of limiting hydrogen to water ratios and carbon monoxide to carbon dioxide ratios.

The importance of Everett's research is two-fold: first, it suggested the hydrogen to water or the carbon monoxide to carbon dioxide ratios may be used to control carbon deposition; secondly, he was one of the first to use an equilibrium phase diagram as a means of analyzing a complex reaction system.

Karcher and Glaude (1971) also determined that water was a "strong" carbon deposition inhibitor. In their investigation a steel sample was suspended from an electrobalance into a combustion tube. Normal operating temperature was 823 K. Using argon gas as a carrier median, various amounts of carbon monoxide, hydrogen, and inhibitor were passed over the steel samples, carbon deposition being monitored by changes in the sample mass.

Figure 9 shows some of the data reported. The first plot shows the ratio of carbon deposition rates with and without water versus the parts per million of water by volume in the gas stream. Replotting the data against the ratio of partial pressure of hydrogen-to-water gives the second plot. In Figure 9 the data for two concentrations of hydrogen and

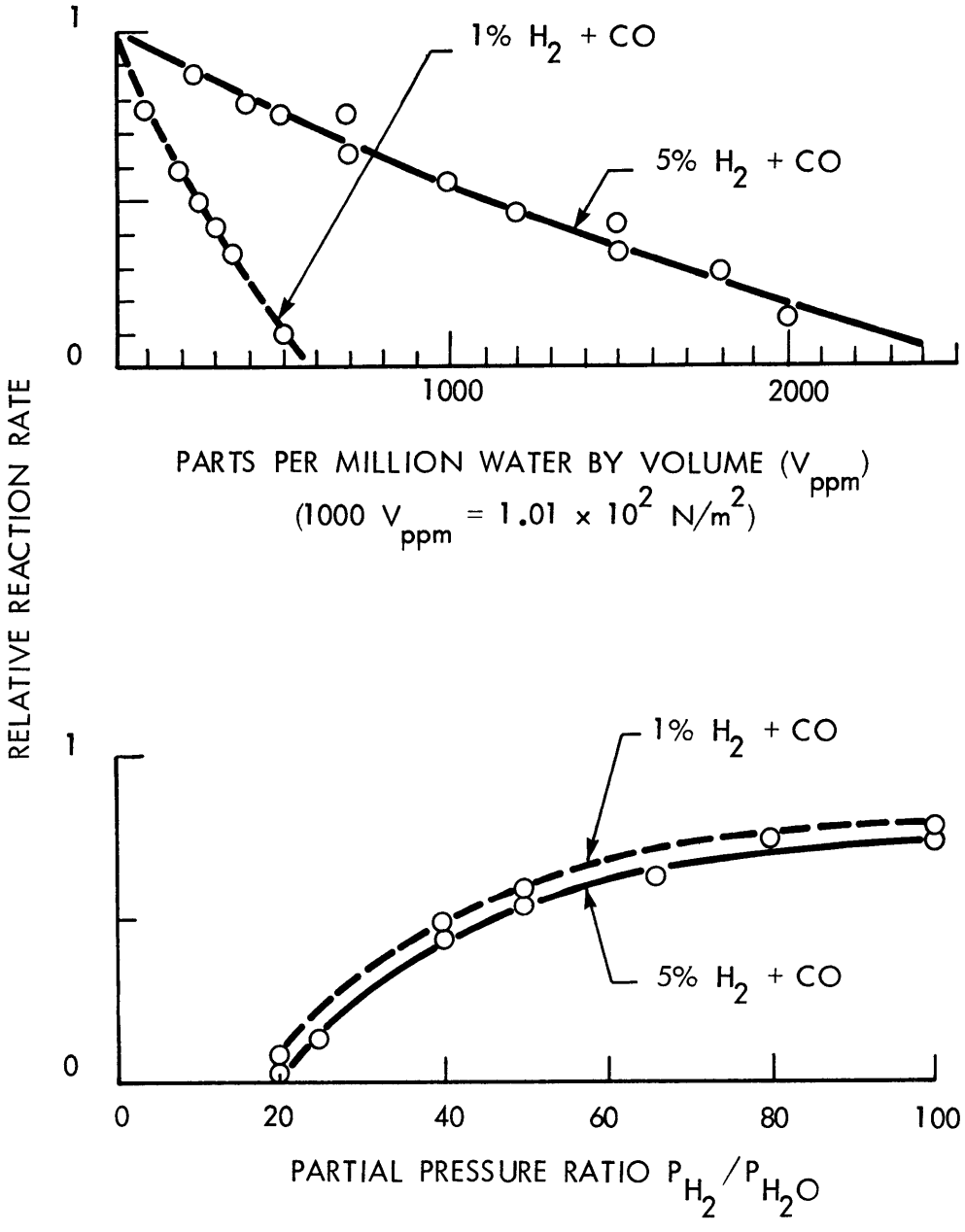

FIGURE 9
EFFECT OF WATER ON CARBON DEPOSITION AT 823 K
(KARCHER and GLAUDE, 1971)

carbon monoxide are reduced to one curve when plotted on these coordinates, thus, it is the ratio P_{H_2}/P_{H_2O} which is important in determining the carbon deposition rate. Also apparent is that at a ratio of P_{H_2}/P_{H_2O} of 20, the rate of carbon formation is zero. The cause of this apparent "equilibrium" is not known. Karcher and Glaude speculated that the phenomenon observed was due to competitive adsorption of the inhibitor on the catalyst sites with respect to the reaction partners carbon monoxide and hydrogen. In view of the fact that under the conditions reported, a P_{H_2}/P_{H_2O} of 20, metallic iron would be the stable equilibrium phase; this seems reasonable.

In a similar manner, Karcher and Glaude found carbon dioxide inhibited carbon formation from gas mixtures of carbon monoxide and hydrogen. However, with carbon dioxide, unlike the results found for water, carbon deposition could never be completely stopped. They speculated that the behavior of carbon dioxide may reflect side reactions such as reaction F. Reaction F would produce water which in turn was the actual inhibitor.

Although possible, the results of Manning (1976) and Everett et al. (1967) indicate that if the carbon dioxide concentration is high enough, carbon deposition will cease.

2.1.2 Reverse Water-Gas Shift Reaction

A detailed study on the reverse water-gas shift reaction was done by Kusner (1962).

$$CO_2 + H_2 \rightleftarrows CO + H_2O \qquad (F)$$

The reaction was carried out in a continuous flow vertical reactor, the reactor tube being positioned in an electric furnace which provided heat for the preheating of reaction gases and for the heat of reaction. A reduced iron catalyst was positioned mid-way up the reaction tube on a support grid. Inlet and exit gas compositions were monitored using a gas chromatograph.

Several different iron catalysts were tried and all were found to be active. Normal catalyst preparation involved grinding the iron or iron-oxide powder, pelletizing with a starch binder, followed by drying and firing to burn off the starch binder and to partially sinter the pellets. After final reduction in hydrogen at 1092 K, they were cooled (in hydrogen), crushed, and sieved. The final average particle size was 3 mm, the density 3.07 g/cc, the porosity 61% and the BET surface area 0.11 m^2/g. The amount of catalyst used ranged from 100 to 600 g, corresponding to a packed bed height between 2.6 and 15.6 cm. The bed porosity was determined to be 0.46.

Experiments were performed with hydrogen-to-carbon dioxide ratios between 0.5 and 3.0. Normal operating temperature was approximately 922 K. Reynolds numbers, based on particle diameter, varied between 1.7 and 16.0. This corresponded to the laminar flow regime with some excursion into the transition region.

In order to determine the equilibrium composition to be expected from a given inlet hydrogen-to-carbon dioxide ratio, Kusner constructed the phase diagram shown in Figure 10. Fixing the system temperature and pressure, and recognizing that the stoichiometry of the process is such that the amount of carbon monoxide formed equals the amount of water formed, allowed Kusner to construct a process operating line based on the inlet H/C ratio which fixed the system composition. For example, if one fixes the hydrogen to carbon ratio at X, in the given coordinate system, one would follow an operating line equal to 2X (which is fortuitously equal to the inlet H_2/CO_2). When the appropriate equilibrium curve (fixed by temperature, pressure, and C/H) is intercepted, the coordinates for the point give the equilibrium gas composition. The equilibrium solid phase expected was also plotted on this diagram in similar fashion.

Figure 11 is a plot of conversion versus inverse space velocity (time required to process a volume of feed at a given catalyst loading). At a fixed inverse space velocity, conversion was seen to increase with particle Reynolds number. Based on these initial results, Kusner modeled his system as an isothermal, packed bed plug flow reactor under mass transfer control. He assumed, initially, no axial or longitudinal diffusion.

This model, however, did not adequately describe the observed quantitative behavior. Having observed some carbon

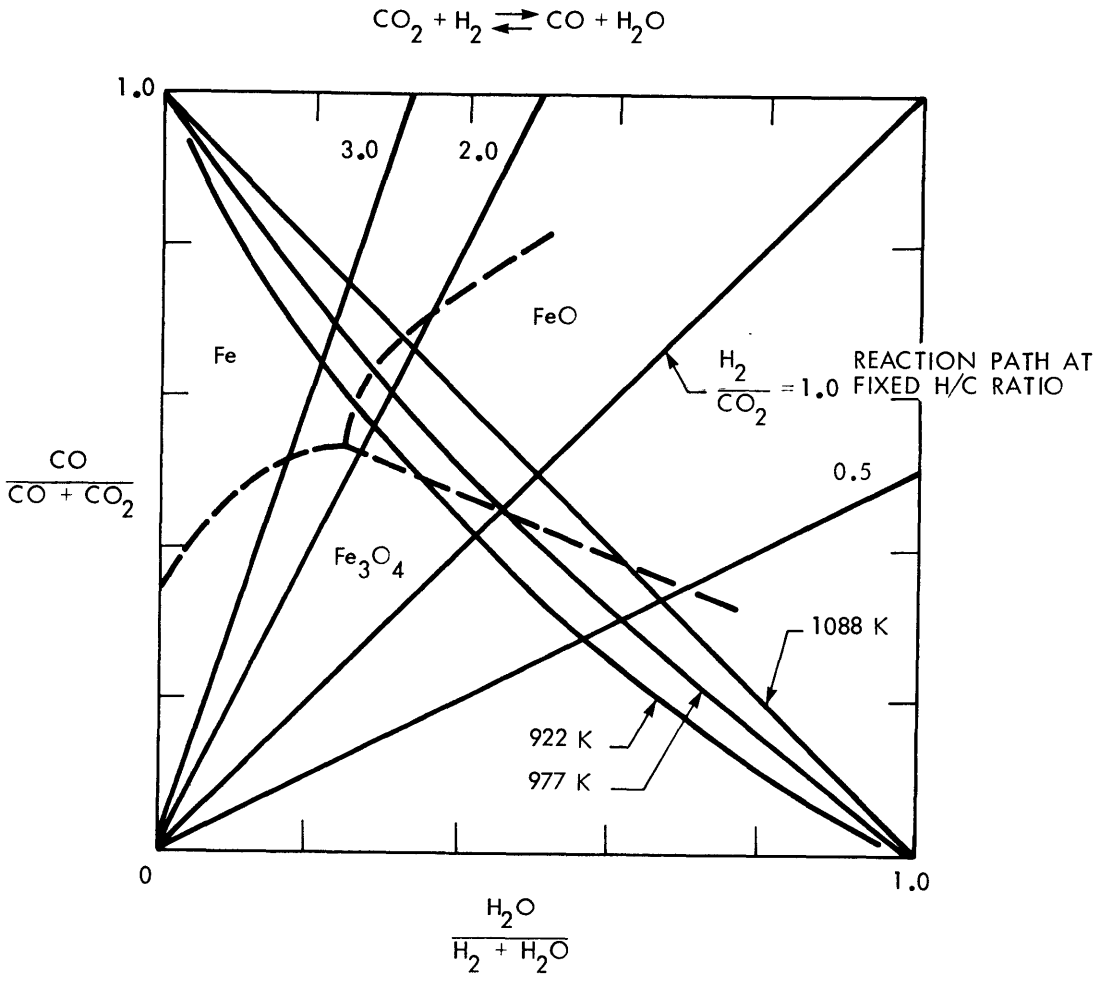

FIGURE 10

PHASE DIAGRAM FOR THE REVERSE WATER–GAS SHIFT REACTION (KUSNER, 1962)

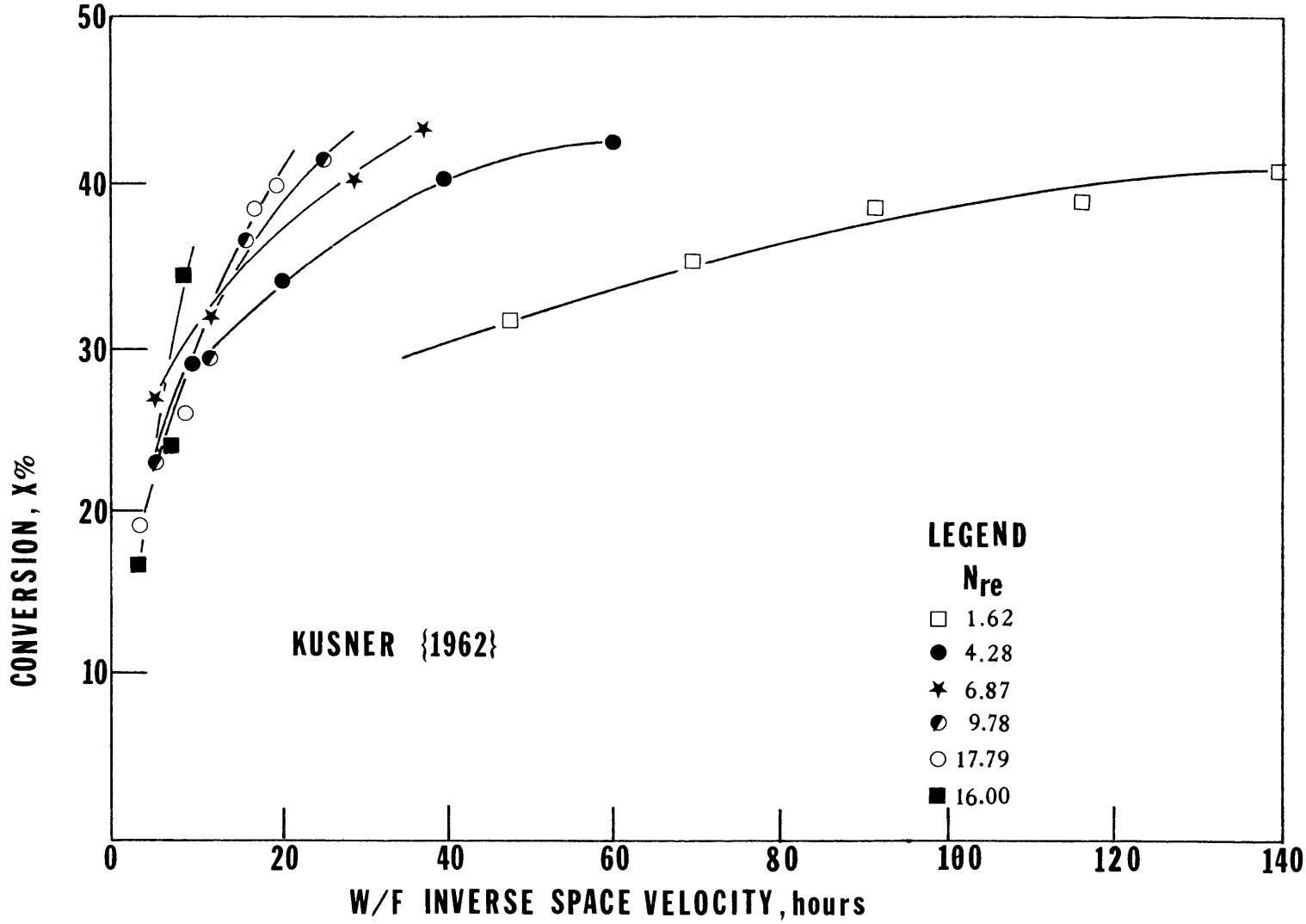

Figure 11 CO_2 Conversion in a Packed Bed For The Reverse Water-Gas Shift Reaction

monoxide and water prior to the catalyst bed, Kusner assumed that axial and longitudinal diffusion may be important.

Kusner next modelled his system as (N) mixed reactors in series and also as a plug flow reactor with axial and longitudinal diffusion. The models both appeared to describe qualitatively the behavior observed but no quantitative comparison could be made.

The importance of Kusner's work lies in the fact that he has conclusively shown that the reverse water-gas shift reaction occurs at a rapid rate in a packed bed at 922 K without carbon formation. Also important is the implication which can be drawn from his phase diagram analysis. That is, both iron and various iron oxides are catalysts for the reaction.

Additional evidence suggesting that iron oxide is a catalyst for the reverse water-gas shift reaction was provided by Barkley et al. (1956).

Barkley studied the reverse water-gas shift reaction over a promoted iron oxide catalyst. The catalyst was in the form of cylindrical pellets 3 mm in diameter and 1.75 mm in length. The bulk density of the catalyst was 300 g/cc. The reactor consisted of a vertical Vycor tube housed in an iron pipe to facilitate temperature distribution. The entire reactor assembly was set in a split type, heavy duty electric combustion furnace with the catalyst being supported on a perforated porcelain dish. The bed height varied between 1.3 and 6.5 cm. Reactor feed rates varied between 0.02 and 0.22 M^3/Hr. Hydrogen-to-carbon dioxide ratios varied from 4.0 to

0.25. Samples of both feed and product gases were analyzed for carbon dioxide, carbon monoxide, and hydrogen. The quantity of water vapor formed was obtained by material balance. No other gases were found and no carbon formation was reported.

Figure 12 is a plot from Barkley's data for conversion expressed as lb-moles CO_2 converted per lb-mole CO_2 fed versus inverse space velocity (W/F). Comparing Figure 11 of Kusner's data with Figure 12, one can see that the general shape of the curves are similar. The curve for a hydrogen-to-carbon dioxide ratio of 4.0 in Figure 12 shows an approach to equilibrium of 88%. Similarly, for a hydrogen-to-carbon dioxide ratio of 3.0 in Kusner's study, the approach to equilibrium is approximately 95%. Unlike Kusner, Barkley's apparatus showed no mass transfer limitations. This was determined by varying the amount of catalyst and the feed rate of CO_2 independently while maintaining the W/F (inverse space velocity) constant. No appreciable effect on conversion was observed, thus indicating no mass transfer limitations.

Barkley proposed the following reaction mechanism for the reverse water-gas shift reaction:

A) A molecule of carbon dioxide is adsorbed on a single active site.

B) The adsorbed carbon dioxide molecule reacts with hydrogen to form a molecule of adsorbed carbon monoxide and a molecule of water in the gas phase (rate controlling step).

C) The molecule of carbon monoxide is desorbed.

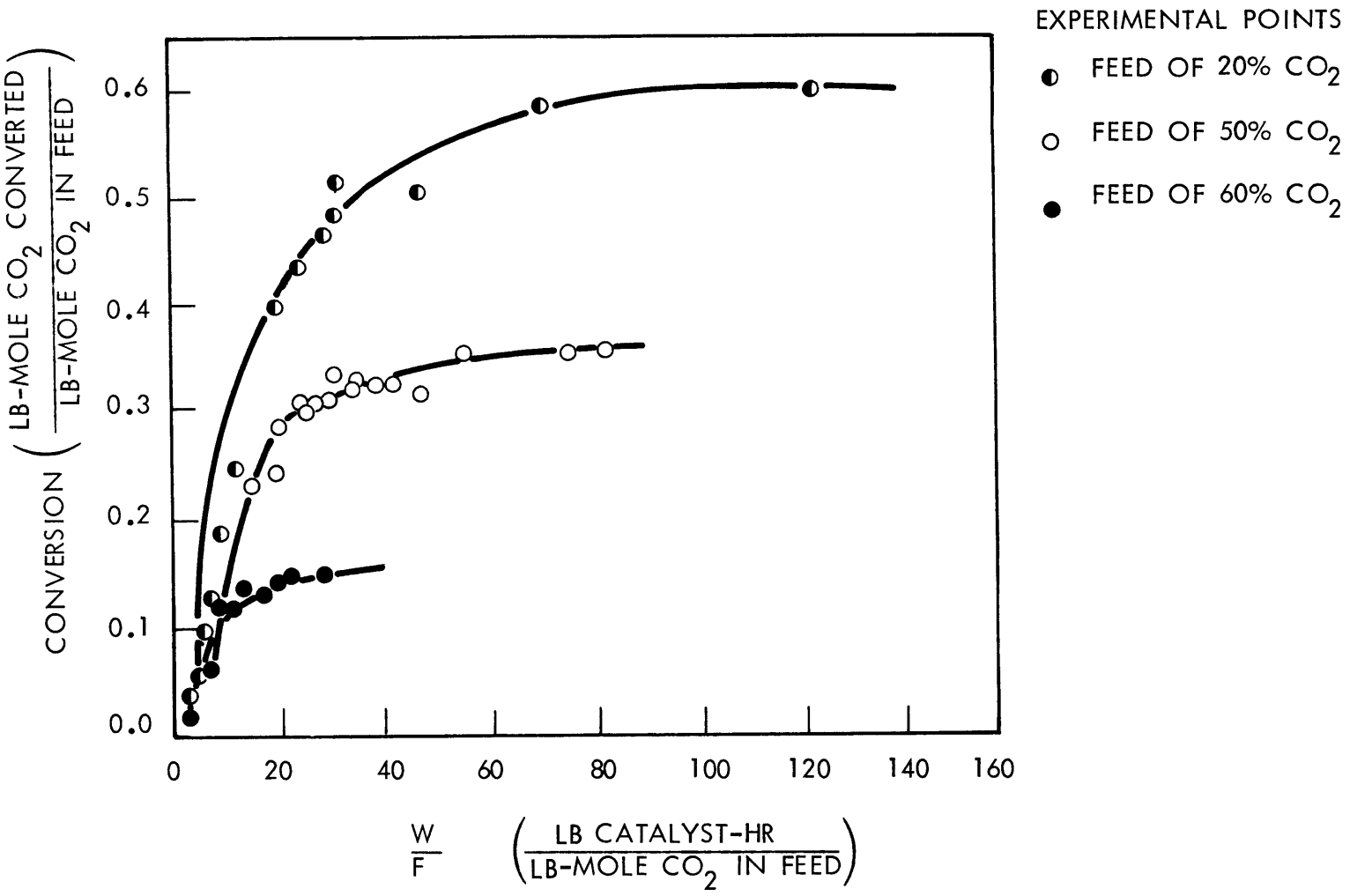

FIGURE 12 CONVERSION VERSUS W/F (BARKLEY et al.,1956)

Using this reaction mechanism and a least square regression analysis, Barkley found the following rate expression fit the obtained data:

$$r = k \left(\frac{P_{CO_2} P_{H_2} - P_{CO} P_{H_2O}}{1 + K_A P_{CO_2} + K_R P_{CO}} \right) \qquad (2)$$

Although this mechanism is intriguing, the fitted constants (i.e., k, K_A, K_R) were not presented, since temperature control in Barkley's reactor was reported poor. Temperatures were reported to fluctuate as much as 50 K.

The importance of this work is that, once again, evidence indicates the reverse water-gas shift reaction occurs readily in a packed bed.

2.1.3 Methane Formation

Methane formation has been found to occur in all Bosch processes. The mechanism by which it forms has never been clearly understood. This lack of understanding is due in no small part to the complexities of the Bosch reaction sequence. The following reactions are suggested as possible methane formers.

2.1.3.1 CH_4-H_2-C System

Browning et al. (1951) studied the carbon-hydrogen-methane system in the presence of an iron catalyst.

$$2H_2 + C \rightleftarrows CH_4 \qquad (G)$$

The apparatus consisted of a sample container, a trap

for removing water during analysis, a copper oxide trap for conversion of hydrogen to water during analysis, a circulating pump, and a by-pass to allow gases to be either circulated through the catalyst or be by-passed through the analytical train.

Prior to a run, a synthetic ammonia catalyst was reduced in hydrogen at 773 K. The reduced iron catalyst was then carbided to cementite (Fe_3C) in butane at 548 K. Heating to 773 K for 72 hours decomposed the cementite to carbon and iron. The temperature was then lowered to 548 K and hydrogen was again introduced to convert any remaining cementite to iron. During this last step, the carbon formed during cementite decomposition remained relatively unaffected.

Figure 13 represents the data obtained by Browning (solid line), as well as that reported by Rossini (1947) (dotted line). The apparent equilibrium values reported by Browning lay below those reported by Rossini. Comparing the Gibbs energies they calculated with those reported by Rossini, Browning determined the Gibbs energy of formation of the carbon in their system was approximately 300 calories/mole less than the β-graphite used in Rossini's work. Browning approached the "equilibrium" from both the hydrogen and methane-rich sides, obtaining good agreement. However, the conversion of methane when approaching from the methane-rich side was small. Thus, further verification from the methane-rich side would be desirable.

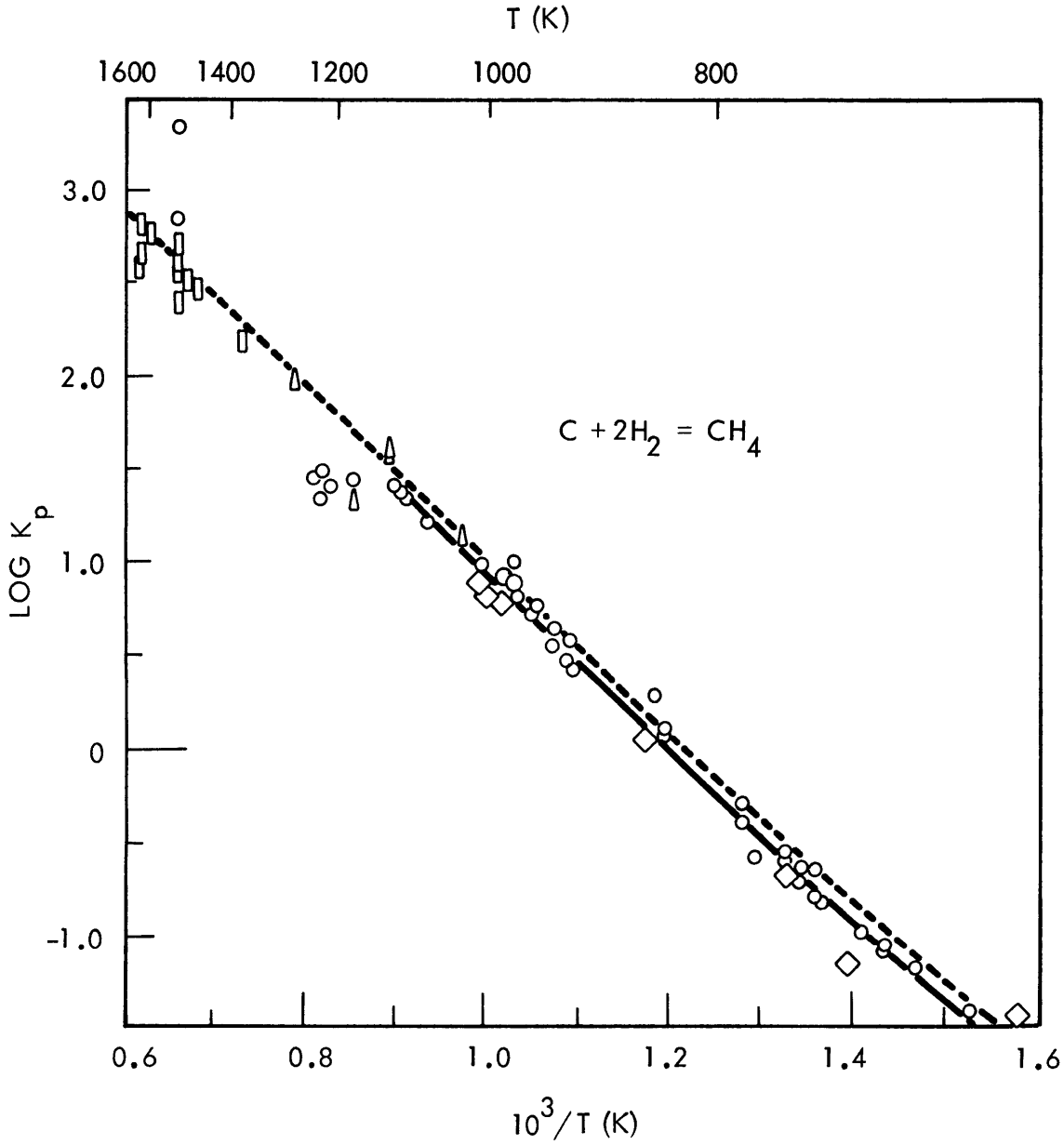

FIGURE 13
EQUILIBRIUM DATA FOR REACTION (G)
(BROWNING and EMMETT, 1951)

Although Figure 13 indicates good agreement with Rossini and others, there remains a problem in the equilibrium study as described.

From a phase rule analysis on Browning's system, n, the number of components, equals 3 (i.e., H_2, C, CH_4), the temperature was fixed but not pressure. Given two phases exist (i.e., carbon and gas) and the number of independent reactions, R, equals 1. The number of intensive variables left to fix the system is 1 (f = 3 + 2 - 2 - 2 = 1).

There are two possible explanations for this, both speculative; one, the experiment as reported is inaccurately described; second, some Fe_3C remains after the final hydrogen reduction. The implication of some Fe_3C remaining is as follows: in this temperature range, reaction G must be faster than reaction H-A in both the forward and reverse direction.

$$2H_2 + Fe_3C \rightleftarrows 3Fe + CH_4 \qquad \text{(H-A)}$$

Again, this is speculative and requires data for substantiation.

2.1.3.1.1 Recent MIT Work

Manning (1975) reacted methane and hydrogen over 250 mg of steel wool catalyst which had had approximately 375 mg of carbon deposited on it. The reaction was carried out at a temperature of 823 K under a total pressure of 1.01 X 10^5 N/m^2. The carbon was deposited using a 1:1 molar ratio of carbon monoxide-to-hydrogen at 823 K.

Pure hydrogen was fed to the reactor for one hour; the reactor effluent indicated a hydrogen conversion of 0.24 -

.54%. This corresponded to an outlet concentration of only 0.17 to 0.27% methane. During this same time period, a linear carbon weight loss was observed (Figure 14). As indicated by Figure 14, the carbon weight loss was in excess of 75 mg.

Manning increased the methane content to 75% for two hours. Figure 14 indicates no weight loss or gain was noted. There was no variation in the effluent and this also indicates that no reaction had occurred. Dropping the methane content to 60% for 1.5 hours again produced no apparent reaction. A mixture of 25% methane-75% hydrogen was next run through the reactor for 2.5 hours. Figure 14 indicates 35 mg of carbon were lost. The slope of the 75% hydrogen mixture is less than that for the 100% hydrogen mixture.

Manning suggested the following reactions as the probable sources of methane:

$$2H_2 + Fe_3C \rightleftarrows 3Fe + CH_4 \qquad K_{P_{823\ K}} = 2.48 \qquad \text{(H-A)}$$

$$2H_2 + C \rightleftarrows CH_4 \qquad K_{P_{823\ K}} = 0.966 \qquad \text{(G)}$$

In an attempt to determine the mechanism for carbon formation, pure hydrogen was passed over 450 mg of activated charcoal (BET area 850 m^2/g) in the absence of iron. No methane was detected in the reactor off-gas. Manning concluded that reaction H-A was therefore responsible for methane formation. He explained the 75 mg carbon loss by assuming that cementite production is occurring faster than its reduction (only 17 mg of carbon would have completely carbided the catalyst.)

This hypothesis is suspect because other established

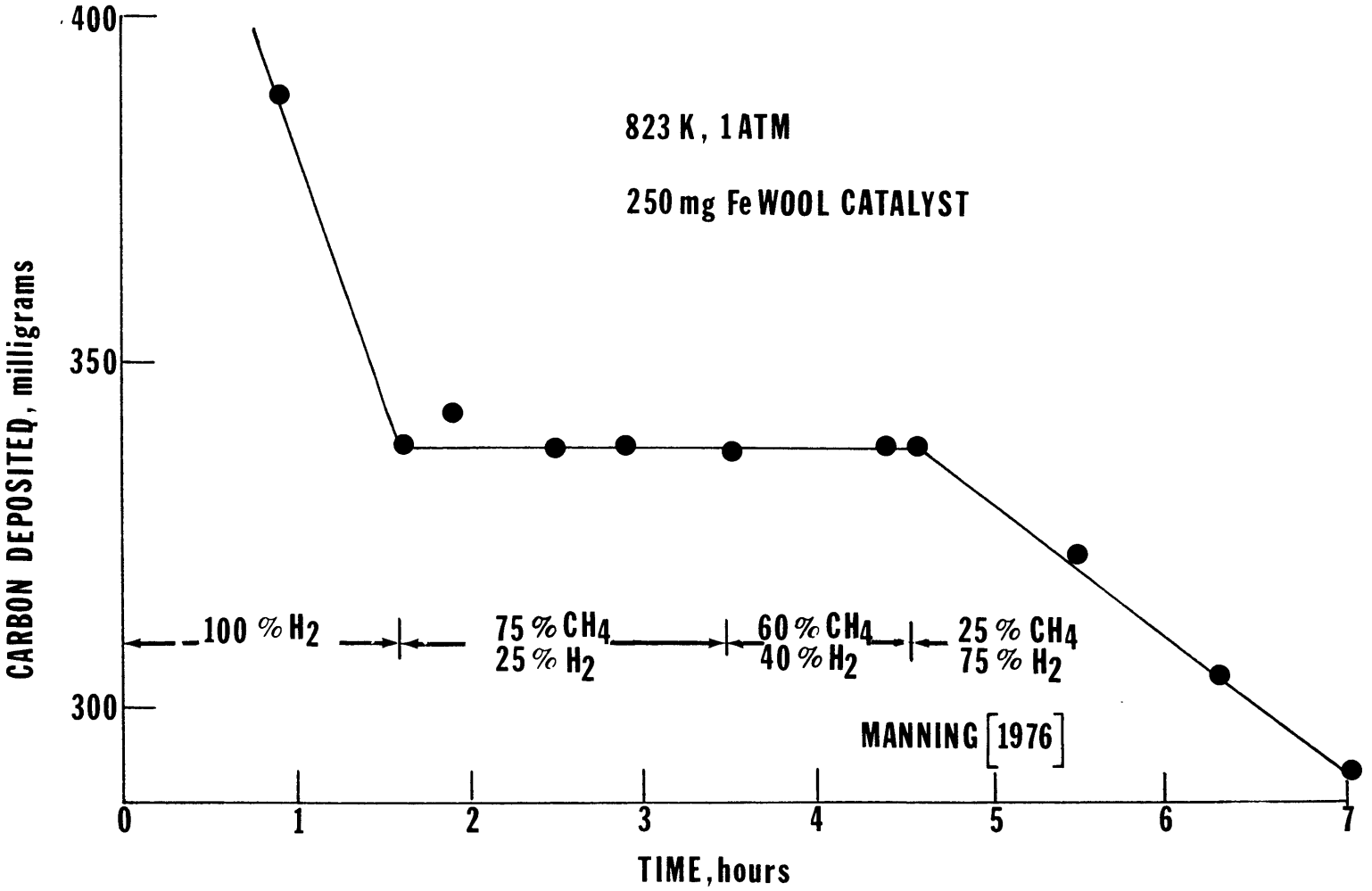

Figure 14 Carbon Deposition From CH_4-H_2 Mixtures

methane catalysts do not form carbides in the temperature range where they are known to catalyze methane formation. Thus, a carbide species as an intermediate in methane formation is dubious.

From a thermodynamic point of view reaction H-A and G would proceed to the right for the runs where the hydrogen concentrations were 100% and 75%. For the runs of 25% and 40% hydrogen, reaction G would be expected to deposit carbon while reaction H-A would be expected to form cementite (Fe_3C).

The implication is that methane decomposition may be inhibited by cementite formation. This, however, is speculative and more data are needed before a definitive statement can be made.

2.1.3.2 CH_4-H_2-Fe_2C-Fe, CH_4-H_2-Fe_3C-Fe Systems

Browning et al. (1950) also studied the equilibrium represented by reactions H-B and H-A.

$$2H_2 + Fe_2C \rightleftarrows 2Fe + CH_4 \qquad \text{(H-B)}$$

$$2H_2 + Fe_3C \rightleftarrows 3Fe + CH_4 \qquad \text{(H-A)}$$

Hagg carbide (Fe_2C) was prepared by reducing an iron synthetic ammonia catalyst in hydrogen at 773 K prior to carbiding. The carbiding gas was either carbon monoxide, butane, or methane. Carbiding was done at 473-573 K; the amount and type(s) of carbide formed was determined by x-ray diffraction patterns. The surface area of the catalyst was determined by standard BET methods and was found to be 17 m^2/g.

Cementite (Fe_3C) was prepared by heating Hagg carbide to 748-773 K for three hours. Browning indicated this treatment caused complete disappearance of Fe_2C lines and the appearance of Fe_3C lines in an x-ray diffraction pattern. Figure 15 is a plot of Browning's data, where log K_P is defined as

$$K_P = \frac{(X_{H_2})^2}{(X_{CH_4})} \tag{3}$$

Curves A, B, and C are plots of the best values of the "equilibrium" data for the systems C_β-CH_4-H_2 (as given by Rossini {1947}), Fe_3C-Fe-H_2-CH_4, and Fe_2C-Fe-H_2-CH_4 (Browning et al.), respectively. Figure 15 shows that, below approximately 670 K, curves B and C follow linear behavior. However, above 670 K the data appears to lie halfway between curve A and curve B. The implication of these data is that below 670 K reaction H-A and H-B are kinetically more favorable than reaction G. Above 670 K, however, the rate of reaction G becomes more significant.

A phase rule analysis on the H_2-CH_4-Fe_2C-Fe and H_2-CH_4-Fe_3C-Fe systems indicates only one intensive variable need be fixed to completely specify the equilibrium state. From Figure 15 and from the fact that Browning occasionally reported carbon diffraction lines when preparing carbides, one can speculate that some carbon is present in all the "equilibrium" systems measured. This explanation will satisfy the phase rule analysis.

One note of caution is necessary in evaluating Browning

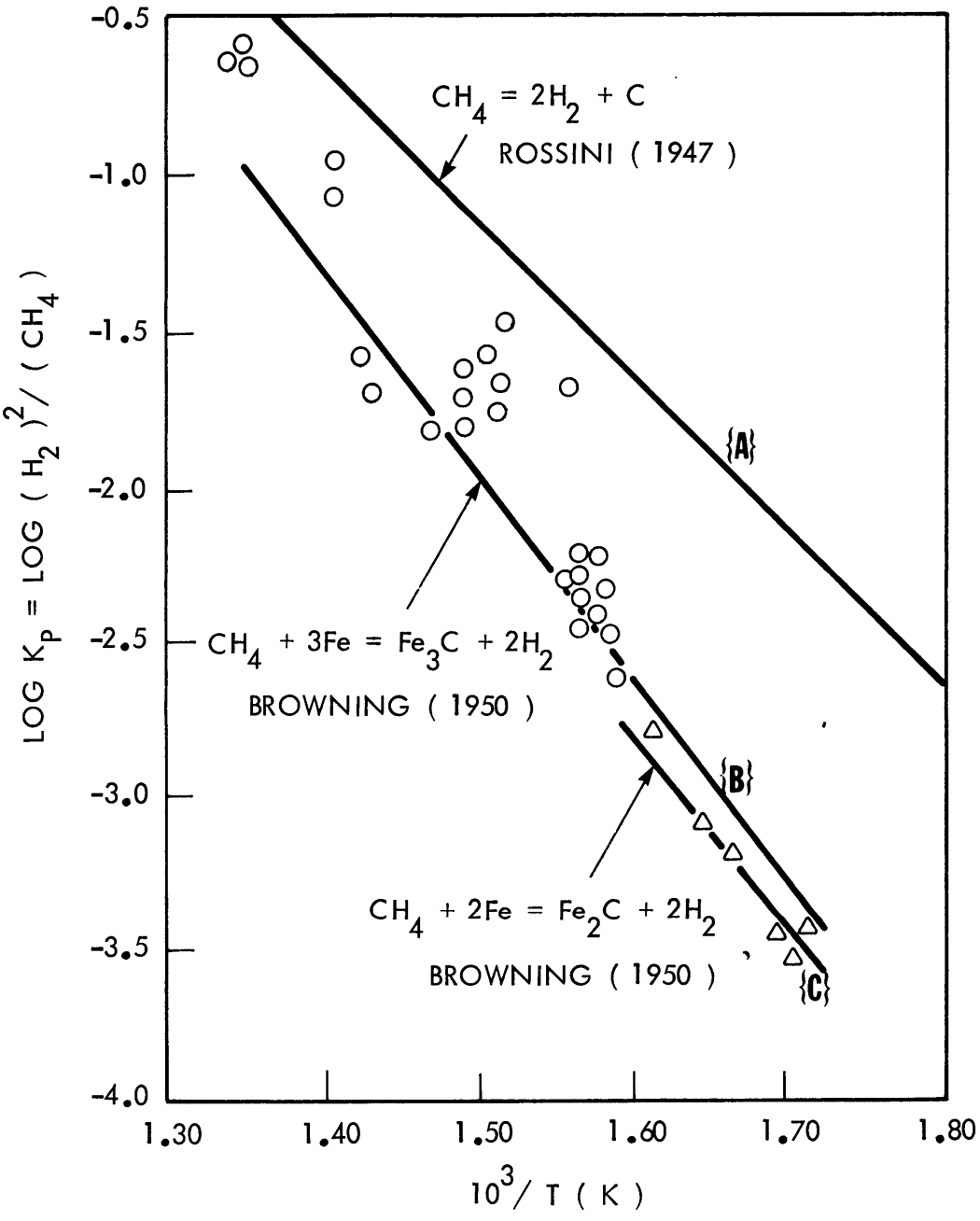

FIGURE 15
EQUILIBRIUM STUDIES OF CH_4-H_2-Fe-Fe_2C AND
CH_4-H_2-Fe-Fe_3C SYSTEMS

et al.'s data: the methane content in the systems was obtained by difference, that is, no true material balance was performed on the system; the hydrogen content was determined after it was converted to water.

2.1.3.3 H_2-CO-CH_4-H_2O System

The reaction of carbon monoxide and hydrogen to give methane and water is termed methanation, reaction K.

$$3H_2 + CO \rightleftarrows CH_4 + H_2O \qquad (K)$$

Reaction K is normally run over a nickel catalyst at 523-723 K (Vanice, 1976). However, nickel is not the only active catalyst for methanation. The following metals were described by Vanice (1976) as good methanation catalysts. In decreasing order of activity: Ru, Ir, Rh, Ni, Co, Os, Pt, Fe, and Pd. In general, methanation catalysts deactivate due to sulfur compounds, sintering, and carbide formation.

2.2 Metallurgical Considerations

The gas phase reactions which comprise the Bosch process are seen to be catalyzed by transition metals. The literature indicates that the solid phase and/or phases of the catalyst may change during reaction. The catalytic effect of these new phases are not clear, however, indications are that iron oxides and/or iron carbides may not be catalysts for carbon deposition, carbon deposition being an integral part of the Bosch sequence. Thus, a thorough knowledge of the thermodynamics and kinetics of oxide and carbide formation is necessary.

2.2.1 Thermodynamics of the Iron-Iron Oxide System

Figure 16 is a phase diagram representing the iron-iron oxide system. The solid phase composition is fixed, at a specific temperature, by adjusting the oxygen activity* to the desired value. The oxygen activity in the system can be maintained at a desired value by fixing the hydrogen-to-water ratio according to reaction B or, alternatively, by the carbon monoxide-to-carbon dioxide ratio, reaction L.

$$H_2 + 1/2\ O_2 \rightleftarrows H_2O \qquad (B)$$

$$CO + 1/2\ O_2 \rightleftarrows CO_2 \qquad (L)$$

If carbon monoxide, carbon dioxide, hydrogen, water, and oxygen are all present in the equilibrium gas mixture, then reaction F can be

$$H_2 + CO_2 \rightleftarrows CO + H_2O \qquad (F)$$

used in conjunction with reaction B or reaction L to fix the solid phase composition.

It is of interest to note the wustite phase field is of variable composition. That is, at a set temperature, the activity of oxygen varies across the phase field. Also, the gentle slope of the wustite/iron, wustite/magnetic phase boundaries must be accounted for in determining oxygen partial pressure above a desired equilibrium phase. A further compli-

---

*Note: $a_{O_2} = \frac{\hat{f}_{O_2}}{f^{\circ}_{O_2}}$ $\qquad f^{\circ}_{O_2} \rightarrow 1$ and $f_{O_2} \cong P_{O_2}$

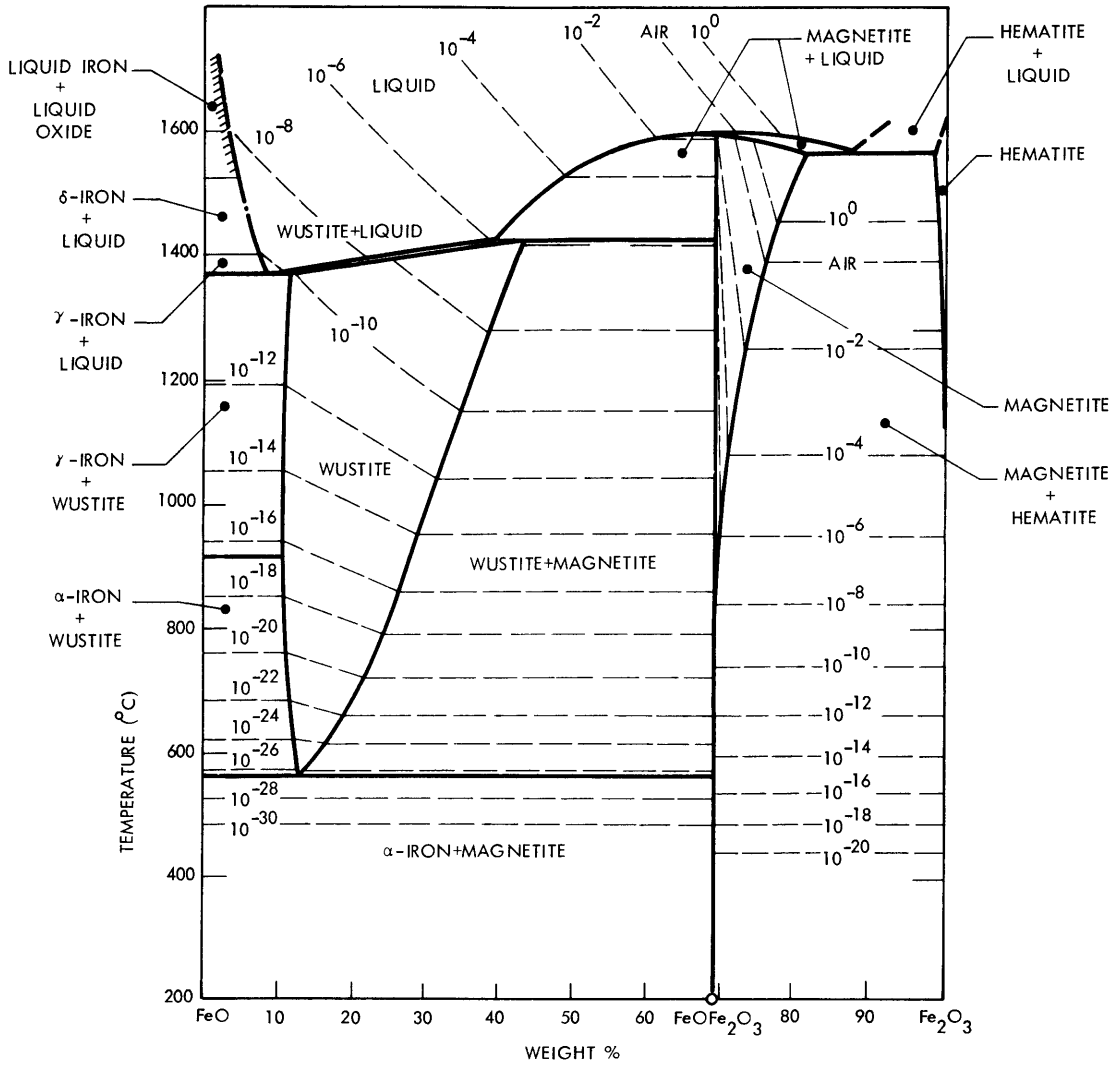

FIGURE 16

IRON-IRON OXIDE PHASE DIAGRAM

(MUAN and OSBORN, 1965)

cation, illustrated by Figure 16, is that the stable oxide phase in equilibrium with alpha-iron is a function of temperature. Below 833-843 K, magnetite (Fe_3O_4) is the stable oxide phase; while above 833-843 K, wustite is the expected oxide phase.

2.2.2 Solid-Gas Reactions - Oxidation and Reduction of Iron and Iron Oxides

The complexity of the iron-iron oxide phase diagram is reflected in the voluminous and often confusing literature concerning iron oxidation and/or iron oxide(s) reduction. Additional complications arise from the fact that structural changes occur during reaction and these affect the kinetics. There are, however, three major mechanisms which have been successful in explaining observed data both qualitatively and quantitatively. Each describes the kinetics depending upon initial structure and temperature. The three proposed mechanisms are as follows:

A) Gas-solid reactions combined with solid-state diffusion

B) A shrinking core model which assumes a nonporous unreacted core and a porous product layer

C) A shrinking core model for a porous particle assuming diffusion and/or mixed diffusion-interfacial control

A brief description of each mechanism is felt necessary to insure a better understanding of the process or processes

that will occur on the Bosch catalyst.

2.2.2.1 Gas-Solid Reaction and Solid State Diffusion

When the solid product layer is nonporous, forming a dense layer around the reactant solid, the transport of matter across the product layer occurs by solid state diffusion. Solid state diffusion has been shown to control metal oxide reduction and metal oxidation under certain conditions.

Ladler and Komack (1966) studied the partial reduction of wustite with hydrogen.

$$Fe_{1-y_1}O \rightarrow Fe_{1-y_2}O$$

They interpreted their results based upon a model which assumed the overall rate was controlled by chemical reaction at the solid-gas interface and solid state diffusion of iron within the oxide. Figure 17 illustrates the proposed mechanism.

Assuming the solid to be a slab of thickness, (L), they derived the transport equation for the undirectional diffusion of iron. Applying the appropriate boundary conditions they obtained the iron concentration profile as a function of thickness (y) and time (t). This is shown in Figure 17. As additional proof of the validity of the model, the iron concentration profile was used to derive an expression for the overall conversion ($\underline{X}$) as a function of reduced time ($4D_s/tL^2$).

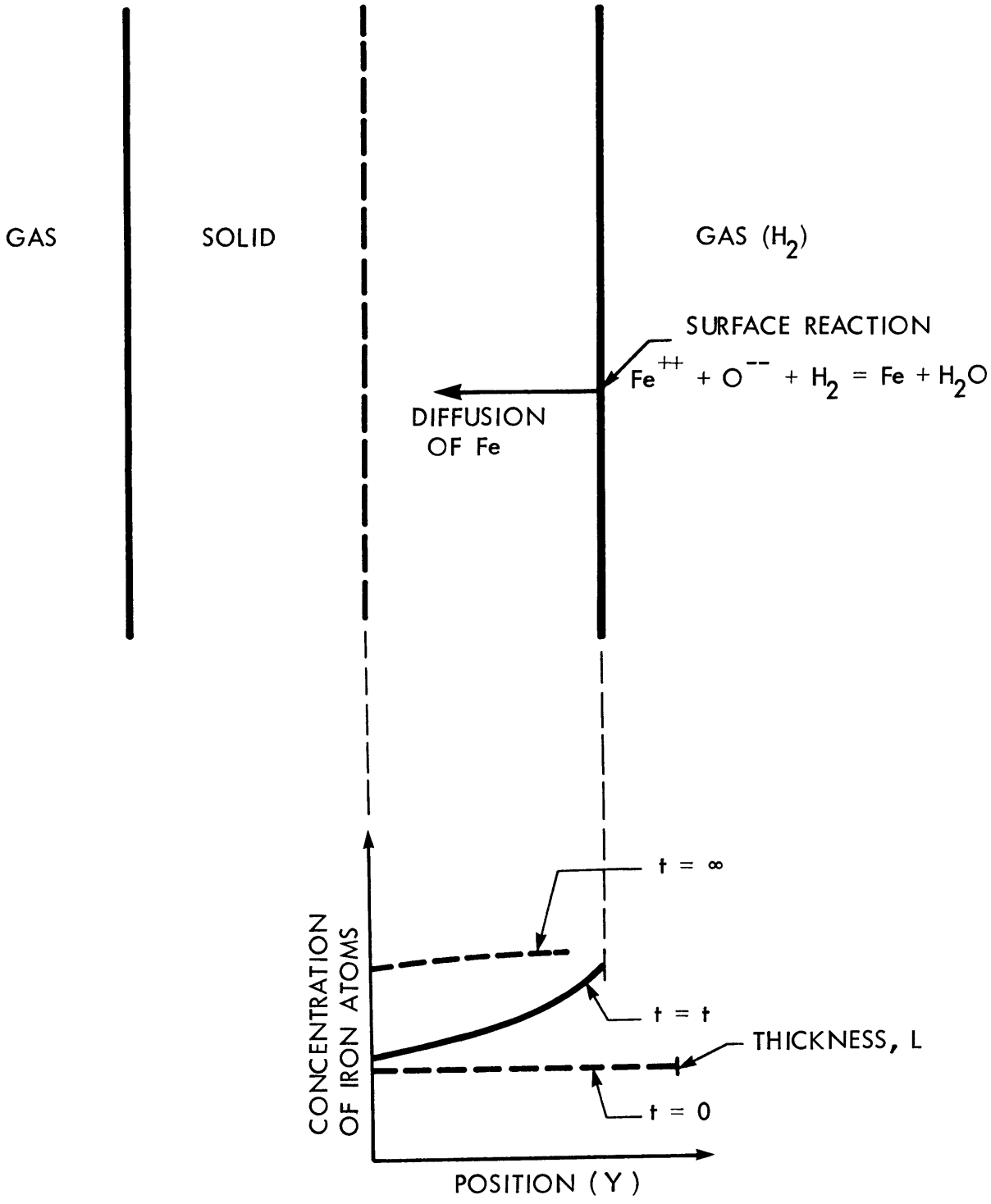

FIGURE 17

COMBINED SURFACE REACTION WITH SOLID STATE DIFFUSION

(SZEKELY et al.,1976)

$$\underline{X} = 1 \sum_{n=1}^{\infty} 2\exp\left(-4 \frac{D_s t}{L^2} \beta_n^2 \right) \left(\beta_n^2 + \left(\frac{2D_s \beta_n^2}{k\ L}\right) + \frac{2D_s \beta_n^2}{k\ L} \right)^{-1} \qquad (4)$$

Landler and Komack then used this to determine the diffusivity of iron and found it to be reasonable and consistent.

This proposed model is slow relative to the other two mechanisms and would require a high activation energy. Edstrom (1955) has demonstrated that the rate of iron ion mobility in wustite varies over one hundred fold between 973-1273 K. Assuming a rate expression of the form

$$R = k\ e^{-E/RT} \qquad (5)$$

one can calculate an $E/R = 1.90 \times 10^4$ K. Extrapolating to 900 K, the relative rate is $0.007\ R_{1273\ K}$. With an iron mobility this low, iron oxidation or reduction would be very slow in the temperature range of interest in the Bosch process ($\leq$900 K).

If solid state diffusion is controlling oxidation or reduction, the weight gain or loss during reaction is initially more rapid. As the outer surface is reduced (oxidized), a nonporous shell is formed, the thickness of which increases slowly with time. Frequently, on reaching a critical thickness, reaction essentially stops (i.e., diffusion distance is large). Thus, if seen in a metallograph, one would expect a single, usually thin nonporous oxide or iron layer.

2.2.2.2 Nonporous Shrinking Core Model With Porous Product Layer

Spitzer et al. (1966) developed a shrinking core model for the reduction of dense hematite (Fe_2O_3) spheres. It was assumed that iron oxide reduction went through the following steps:

$$H_2/CO + Fe_2O_3 \rightarrow Fe_3O_4 \rightarrow Fe_{1-y}O \rightarrow Fe + H_2O/CO_2$$

All oxygen removed was assumed to occur at the $Fe/Fe_{1-y}O$ interface, while reduction of the intermediate oxides occurred by solid state diffusion. The oxygen density at the core was assumed constant.

They proposed the following steps to occur in series:

I. Transport of gaseous reactants from the bulk to the outer surface of the particle

II. Diffusion of reactant through the porous iron layer to the surface of the unreacted core (the $Fe/Fe_{1-y}O$ interface)

III. Chemical reaction of the gaseous reactant with solid oxide to form gaseous product

IV. Outward diffusion of the gaseous product through the product shell (iron layer)

V. Transfer of the product species from the outer surface to the bulk gas stream

An illustration of the proposed model is shown in Figure 18 along with the electrical circuit analogy used in the

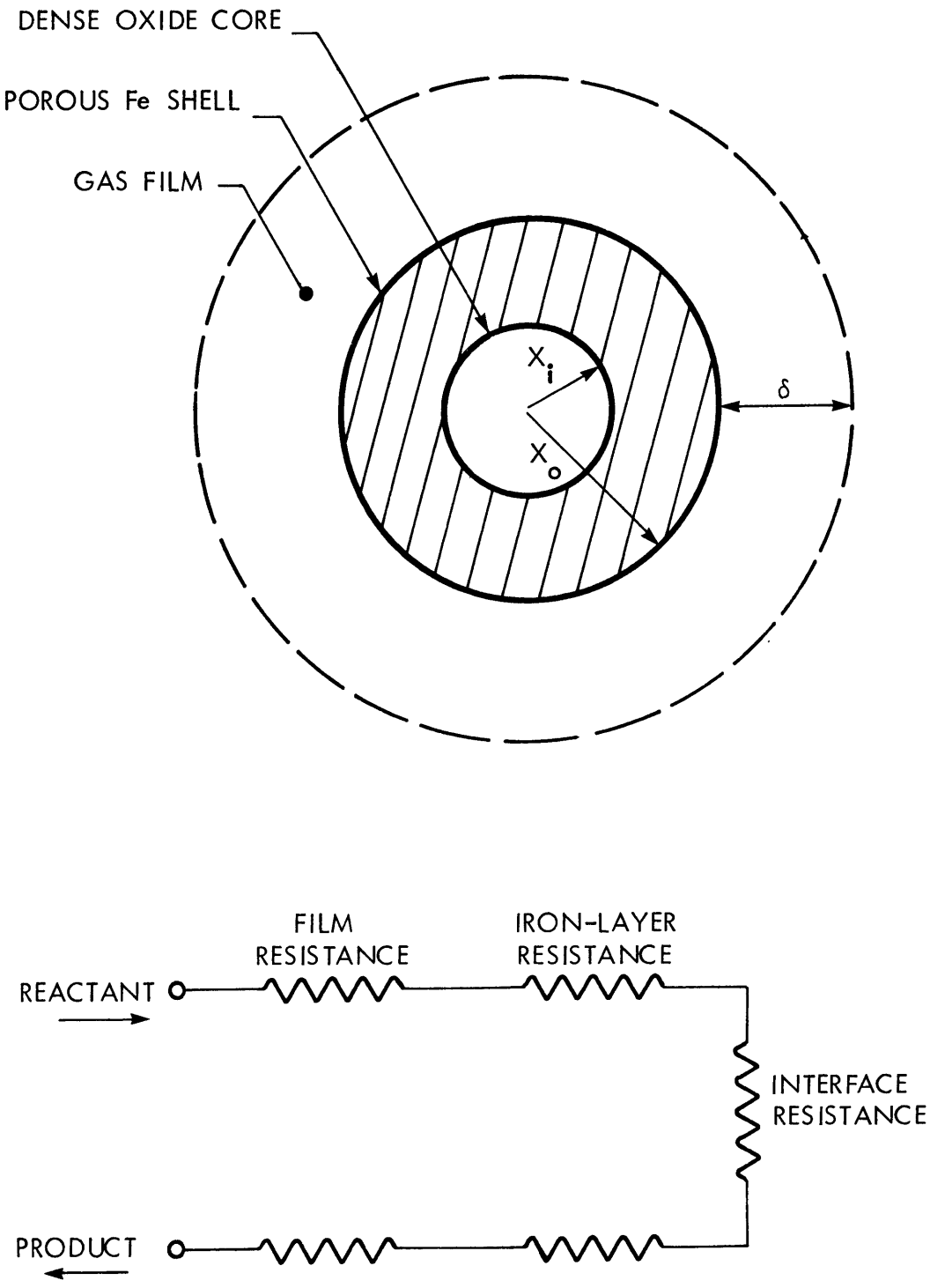

FIGURE 18

NON-POROUS SHRINKING CORE MODEL WITH POROUS PRODUCT LAYER (SPITZER et al.,1966)

mathematical derivation.

The gas film, shell layer and interface resistances* were combined in Ohm's law fashion, and an equation describing the rate of change of core radius was generated.

$$\frac{dX_i}{d\theta} = \frac{-k_{ov}}{R_g TCO} \left[P_A^{(b)} - \frac{P_B^{(b)}}{K_e} \right] \tag{6}$$

where:

$$k_{ov} = \frac{1}{\frac{X_i^2}{X_o^2 \alpha} + \frac{X_i (X_o - X_i)}{X_o \beta} + \frac{1}{k_r}} \tag{7}$$

The terms in the denominator were identified as, respectively, the gas film resistance, the shell layer resistance, and the interface resistance.

This model predicted well the linear rate of advance observed by McKewan (1962). Adopting a Langmuir-Hinshelwood rate expression, the model was also able to predict the observed behavior of rate as a function of hydrogen pressure. Since the Langmuir-Hinshelwood formulation requires that strongly adsorbed species be present in the denominator, Equation 8 implies that water is more strongly adsorbed than hydrogen on iron and iron oxide.

---

* See Appendix 7-1.

$$r_o = \frac{\frac{k_r}{R_g T}\left(P_{H_2}^{(b)} - \frac{P_{H_2O}^{(b)}}{K_e}\right)}{\left(1 + \frac{K_a^{H_2O}}{R_g T} P_{H_2O}^{(i)}\right)} \qquad (8)$$

If the solid-gas reactions on the Bosch catalyst followed this mechanism, a metallograph would show a single linearly advancing interface of porous material.

2.2.2.3 Shrinking Core Model for a Porous Particle

The equilibrium diagram in Figure 16 indicates that, depending on the kinetics of individual phase changes, as many as three interfaces could conceivably exist. In recognition of this problem, Spitzer et al. (1966) extended their shrinking core model to the reduction of porous hematite spheres. The situation is illustrated in Figure 19. The electrical circuit diagram was again used as the model for the mathematical formulation. The formulation, as before, followed an Ohm's law analysis.

Each interface was proposed to move at a rate determined by the specific rate constant for the surface reaction and by the gas composition present at the interface. For reversible, first-order kinetics, there were three equations generated of the form:

$$\frac{dX_i^{(t)}}{d\theta} = \frac{-\,k_r^{(t)}}{R_g T\, C_o^{(s)}\,\theta^{(t)}} \left(P_A^{(t)} - \frac{P_B^{(t)}}{K_e^{(t)}}\right) \left| \begin{matrix} s \to t \\ w \to Fe \\ m \to w \\ h \to m \end{matrix} \right| \qquad (9)$$

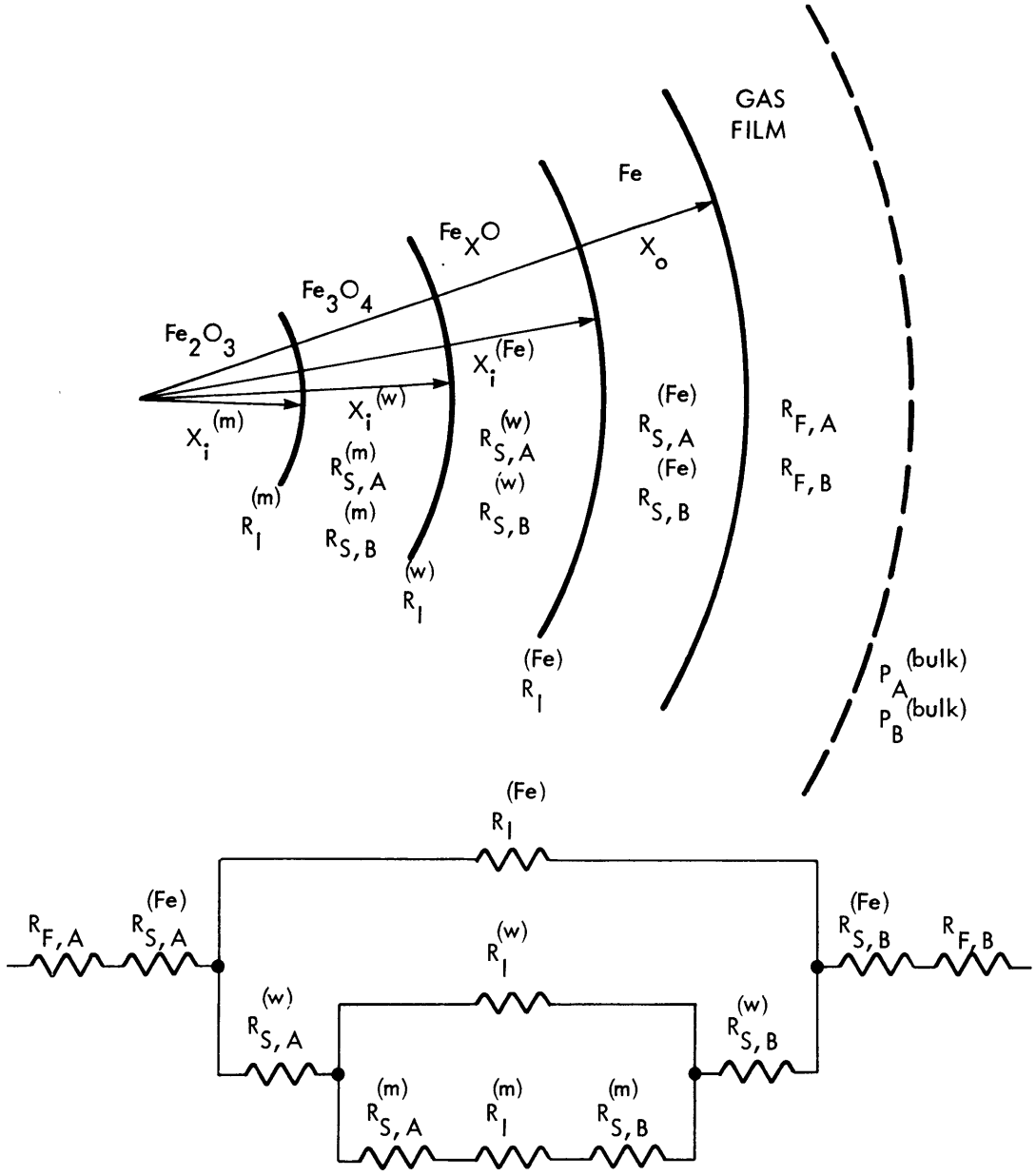

FIGURE 19

SHRINKING CORE MODEL FOR POROUS PARTICLE

(SPITZER et al.,1966)

where s is a mnemonic index for the reactant oxide, t is a mnemonic index for the product, and the s→t box signifies that equation 9 applies to all three interfaces.

Specific rate constants for each interface were determined by fitting the model to the data of McKewan (1964). An interesting parametric study was then made using this model.

Figure 20 is a computer generated plot of core radii (cm) versus reaction time, θ (min) for hematite reduction in pure hydrogen at 1173 K and 1.01 X 10^5 N/m^2. Similar to the dense pellet model, a linear advance of the reaction interface was predicted. However, according to this model, thin layers of magnetite and wustite are also predicted.

The interesting thing about this model is that it predicts a substantial increase in wustite layer thickness with addition of water, while the magnetite layer thickness does not increase greatly. If the P_{H_2}/P_{H_2O} is adjusted to a value only slightly above the equilibrium P_{H_2}/P_{H_2O} for wustite, Figure 21 is generated. Figure 21 indicates that for the first ten minutes no iron will be formed. Again, a thick wustite layer was predicted.

This type of system response results because the P_{H_2}/P_{H_2O} ratio is much smaller for the α-Fe/$Fe_{1-y}O$ equilibrium than for either the $Fe_3O_4/Fe_{1-y}O$ or the Fe_2O_3/Fe_3O_4 equilibriums. Therefore, at a given P_{H_2}/P_{H_2O} the driving force for reaction (i.e., distance from equilibrium) is greater for reduction of the Fe_2O_3, and Fe_3O_4 phases than for $Fe_{1-y}O$.

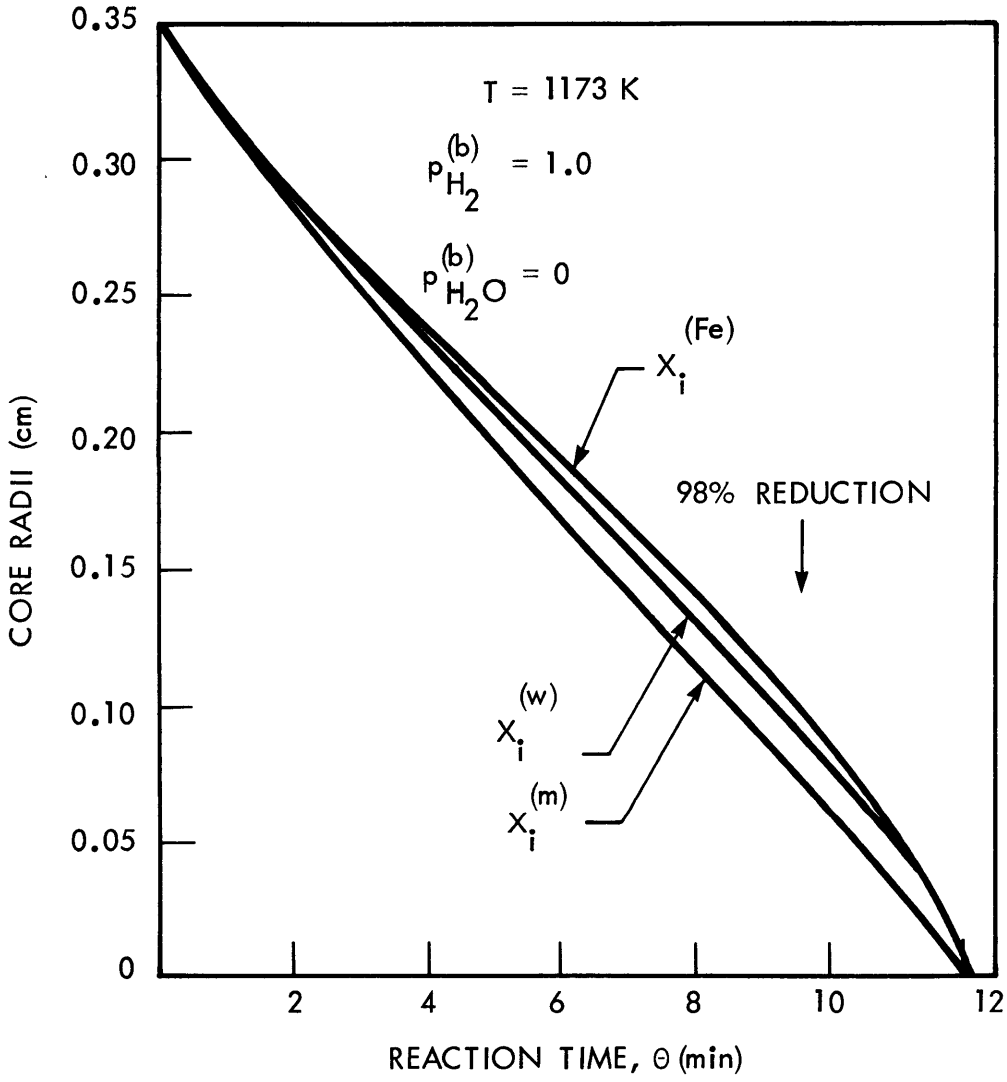

FIGURE 20
CORE RADII MOVEMENTS COMPUTED FOR POROUS PELLET MODEL
(SPITZER et al.,1966)

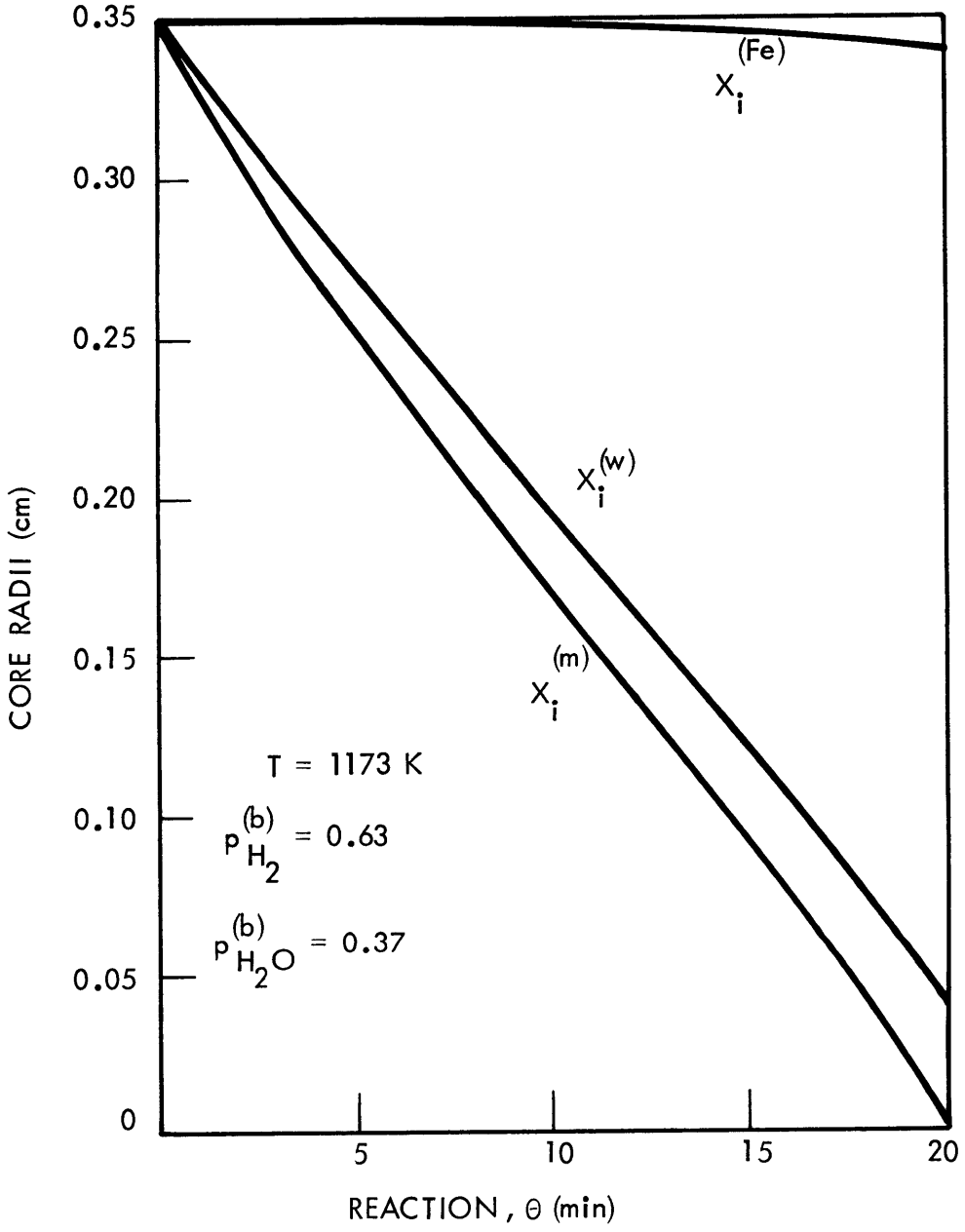

FIGURE 21
DELAYED ADVANCE OF IRON/WUSTITE INTERFACE POROUS PELLET MODEL
(SPITZER et al.,1966)

Also, since the various oxide phases are considered porous, these "faster" reactions produce water which maintains the local water concentration higher at the $Fe_{1-y}O/\alpha$-Fe interface than in the bulk gas phase. This in turn surpresses the reaction rate further for the conversion of $Fe_{1-y}O$ to α-Fe.

A comparison between morphologies predicted from the dense pellet model to that for the porous pellet model (Figure 22) shows that complete reduction is 1.5 faster in the porous pellet than in the dense pellet. Also, the dense pellet model predicts, at the same P_{H_2}/P_{H_2O}, a dense wustite layer. The porous pellet model predicts a substantially thicker porous layer.

From the kinetic analysis presented above, the following conclusions can be drawn. Depending on whether the steel wool catalyst behaves as a dense or porous solid and, depending on the mobility of iron ions at the temperature of interest, different morphologies can be predicted. If solid diffusion is important, the rate of oxidation and reduction will be substantially slower. Under certain conditions metastable multiple oxide phases are possible. The number and thickness depend on the temperature, past history (i.e., porous, non-porous), magnitude of the oxygen chemical potential, time at a fixed oxygen activity, and structural changes which may occur during reaction or during oxidation.

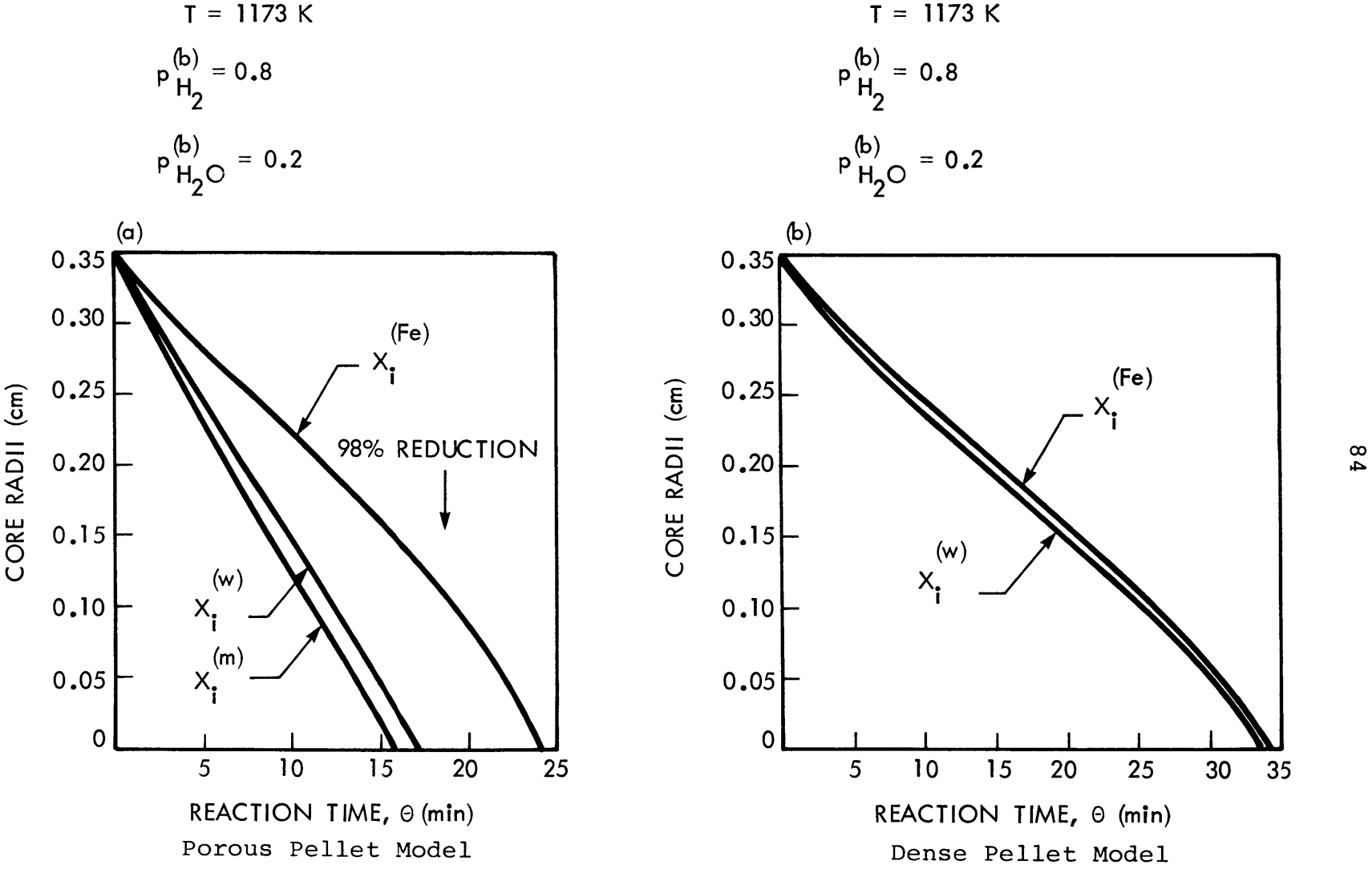

FIGURE 22 COMPARISON OF WUSTITE LAYER THICKNESS BETWEEN POROUS PELLET MODEL AND DENSE PELLET MODEL (SPITZER et al.,1966)

2.2.3 Iron-Carbon System

2.2.3.1 Thermodynamics of the Iron Carbon-System

Figure 23 (1958) is the standard phase diagram for the Fe-$C_\beta$system in the form of a double line diagram. The curves for the metastable Fe-Fe_3C system are drawn as solid lines. Those for the stable Fe-C_β are represented by dashed lines. Figure 23 is not a true equilibrium phase diagram because Fe_3C is not an equilibrium phase. Graphite is the stable carbon phase and cementite will eventually decompose to graphite. In ordinary steel, however, graphite precipitation is virtually never observed. Iron super saturated with carbon will precipitate cementite, not graphite. This is due to the fact that nucleation of cementite in iron occurs much more readily. Thus, when carbon is precipitated from solid solution of alpha (bcc) or gamma (fcc) iron, the resulting phase is almost always cementite (Reed-Hill, 1973).

Other iron carbides can form when iron solutions are supersaturated with carbon, but these are less stable than cementite (Cahn, 1965) and form only under special conditions. The most frequently observed of these less stable carbides is Hagg carbide. Hagg originally reported its measurement in 1932. Later, Jack (1946) and Jack and Wild (1966) reported its actual structure to be Fe_5C_2. Cohn et al. (1949) reported Hagg carbide would decompose to cementite above 773 K.

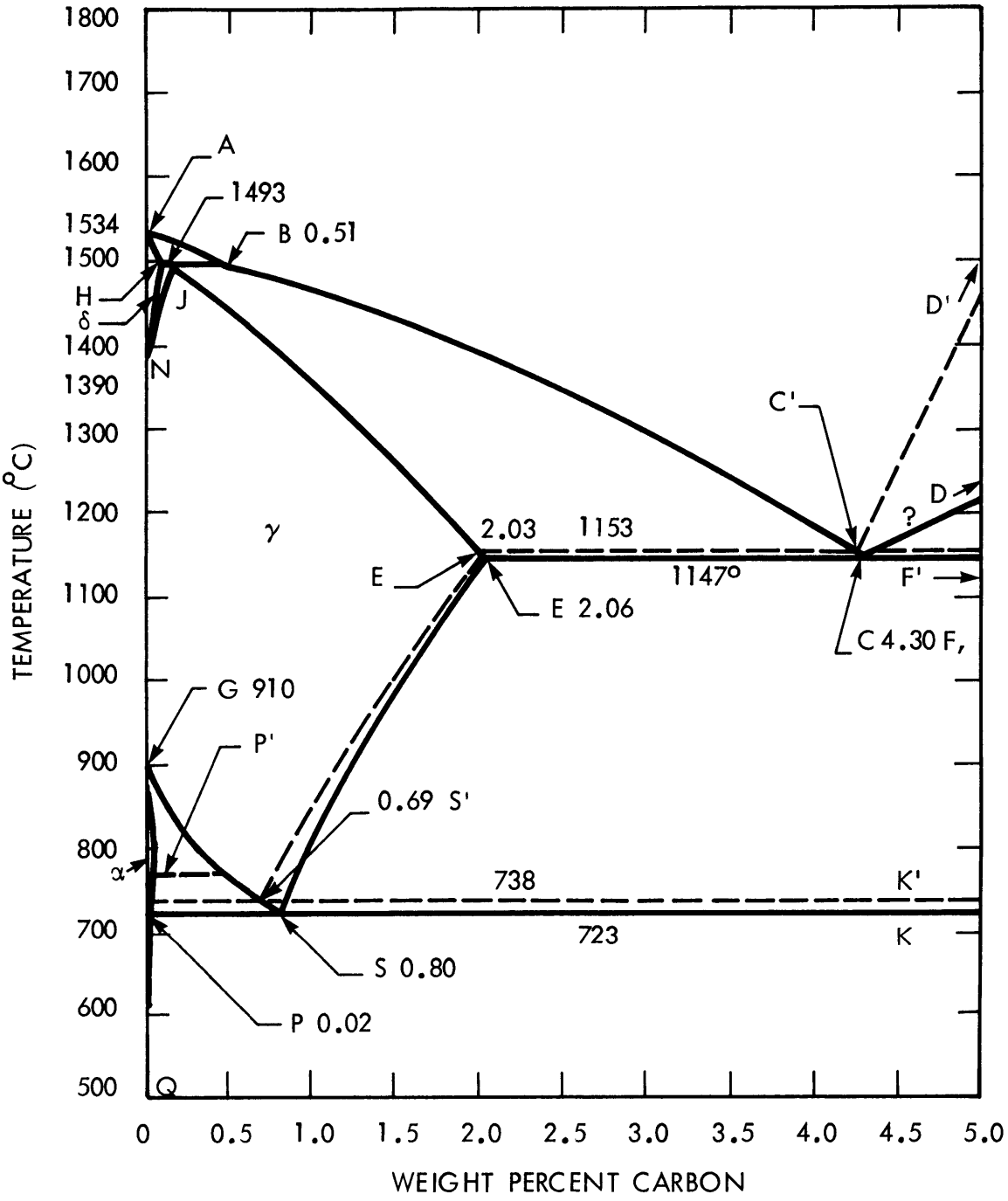

FIGURE 23

CARBON-IRON PHASE DIAGRAM (WEIGHT PERCENT)

2.2.3.2 Structural Change and Cementite Formation

Podgurski et al. (1950) determined that Hagg carbide could be produced from a variety of different gases. Using hydrocarbons such as butane, propane, and pentane, complete carbiding was reported in just a few hours in the temperature range 548-598 K. Methane was also used; however, the rate of carbiding was very slow. Carbon monoxide was tried, but free carbon was found to form and for that reason the carbiding temperature was lowered to 473-498 K. The Fe_2C and Fe_3C formed from carbon monoxide were found to be more stable than those from other carbiding gases. Podgurski suggested that iron oxide may help stabilize carbides; some iron oxide was produced when carbon monoxide disassociated.

Cementite (Fe_3C) was formed from Hagg carbide by reaction M,

$$Fe + Fe_2C \rightarrow Fe_3C \qquad (M)$$

The normal temperature used was 773 K and reaction took three to four hours.

The Fe-C system is a complex one. Metallurgists have for a long time recognized the time-temperature history of an iron-carbon alloy has a profound effect on its structure. In order to be able to adjust physical properties of these alloys an understanding of the time-temperature effects was necessary.

The time-temperature history of a metal catalyst, such as the Bosch catalyst, is also important. Hot spots developing in the bed and/or the cooling rate for the reactor can have

an enormous effect on the final structure and phases observed after completion of an experiment.

A convenient way to represent the effect of temperature excursions on final structure is the so-called Time-Temperature-Transformation diagram (T-T-T diagram). Figure 24 is a typical isothermal T-T-T diagram for eutectoid steel. Depending on the path chosen to bring the steel to room temperature, different structures and phases will be observed.

For example, path 1 shown in Figure 24 shows eutectoid steel quench-cooled to 600°C from above the eutectoid temperature. The steel is held at 600°C for approximately 20 seconds; this converts all the austenite to pearlite, pearlite being a specific cementite-α-Fe structure. When quench-cooled to ambient temperature no structural change will occur since all the austenitic steel has already been converted to pearlite.

On the other hand, if one follows path 2, only 50% of the austenite is converted to bainite before quench-cooling. Thus, the remaining austenite will convert to martensite on quench-cooling to ambient temperature. Bainite and martensite are specific structures common in steel processing (Reed-Hill, 1973). An additional complication arises from the fact that for a gradual cooling rate, the envelope for austenite to pearlite transformation will shift to the right. Thus, a mixture of several different structures is possible.

This may account for some of the dispute in the literature on what is the actual catalyst for carbon deposition. The structure and phases observed on completion of the reaction

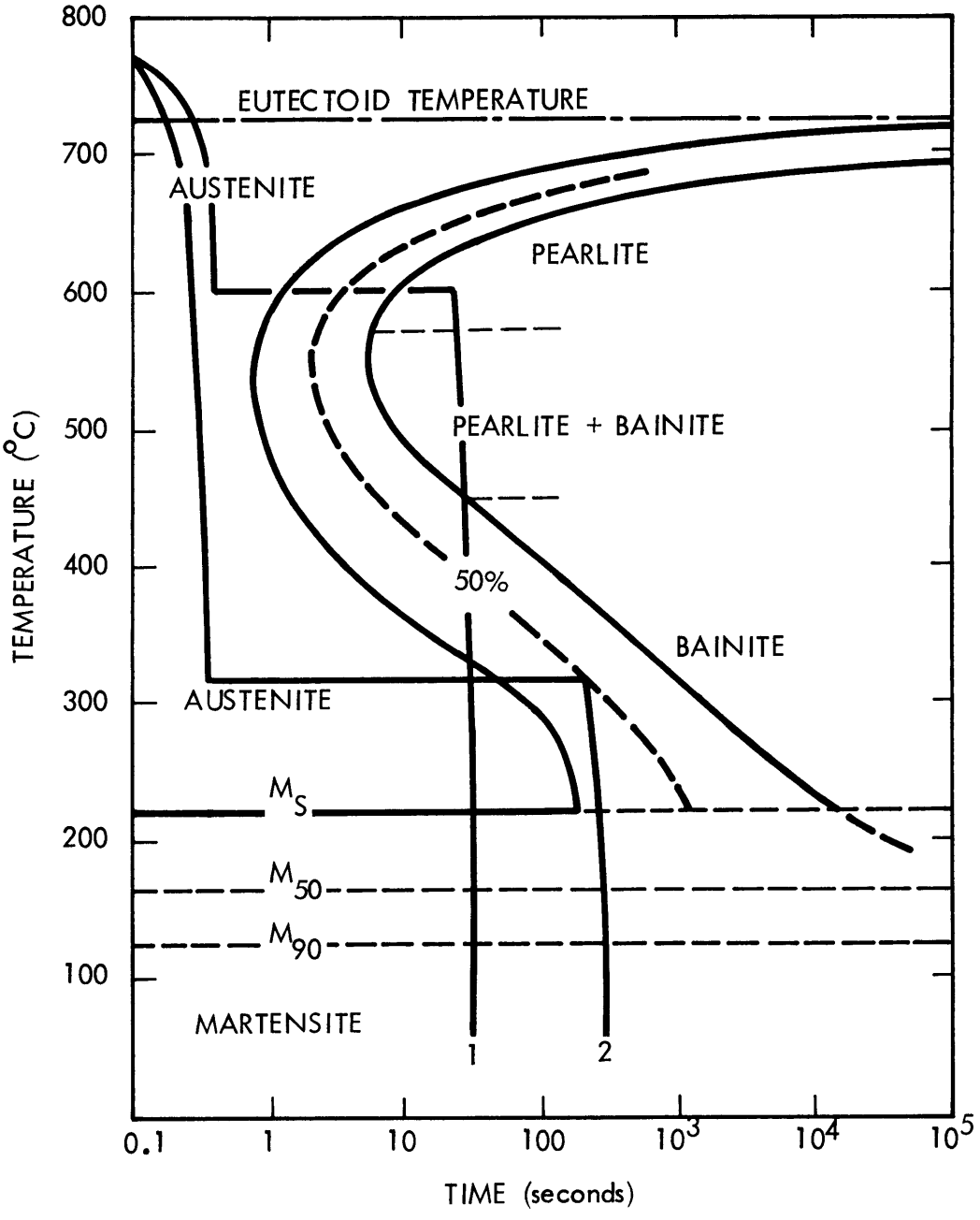

FIGURE 24

COMPLETE ISOTHERMAL TRANSFORMATION DIAGRAM FOR EUTECTOID STEEL

(REED-HILL, 1973)

may not necessarily be that available during reaction.

2.2.3.3 Carbon Fiber Formation

Fiber formation is a peculiar by-product of almost all carbon deposition experiments. Fibers form on many transition metals, notably nickel and iron. The mechanism for fiber growth has been speculated upon by many, however, no complete mechanism has been proposed thus far which can explain the often conflicting data. The fibers themselves are extremely uniform in diameter, usually between 500 - 1000 Å in thickness (MacIver et al., 1955), come in the shape of flat ribbons, solid or hollow tubes, and some are even twisted. Crystals are often found at the end of these filaments and in some cases iron fragments are found throughout their length (MacIver et al., 1955). The filaments have lengths over 1 μ and BET areas up to a range of over 100 m^2/g. Fiber C/Fe ratios were sometimes well in excess of 100 and the C/H atomic ratios in the filaments varied between 10 and 30 and,were found to increase with temperature (Walker et al., 1959).

Ruston et al. (1969) performed the most detailed metallurgical investigations on the structural changes which occur on the surface and within the bulk of an iron catalyst during carbon deposition. Utilization was made of optical and electron microscopy, metallographic etching, and x-ray and electron diffraction. Observations were made to determine what occurred on the surface, in the bulk and what solid phases

formed during the reaction. All experiments were carried out with crystalline, metallographically polished iron with pure carbon monoxide at a pressure between 0.01 to 1.01 x 10^5 N/m^2 and at 823 K.

Two types of carbon were generally found on the surface of their samples after exposure to carbon monoxide. The first was a lamellar form of carbon located close to the metal surface. Ruston speculated that this probably came from decomposition of Fe_3C (cementite) crystals on the surface. The second was a filamentous form which they proposed originated from small crystals of iron carbide epitaxially grown on the surface of metal grains.

The following mechanism was proposed for the formation of the lamellar form of carbon. Carbon monoxide first adsorbs on the reduced iron surface . Depending upon the temperature and carbon monoxide concentration, some carbon monoxide decomposed to carbon and oxygen atoms; the oxygen atoms reacted with adsorbed carbon monoxide to form product carbon dioxide; the carbon atom, being relatively mobile, diffused into the α-iron along intergranular paths. Supersaturated carbon solutions precipitated cementite (Fe_3C) at intergranular sites creating stress in the metal. The stress was released by creep within the surface region; in the absence of compressive stress on the surface, the Fe_3C decomposes to iron and lamellar carbon.

Metallographic examination of the catalyst cross section indicated the phenomenon of carbon deposition was always

accompanied by the formation of cementite within the bulk of the metal. Again, the cementite appears to form almost exclusively at intergranular sites.

To explain the observed fiber growth, Ruston proposed the following reaction sequence. The crystallite formed from cementite decomposition and reacted with carbon monoxide to form Fe_7C_3. The shape and distribution of these small crystals depend on the orientation of the original iron crystals. The small crystals of Fe_7C_3 were lifted off the metal substrate by carbon formed by catalytic decomposition of carbon monoxide on their surface. This carbon diffused around the back forcing the crystallite of the surface. The small crystals continued to function as a growth center and were carried upward by the growing filaments. They also noted that this process did not continue indefinitely as the Fe_7C_3 crystallite disintegrated, leaving behind iron-rich fragments as the carbon filament grew. The crystallite was no longer active when the carbor-iron filament dropped to less than about 3 wt% Fe (C/Fe atom ratio = 150).

Ruston's findings are valuable for their insight into the overall process occurring on the surface of polycrystalline iron. However, several objections have been raised to his conclusion that the small crystallites grown on single crystal iron surfaces are Fe_7C_3. Ruston formed this conclusion primarily on the basis of x-ray diffraction data yet both Renshaw et al. (1970) and Ratcliff (1968) contend that his reported x-ray diffraction data are open to other interpretations.

Also, Ruston does not elucidate the mechanism to explain how the original crystallite is lifted off the surface, this issue being perhaps the most important and least understood part of fiber formation.

Robertson (1970) studied carbon formation from methane over iron, nickel, and cobalt surfaces at 923 K and 1023 K. Using transmission electron microscopy, he established two distinct types of carbon were formed. One he designated "flake" carbon, and the other "polycrystalline".

From electron and x-ray diffraction properties, Robertson discovered that the "flake" carbon was highly crystalline and graphitic in nature. This layered form of carbon was very similar to the "lamellar" form reported by Ruston. Surface perfection and reactivity studies also revealed the equivalence of "flake" carbon to natural or synthetic graphite. Only trace amounts of metal substrate were found in this form of carbon. This high degree of crystalline graphite perfection in "flake" carbon is very unusual below formation temperatures in excess of 2000 K.

The second form of carbon was deemed "polycrystalline". This fibrous form of carbon was similar to that reported by Ruston. These fibers grew from the main body of the deposit and ranged in length between 2400 to 14,000 Å and, in width, between 600 to 1350 Å. In a similar manner to Ruston et al. (1969), Robertson (1970) reported: "Dispersed throughout this type of carbon are discreet electron-dense "kernels"; these are surrounded by much more electron transparent bands which

display diffraction contrast effects along their lengths."

Boehm (1973) studied the nature of carbon fibers deposited from hydrogen-carbon monoxide mixtures over nickel deposited from nickel carbonyl, iron deposited from iron carbonyl, Raney nickel, and powdered iron. Runs were made in the temperature range 753-973 K; no pressure was indicated. By comparing the resultant carbon, several conclusions were drawn: first, nickel and iron form different types of carbon fibers. The fibers formed on nickel were hollow, thin-skinned tubes, while those formed on iron were finer, denser fibers apparently containing bands and kernels of iron. Boehm concluded that the formation of carbon fibers on nickel and iron followed different mechanisms. The tubular carbon fibers on nickel were explained by assuming that nickel in the form of globular particles and chains of fused particles (analogous to carbon blacks) had formed during pyrolysis of the carbonyl. Subsequent deposition of carbon on the nickel surface and leaching of the nickel during hydrochloric acid washing of the carbon served to leave only the outside carbon shell.

The carbon fibers formed from either iron carbonyl or reduced iron oxide appeared in a variety of shapes. Helically twisted filaments, tubes, and straight strands were all found. Indeed, some of the straight strands were noted to show low contrast indicating ribbon-like structures rather than a rod-like structure of circular or rectangular cross-section. Boehm also reported that extensive fibrous growth was only noted for carbon monoxide-hydrogen mixtures. In a

pure carbon monoxide stream, only "empty skins" and "densely agglomerated material" were reported.

Boehm proposed a mechanism to explain the ribbon-like carbon fibers as well as the twisted carbon fibers he noted in his study. He suggested that carbon filaments grow only from certain crystal faces of a carbided catalyst, the growth rate being controlled by the diffusion of carbon atoms to these specific crystal faces. Disorganized or poorly crystalline carbon in contact with other crystal faces of the carbide phase would be transported by diffusion to the thermodynamically more favorable, well-organized carbon phase. An illustration of this mechanism is shown in Figure 25.

There are several inherent problems in this proposed mechanism of Boehm's. One is that disorganized carbon is assumed always available for diffusion into the carbide crystallite. The formation and transport mechanism for this disorganized carbon to reach the crystallite is not discussed. Also, the direction of the specialized nucleation points must always be oriented in such a way as to give vertical fiber growth, as is almost always found. The reason why the helix structure is developed is unclear. Fourthly, and most importantly, no mechanism is proposed to explain the crystal heads noted in almost all fibers. These points cast some doubt on the proposed mechanism.

Baker et al. (1972) advanced a hypothesis which attempted to explain both the "hollow core" reported by many authors and the "kernel" of metal or carbide at the fiber tip. The

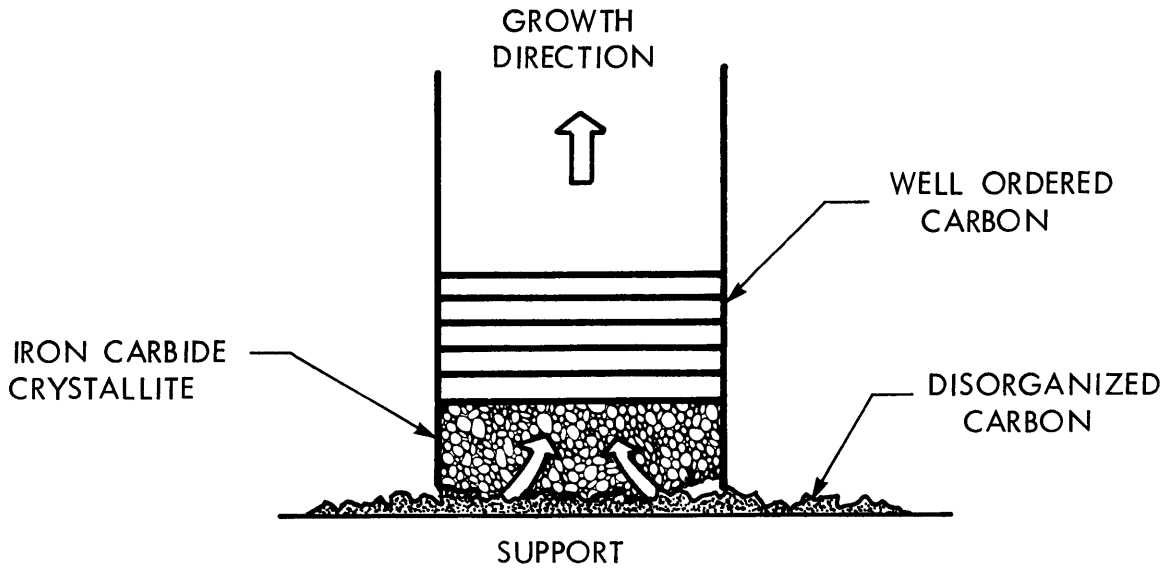

GROWTH OF RIBBON-LIKE FIBERS

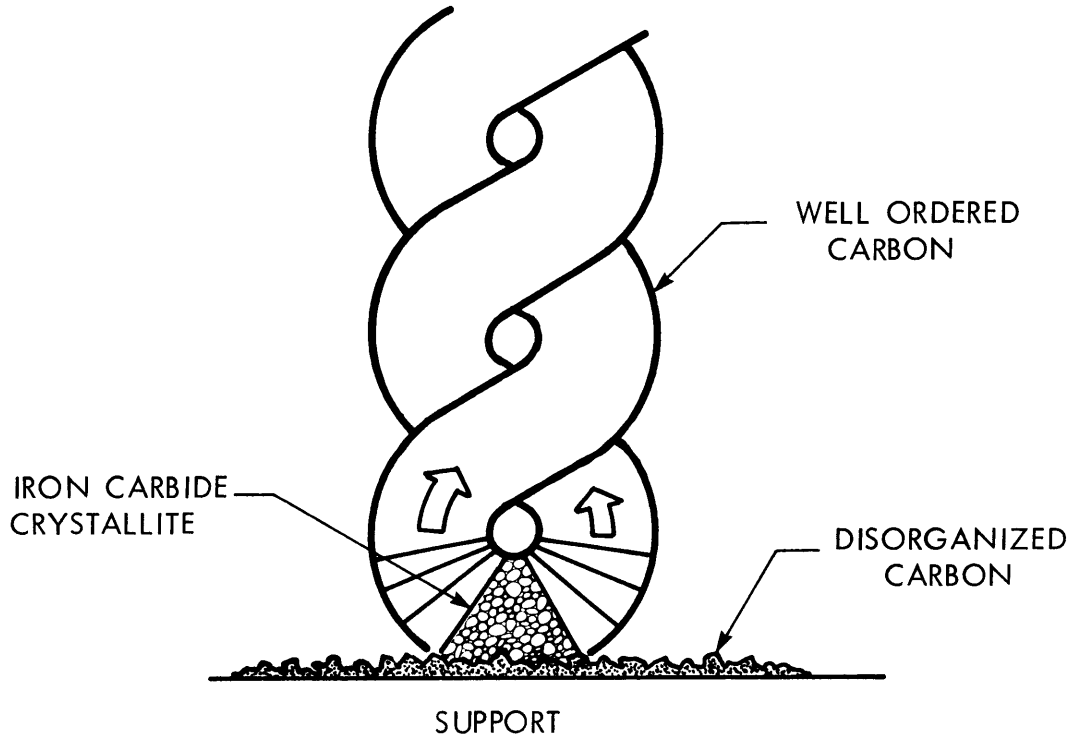

GROWTH OF TWISTED FIBERS

FIGURE 25

FIBER GROWTH MECHANISMS (BOEHM, 1973)

proposed model is shown in Figure 26. In step (a), a crystallite has been liberated from the support (for iron this could be by the mechanism proposed by Ruston et al., 1969). Gas phase components such as methane, acetylene, or carbon monoxide are then free to react and deposit carbon on the crystallite as shown in (b). Carbon from the decomposed gases can be taken into solution in the metal, diffuse through the crystallite to be deposited predominantly in the protected regions to produce the situation shown in step (c). The precipitation of carbon at the rear of the particle builds up a deposit of carbon which forces the particle away from the support as shown in (d). If diffusion through the particle is slow enough to limit the rate of the above process, then eventually the surface of the entire crystallite will be covered with carbon and catalytic activity will cease as shown in (e). The shape of the catalytic crystallite and differing diffusion paths lead to the hollow core shown in (d) and (e). Baker alleged that the diffusion of carbon through the crystallite was caused by a thermal gradient. They proposed an exothermic reaction occurring at the exposed surface caused temperature gradients across the particle. In support of their hypothesis, they pointed out that the activation energy for the observed reaction was the same as the reported activation energy for the diffusion of carbon in nickel. Manning (1976) correctly pointed out, however, that the solubility of carbon increases with temperature to 996 K then decreases. Thus, a thermal gradient as the driving force for carbon solution and

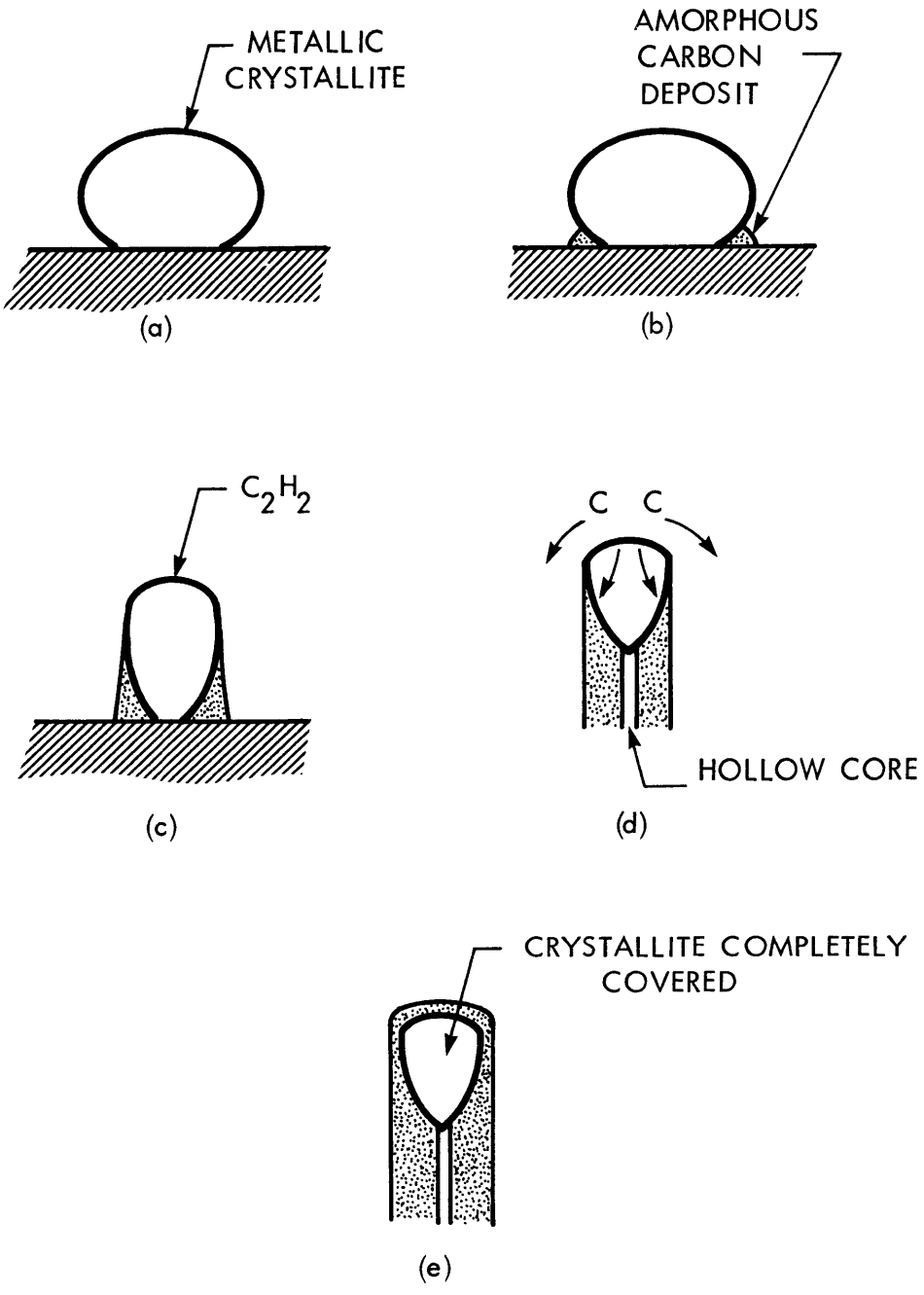

FIGURE 26

FIBER GROWTH MECHANISM (BAKER et al.,1972)

then dissolution appears inconsistent with this fact.

Baker et al. (1972), using controlled atmosphere electron microscopy, also studied the deposition characteristics of various gas mixtures containing carbon dioxide, carbon monoxide, and methane. Single crystal graphite substrates were used onto which iron films could be evaporated. The gas mixtures used were pure carbon dioxide; pure methane; and a 97.5% carbon dioxide, 1.5% carbon monoxide, 1.0% methane mixture. Reaction temperatures varied between 725 K and 1265 K, while pressures were in the order of 8 kN/m^2. Reaction times were thirty to sixty minutes.

Baker observed two types of carbon formation which he deemed "Type I" and "Type II". "Type I" carbon formation was a flocculent amphorous deposit which only formed in the presence of iron particles, if methane was a component in the gas mixture and only when under an electron beam. In addition, this flocculent amphorous deposit was only found above a temperature of 900 K.

"Type II" carbon was identified as crystalline platelets of graphite (these are very similar to Robertson's "flake" carbon (1970) and Ruston's "lamellar" carbon (1969). This type of formation was only observed at temperatures above 1200 K and only occurred around iron particles greater than 60 nm in diameter. During this investigation they noticed a high degree of iron crystal mobility. Iron particles 10 nm in diameter diffused along the graphite substrate and coalesced to form spheres 80 nm or more in diameter. Smaller

iron particles were observed to remain mobile and aggregated until they were large enough for platelet growth to begin. Type II carbon was found to occur even if only pure argon (i.e., inert atmosphere) was fed as the gas phase. However, Type II formation only occurred in an iron-graphite system; never if either of these (iron or graphite) were used alone. This lends support to the hypothesis of Baker et al. and Ruston et al. that suggested that lamellar (platelet) carbon is found by Fe_3C disintegration.

Assuming first that some carbon (i.e., graphite) dissolves in these iron particles at the reaction temperature (i.e., 1225 K), Baker postulates the following as the mechanism for Type II formation. At 1225 K the stable Fe-C phase is austenite and in order to maintain the concentration of dissolved carbon at the saturation level for 1225 K, cementite is precipitated. At temperatures above 975 K, the rate of decomposition of cementite to form iron and graphite increases rapidly with increasing temperature. Under the present slow cooling conditions, it is probable that decarburization of austenite will occur, the carbon precipitating as cementite, which in turn will undergo decomposition to form iron and graphite, the latter crystallizing on the edges of the metal particles. If iron particles lose mobility when carbide forms, then carbon transpiration could then take place within the particle causing graphite to crystallize and grow from the gas-cooled upper surfaces. Since carbon dissolves in iron faster from graphite than from other carbonaceous

materials, a high concentration of carbon in iron would be expected to build up readily in the present system. Baker did not observe any fibrous carbon formation in this continuous electron microscopy study. From the work of Ruston et al. (1969), one can say that the probable reason for this was that the partial pressures of the carbonizing gases were very low and also the residence times very short. Ruston et al. (1969) concluded that fiber formation was a function of both residence time and carbon monoxide partial pressure.

Thomas, Thrower, and Walker (1973) studied the growth of filamentary carbon on metallic surfaces during the pyrolysis of methane and acetone. This was done with the use of transmission electron microscopy. They found that neither nickel nor iron produced fibers when heated in ultra-pure methane at temperatures below 1173 K. Above 1173 K both nickel and iron catalyzed fiber growth, nickel being the most active. At this temperature, Thomas also reported platelet formation was observed. This plate formation was of the same type as that found by Baker (1972), Robertson (1970), and Ruston (1969). Thomas next ran commercial grade methane over identical catalyst at 1173 K and found that filament growth did occur. In fact, using commercial grade methane, Thomas was able to get significant fiber formation at temperatures as low as 773 K. This would then seem to indicate that trace impurities present in methane play a major role in the production of filaments at low temperatures.

Acetone, a frequent impurity in methane, was then fed

over the iron catalyst. Iron promoted deposit formation at 673 K, but they found no observable effect on nickel. The deposit found was lamellar in nature. Pyrolysis of acetone at 773 K, however, gave rise to filament formation, each filament associated with a dense particle at its dip. The appearance of these filaments was similar to those found by Robertson (1970). If one checks back into Robertson's work (1970) on methane pyrolysis, one finds that Robertson (1968) in a later work comments on the possibility that carbon deposits could arise from breakdown of trace impurities in the methane employed in his investigations. The fact that impurities may have caused the carbon fiber formation not the methane levels, lends credence to the mechanism proposed by Baker et al. (1972). That is, only carbon-bearing gases which deposit carbon exothermically produce carbon fibers. However, the inconsistency suggested by Manning (1976) is still left unanswered.

3. Apparatus Design Rationale

In order to achieve the previously stated thesis objective, the following design criterion had to be met by the experimental apparatus:

1. Gases, both pure and of specified composition, were to be metered and preheated before entering the reactor. Provisions were necessary for on-line inlet and exit gas analysis. Steady flow conditions, as well as the capability for rapid changes from one composition to the next, were necessary.

2. The reactor had to be capable of operating isothermally. A provision was also necessary to monitor changes in mass of the catalyst as oxidation or carbon deposition proceeds. The capability to monitor continuously catalyst bed temperature was also desirable.

3. Provision must be made to facilitate the determination of experimental run conditions. This is, to solve numerically the appropriate equilibrium relationships and establish the necessary flow condition to achieve a given gas composition over the desired solid phase. This procedure must allow variations in the P_{H_2}/P_{H_2O} ratio at fixed C/H or O/H values.

4. Data acquisition had to be fast and accurate. A continuous record of all pertinent temperatures, as well as a record of the analysis for exit and inlet gas samples were

necessary. Finally, to facilitate data interpretation, it would be necessary to formulate a computer program. This program should have the ability to indicate the equilibrium solid phases present.

The above design criteria were met by the experimental apparatus and procedures described below. As such, they provided an efficient and reliable research tool to explore the multi-faceted Bosch reaction sequence.

3.1 Experimental Apparatus

The experimental apparatus can be broadly divided into three subsections: the feed-gas delivery system in which the inlet gases are individually metered, mixed, and delivered dried or saturated with water; a reactor section consisting of a quartz preheater, quartz reactor tube, and catalyst assembly mechanism; and a data acquisition sub-system.

3.1.1 Feed-Gas Delivery System

Figure 27 is a schematic of the feed-gas delivery sub-section. The gases used during the investigation and a typical analysis of each is given in Table 1.

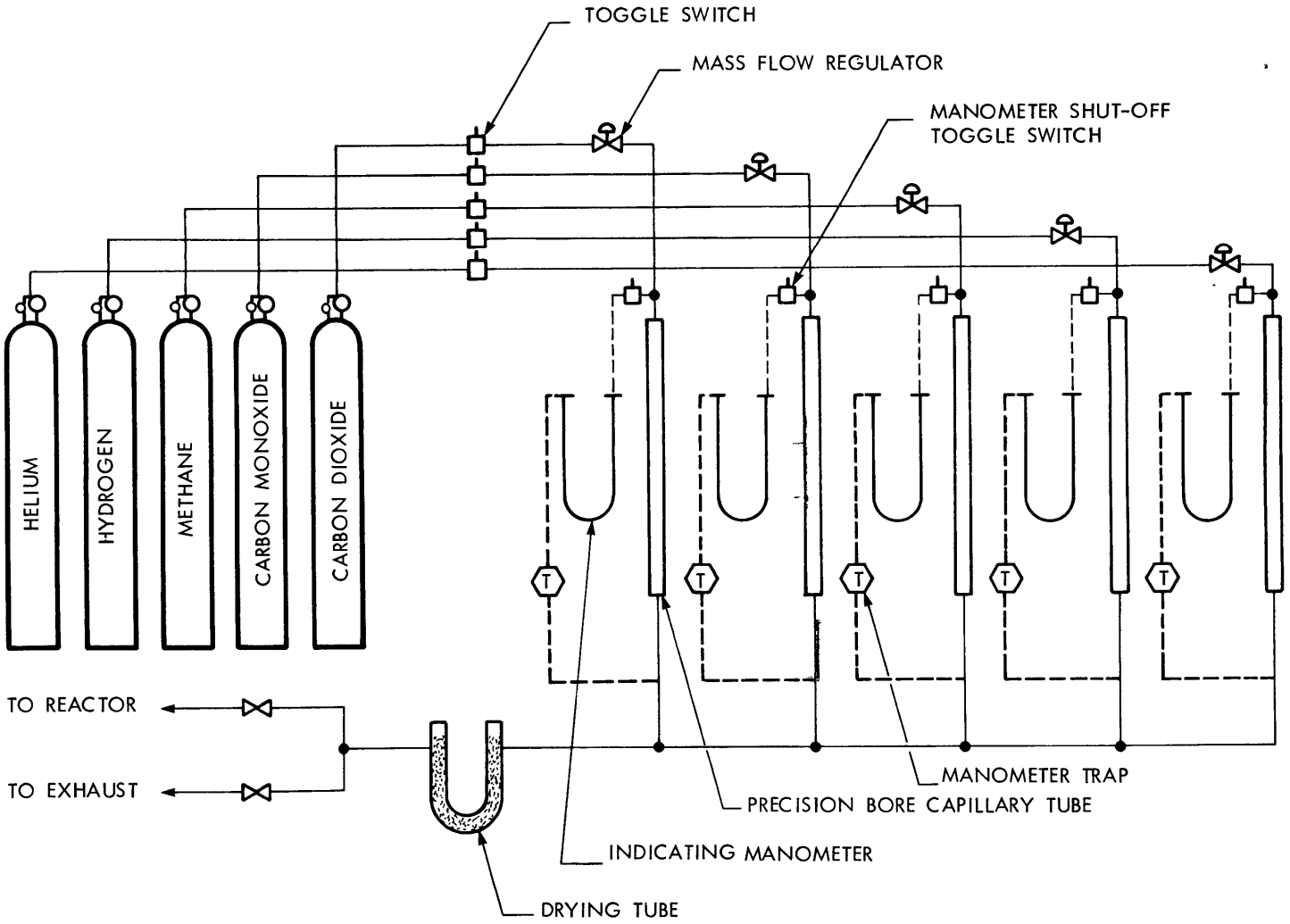

FIGURE 27 FEED GAS DELIVERY SYSTEM

Table 1 Feed-Gas Analysis

	CO_2	O_2	N_2	Dew Point
Hydrogen Prepurified Grade		<20 ppm		213.6 K
Methane (Cp Grade)	0.2 mole %	0.005 mole %	0.6 mole %	
Carbon Dioxide (Bone Dry Grade)	99.95 mole %	0.05 mole %		238.6 K
Carbon Monoxide (Cp Grade)	50 ppm	600 ppm	1500 ppm	
Helium (High Purity Grade)	1 ppm	1 ppm	14 ppm	

The gases were individually fed to Brooks Model 8944 mass flow regulators equipped with digital valve stems for reproducibility and inlet line filters capable of entraining particulates > 2 μm. Inlet pressures of 3.45×10^5 N/m^2 (50 psig) maintained choke velocities across the individually sized flow regulators. Precision bore capillary tubes (I.D. ±0.007 mm of specified value and 91.5 cm in length) in combination with manometers containing Meriam high vacuum manometer fluid (specific gravity equals 1.04) were used to obtain calibration curves of flowrate in cm^3/s versus pressure drop in cm of Meriam fluid for each reactant gas. These calibration curves, corrected to standard temperature and pressure, were used to establish the desired gas phase composition. The gases were mixed and dried in a 15.24 cm Kimax U-tube filled with

indicating dessicant (Grade 42, Silica gel 6-16 mesh, Fisher Scientific Company). The mixed gases were then either fed to the reactor or by-passed to the atmosphere.

When the gases were sent to the reactor, they could be fed either dry or saturated with water. Figure 28 illustrates the components and flowpaths for the saturator system. The feed gases flowed through a preheater constructed from a 3 m length of 0.64 cm I.D. refrigeration tubing. Heat was supplied by a Briskeat-silicone-rubber-imbedded flexible heating tape, the power output being controlled by a Superior Electric Company Powerstat. Asbestos insulating tape was used to reduce heat losses. The gases from the preheater (attaining temperatures as high as 333 K) entered three 1000 ml Pyrex three-necked flasks. These flasks were connected in series and submerged in a 55.32 liter Precision Scientific Company constant temperature bath. A Chemical Rubber Company contact heater maintained the bath temperature to ±0.1 K. The bath circulation was provided by a motor-impeller assembly. During normal operations, each bubbler contained 900 cm^3 of water. The gas stream was fed to each bubbler through Pyrex-fritted gas-dispersion tubes; the gas stream passing from bubbler to bubbler through 0.95 cm Vycor tubing which was also kept submerged. After the third bubbler, the gases passed into a 20.5 cm deep vertical bed packed with 0.38 cm O.D. glass-beads, and 5 cm of quartz wool. This assembly was used to eliminate any entrained water droplets in the saturated gas stream. The feed gas stream then entered the reactor through

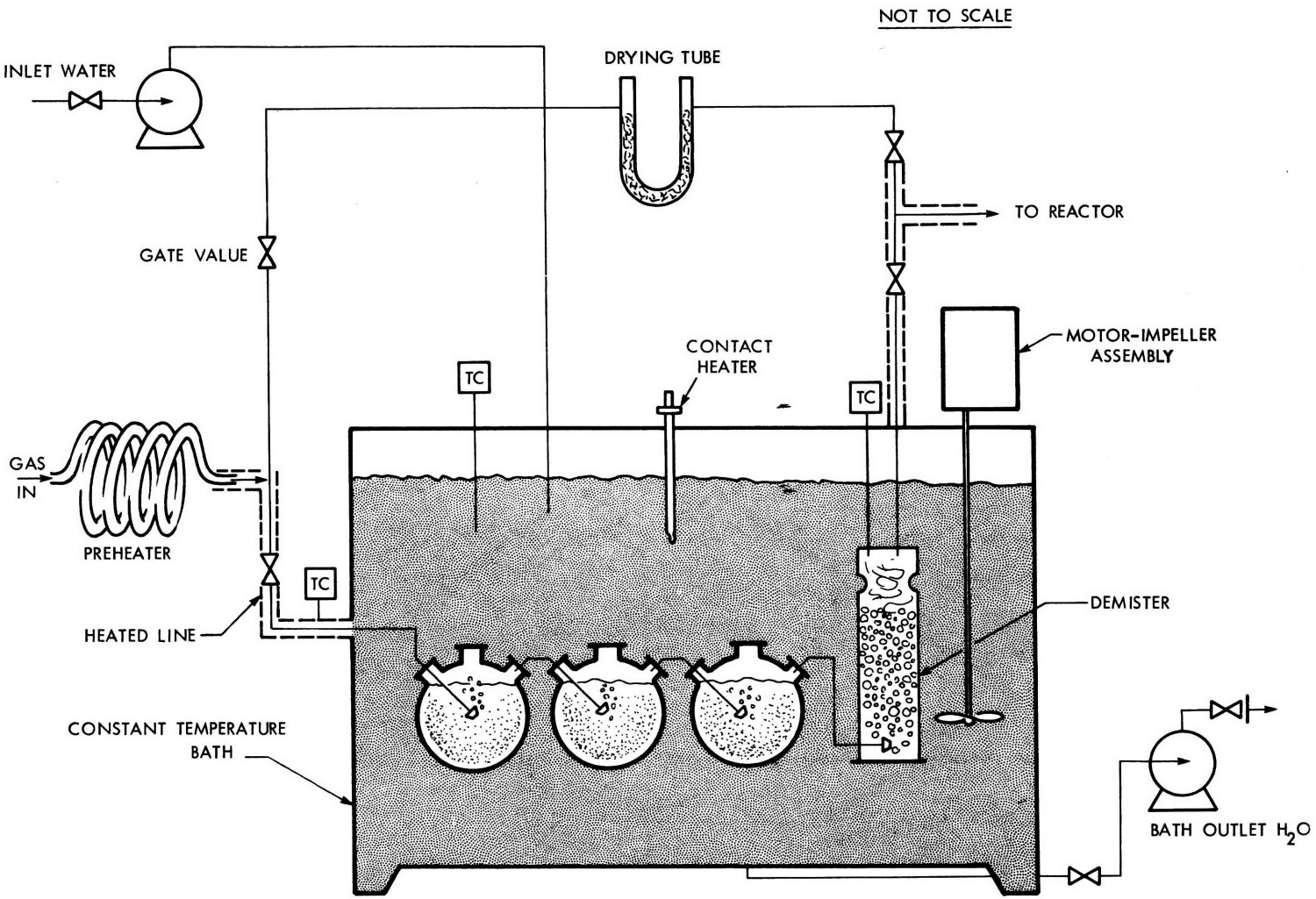

FIGURE 28 SATURATOR SUB-SECTION

heated feed lines. A combination of March Company centrifugal pumps (maximum capacity 6.0 liters/min) and a 1.27 cm NUPRU regulating valve allowed readjustment of the bath and bubbler temperatures in 3 to 5 minutes. The highest water partial pressure attained was 3.13×10^4 N/m^2 (30%). As indicated in Figure 28, 3 chromel alumel thermocouples were used to monitor the gas temperature just prior to entering the first bubbler, the exit gas temperature and the bath water temperature.

If the gases were to be fed dry, after passing through the copper preheater, they were sent through another dessicant-drying tube and on to the reactor.

3.1.2 Reactor Section

The reactor consisted of three basic parts: the pre-heater and lower reactor support tube; the top section of the reactor support tube; and the catalyst assembly. Figure 29 illustrates the top and lower reactor sections including the preheater.

3.1.2.1 Preheater and Lower Reactor Support Tube

The preheater was constructed from a 6 m quartz tube with a 7 mm I.D. formed into a helical coil. The preheater coil extends from approximately halfway up the top reactor section down over the entire length of the lower reactor support tube and connects at the base. Mounted concentrically around the reactor support tube, it has an inside diameter of 60 mm. The lower reactor support section was constructed from a

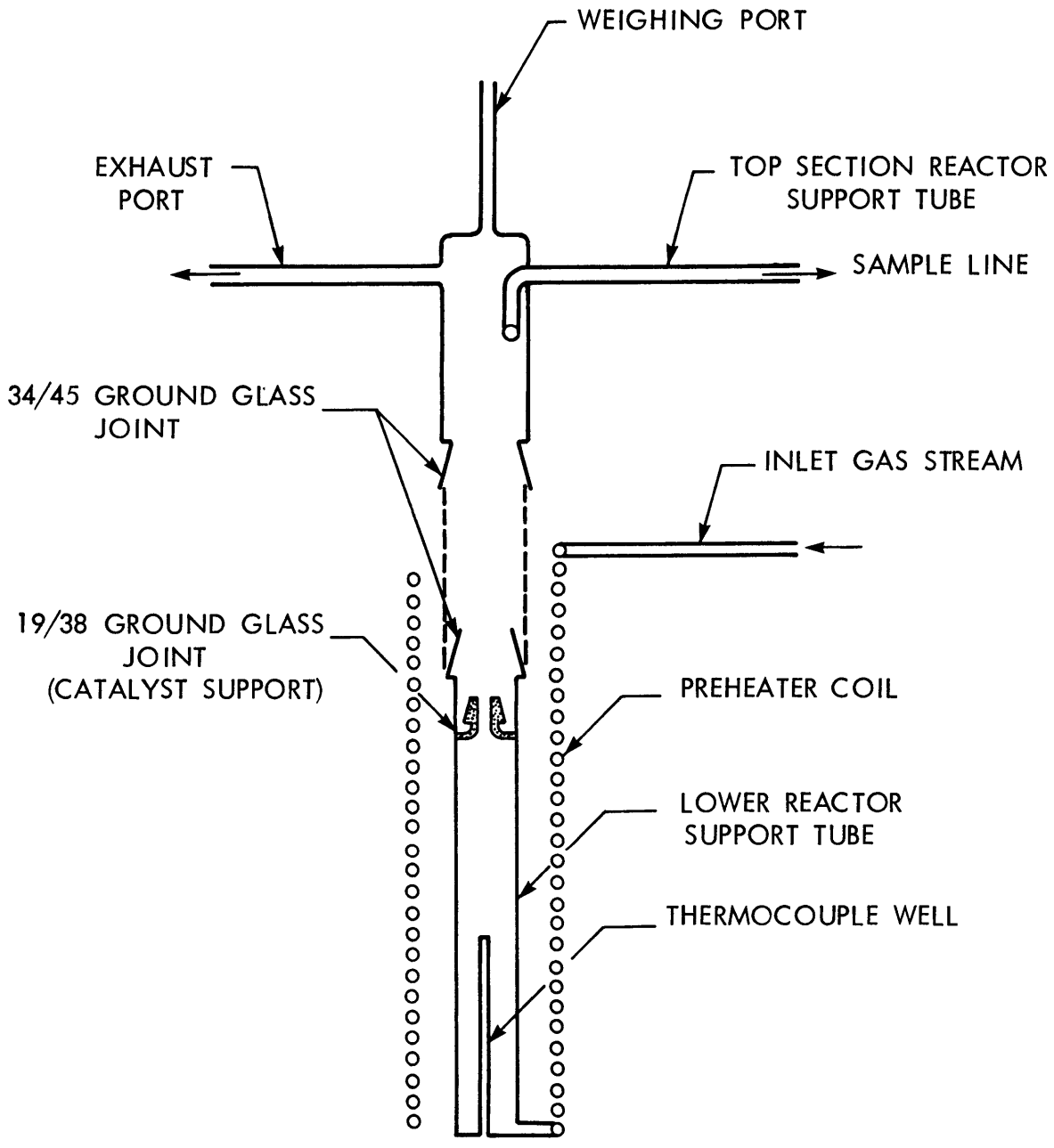

FIGURE 29

TOP AND LOWER REACTOR SECTION INCLUDING PRE-HEATER

28 mm I.D. quartz tube 28 cm in height. A 34/45 tapered male ground glass joint is attached to one end, the other is connected to the preheater. A 110 mm quartz thermocouple well is provided at its base to support a two-hole Alundum thermocouple sheath used to position two 0.051 cm type K chromel-alumel thermocouples. One thermocouple activates a Thermolyne proportional controller used to maintain reactor temperature, the other provides a continuous indication of the reactor temperature. Located 20 mm from the base and on the inside wall of the reactor support tube is a 19/38 male ground glass joint used to support the catalyst assembly. Figure 30 illustrates the temperature profile obtained over the catalyst mechanism at typical run condition (i.e., reactor set temperature 823 K, pressure = 1.01 X 10^5 N/m^2, flowrate He = 20 cm^3/s {STP}).

3.1.2.2 Top Section Reactor Support Tube

The top section consisted of a 28 mm I.D. quartz tube 15.24 cm in height. The lower end was fitted with a female 34/45 ground glass joint, the upper end had an 8 mm I.D. quartz tube concentrically mounted. This concentric 8 mm tube was used as a weighing port.

Mounted at 90° angles to the support tube center-line were two additional 8 mm I.D. quartz tubes. One of these extensions was used as an exhaust line, the other had a 2.6 cm elbow extending into the effluent stream and was used as a sample line.

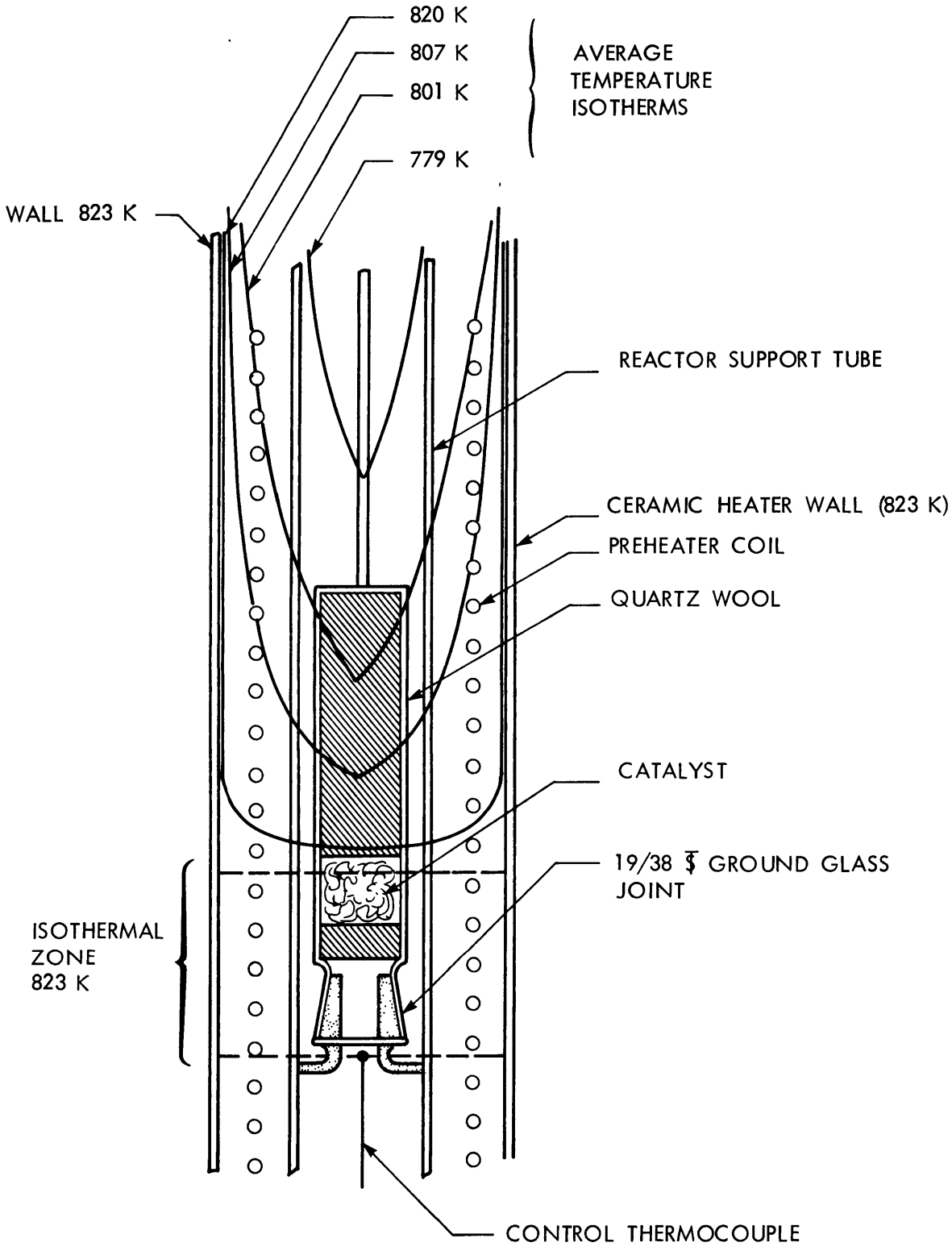

FIGURE 30

REACTOR TEMPERATURE PROFILE

3.1.2.3 Catalyst Assembly

Figure 31 is a representation of the catalyst assembly which consisted of a 120 mm, 20 mm I.D. quartz tube with one end fitted with a 19/38 female tapered ground glass joint. Attached to the catalyst carrier was a concentrically positioned quartz tube 23.62 cm in height with an inside diameter of 2 mm. A 1.5 mm I.D. Alundum sheath provided support for a chromel-alumel thermocouple which was positioned in the catalyst bed. A standard Omega Engineering Company thermocouple connector attached to the quartz tube suspension bar allowed continuous recording of the catalyst bed temperature. A matched thermocouple connector suspended from a Sartorius electrobalance allowed weight measurements to be made periodically during an experiment.

The entire three-piece reactor assembly was housed in a heating furnace (Figure 32). Two Thermcraft Model RH 254 semicylindrical ceramic heating elements 75 mm in diameter and 30.5 cm in length encompass the preheater-reactor heated cavity. These heating elements were wired in parallel to a 220 volt electrical line and were capable of delivering a maximum power output of 2300 watts. The temperature in the cavity was maintained by a Thermolyne Dubuque III solid state proportional controller activated by a chromel-alumel thermocouple. The Dubuque III controller maintained the set value to ±10 K and, in combination with the heating elements, had a range of 1450 K. The heating elements are enclosed by 10.92

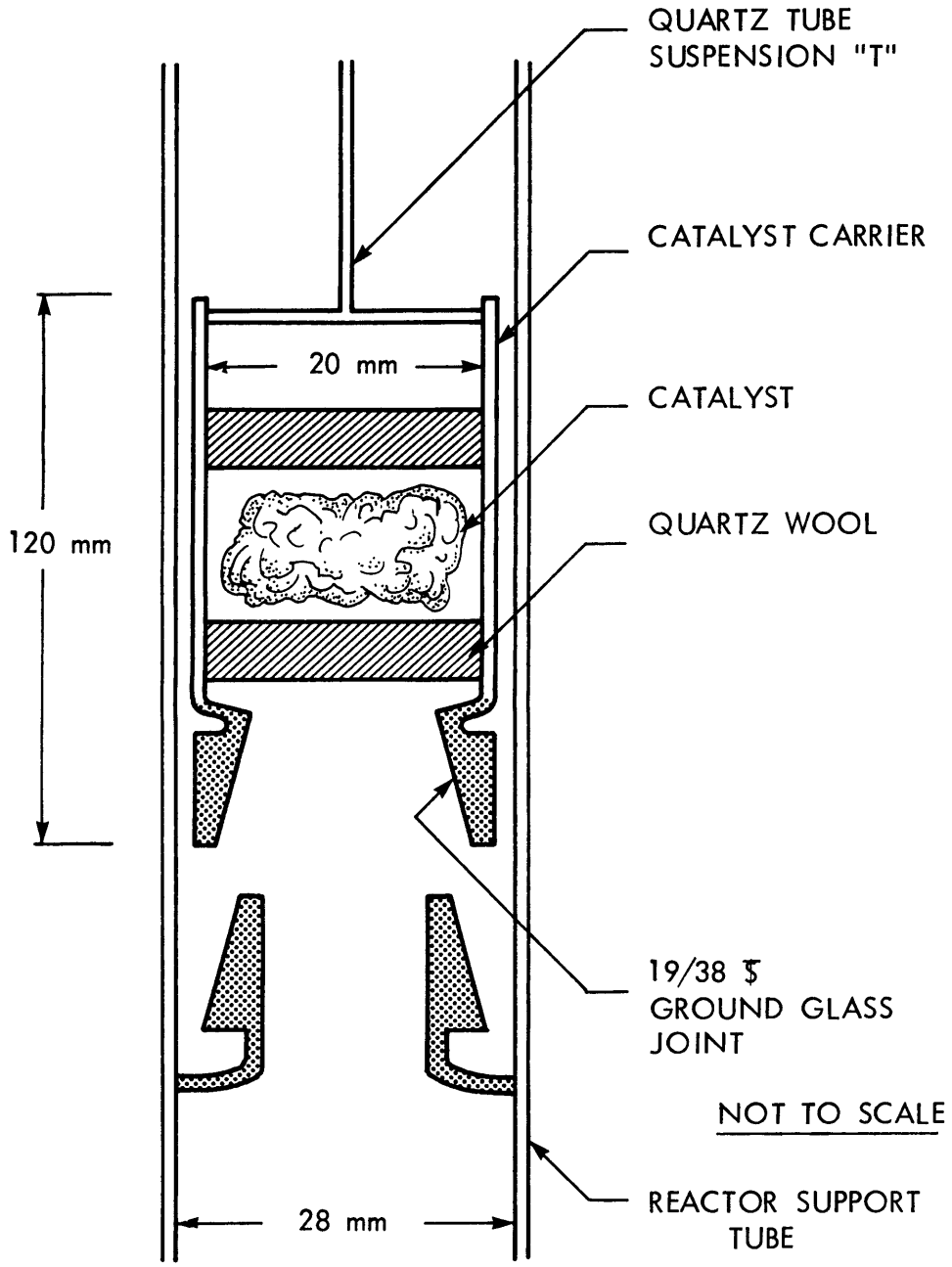

FIGURE 31

CATALYST CARRIER IN SUPPORT TUBE

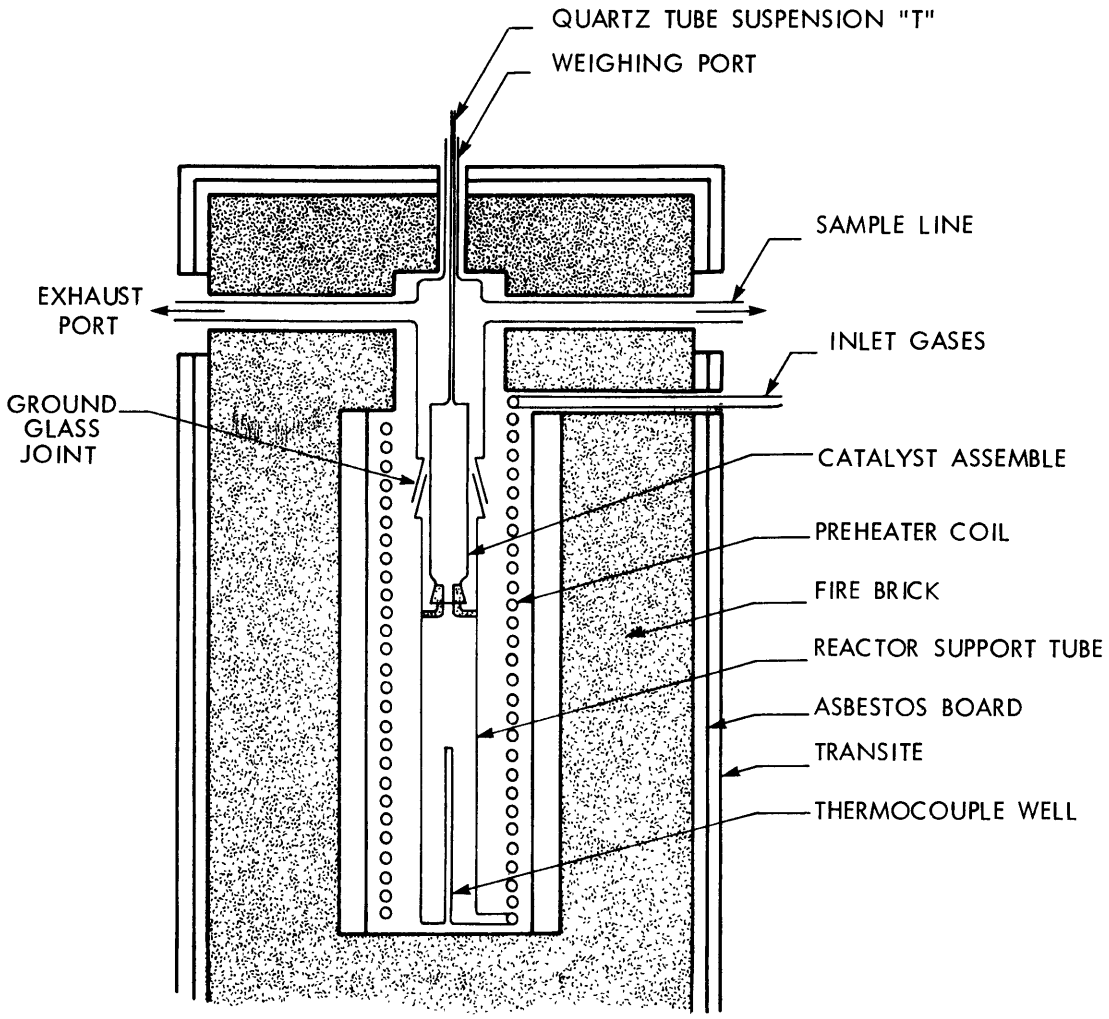

FIGURE 32 REACTOR ASSEMBLY IN FURNACE

cm of Babcock and Wilcox type K-30 insulating firebrick which in turn was enclosed by 6.5 mm of asbestos board. The entire furnace was structurally supported by an outer layer of 6.5 mm Transite, an asbestos-concrete composite.

3.1.3 Data Acquisition Section

Inlet and exit gas samples were analyzed using an on-line series 700 Hewlett-Packard gas chromatograph with a thermal conductivity detector.

Table 2 is a summary of critical operating parameters.

Table 2 Critical Gas Chromatograph Parameters

Filaments	GOW-MAC Rhenium Tungsten Code 13.002 (wx)
Sample Size	0.25 cm^3
Carrier Gas Flowrate	30 cm^3
Column Operating Temperature	348 K
Detector Operating Temperature	473 K
Detector Filament Current	200 m A

Porapak Q and Porapak QS were used interchangably as packing in the analytical columns. These columns were hand-packed in 3.15 mm X 3 m Teflon tubes which were subsequently made into coils in order to fit into the chromatograph oven. A special carrier gas mixture supplied by the Matheson Gas Company of Massachusetts (19.5% He, 8.5% H_2) allowed direct measurement of hydrogen by the method recommended by Purcell and Ettre (1965). Following the method described by Dal Nogare

and Juvet (1962), an external standard was used to determine response factors of the thermal conductivity detector. These in turn were used to calculate component compositions (except hydrogen).

An Autolab 6300 digital integrator in conjunction with a Honeywell chromatograph recorder was used to give a quantitative as well as visual record of all samples analyzed. The Autolab 6300 was found to have a precision of 0.8% and an accuracy of 1.0% of the indicated values.

An on-line sample valve system was used to obtain reproducible samples for injecting into the gas chromatograph. A Hewlett-Packard Model 19020 sample valve-sample loop assembly was housed in an insulated aluminum box. Cartridge heaters imbedded in an aluminum block provided a constant temperature heat sink. The temperature of the sample valve system was maintained to ±0.1 K by a model 220 Hewlett-Packard temperature controller activated by an iron-constantan thermocouple. A series of inter-connected toggle switches allowed the selection of samples of inlet, outlet, and standard gases. Another toggle switch allowed the entire sample valve system to be evacuated. During normal operation a vacuum would be drawn on the sample valve system. With the desired toggle switch open, gas entered the sample valve system until the pressure in the sample loop equaled the barometric pressure. The sample loop pressure was measured using a U-tube mercury manometer, one leg of which was open to the atmosphere. The sample size used in the course of the investigation was 0.25

cm^3 although the capability was available for larger or smaller sized samples, if desired.

Temperatures were continuously monitored by a Honeywell 27 channel multipoint recorder with an accuracy of ±3 K. An Omega Engineering Company series 200 digital pyrometer allowed instantaneous analysis of the catalyst bed temperature, reactor center line temperature, and the water saturator temperatures. Accuracy was specified to be ±0.25% of the indicated reading.

The raw data were reduced using a modified data reduction computer program originally developed by Manning (1975). A copy of this analytical program is given in Appendix 7.4.

3.2 Experimental Procedure

The experimental procedure varied depending on the specific test objectives; but, as a general rule, the following procedures were used.

3.2.1 Determination of Run Conditions

The experimental procedure in this thesis centered on determining the catalytic effects of iron oxides and iron carbides on carbon deposition. The method chosen for use during the investigation was to vary the P_{H_2}/P_{H_2O} ratio at a fixed O/H or C/H value and through the use of triangular phase diagrams (Appendix 7.2),determine the iron-iron oxide, iron-iron carbide phase boundaries; the initial assumption being that carbon deposition is not catalyzed by either iron oxides or iron carbides.

To achieve this end, it was necessary to develop a computer program which, for a 5 component gas mixture at fixed temperature, pressure, C/H or O/H, and desired P_{H_2}/P_{H_2O} ratio, gave an overall gas composition lying in the desired solid phase envelope.

A convenient mathematical "trick" was used to achieve a rigorous solution. This was to assume all solid phases which could be present were catalysts for all gas phase reactions.

From the Gibbs phase rule: the number of components, N = 5 (CH_4, H_2, CO, CO_2, H_2O), temperature and pressure were fixed along with either the C/H or O/H ratio, and the desired P_{H_2}/P_{H_2O} ratio chosen. The number of degrees of freedom then equals, f = 5 + 2 - 1 - 4 - R = 2 - R.

The number of independent reactions must be two to fix the gas phase composition. Reactions B and K were chosen.

Therefore, by specifying the temperature, pressure, C/H or O/H ratio,and the P_{H_2}/P_{H_2O} ratio, the equilibrium gas phase composition could be numerically solved for and specified along with the associated flow settings. Figure 33 and 34 are examples of typical output from the program used to set up experimental conditions. The phase diagram shown in Figure 34 is generated simultaneously with the numerical solution to give a visual check on the position of the projected reactant gas composition.

RUN NUMBER A- 51
TEMPERATURE 800.K , PRESSURE 1.ATM.

CONDITION 1, PH2O/PH2 0.42, C/H 0.24, O/H 0.17
GAS COMPOSITIONS

PCO2	PCO	PCH4	PH2O	PH2	PTOTAL
0.117493	0.065903	0.416459	0.118352	0.281790	0.999999

PERCENTAGE H 70.75 PERCENTAGE O 12.02 PERCENTAGE C 17.21

FLOW SETTING

6.462116	4.718698	35.399093	49.425949	9.299097

CONDITION 2, PH2O/PH2 0.39, C/H 0.25, O/H 0.17
GAS COMPOSITIONS

PCO2	PCO	PCH4	PH2O	PH2	PTOTAL
0.122386	0.073508	0.436562	0.103546	0.263994	0.999998

PERCENTAGE H 70.18 PERCENTAGE O 11.93 PERCENTAGE C 17.88

FLOW SETTING

6.731242	5.263215	37.107841	46.774284	8.711818

CONDITION 3, PH2O/PH2 0.33, C/H 0.27, O/H 0.17
GAS COMPOSITIONS

PCO2	PCO	PCH4	PH2O	PH2	PTOTAL
0.129538	0.091551	0.475464	0.075860	0.227580	0.999995

PERCENTAGE H 69.07 PERCENTAGE O 11.74 PERCENTAGE C 19.17

FLOW SETTING

7.124616	6.555103	40.414459	40.793052	7.510158

CONDITION 4, PH2O/PH2 0.25, C/H 0.30, O/H 0.17
GAS COMPOSITIONS

PCO2	PCO	PCH4	PH2O	PH2	PTOTAL

Figure 33 Example of Experimental Set Conditions

0.131625 0.120905 0.519347 0.046562 0.181550 0.999992

PERCENTAGE H 67.81 PERCENTAGE O 11.52 PERCENTAGE C 20.65

FLOW SETTING

7.239427 8.656816 44.144554 31.917293 5.991176

CONDITION 5, PH2O/PH2 0.20, C/H 0.32, O/H 0.17

GAS COMPOSITIONS

PCO2	PCO	PCH4	PH2O	PH2	PTOTAL
0.126634	0.149165	0.546503	0.029612	0.148063	0.999979

PERCENTAGE H 66.95 PERCENTAGE O 11.38 PERCENTAGE C 21.66

FLOW SETTING

6.964885 10.680233 46.452781 24.195034 4.886093

CONDITION 6, PH2O/PH2 0.15, C/H 0.34, O/H 0.17

GAS COMPOSITIONS

PCO2	PCO	PCH4	PH2O	PH2	PTOTAL
0.115832	0.181921	0.566275	0.017728	0.118191	0.999949

PERCENTAGE H 66.19 PERCENTAGE O 11.25 PERCENTAGE C 22.54

FLOW SETTING

6.370766 13.025583 48.133377 15.978784 3.900330

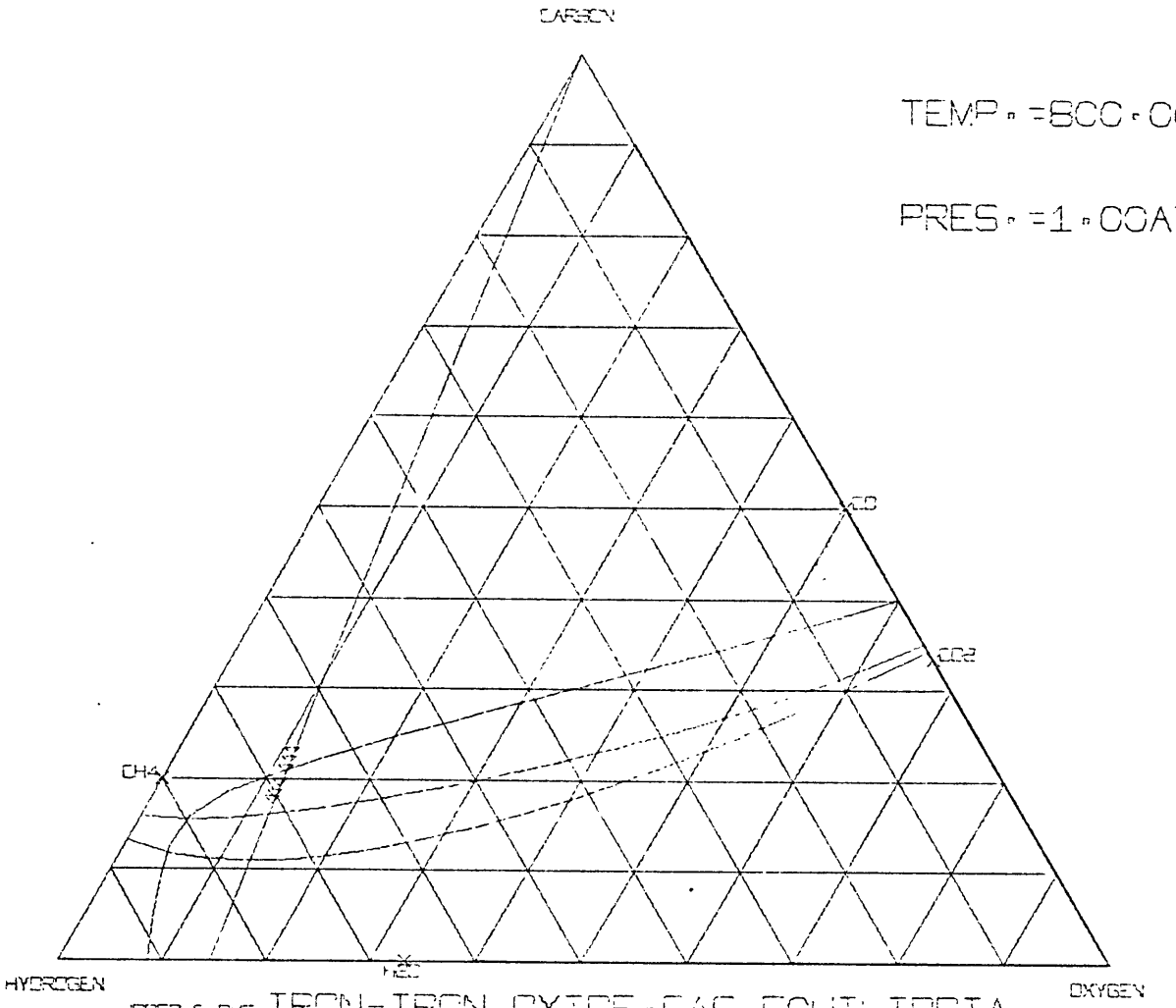

Figure 34 Visual Check on Experimental Set Conditions

3.2.2 Equipment Start-Up

Initially, each piece of electronic equipment was turned on for at least thirty minutes prior to run time. This allowed sufficient time for steady-state behavior to be established in all electrical components. During this thirty minute warm-up period, the catalyst assembly was prepared for the experiment.

The quartz catalyst assembly was first weighed on the Sartorious pan balance to an accuracy of ±1 mg. An appropriate length of quartz wool was then inserted into the catalyst assembly; the assembly was again weighed and the weight recorded. The next step was to weigh out the amount of catalyst desired and insert this into the catalyst carrier. Normally 450 mg of number 2 steel wool were loaded and positioned in the assembly so as to be completely encompassed by the isothermal region (Figure 30). In Table 3 both the composition of the steel wool catalyst and the surface area are shown.

Table 3 Catalyst Composition

ELEMENT	WT %
Fe	≃ 98.882
Mn	0.700
C	0.360
P	0.040
S	0.018
N	0.400 ppm

BET Area by Krypton Adsorption: 389 cm^2/g

At this point, a check was performed to ascertain if the combined weight of the quartz catalyst assembly, quartz wool, and steel wool catalyst was equivalent to that calculated from the individual components. A tolerance of ±2 mg was allowed; if a difference of more than 2 mg was observed, the catalyst loading procedure would be repeated. A final piece of quartz wool was inserted below the catalyst to hold the steel wool in place as well as to distribute evenly the gases as they enter the catalyst bed.

The catalyst assembly was then placed in the lower reactor support tube; the top section of the support tube placed over it and the upper portion of the furnace, in turn, over that. The furnace was next centered under the Sartorious electrobalance and all associated lines connected. When in the furnace, the catalyst assembly was weighed by attaching a monofilament Nylon line to the quartz tube suspension bar. The pre-furnace weight measurements were used as a criterion to determine if the catalyst assembly was freely suspended. Adjustments were made by positioning of the overhead Sartorious balance.

The next step in the start-up procedure was the heating of feed and sample lines, the sample valve system, the saturator subsystem, and the reactor furnace.

The feed and sample lines were heated using powerstats which controlled Briskeat heating tapes. Line temperatures were maintained at approximately 423 K.

The sample valve subsystem was heated by two 65-W

cartridge heaters. A 220 Hewlett-Packard proportional controller maintained the sampling system at 423 K.

The saturation preheater powerstat was next set to the desired levels. This was closely followed by setting the bath contact control heater to the appropriate temperature. The saturator bath temperature often took several hours to reach steady state; and, thus, the bath contact heater was often energized several hours prior to the anticipated run time. If water was not to be a component in the reaction mixture, the saturator system would be by-passed and neither the preheater nor bath heater were turned on.

Prior to activating the furnace heaters, a helium feed rate of 20 cc/s (STP) was fed through the appropriate feed lines to the reactor. The Dubuque III reactor controller was then set to 673 K and activated.

While the system components were being heated, a vacuum was drawn on the sample valve system. A vacuum of at least 400 N/m^2 was used as a criterion of whether the sample valve was vacuum tight. If a vacuum of 400 N/m^2 could not be drawn on the sample valve system, corrective action was taken.

After all initial set temperatures were obtained, an external standard was flushed three times through the sample valve system; and, four 0.25 cm^3 samples were sequentially fed to the chromatograph analytical columns.*

---

* All critical gas chromatograph conditions (Table 2) were set 24 hours prior to start-up in order to establish steady state.

Their peak shapes were noted and integrated areas recorded. These established the response factors for the thermal conductivity cell necessary for the data reduction program (Appendix 7.4.1).

If the water saturator was operational, the helium feed gas would be by-passed through the bubbler; this eliminated the water vapor initially accumulated in the closed saturator loop. The helium was then shut off and 10 cm^3/s (STP) of CO_2 would be passed through the bubbler. Two calibration samples were then taken; hydrogen at 20 cm^3/s (STP) was turned on; the saturator was by-passed (i.e., hydrogen was fed dry); and, the furnace temperature set to the experimental run conditions. These calibration samples were necessary to establish the thermal conductivity cell response factor for water, which was not present in the external standard. Carbon dioxide was used as the carrier gas because its response gave the best precision (<0.8% error) of all gases measured.

Steel wool which has been oxidized by carbon dioxide or water and then reduced in hydrogen, had been shown by Manning (1975) to have a high initial activity. This was desirable since this increased activity allowed a larger variety of conditions to be tested in a given time period (10 to 18 hours on stream).

The reactor was allowed to come up to temperature in hydrogen; the hydrogen was then by-passed out of the reactor and the catalyst assembly was attached to the Sartorious electrobalance. The weight of the assembly was taken, recorded, and used as an initial starting weight in the data reduction program.

Two samples of pure hydrogen were also taken to measure impurities as well as to establish the hydrogen calibration curve following the method of Purcell and Ettre (1965).

3.2.3 Run Procedures

The desired gas compositions were obtained by adjusting the Brooks mass flow regulators in combination with the appropriate manometers. The desired settings were obtained from the predetermined calibration curves. Approximately one minute was necessary to obtain steady-state behavior.

Throughout the duration of the run, inlet and exit gas samples were taken every six minutes. The following procedure was normally followed: first, a vacuum of 400 N/m^2 was continuously drawn on the sample valve system; second, prior to the injecting of any sample, the sample loop was flushed three times with the desired gas mixture; third, the appropriate sample was drawn into the sample valve loop, the temperature and pressure recorded and the sample injected into the analytical columns. Two inlet gas samples, a weight reading, then a sequence of effluent samples was the normal sequence followed.

Weight measurements were taken periodically (usually every 12 minutes) by exhausting the reaction gas to the atmosphere and attaching the catalyst assembly to the electrobalance. During weight measurements, the furnace would be automatically shut off while the gases were by-passed to the atmosphere. This was done as a safety precaution. The reactor

center-line temperature would drop as much as 5 K during these weight measurements. Upon completion of the weighing procedure, the furnace would automatically come back on and, the center-line set temperature was quickly obtained.

A continuous record of all pertinent temperatures was kept with a 27 channel Honeywell recorder. An instantaneous reading of catalyst bed temperature, reactor center-line temperature, and saturator temperatures were obtained with an Omega 200 series digital pyrometer.

3.2.4 Shut-Down Procedures

At the conclusion of a given run, all reactant gases were shut off and 20 cm^3/s (STP) of helium was fed to the reactor. All powerstats were turned down and the Dubuque III furnace controller shut off. Helium flow was continued until the center-line temperature was at ambient temperature.

The feed and sample lines were next disconnected from the furnace and the furnace was, in turn, taken out from under the Sartorious balance. The catalyst assembly was removed from the furnace and visually examined; any pertinent observations were recorded. The catalyst and deposited carbon were then put in specimen bottles, sealed, and labelled.

4. Results

4.1 Preliminary Experiments

In the first experiments binary gas mixtures were normally used. In all cases, the catalyst charge was 250-500 mg of steel wool and the reactor temperature was approximately 825 K. The total reactor pressure was 1 atmosphere.

4.1.1 Hydrogen-Carbon Monoxide Mixtures

The initial experiments were made to determine the maximum amount of carbon that could be deposited per unit weight of catalyst as well as to elucidate the carbon deposition mechanism. Figure 35 illustrates the typical behavior observed. In this experiment 450 mg of steel wool catalyst were exposed to a gas mixture of 50% hydrogen-50% carbon monoxide.

Carbon deposition was periodically measured by weighing the catalyst assembly and determining the differential weight change. Correcting for the time off stream, these measurements were used to determine change in rate as a function of time. As shown, the rate of carbon deposition is seen to increase rapidly with time reaching a maximum of 38 mg/min after approximately 204 minutes. The rate was then observed to fall. The minimum P_{H_2}/P_{H_2O} was found to coincide with the point of maximum carbon deposition rate; the minimum P_{H_2}/P_{H_2O} value being equal to 11.0. The reason for the rapid drop-off in rate is unclear. The bulk P_{CO}/P_{CO_2} and P_{H_2}/P_{H_2O}

RUN A-4.0

TEMPERATURE 823 K

PRESSURE 1.01×10^5 N/m^2

CATALYST CHARGE 450 mg

CO/ H_2 FEED RATIO = 1.0

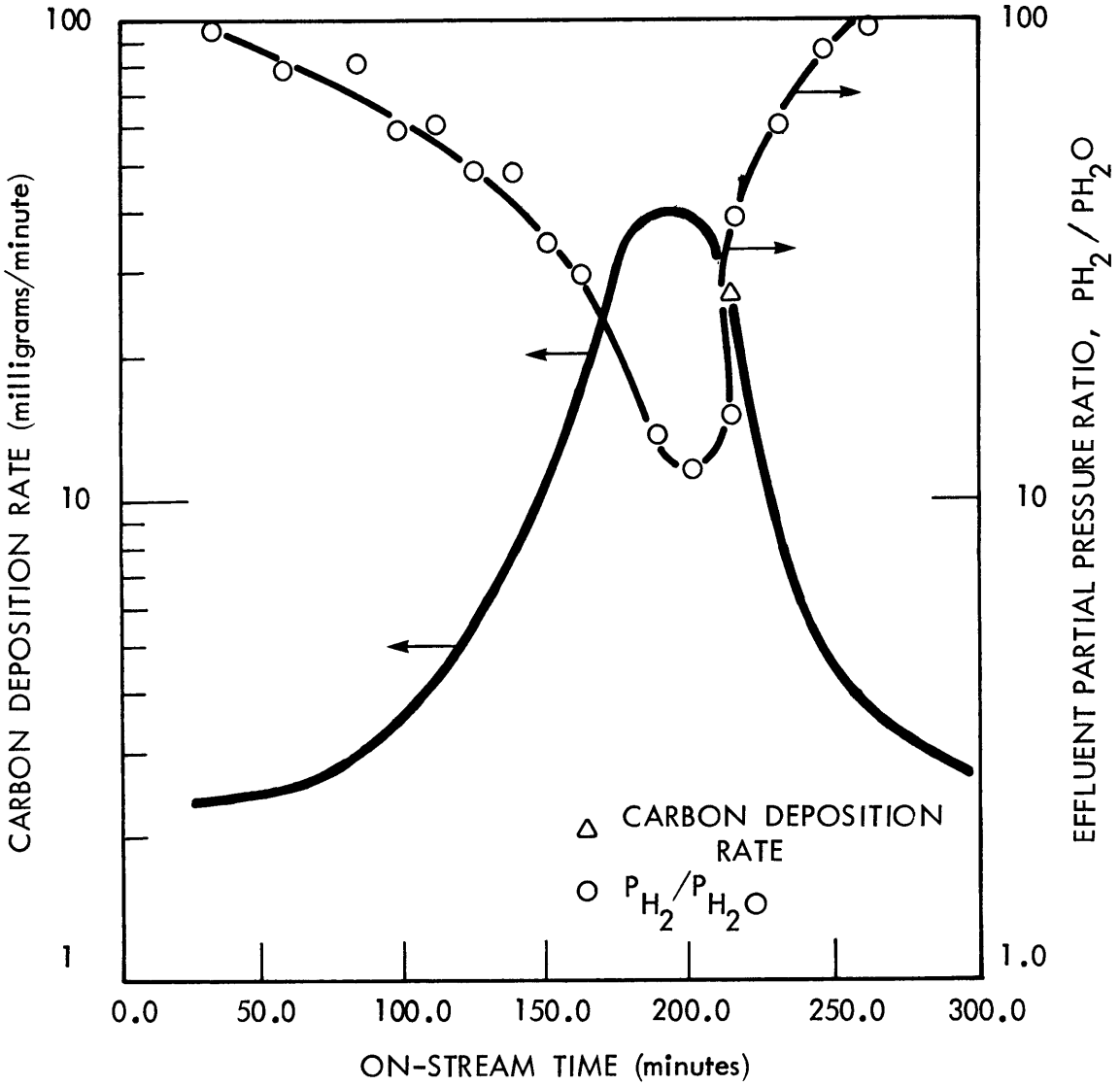

FIGURE 35

CARBON DEPOSITION RATE AND P_{H_2} / P_{H_2O} RATIO VERSUS ON-STREAM TIME

ratios were not in the range where oxide would be expected to form. The catalyst assembly was securely fastened down, eliminating any possible gas by passing the catalyst bed. Slight pressure fluctuations were noted in the reactor back pressure; this suggested plugging with concomitant channeling in the catalyst bed itself. Visual examination of the catalyst bed did indicate a dense packed carbon slug. However, no preferential area of carbon deposition, indicating channeling, was observed. It is interesting that 30% of the total carbon deposited occurred after the fluctuations were recorded in the reactor. This indicated that a substantial portion of the catalyst was seeing reactant gases during the entire experiment. Also, the minimum P_{H_2}/P_{H_2O} at which carbon deposition stopped was found to correspond to that observed by Everett (1967). Their value was reported to be ten.

During the entire experiment, the conversion of hydrogen was virtually constant at less than 1.5%. The carbon monoxide conversion was observed to increase to a maximum of 15%. When conversion of carbon monoxide was $\geq$ 9%, based on the Boudouard reaction, the amount of carbon predicted was within 70% of that found.

Interestingly, no methane was observed until the rate of carbon deposition was almost at a maximum; and then only trace amounts were observed. However, once begun the methane concentration remained virtually fixed until run completion. The final catalyst weight recorded was 3.048 grams, corresponding to a C/Fe atom ratio of 32. Walker et al. (1959) reported

C/Fe ratios as high as 100, before catalyst deactivation.

In an effort to explain this rather odd behavior, an experiment was run at identical conditions with a chromel-alumel thermocouple imbedded in the catalyst bed. The bed temperature was recorded periodically using a potentiometer. Figure 36 illustrates a temperature rise of 100°K occurred in the catalyst bed during the period of rapid carbon deposition. A plot of volume percent CO_2, H_2O, and CH_4 in the effluent indicates the time of maximum temperature rise corresponds to the time when CO_2, H_2O, and CH_4 reach their maximum concentrations (see Figure 36). Although CO_2 and H_2O concentrations were seen to fall off after the peak temperature was achieved, methane concentration appeared to stay fixed.

The following conclusions may be drawn from Figure 36. The increase in carbon deposition rate with time noted by Manning is, at least in part, due to a rapid temperature rise in the catalyst bed. Methane formation appeared to be significant only after the hot spot developed in the bed. This is in agreement with the observation made by Browning et al. (1950) who indicated reaction G interfered with his equilibrium

$$2H_2 + C = CH_4 \qquad (G)$$

measurements at temperatures above 930 K (which is approximately equal to the hot spot temperature).

At high carbon monoxide conversion (i.e., $\geq$ 9%), carbon

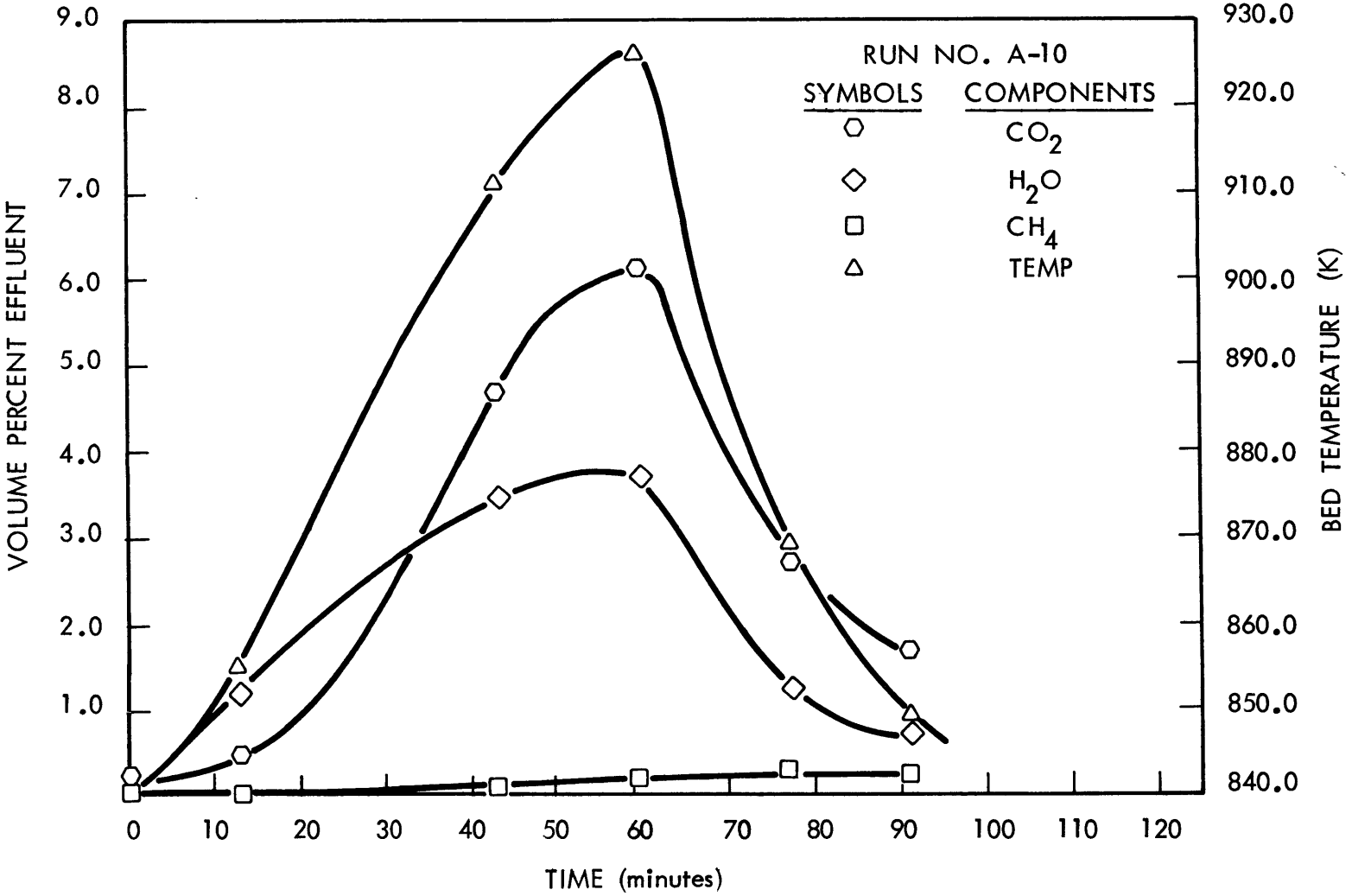

FIGURE 36 VOLUME PERCENT EFFLUENT VERSUS TIME AND BED TEMPERATURE VERSUS TIME

deposition appears to come primarily from the Boudouard reaction.

$$2CO = CO_2 + C \qquad (D)$$

It is believed that the drop in carbon deposition rate and temperature were probably due to channeling in the bed; and thus, no conclusive statements concerning the observed temperature or concentration peaks could be made.

4.1.2 Surface Oxidation Study

Next, experiments were run to verify the proposed inhibiting effect of iron oxide. Figure 37 is representative of the behavior observed when binary gas mixtures of carbon monoxide and carbon dioxide were run over a pre-carboned steel wool catalyst at 825 K and 1.01 X 10^5 N/m^2.

A 50% H_2- 50% CO mixture was first used to deposit 650 mg of carbon on 251 mg of iron catalyst. A stream of carbon dioxide was next fed to the reactor. Figure 37 shows carbon deposition immediately stopped. The small increase in weight is presumably due to oxide formation (reaction J-A). It was thought that reaction D would proceed in the reverse direction, but these data suggest that oxide formation is fast and also, that iron oxide (Fe_3O_4) apparently is not catalytic for reaction of carbon with carbon dioxide.

Following oxidation with carbon dioxide, binary gas mixtures having P_{CO}/P_{CO_2} ratios of 1.13 and 4.00 were alternately fed to the reactor. At a value of 1.13, no carbon deposition was observed. The equilibrium concentration of

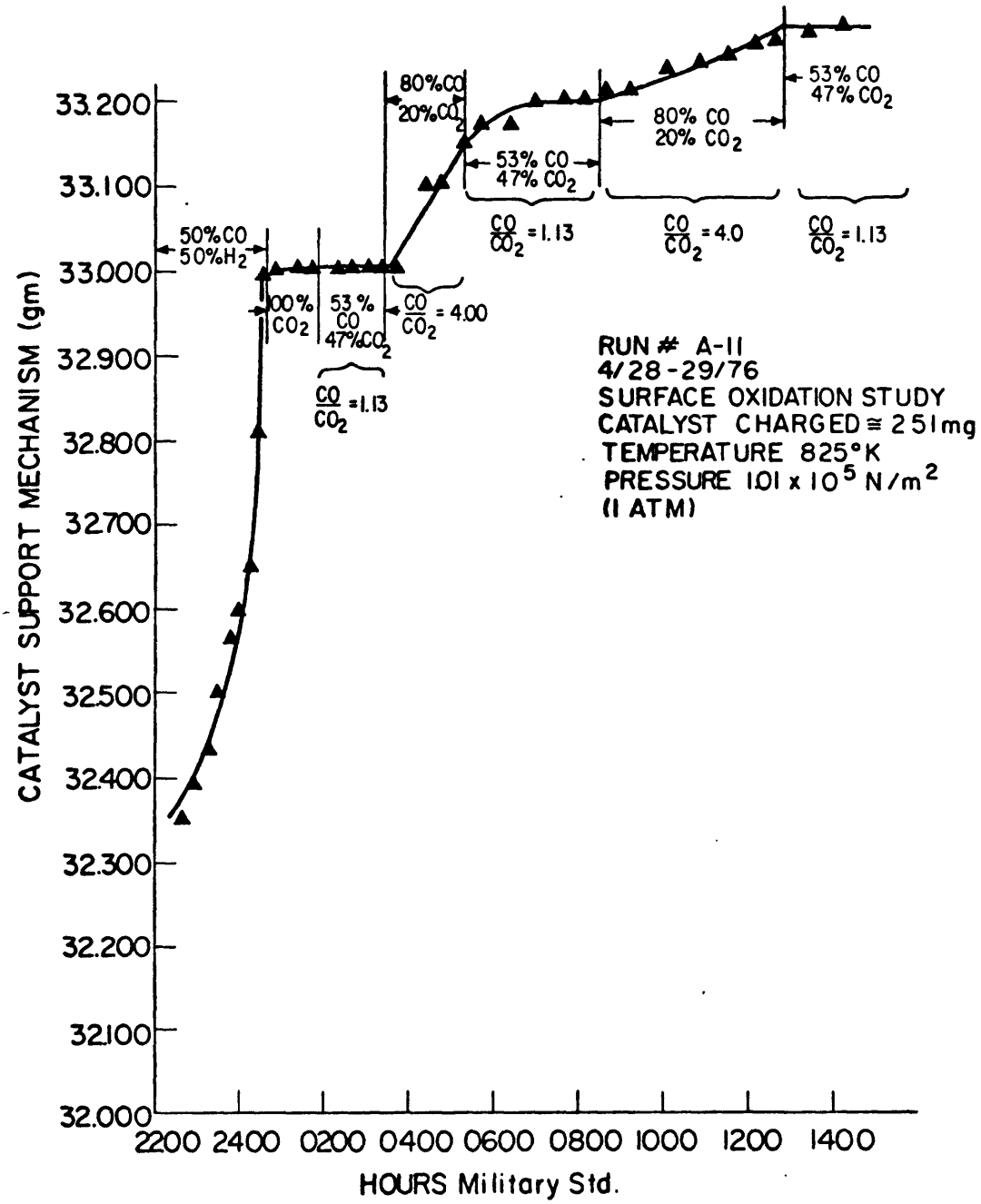

FIGURE 37 EFFECTS OF OXIDE INHIBITION IN BINARY GAS MIXTURES OF CO-CO_2

carbon monoxide for reaction D is 13%; thus, carbon deposition would be expected. However, at a P_{CO}/P_{CO_2} ratio of 1.13, α-Fe is at equilibrium with Fe_3O_4 (reaction J-A). It is believed that the "catalyst" was in the oxidized state and as such was not a catalyst for carbon deposition.

In support of this hypothesis, when the P_{CO}/P_{CO_2} ratio was increased to 4.0 (i.e., strongly reducing atmosphere), rapid carbon deposition occurred. This reducing atmosphere favored α-Fe formation which in turn catalyzed reaction D.

The step-like system response shown in Figure 37 was typical. The system was seen to respond more sluggishly after the initial oxidation and reduction. This behavior is due to the increased carbon deposition on the catalyst bed which acts to dilute the effective area.

Quantitatively, the amount of carbon formed was usually within 10% of that predicted by carbon monoxide conversion. However, variations as high as 50% were noted. Considering the degree of carbon monoxide conversion (i.e., < 1%), this discrepancy was considered reasonable.

Figure 37 implies that reaction D is inhibited by the formation of iron oxide in both the forward and reverse direction. The quantitative results show that carbon deposition can be accurately represented by the Boudouard reaction.

4.2 Oxide Inhibition in 5 Component Gas Mixtures

The results from the preliminary experiments verified that iron oxide (Fe_3O_4) will inhibit carbon deposition from

binary gas mixtures of carbon monoxide and carbon dioxide. The next step in the investigation was to determine the effect of oxide formation on carbon deposition under normal Bosch operating conditions, i.e., those in which there is a gas phase consisting of methane, hydrogen, carbon monoxide, carbon dioxide, and water. The iron catalyst would have carbon present along with small amounts of iron oxide and/or iron carbide.

In order to study and evaluate the inhibiting behavior of iron oxide(s), a series of experiments were performed to determine: the effect(s) of oxidation and reduction on catalyst structure prior to and during reaction, to ascertain whether the system response was more sensitive to variations in P_{H_2}/P_{H_2O} or the P_{CO}/P_{CO_2} ratio, and, finally, to determine the precise location of the phase boundary for the α-iron/wustite and α-iron/magnetite systems. The phase boundary location was determined by the point where carbon deposition was observed to start and stop.

4.2.1 The Effects of Preconditioning at 900 K

Manning (1976) reported the initial rate of carbon deposition increased substantially on preoxidation of the steel wool catalyst. In order to be able to utilize this effect, a clear understanding of the oxidation-reduction process and/or processes occurring on the catalyst surface was necessary.

A series of micrographs of an unconditioned #2 steel

wool fiber is shown in Figure 38. Micrograph (a) is an overview of the entire fiber. Micrographs (b), (c), and (d) are high-magnification photographs illustrating three distinctive surface structures. The top region of the fiber (micrograph {b}) is seen to be a relatively smooth area, showing some stress cracks and holes. Micrograph (c) illustrates the central region of the fiber. Here the structure appears to be layered. The lower section of the catalyst fiber seems to be a combination of the top and central regions showing both regular layering and periodic cracks and holes. This type of surface structure was found on all unconditioned #2 steel wool fibers and is apparently the result of the continuous shaving process used in steel wool manufacture. Surface area measurements using BET methods with krypton adsorption indicated an area of 389 cm^2/g for the unconditioned catalyst.

The steel wool catalyst prior to introduction of the reactant gases was typically preconditioned according to a standard procedure. This procedure consisted of oxidizing in a carbon dioxide-water atmosphere for several hours at 900 K and 1.01 X 10^5 N/m^2. This step was followed by reduction in a flowing stream of hydrogen.

Scanning electron micrographs of the preconditioned catalyst are shown in Figure 39. Micrographs (a) and (b) are different areas of the same fiber. Note the sponge-like appearance which has led to this type of structure being named "sponge-iron". Electron micrograph (c) clearly shows the sintered iron grains which make up this porous structure.

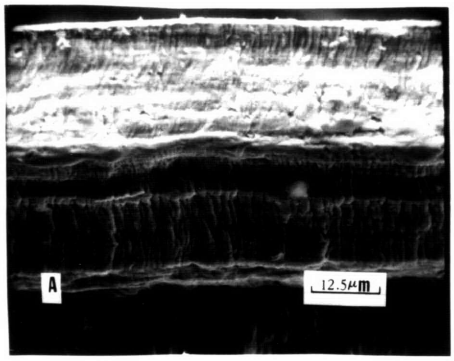

OVERVIEW, STEEL WOOL CATALYST

{unconditioned}

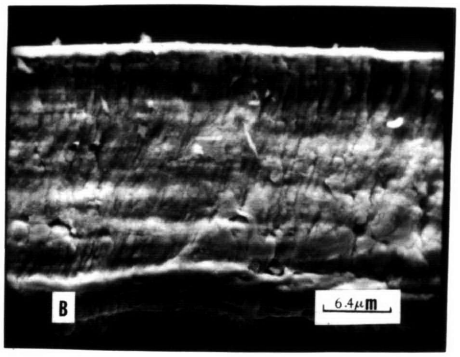

TOP REGION, STEEL WOOL CATALYST

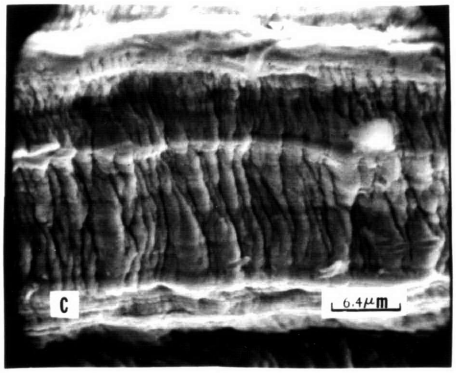

CENTRAL REGION,
STEEL WOOL CATALYST

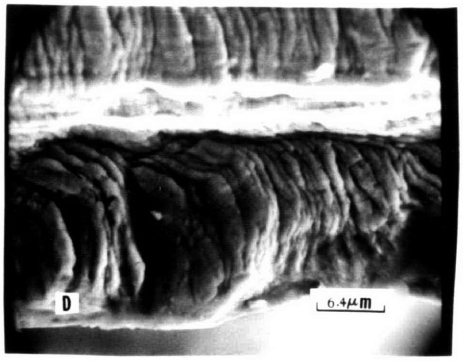

BOTTOM REGION
STEEL WOOL CATALYST

FIGURE 38 UNCONDITIONED #2 STEEL WOOL CATALYST

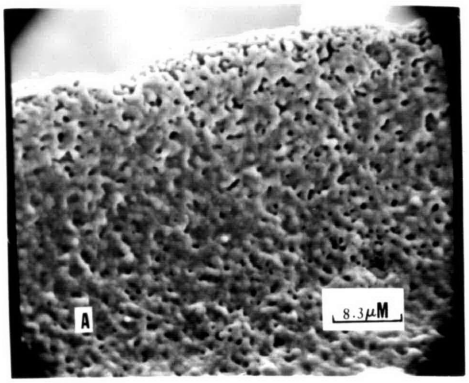

PRECONDITIONED CATALYST

AT 900 K

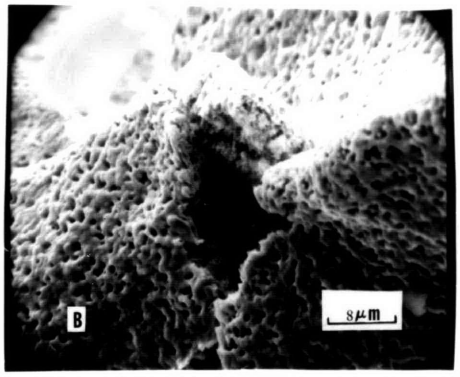

SPONGE–IRON STRUCTURE

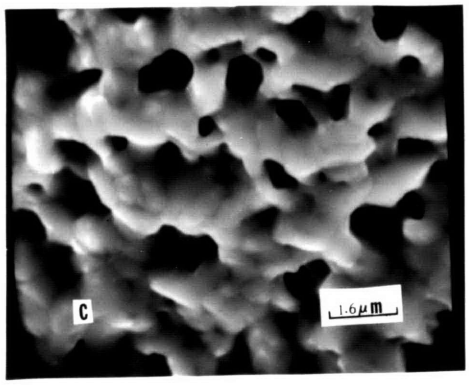

SPONGE–IRON MORPHOLOGY

note: sintered iron grains

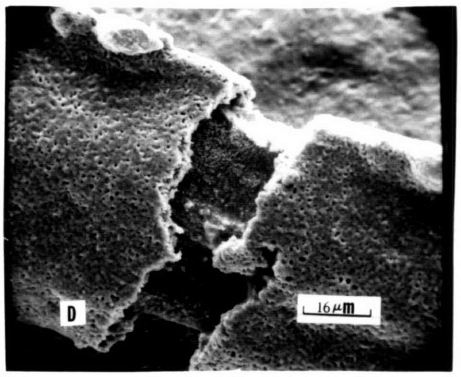

FISSURE SHOWING SHELL AND CORE MORPHOLOGY

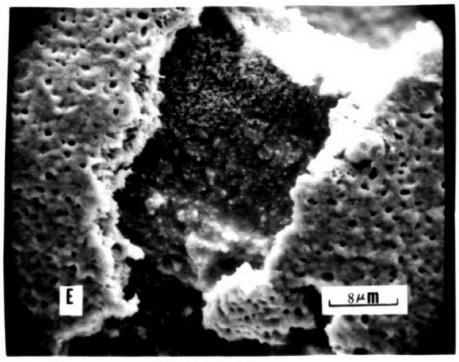

STRUCTURE INDICATING MULTIPLE OXIDE FORMATION

FIGURE 39 PRECONDITIONED CATALYST AT 900 K

Also shown in Figure 39 are two micrographs of a fissure observed on another catalyst strand.

The shrinking-core type behavior described by Spitzer et al. (1966) is clearly shown in micrographs (d) and (e). The porous shell is seen to be composed of two distinct layers, indicating multiple oxide formation. As discussed by Spitzer (section 2.2.2.3), multiple layers will be observed if the catalyst behaves as a porous particle under diffusion control. BET surface area measurements indicated an area of 1912 cm^2/g. This corresponds to an increase in effective surface area of 500% relative to the unconditioned catalyst.

The electron micrographs shown in Figures 38 and 39 indicate the reason for the increase in initial reaction rate noted by Manning, the increase being the result of the increased effective surface area. Figures 38 and 39, however, point out a much more important structural effect. This is the possibility of multiple oxide formation with its concomitant kinetic problem. Spitzer et al. (1966) clearly showed that if multiple oxide formation occurs, depending on the past history of the oxygen activity and the time at a given oxygen activity, the response of the system to changes in oxygen activity will vary. That is, changing P_{H_2}/P_{H_2O} and/or P_{CO}/P_{CO_2} ratios will cause a different response. This would indicate a system response time is to be expected and that this response time may vary.

4.2.2 Carbon Deposition-Control by P_{H_2}/P_{H_2O}

The question arises as to whether the P_{H_2}/P_{H_2O} or P_{CO}/P_{CO_2} ratio controls oxidation and reduction on iron catalysts. This question as well as the question of the inhibition of carbon deposition in a five component gas mixture was next examined.

In run A-18, 415 milligrams of steel wool catalyst were oxidized in a flowing stream of 77.2% carbon dioxide-22.8% water at 900 K and 1.01 X 10^5 N/m^2.

The P_{H_2}/P_{H_2O} ratio was varied between a value of ∞ (i.e., no water) and a value of 1.0. The remaining gas compositions were set so that reaction D proceeds to the right while; at this P_{CO}/P_{CO_2} ratio, reaction J-B should proceed in the direction to reduce iron oxide (i.e., to the left).

$$2CO \rightarrow CO_2 + C \qquad (D)$$

$$CO_2 + (1-y)\ Fe \leftarrow F_{1-y}O + CO \qquad (J\text{-}B)$$

If the surface condition is controlled by reaction N-A, alternating the P_{H_2}/P_{H_2O} ratio between a value of ∞ and 1.0 should effect carbon deposition.

$$H_2O + (1-y)\ Fe \rightleftarrows Fe_{1-y}O + H_2 \qquad (N\text{-}A)$$

The results from A-18 are shown in Figure 40. As shown, carbon deposition was controlled by adjusting the P_{H_2}/P_{H_2O} ratio which in turn controlled the surface condition according to reaction N-A. Also, as had been expected,

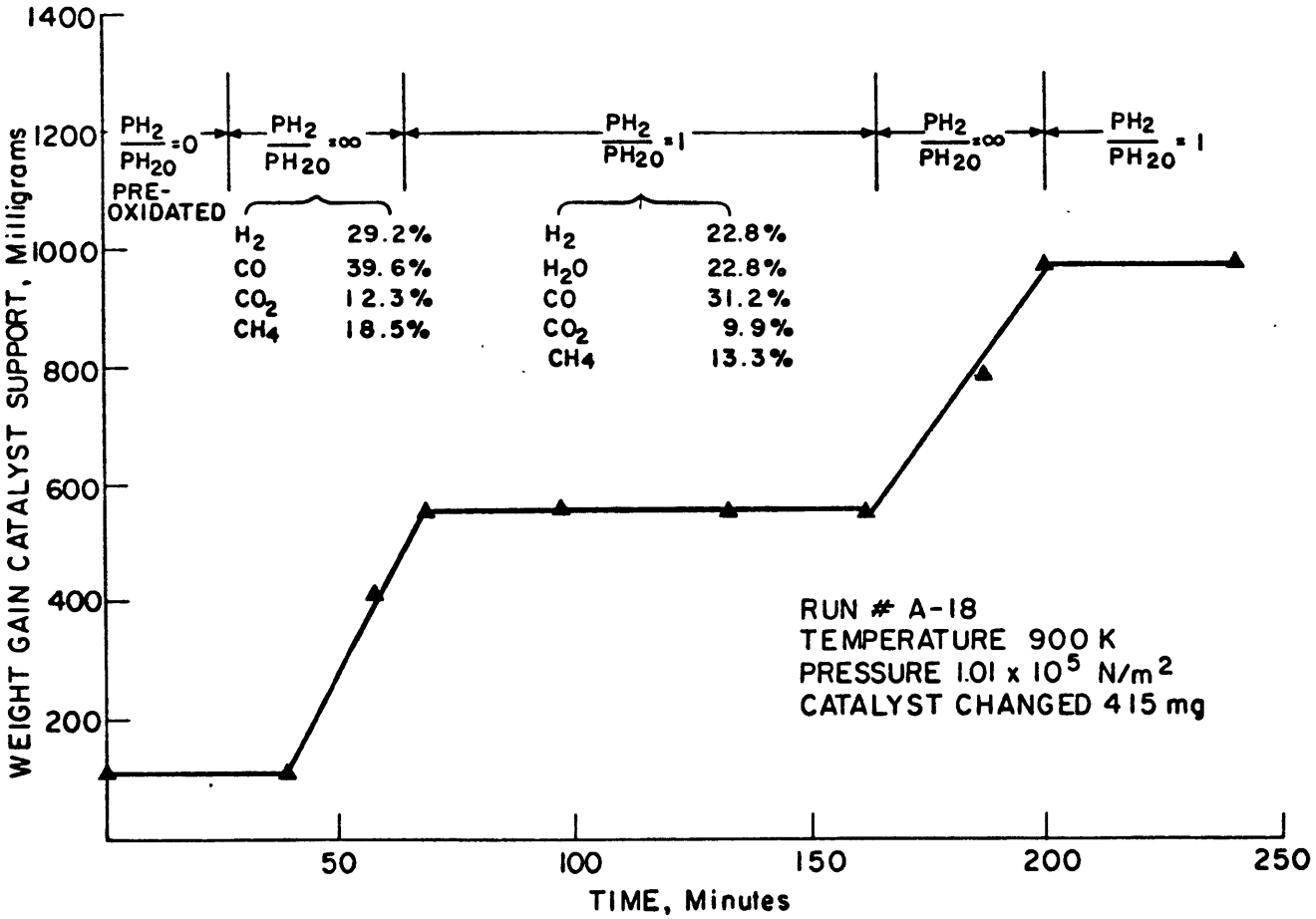

FIGURE 40 CONTROL OF CARBON DEPOSITION THROUGH VARIATION IN PH_2/PH_2O RATIO

iron oxide appeared not to be a carbon deposition catalyst. Unfortunately, due to the inherent error in effluent concentration measurements, at low conversions, nothing quantitative could be said about the reaction mechanism.

The effect of deposited carbon on the response of the metallic iron catalyst was next explored. This was necessary because a Bosch catalyst will routinely have carbon deposited on it. Run A-19 is representative of the behavior found. Initially, a P_{H_2}/P_{H_2O} ratio of (∞) was used to deposit approximately 350 mg of carbon on 415 mg of steel wool catalyst. The reactor set temperature was 900 K and the total pressure 1.01 X 10^5 N/m^2. As shown in Figure 41, no appreciable weight gain was noticed with P_{H_2}/P_{H_2O} ratios between 1.0 and 2.26. Upon changing the P_{H_2}/P_{H_2O} to 4.58, rapid carbon deposition was observed. This behavior is in complete agreement with the results shown from A-18 and indicates that reaction N-A controls the surface condition, the P_{H_2}/P_{H_2O} ratio at equilibrium for reaction N-A being 2.75.

Although only runs which approach the iron-iron oxide equilibrium from the oxide side of reaction N-A were shown, the same type of behavior was observed coming in from the reduced side.

The runs approaching the phase boundary from the reduced side were not shown because carbon deposit was rapid and it could only be shut off once before the catalyst assembly exceeded its design capacity. That is, the pressure drop across the bed became so great it equaled its weight. This,

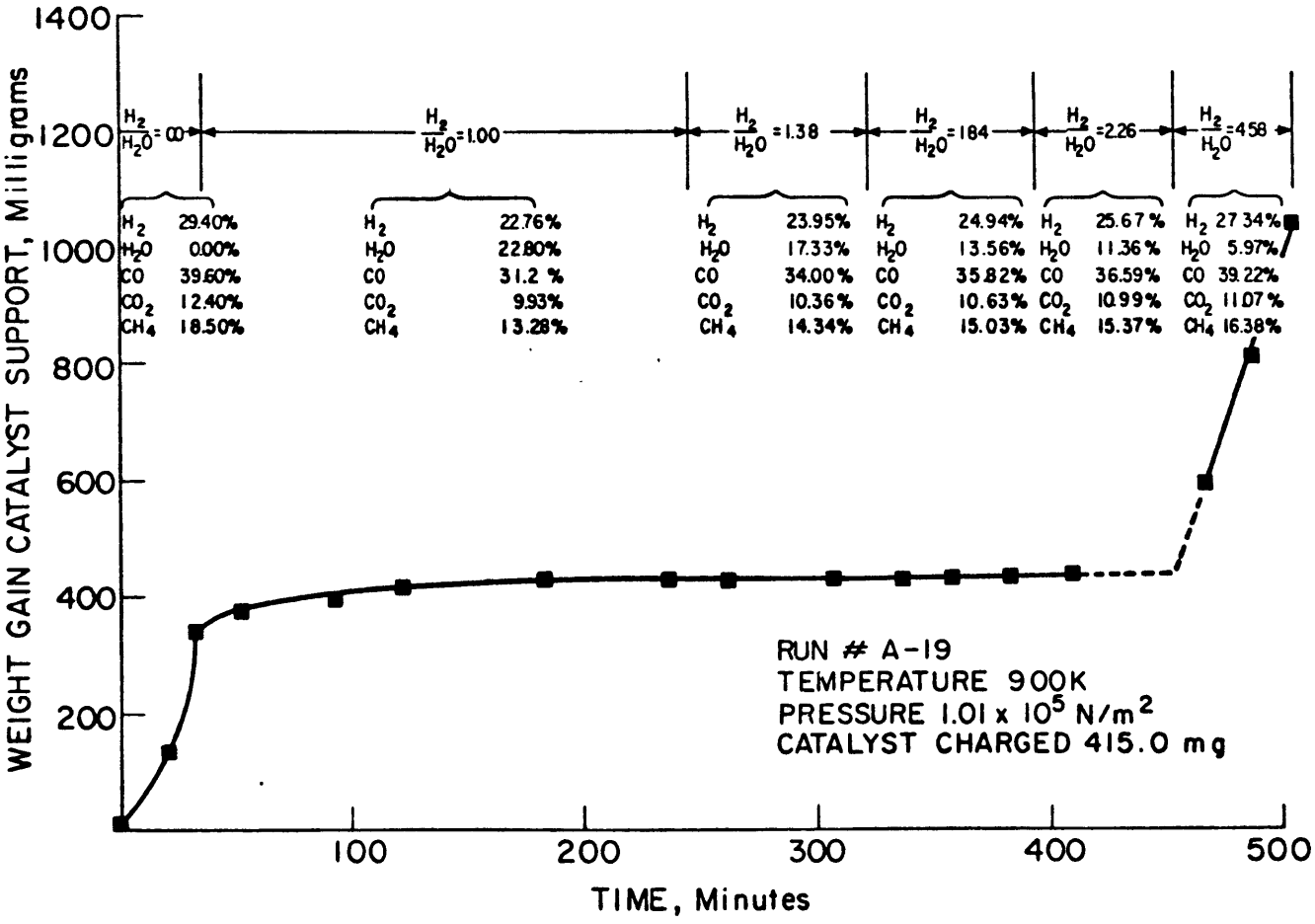

FIGURE 41 CARBON INHIBITION AS A FUNCTION OF PH_2/PH_2O RATIO

in turn, caused the assembly to float. In all cases, carbon deposition ceased when the water content was above that for equilibrium according to reaction N-A.

The question may arise as to the effect of oxide inhibition on reaction

$$CO + H_2 \rightleftarrows H_2O + C \qquad (E)$$

From the data of Figure 40 and 41 it is evident that reaction D is inhibited by oxide formation, but what of reaction E? Run A-19 indicates this reaction is also inhibited by oxide formation. Thus it can be conclusively stated that oxide formation inhibits deposition from both reaction D and reaction E at 900 K. Also, once again, the surface condition is controlled by reaction N-A through adjustments in the P_{H_2}/P_{H_2O} ratio.

4.2.3 Structural Changes During Reaction

In varying the P_{H_2}/P_{H_2O} ratio to control carbon deposition, the discussion in Section 4.2.1 indicated the catalyst structure may change. In addition, carbon deposition has been shown to alter the catalyst structure (Section 2.2.3.3). In order to better understand these simultaneous structural changes, a metallurgical examination was performed.

Figure 42 shows a series of electron micrographs of the catalyst from run A-18. Micrograph (a) reveals the shell and core type structure formed during reaction. This type of morphology results from the oxidation-reduction sequence used in run A-18. Carbon-bearing gases diffused through the porous iron shell depositing carbon along its length. This

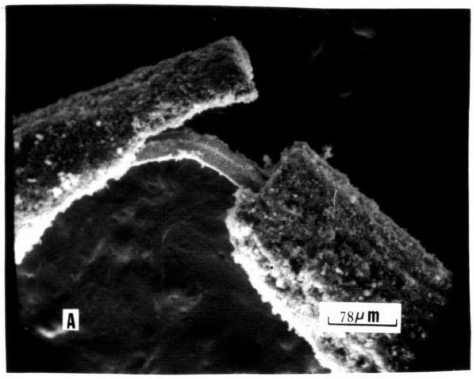

CATALYST FIBER RUN A-18
OXIDATION-REDUCTION MORPHOLOGY

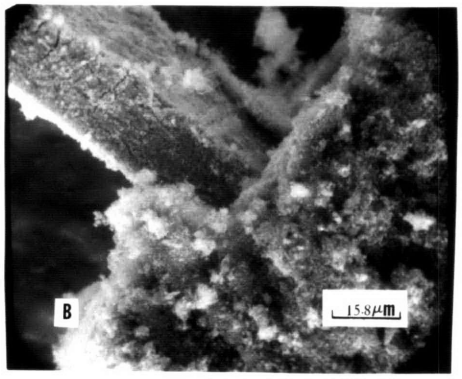

SHELL AND CORE STRUCTURE

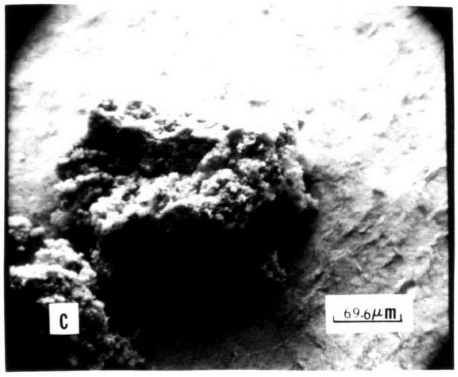

PORTION OF EXTERIOR SHELL
{gold coated}

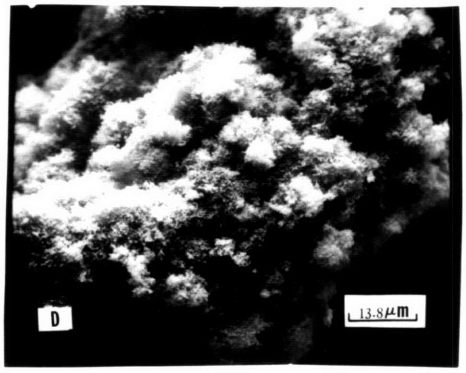

NODULE-STRUCTURE OF EXTERIOR SHELL

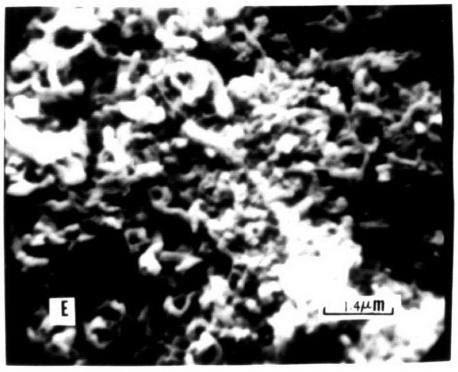

TUBULAR AND CIRCULAR CARBON FIBERS

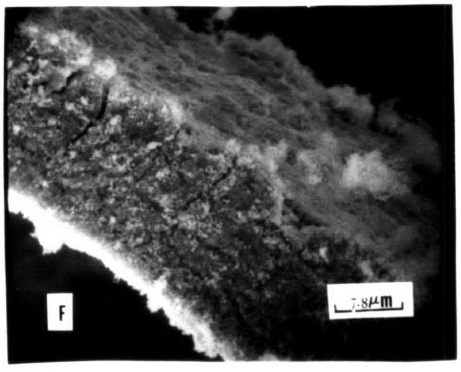

CORE REGION, RUN A-18

FIGURE 42 CATALYST STRUCTURE AFTER REACTION, RUN A-18

carbon deposition appears to make the exterior shell brittle, breaking away easily from the more structurally solid core. A high magnification photograph of the shell surface is shown in micrograph (b). Carbon fibers are seen to form in bundles or nodules. Transmission electron micrographs indicate these nodules are large chunks of electron-dense material, presumably iron or iron compounds. A small portion of the exterior shell was removed for examination and is shown in micrographs (c), (d), and (e). Again the nodule-like fiber bundles are clearly shown. In micrograph (e) carbon fibers can be seen having both tubular and circular shape.

Interestingly, the core region shown in micrograph (f) is relatively smooth showing none of the surface features noticed on the untreated steel wool. Also, very little carbon was deposited on the core fiber indicating both its low effective surface area as well as probable diffusion limitations through the shell for carbon-bearing gases.

4.2.4 Structure of Carbon Fibers

Manning (1976), Walker et al. (1959), and Baker et al. (1972) and many other investigators have observed carbon fiber formation occurring during carbon deposition experiments. Manning reported flat ribbon-shaped fibers, while Walker and Ruston observed both tubular and coil-shaped fibers which were hollow and often, although not always, associated with an electron dense tip. Transmission electron microscopy (TEM) was used to observe the type or types of fiber formed in this

investigation.

Figure 43 is a TEM micrograph of a typical carbon fiber found in the exterior shell region of a catalyst fiber from run A-18. Three points are worth mentioning: first, the "camel" shaped fiber is suspended securely from the main catalyst surface by carbon fibers. This is indicative of the type of shell structure developed during carbon deposition. The shell region appears to consist of an intricate network of interwoven fibers connected securely by fiber bundles or nodal points. These nodal points consist of iron and/or iron compounds. Second, in agreement with Baker and Walker, the fiber shaft appears to be hollow. Third, most fibers were observed to have an electron dense tip.

Electron diffraction patterns were taken of the head and shaft regions of the fiber. The results are shown in Table 4.

The electron dense tip was seen to have some Fe_3O_4 and Fe_2O_3, along with some graphite (well ordered). A small amount of α-Fe was observed along with what appears to be $Fe_{20}C_9$.* The shaft region had intense patterns for graphite and indicated trace amounts of Fe_2O_3 and α-Fe. Very little Fe_3O_4 and no iron carbide was found on the shaft. These results agree for the most part with those of Walker and

---

*The diffraction patterns for various carbides are very similar. Consequently, identification is often a matter of experience and judgment.

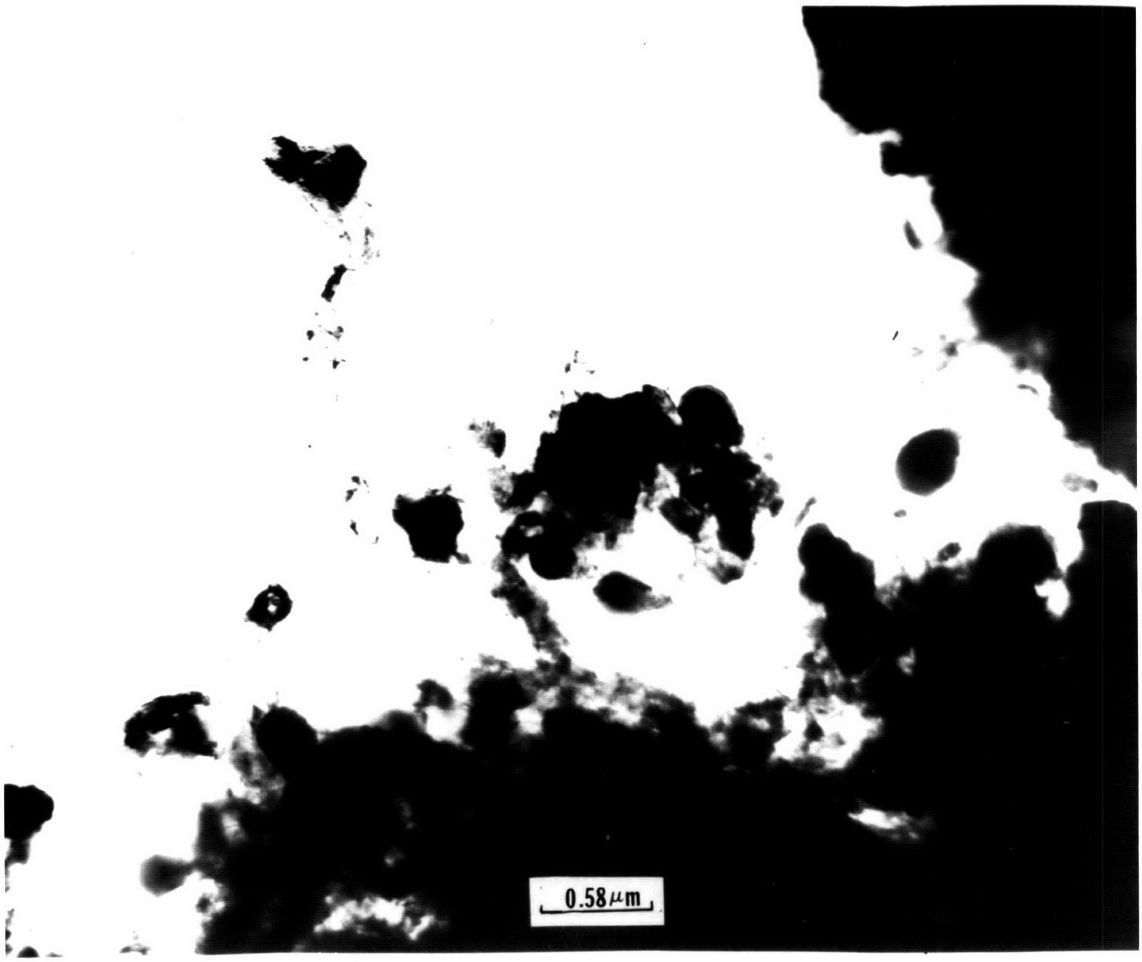

FIGURE 43 CARBON FIBER FROM EXTERNAL SHELL REGION , A-18

Diffraction Pattern	Experimental Data d (A)	I/IO Visual Est.	Graphite ASTM Card 13-148		Graphite ASTM Card 12-212		α-Fe ASTM CARD 6-0696		"Fe-C" 6-0686		ε-Fe_2C 6-0670		$Fe_{20}C_9$ 8-370 9-369		Fe_3C 6-0688		α-$Fe_{20}O_3$ 13-534		Fe_3O_4 11-614		Fe_xO 6-0615	
	3.49	100	3.35	100	3.37	100											3.66	25				
Electron	2.07	60	2.04	50	2.04	3	2.03	100			2.08	100	2.08	100	2.06	70	2.07	2	2.09	70		
Dense	1.73	50							1.72	60			1.73	50	1.76	15			1.71	60		
Tip	1.27	20	1.23	90	1.23	6					1.24	60					1.26	8	1.26	10	1.24	15
	1.17	20	1.15	90	1.16	6	1.17	30	1.17	30	1.16	60					1.19	10				
	3.49	100	3.35	100	3.37	100											3.66	25				
Shaft	2.05	80	2.04	80	2.04	3.	2.03	100			2.08	100					2.07	2	2.09	70		
Region	1.27	10	1.23	90	1.23	6					1.24	60					1.26	8	1.26	10	1.24	15
	1.18	20	1.15	90	1.16	6	1.17	30	1.17	30	1.16	60					1.19	10				

TABLE 4 Electron Diffraction Pattern Head and Shaft of Carbon Fiber

Ruston. The high intensity hematite (Fe_2O_3) and magnetite (Fe_3O_4) diffraction patterns are presumably due to the oxidation-reduction sequence used in run A-18.

A variety of tubular shaped fibers were formed. Figures 44 and 45 show two additional types. Figure 44 is a micrograph of a fiber taken into the direction of growth. Again, the hollow shaft is seen along with the electron dense tip. Interestingly, in all micrographs taken in the growth direction, a slit or hole is noticable in the tip.

Figure 45 is a circular-shaped fiber. The hollow shaft is again seen, but this fiber has no metallic tip. The graphitic nature of the skin is shown in Figure 45 along with indication of disintegration fragments of iron and/or iron compounds.

Electron diffraction patterns on all fibers formed gave similar results to those presented in Table 4. No ribbon-shaped fibers were formed nor were any coiled fibers in evidence.

4.2.5 $Fe_{1-y}O/\alpha$-Fe Phase Boundary

Having determined that carbon deposition can be controlled by adjusting the P_{H_2}/P_{H_2O} ratio, the next step in the investigation was to determine precisely the location of the wustite/α-iron phase boundary.

The iron-iron oxide, graphite-gas and iron-iron carbide phase boundaries can be conveniently plotted on a triangular phase diagram. Figure 46 shows such a representation with

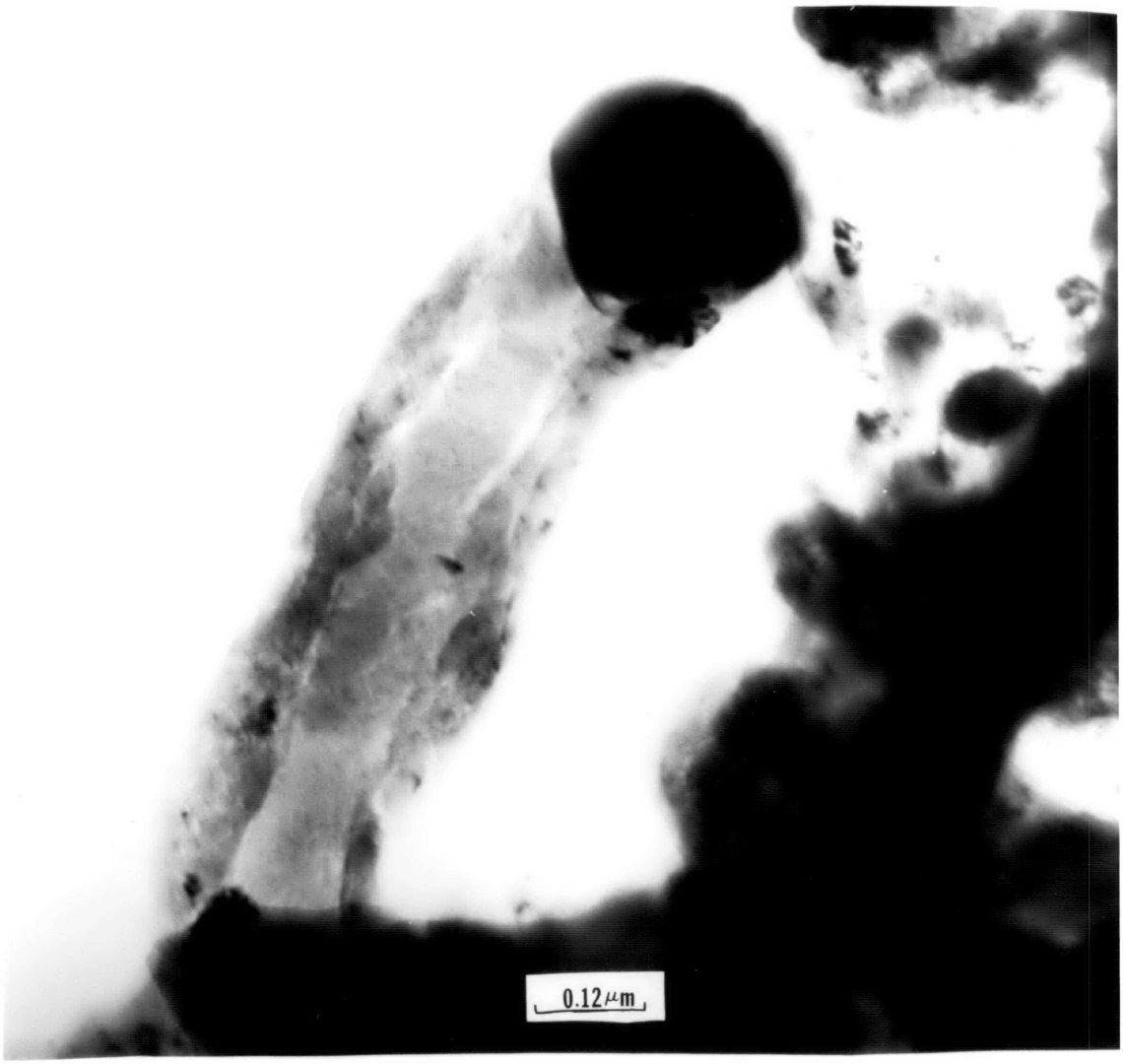

FIGURE 44 CARBON FIBER-MICROGRAPH TAKEN IN GROWTH DIRECTION

FIGURE 45 CIRCULAR-SHAPED CARBON FIBER

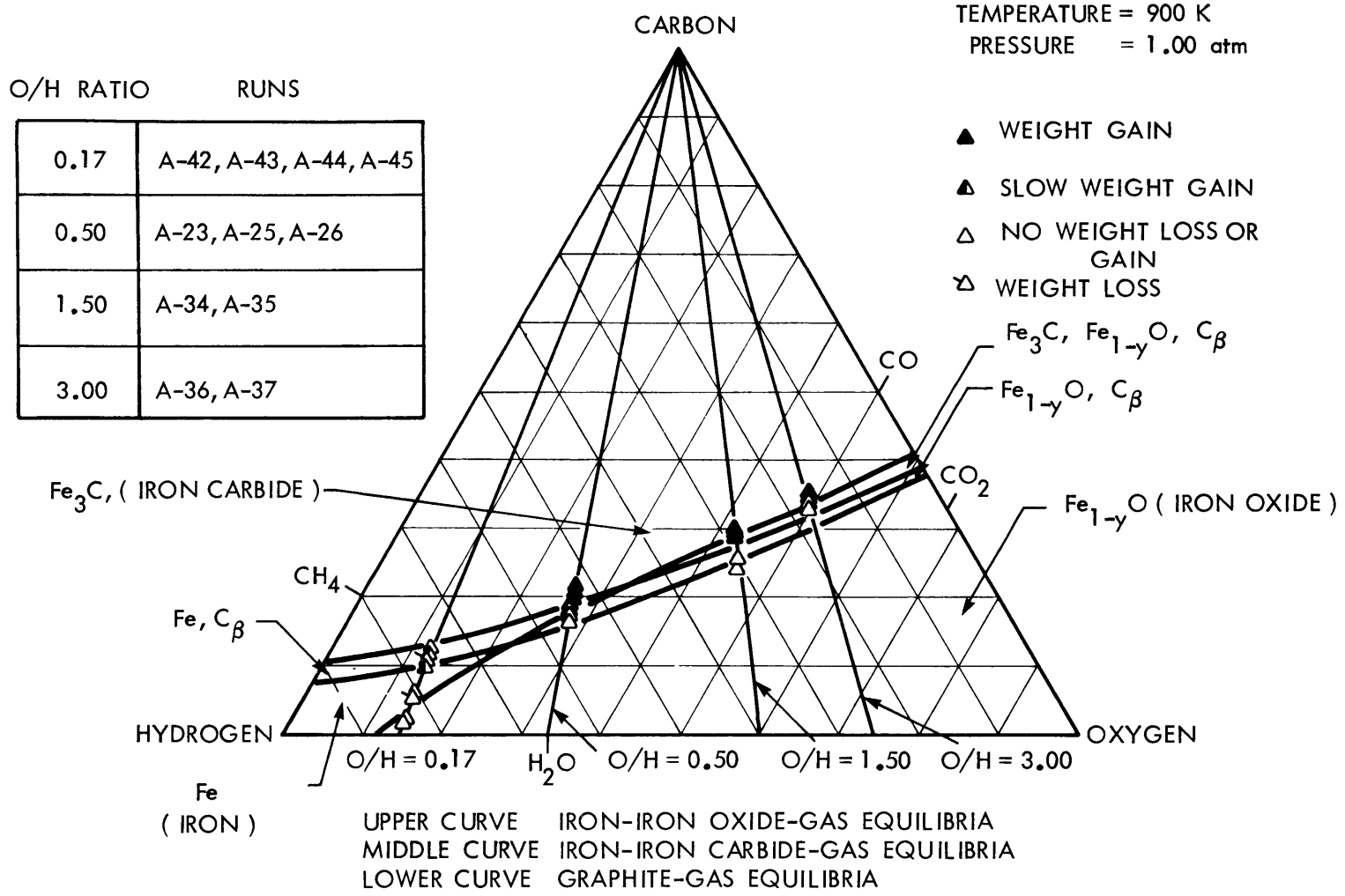

FIGURE 46 DETERMINATION OF THE IRON/WUSTITE PHASE BOUNDARY IN A FIVE COMPONENT GAS MIXTURE AT VARIOUS O/H RATIOS

several runs plotted at various O/H ratios. With the one exception of O/H = 0.17, all the data shown represents well the conclusion established earlier; that is, that iron oxide inhibits carbon deposition. Also, the phase boundary itself appears to be located at the predicted region from theoretical calculations. Due to the proximity of the various phase boundaries at 900 K, these data with some additional data are best represented as shown in Figure 47.

Figure 47 is a plot of the percentage of the theoretical P_{H_2}/P_{H_2O} for the surface controlling reaction N-A, versus the experimental P_{H_2}/P_{H_2O} ratio. Each data point is seen to have associated with it error bars as determined by a propagation of error analysis (Appendix 7.4.2).

Figure 47 indicates some scatter was associated with different run conditions. That is, occasionally, carbon deposition did not stop or begin when expected. Most of this scatter is within 10% of the equilibrium P_{H_2}/P_{H_2O} ratio. Again a propagation of error analysis indicates the maximum error in P_{H_2}/P_{H_2O} ratio could be as high as 11%. Undoubtedly, part of this scatter comes from normal inherent error associated with the experimental procedure, data collection, and data analysis methods.

Since a propagation of error analysis gives the maximum error possible, it is felt that some of the scatter shown possibly reflects another process which affects the <u>rate</u> of either carbon deposition or oxide formation. An intriguing possibility is the formation and reduction of multiple oxide

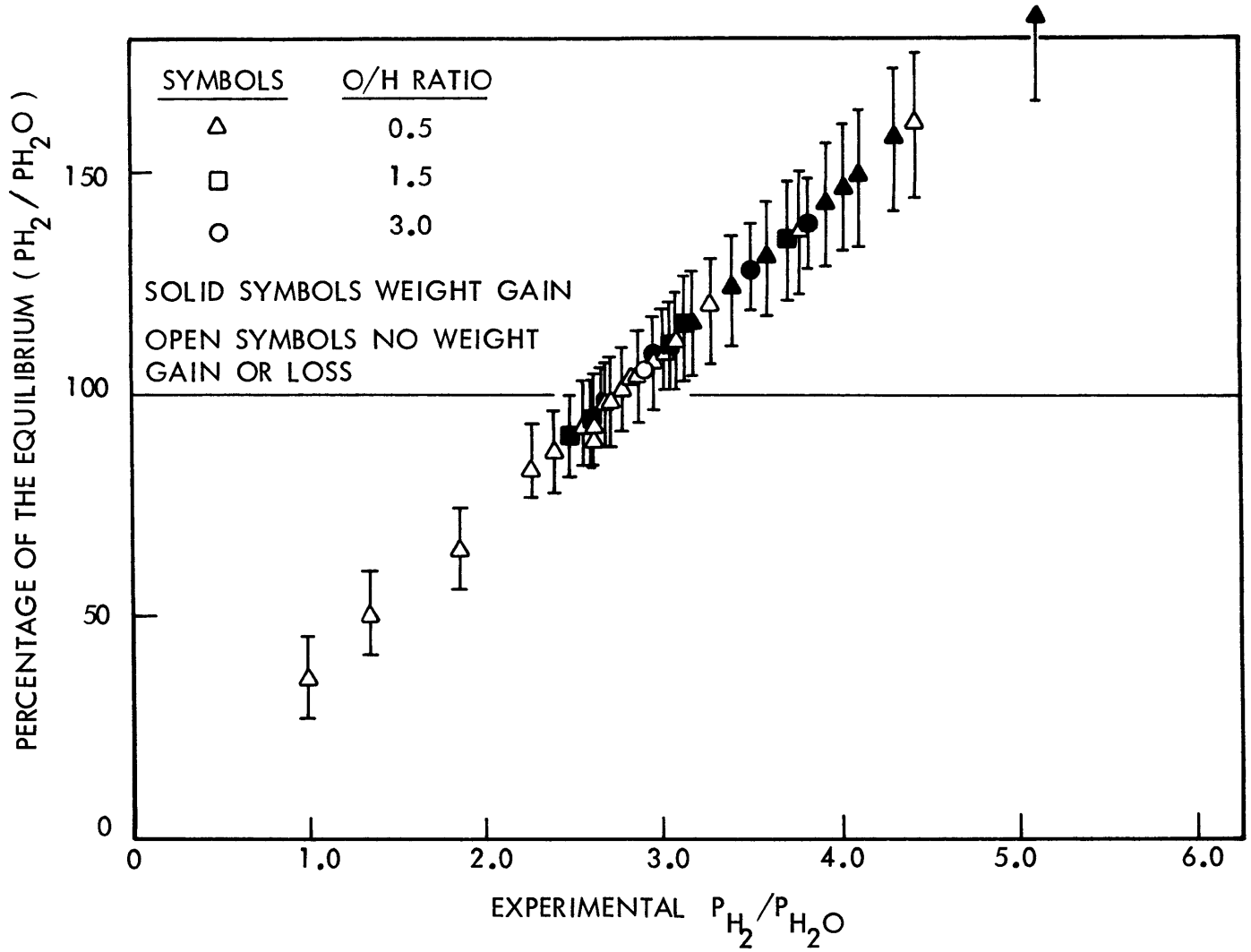

FIGURE 47 PERCENTAGE OF THEORETICAL $P_{H_2}/P_{H_2O}\big|_{eq}$ VERSUS EXPERIMENTAL P_{H_2}/P_{H_2O} FOR VARIOUS O/H VALUES

phases. It was shown in Section 4.2.1 that multiple oxide formation does in fact occur on the steel wool catalyst. However, multiple oxide formation can only occur if the oxygen activity in the system at some time exceeds that necessary to support the particular multiple oxide phase of interest. For example, if a layer of magnetite (Fe_3O_4) is to form at 900 K, the oxygen partial pressure (activity) has to exceed that for the equilibrium between wustite and magnetite. While this was clearly the case during normal catalyst pretreatment, it was not generally the case during most of the experimental runs. This fact would normally tend to rule out this effect. However, the results from run A-43 as well as several others suggest that multiple oxides may indeed form.

Run A-43 was carried out to establish the position of the iron-iron oxide phase boundary at an O/H value equal to 0.17. The normal catalyst pretreatment was carried out, i.e., 402 mg of carbon were deposited and an initial set of run conditions fed. This initial set of run conditions created an oxidizing atmosphere with a P_{H_2}/P_{H_2O} equal to 2.38. On conclusion of the first set of run conditions a leak in the inlet line developed and the reactor was immediately shut down.

Figure 48 shows the catalyst carrier after removal from the reactor. Carbon was shown to be preferentially deposited at the bed inlet. It is important to point out that this carbon deposition occurred prior to the time when the inlet leak occurred. Above the carbon bed was a region where very little carbon was observed to deposit , followed by a reddish-

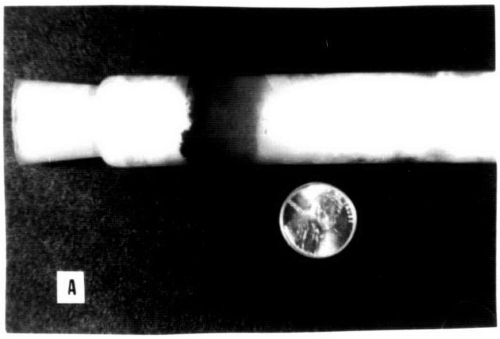

CATALYST CARRIER RUN A–43

note, three distinct regions

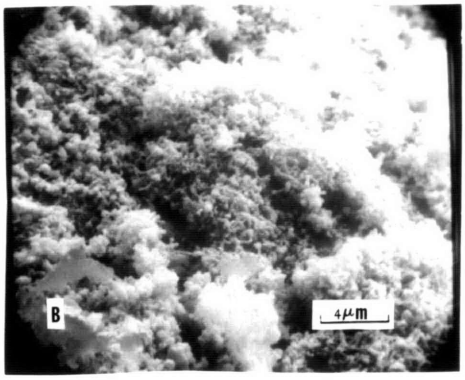

CARBON FIBER FORMATION

{lower region}

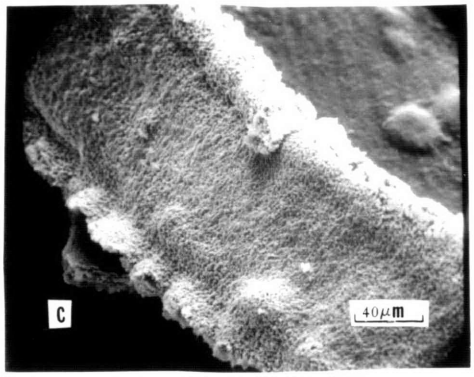

OVERVIEW CATALYST STRAND

{central region}

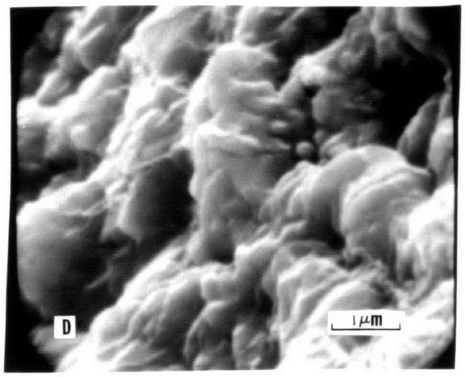

SURFACE STRUCTURE

{central region}

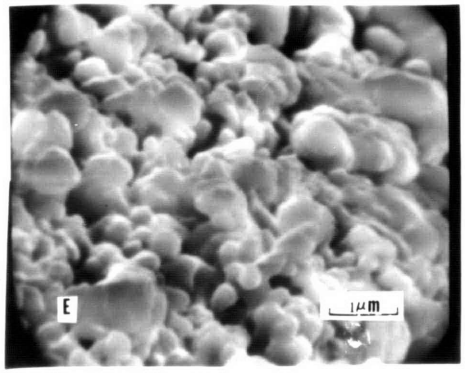

SURFACE MORPHOLOGY

{upper central region}

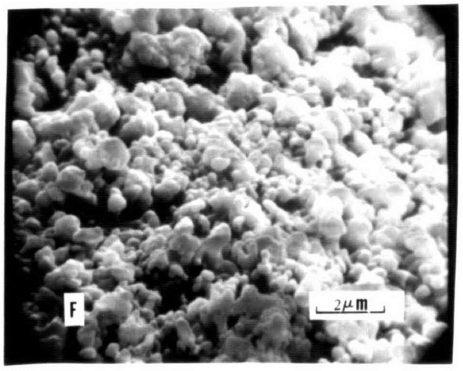

HEMATITE, Fe_2O_3, STRUCTURE

{top region}

FIGURE 48 CATALYST SHOWING STRUCTURAL CHANGE, RUN A-43

orange region where no carbon deposition occurred. This reddish-orange region is Fe_2O_3 (hematite). At this P_{H_2}/P_{H_2O} ratio no Fe_2O_3 should have been able to form. Since similar results were noticed in other runs and, also, since this type of behavior has been reported by Everett et al. (1967) and Wilson (1971) under similar conditions it is felt that this oxide formation is not a function purely of the inlet leak reported. This type of behavior reflects product poisoning; in this case water and carbon dioxide. If product poisoning is occurring, it means that multiple layer formation could take place. If so, this could easily explain the scatter noted in Figure 47 (see Section 4.2.5). Figure 48 is important from another point also: it visually shows that carbon deposition does not occur on oxidized iron.

The three regions observed in Figure 48 provide a unique opportunity for metallurgical examination of what could possibly be the structural change sequence which occurs during reaction.

Micrograph (b) shows the familiar carbon fiber formation which was similar to those seen from micrographs of the shell region from run A-18. A strand taken from the central region is shown in micrograph (c). At first glance the structure looks very similar to the sponge-like structure which develops during preconditioning. However, close examination of the surface shows rough irregular features with significantly less porosity than that observed on a preconditioned catalyst

(micrograph {d}). Micrograph (e) is a high magnification photograph of the surface features just prior to entering the reddish-orange hematite (Fe_2O_3) region. Notice there is more porosity here suggesting less structural sintering. The final micrograph shown in Figure 48 is the Fe_2O_3 surface oxide; note the particle-like nature of the hematite structure and the associated high porosity. It should be remembered in viewing the micrographs in Figure 48 that the original structure was that of sponge-iron developed during standard catalyst preconditioning.

Figure 49 is a final series of micrographs showing the multi-layer structure formed in run A-43. Micrograph (a) is a typical catalyst fiber showing the core and double layer regions. Micrographs (b) and (c) are high magnification micrographs of the double layer structure observed in micrograph (a). These micrographs clearly show two distinct layers, neither of which appear to have any carbon deposited on them. A close examination of the core region micrograph (c) shows what appears to be some kind of projections. A close up of this core region shown in micrograph (d) show iron whiskers. These were identified as pure iron by Energy Dispersion Analysis. It is interesting to compare the core region shown in micrograph (d) with the core region from micrograph (f) in Figure 42. In both photographs very little carbon if any is seen. However, no iron whiskers are noticed in micrograph (f) of Figure 42.

Whiskers are curious structures which have not been fully

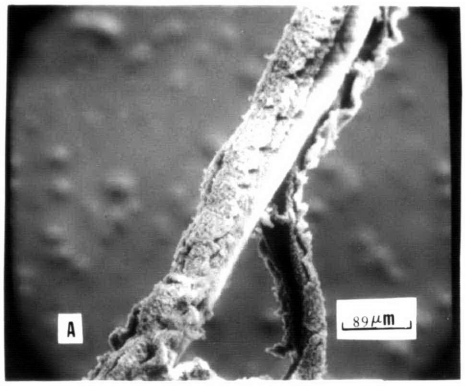

RUN A-43 CATALYST FIBER
note, shell double layer

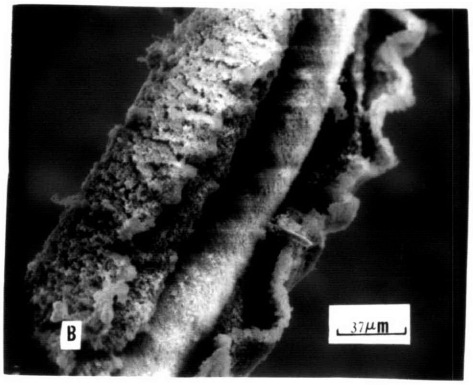

DOUBLE LAYER MORPHOLOGY

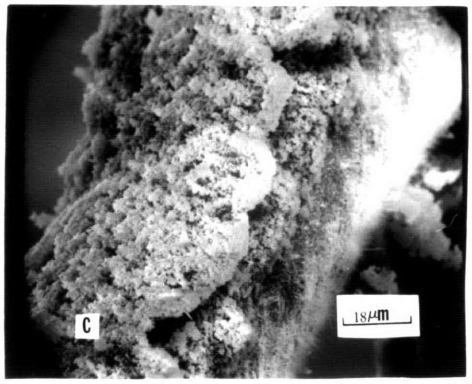

SHELL AND CORE STRUCTURE
note, iron-whiskers on core

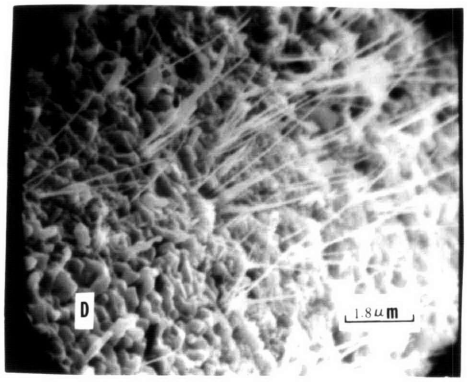

IRON-WHISKER FORMATION

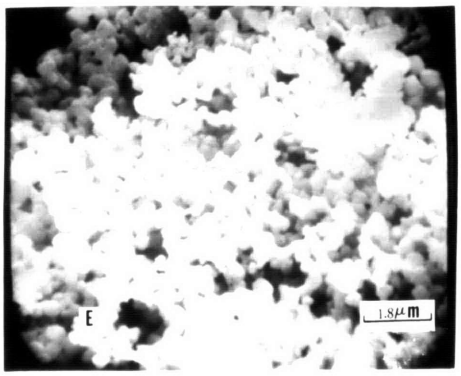

Fe_2O_3 OUTER SHELL

FIGURE 49 CATALYST EXHIBITING MULTIPLE OXIDE FORMATION, RUN A-43

explained. Several theories have been put forth, but none have been experimentally verified. However, whisker formation has been found to frequently occur in structures reduced in hydrogen with hematite (Fe_2O_3) present (Cahn, 1973).

It was mentioned earlier that the data in general agreed with the conclusion that iron oxide is not a catalyst for carbon deposition. However, one of the major problem areas was at low O/H values (i.e., < 0.2). Here the data were inconsistent. The reason for this was that the water concentration was so high that it exceeded system design. Condensation was observed to occur in both the inlet and exit lines. For completeness the runs at O/H values of 0.17 were shown in Figure 46, but the results presented must be viewed with caution.

In conclusion, the α-Fe/$Fe_{1-y}O$ phase boundary is seen to be in the position predicted by theory. The scatter noticed can be justified by consideration of normal error involved in experimentation and data analysis. Also, evidence has been shown which suggest multiple oxide formation can be important in explaining the observed system behavior.

4.2.6 Iron-Iron Carbide Equilibrium

The question of the role of carbides during carbon deposition is a difficult one. The difficulty lies in the fact that carbides are difficult to identify and can form not only during reaction but as the reactor goes through wide temperature fluctuations, such as in a hot spot or during the cooling

down sequence.

Several experiments were run in an attempt to determine the effect of carbides formed during reaction on carbon deposition.

Run A-57 was the initial experiment performed. In run A-57, a 514 mg steel wool catalyst with 577 mg of carbon was exposed to a variety of different methane-hydrogen mixtures at 823 K and 1.01 X 10^5 N/m^2. At all run conditions, the methane content was maintained at a value above that predicted by equilibrium for reaction G, 38%. Thus, reaction G would be expected to proceed to the left.

$$2H_2 + C \rightleftarrows CH_4 \qquad (G)$$

The methane content was adjusted to favor either Fe_3C or α-Fe formation according to reaction H-A.

$$2H_2 + Fe_3C \rightleftarrows 3Fe + CH_4 \qquad (H\text{-}A)$$

Figure 50 represents the results obtained. Condition 1 was run with a methane content of 58%; this corresponded to a composition slightly above the 52% required for equilibrium of reaction H-A.

From equilibrium considerations alone, carbide formation as well as carbon deposition would be expected to occur. As shown a slow weight gain was recorded, however, due to low conversion, it was impossible to determine whether or not carbide formation accounted for the weight gain. The methane content was then reduced to 49% so as to bring the gas composition below the iron-iron carbide phase boundary.

RUN NO. A-57

Condition	%Hydrogen	%Methane	Comment
1	41.23	58.51	Slow Weight Gain
2	50.50	49.29	Very, Very Slow Weight Gain
3	60.57	39.25	No Weight Gain or Loss
4	25.45	74.21	No Weight Gain
5	98.86	00.13	Rapid Weight Loss

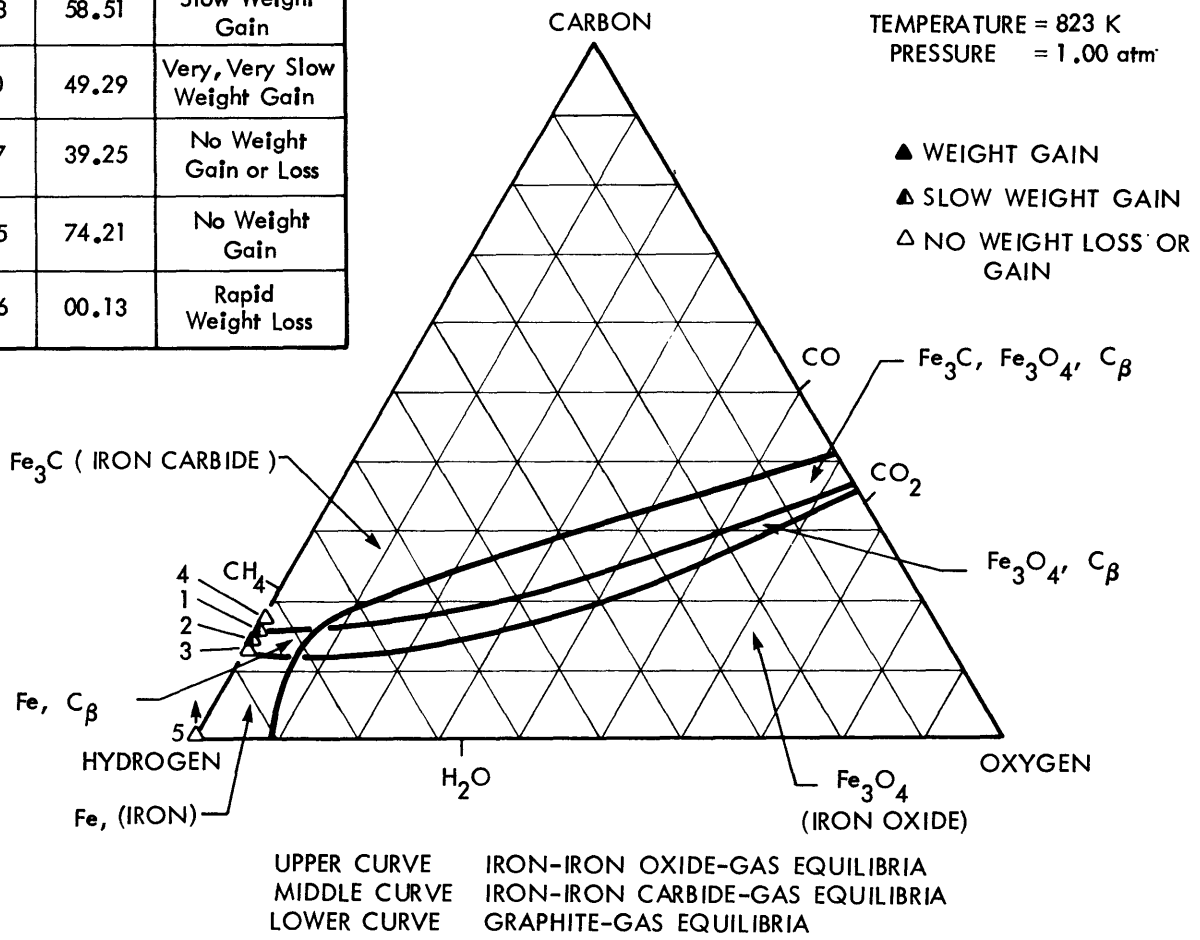

FIGURE 50 EFFECT OF Fe_3C ON CARBON DEPOSITION FROM METHANE-HYDROGEN MIXTURES

According to reaction G carbon should have formed but a methane content this low would require H-A to proceed to the right, thus reducing any carbide present. A slow weight gain was observed but effluent gas composition did not appear to change substantially. For the next two runs at methane contents of 39 and 74%, respectively, there was neither weight loss nor gain. The run at 74% methane should have formed carbide and carbon, however, no weight change was observed nor did the effluent composition change. When the methane content was dropped to less than 1%, rapid weight loss was observed, with methane appearing in the product gas stream.

Manning (1976) suggests that methane formation may be formed through a carbide intermediate, but here is proof that not enough, if any, carbide was formed to account for 115 mg of weight loss which occurred at run condition 5. Condition 1 indicated (assuming the weight gain noted was entirely from Fe_3C formation) that carbide formation is much too slow, from methane, to account for the rate of carbide formation necessary to give the weight loss observed. These observations agree with those observed by Podgurski (1950) who stated that carbide formation from methane was extremely slow. Carbon formation from reaction G at this temperature can also be inferred to be slow by Browning et al.'s (1950) data on α-iron/Fe_3C equilibrium and thus little carbon weight gain would be expected.

In order to confirm these results and to try and establish if Fe_3C is a catalyst for carbon deposition, a series of

runs were performed at 900 K with a five component gas mixture. At this temperature carbon formation from reaction G should become more significant and the rate of carbide formation should also increase.

Runs A-58 and A-59 were performed at fixed C/H values of 0.2 and 0.35, respectively. The catalyst was preconditioned using the standard procedure and a carbon bed laid down. Figure 51 illustrates the observed behavior.

During both experimental runs, weight gain was observed in the region where cementite (Fe_3C) would be expected to be the stable solid phase. However, the effluent in both runs A-58 and A-59 indicated little if any change in methane concentration, and the observed weight gain resulted primarily from carbon monoxide conversion.

There are two reactions which could account for the weight gain observed, reaction I and/or reaction D.

$$2CO + 3Fe \rightleftarrows Fe_3C + CO_2 \qquad (I)$$

$$2CO \rightleftarrows CO_2 + C \qquad (D)$$

From stoichiometric considerations it is impossible to determine if reaction I or reaction D accounts for the weight gain reported. However, the results of the work by Podgurski et al. (1950) and Walker et al. (1959) indicated that carbon deposition resulted when carbiding with carbon monoxide, even at temperatures as low as 598 K. Taking this into account, along with the fact that the total weight gain was 3.5 times that required for complete carbiding (35 mg), suggests that

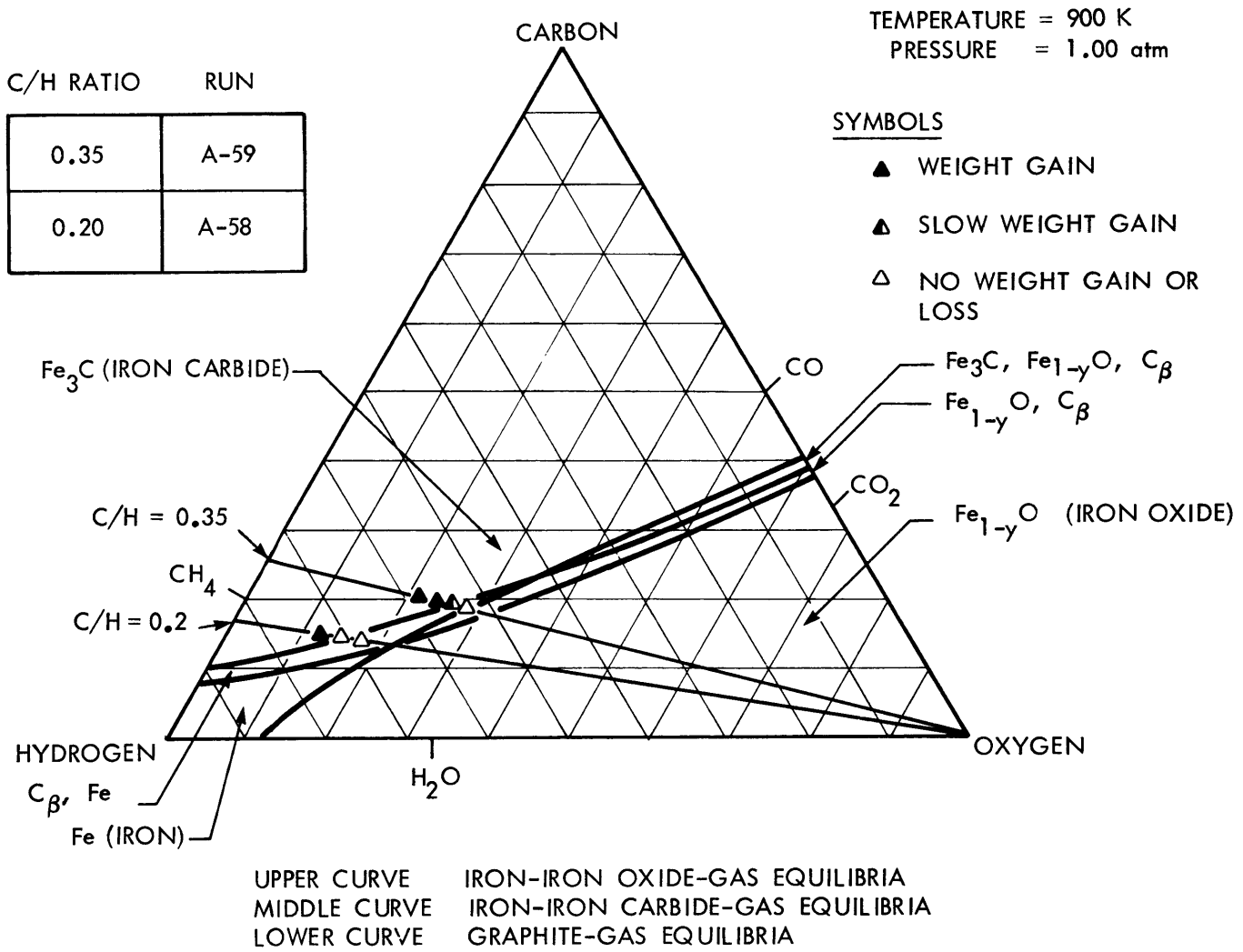

FIGURE 51 DETERMINATION OF IRON / IRON CARBIDE PHASE BOUNDARY IN A FIVE COMPONENT GAS MIXTURE AT VARIOUS C/H RATIOS

the weight gain observed was due to carbon deposition not carbide formation.

These data indicate that at 900 K, carbide formation from methane does not occur readily. The data were inconclusive in determining if weight gain was due to carbon formation entirely or a carbide-carbon combination. For this reason, these data do not conclusively show whether carbide formation inhibits or catalyzes carbon deposition. However, from an operational standpoint, it appears that oxide formation is the more important problem in efficient Bosch reactor operation.

If one looks closely at the data plotted in Figure 51, an interesting question arises: why did not carbon deposition occur in the region between the iron-iron carbide and graphite-gas phase boundaries, i.e., in the region where the stable solid phase should be α-iron and carbon?

The reason appears to be related to kinetics. For example, assuming the rate of reaction E can be represented by a power law relationship:

$$r_{(E)} = \frac{k_1}{R_g T} \{P_{H_2}\} \{P_{CO}\} - \frac{k_2}{R_g T} \{P_{H_2O}\}$$

assuming a one step mechanism

$$K_e = \frac{k_1}{k_2}$$

$$\therefore r_{(E)} = \frac{k_1}{R_g T} \left((P_{H_2}) (P_{CO}) - \frac{(P_{H_2O})}{K_e} \right)$$

or

$$r_{(E)} = \frac{k_1}{R_g T} \left(1 - \frac{\frac{P_{H_2O}}{P_{H_2} P_{CO}}}{\left.\frac{P_{H_2O}}{P_{H_2} P_{CO}}\right|_{eq}} \right) \tag{10}$$

Equation 10 expresses the fact that rate can be related to a driving force or distance from equilibrium (i.e., $\{1 - \frac{\left(\frac{P_{H_2O}}{P_{H_2} P_{CO}}\right)}{\left.\frac{P_{H_2O}}{P_{H_2} P_{CO}}\right|_{eq}}\}$).

A visual representation of this "driving force" is given in Figure 52. In Figure 52 a plot of the percentage of the theoretical equilibrium constant versus the actual experimental ratio for reaction E and reaction D is presented.

$$H_2 + CO \rightleftarrows H_2O + C \tag{E}$$

$$2CO \rightleftarrows CO_2 + C \tag{D}$$

Again, solid symbols represent runs where weight gain was observed; open symbols were runs where no weight change was observed. The data for runs A-58 (triangles) and A-59 (diamonds) clearly show a critical driving force for reaction (distance from equilibrium) must exist before weight gain will be observed. This appears to be true even though α-iron is present to catalyze the reaction.

In order to verify if this critical driving force could account for some of the deviation observed when determining the iron-iron oxide phase boundary, several runs were plotted

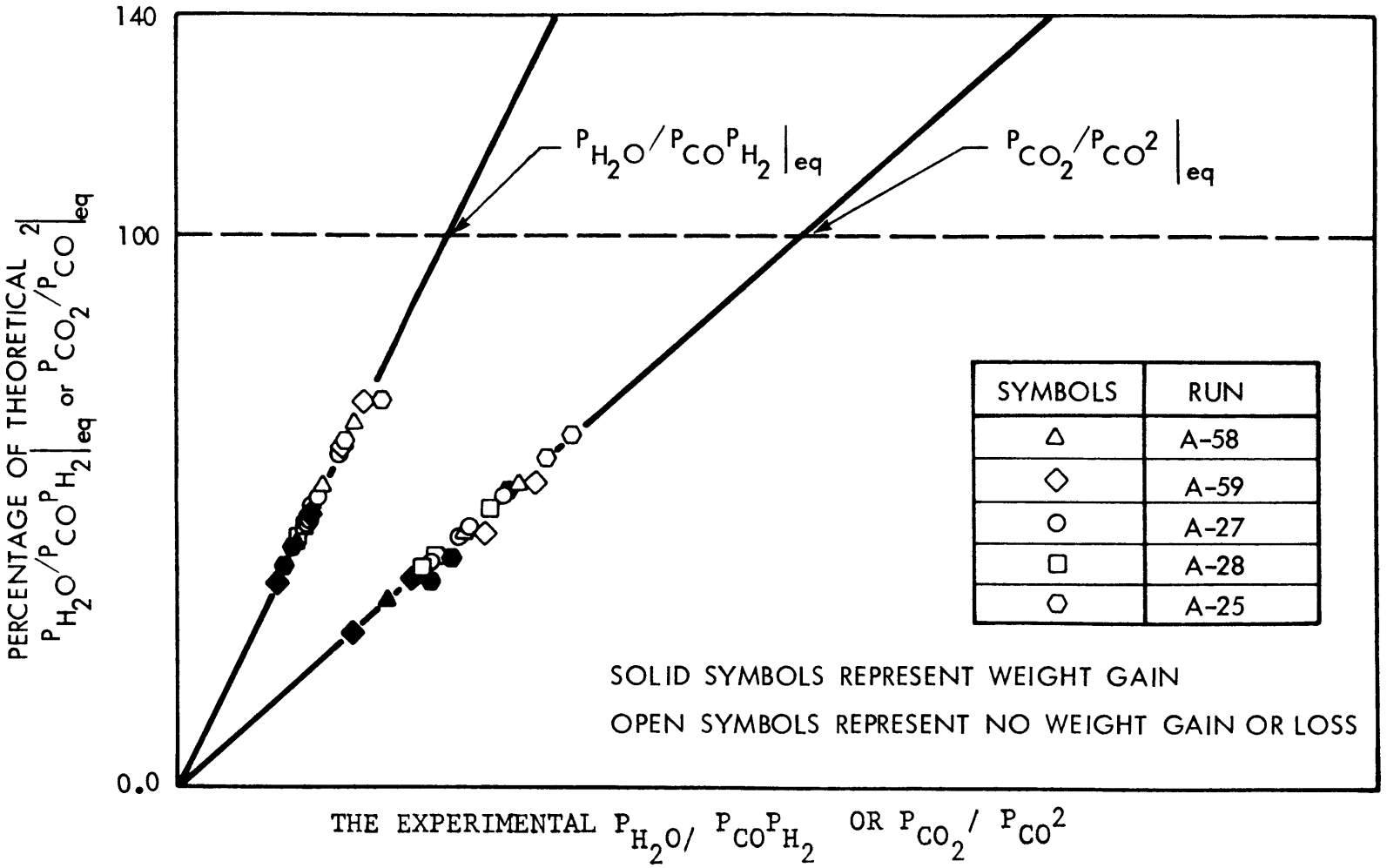

FIGURE 52 PERCENTAGE OF THEORETICAL $P_{H_2O}/P_{CO}P_{H_2}\big|_{eq}$ AND $P_{CO_2}/P_{CO}{}^2\big|_{eq}$ VERSUS THE EXPERIMENTAL $P_{H_2O}/P_{CO}P_{H_2}$ OR $P_{CO_2}/P_{CO}{}^2$

from that study. Runs A-27 (circles) and A-28 (squares) were two runs at an O/H ratio equal to 0.5. No appreciable weight gains were noticed in either runs A-27 or A-28, even though the P_{H_2}/P_{H_2O} ratio was in the region where α-iron would be the expected iron phase. Figure 52 indicates that in both these runs, within experimental error, the critical driving force was not achieved.

Run A-25 is also plotted in Figure 52 and is represented by hexagon-shaped symbols. This run was found to predict accurately the iron-iron oxide phase boundary at an O/H ratio equal to 0.5. Within experimental error, one again sees that carbon deposition will not occur until the driving force for carbon deposition is in the critical region.

It should be pointed out that this critical driving force or distance from equilibrium will not cause carbon deposition to occur if the surface is oxidized (run A-19).

This analysis suggests that two factors are important in determining if carbon deposition will occur: first, the catalyst surface must be in the reduced state; second, the $P_{H_2O}/P_{H_2}P_{CO}$ and/or P_{CO_2}/P_{CO^2} ratio must be sufficiently far away from their equilibrium values to insure a large driving force for reaction.

4.2.7 Effect of Iron-Iron Oxide (Fe_3O_4) at 800 K

Having determined $Fe_{(1-y)}O$ (wustite) is not a catalyst for carbon deposition, the next step was to determine the effect of Fe_3O_4 on carbon deposition, Fe_3O_4 (magnetite) being

the stable oxide in equilibrium with alpha-iron at 800 K.

4.2.8 Catalyst Preconditioning at 800 K

The standard method for preconditioning was used at 800 K. Again, this consisted of running a predetermined carbon dioxide-water mixture over the catalyst at reaction temperature, followed by reduction with hydrogen. Figure 53 is a comparison between the rate of oxidation at 800 and 900 K. As shown the rate of oxidation at 900 K was substantially greater than at 800 K. The behavior shown in Figure 53 at 800 K is characteristic of a process controlled by solid state diffusion. As indicated in Section 2.2.2, if solid state diffusion is important, electron micrographs of the reduced surface should indicate a dense thin iron layer.

In Figure 54 are several electron micrographs of a catalyst strand after standard preconditioning. Micrograph (a) shows a boundary which delineates between the smooth core and the rough, irregular and dense outer surface. The morphology shown in micrograph (a) indicates, in agreement with Figure 53, that solid state diffusion is important in oxidation and reduction at 800 K. Micrograph (b) is a high-magnification photograph of the boundary shown in micrograph (a). Again, notice the rather irregular dense outer shell compared to the featureless inner core. A final micrograph of the outer shell is shown in micrograph (c). In micrograph (c) a crack showing the thin dimensions of the reduced iron skin is shown.

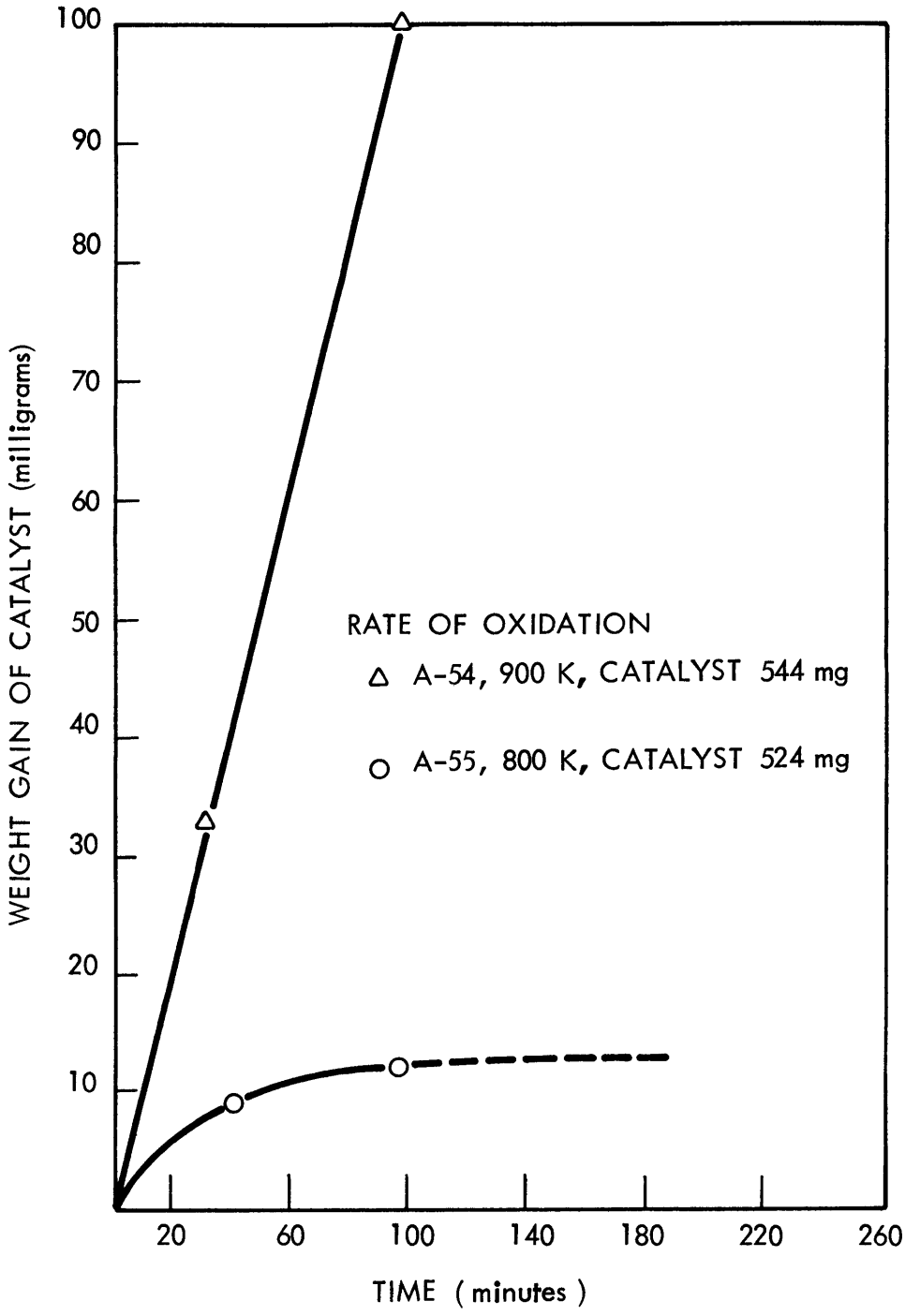

FIGURE 53

WEIGHT GAIN DURING OXIDATION VERSUS TIME AT 800 K AND 900 K

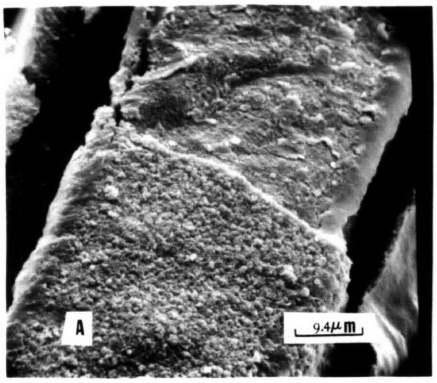

PRECONDITIONED CATALYST
AT 800 K

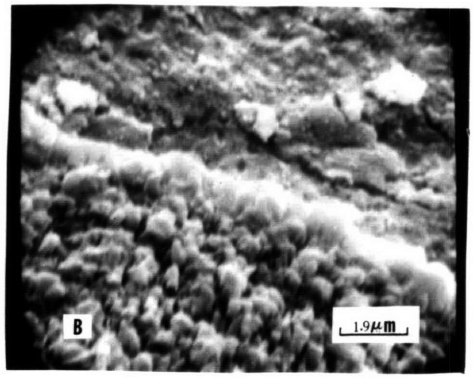

SHELL AND CORE STRUCTURE

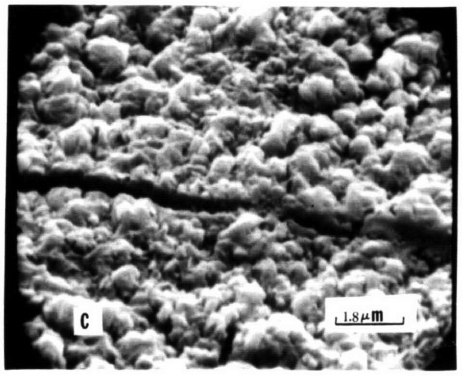

OUTER SHELL

FIGURE 54 PRECONDITIONED CATALYST AT 800 K

The micrographs in Figure 54 and the data shown in Figure 53 indicate that different processes are controlling oxidation and reduction at 800 and 900 K. At 900 K the reduction process is seen to be controlled by the mechanisms involved with gas-solid reactions. At 800 K, however, the overall reduction process appears to be controlled by solid state diffusion.

4.2.9 Carbon Inhibition at 800 K - Fe_3O_4/α-Fe Phase Boundary

The inhibiting effects of Fe_3O_4 on carbon deposition from a five component gas mixture were next investigated. Again, using the procedure outlined in Section 3.2.1, gas compositions were set by adjusting the P_{H_2}/P_{H_2O} ratio at a fixed O/H ratio, temperature and pressure. Figure 55 illustrates the data obtained at three different O/H ratios over a pre-carboned catalyst at 800 K. Two runs were made at each O/H ratio; one approaching the equilibrium phase boundary from the oxide side, the other from the reduced side. As shown in Figure 55, the data are in excellent agreement with the theoretically predicted α-Fe/Fe_3O_4 phase boundary. The effluent concentrations of all runs indicated that methane remained constant; the weight gain observed resulted from carbon monoxide conversion. However, again no definitive statement as to the carbon deposition mechanism could be made.

Considering the scatter observed in the data at 900 K, the excellent agreement between the predicted and experimentally determined phase boundary at 800 K may at first seem

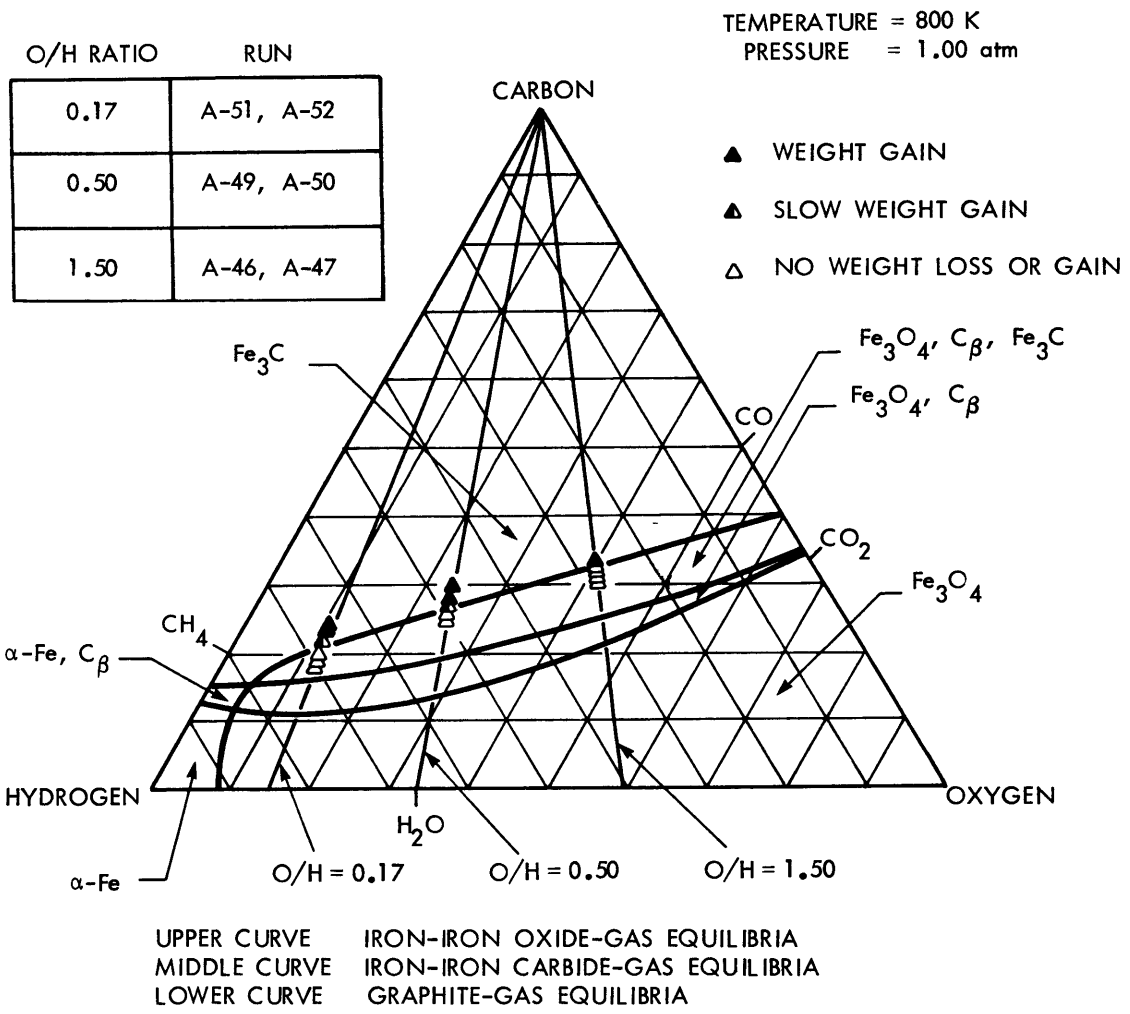

FIGURE 55 INHIBITION OF CARBON DEPOSITION BY Fe_3O_4 AT VARIOUS O/H RATIOS

unusual. However, if one looks at the iron-iron oxide phase diagram in Figure 16, Section 2.2.1, the answer becomes apparent. At temperatures below 833-843 K, the amount of water the system can hold (i.e., oxygen activity) before a second oxide phase forms far exceeds that at temperatures above 833-843 K. Thus, the very serious problem of multiple oxide formation with its concomitant kinetics problems is nonexistent. In fact, in general, at temperatures below 833 K, serious structural change during reaction would not be expected for a steel wool catalyst. That is, structural changes other than those from fiber formation (i.e., sintering, creep).

5. Application of Results

Section 4 presented data which indicated that iron oxides inhibit carbon deposition, one of the important reactions in the Bosch reaction sequence. Also, carbide formation was shown to be slow relative to the rates of oxidation and carbon deposition. Carbide formation, being slow, should not present a problem in an optimal Bosch design. The oxide limitation, however, must be carefully avoided and/or utilized to maximize Bosch efficiency.

The maximum water concentration which can be achieved in the Bosch process, at a specified temperature, is given at the intersection of the graphite-gas/iron-iron oxide phase boundaries.

The reason for this is a complex one. However, one can verify this statement by looking at Figure 56 and visualizing the following.

Envision a series of lines radiating out from the position representing water on the triangular phase diagram. From the properties of equilibrium phase diagrams, any gas mixture having a composition lying closer to the point representing water (for example, point 5) will have a higher water content than another point (point 3) which is further away. Strictly speaking, these points must be colinear with the position representing water.

To the right of the intersection (point 5), the highest water concentration will be given by a gas mixture in

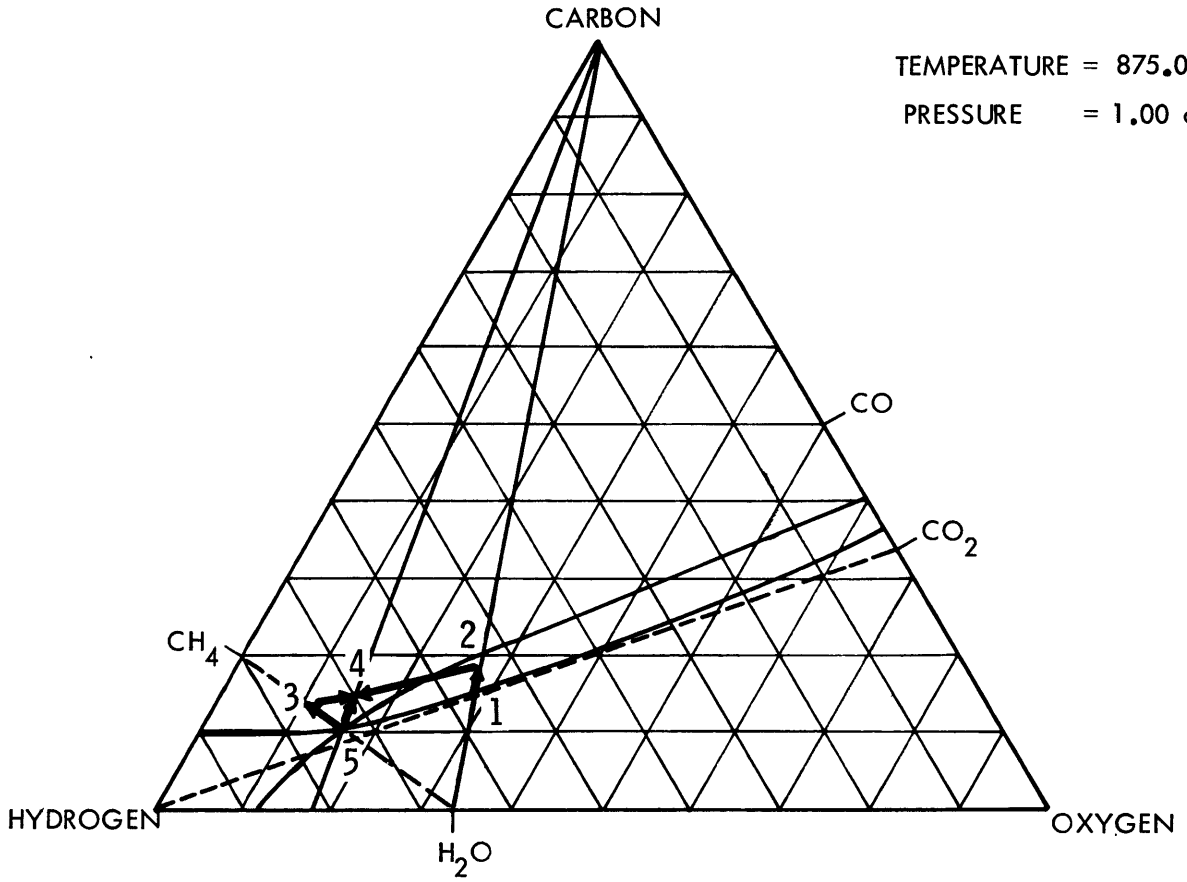

UPPER CURVE IRON-IRON OXIDE-GAS EQUILIBRIA

LOWER CURVE GRAPHITE-GAS EQUILIBRIA

FIGURE 56 OPTIMAL REACTION FLOWPATH FOR THE BOSCH PROCESS

equilibrium with graphite. That is, the graphite-gas phase boundary is closer to the point representing water than is the iron-iron oxide boundary. Unfortunately, the graphite-gas phase boundary lies below the iron-iron oxide phase boundary in the region where iron oxide is the stable iron phase. Therefore, if a gas mixture were to lie in this region, carbon deposition would stop and the gas composition would approach that at equilibrium with iron oxide. Remember, the gas composition in equilibrium with the iron-iron oxide system has a lower water concentration.

The author believes that this is the factor which limited the production of water in previous Bosch prototype reactors.

To the left of point 5, the iron-iron oxide phase boundary is closer to the position representing water than the graphite-gas phase boundary. Thus, to the left of point 5 the graphite-gas phase equilibrium is limiting the maximum water production.

This simple graphical analysis shows that the one point where the maximum water concentration will exist and where there are no limitations imposed on any reaction in the Bosch sequence is point 5. At point 5 iron, iron oxide, graphite, and a gas phase can all exist at equilibrium.

Manning (1976), assuming iron oxides may not be catalysts for carbon deposition, performed some preliminary optimization studies to determine optimal operating conditions. He assumed that the O/H operating ratio was constrained by mass balances

at 0.5 (i.e., the inlet H_2/CO_2 ratio set by system stoichiometry).

Manning investigated a simple recycle Bosch reactor and a variety of different Bosch reactor configurations with prereactors. These prereactors took advantage of the results of Kusner (1962) and Barkley et al. (1952) who determined that the reverse water-gas shift reaction would go to equilibrium in a packed bed; the idea of the prereactor being to take out some of the water prior to entering the Bosch reactor. He determined the prereactor-Bosch reactor configuration to be the most efficient, efficiency being defined as the total moles recycled/mole of CO_2 processed.

The optimal operating conditions in this case would be determined by the intersection of the optimal O/H ratio (i.e., the interaction between the graphite-gas/iron-iron oxide equilibria, where the O/H ratio equals 0.5) with the operating line for the process where the O/H ratio equals 0.5, the operating line being determined by a line drawn from the carbon apex to the point representing water on a triangular diagram. The optimal conditions were determined to be 10.0 total moles recycled/mole of CO_2 processed at approximately 915 K.

As mentioned previously, the optimal O/H ratio (intersection point) is the point, at any given temperature, where one would ideally like to operate. That is, the point of highest water concentration. This optimal O/H ratio will

increase with temperature. Manning limited his analysis to the case where the O/H ratio throughout the system was fixed by the inlet H_2/CO_2 ratio to a value of 0.5.

This limitation can be overcome, however, if one allows for the addition or removal of hydrogen to the system on start-up. A balance can then be made which equates the product of the recycle rate from the Bosch reactor times the water concentration (at the optimum O/H ratio desired) to the rate at which oxygen, hydrogen, and carbon are being fed to the reactor. This type of design is optimal using a shift reactor to initially take out some of the water. A conceptual reactor design is shown in Figure 57. An actual reaction gas flow path is shown in Figure 56 as envisioned on a triangular phase diagram at 875 K.

Initially, 2 moles of hydrogen are mixed with 1 mole of CO_2 and fed to the shift reactor. Point 1 represents the position of the mixture which must fall on the intersection between the O/H operating line for the shift reactor (i.e., 0.5) and a line drawn from the position of carbon dioxide to the position of hydrogen as represented on the phase diagram. Removing the water formed in the shift reactor, the gas mixture moves along the O/H operating line to point 2. The gas mixture at point 2 is mixed with a gas mixture at point 3 to give point 4. The mixture at point 3 was composed of the Bosch reactor effluent at an O/H ratio of 0.204 minus the water formed. At this point, it should be again pointed out

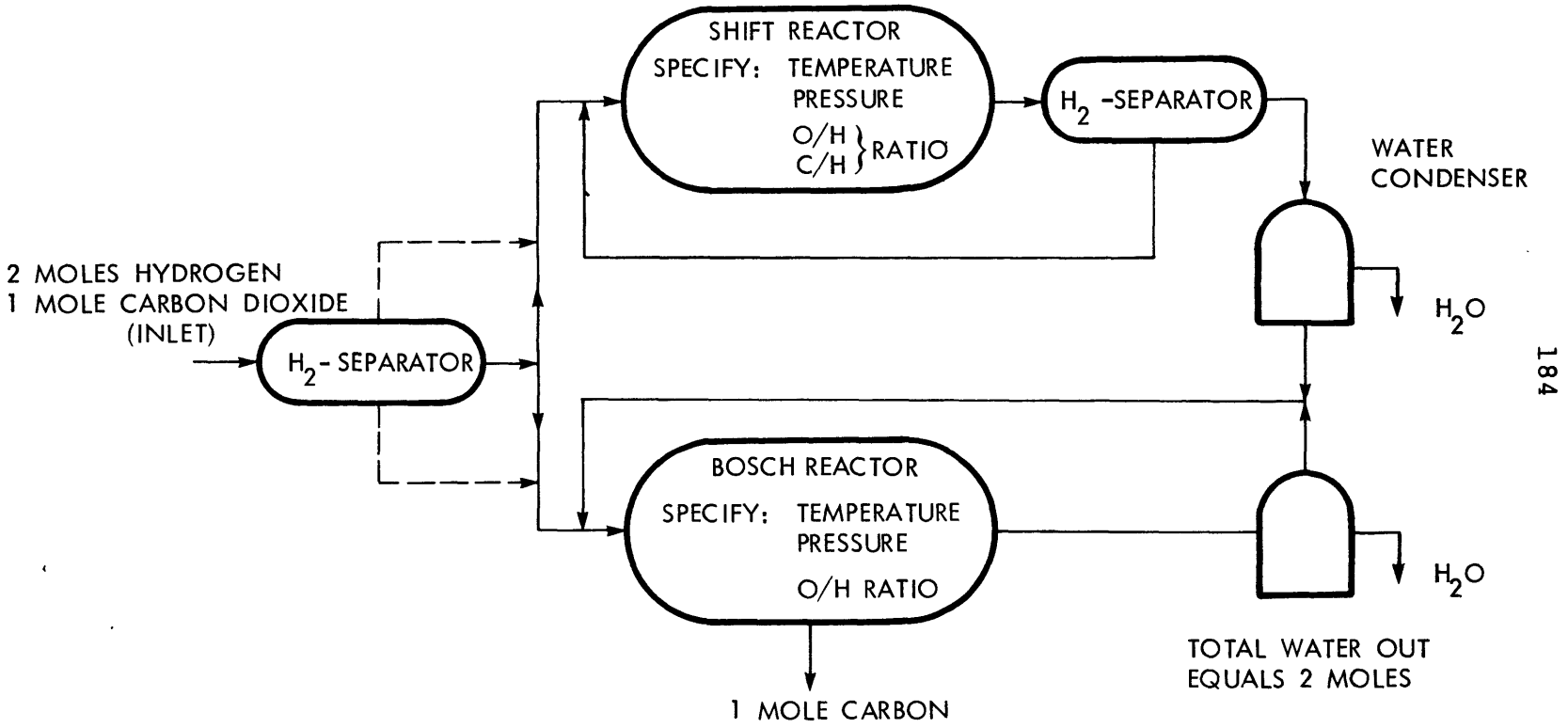

FIGURE 57 DESIGN FOR OPTIMAL REACTOR SYSTEM

hydrogen was added on start-up to initially get this optimum O/H ratio. The gas composition at 4 having an O/H ratio of 0.204 proceeds down the Bosch reactor operating line to the intersection point, at point 5.

Evaluation of this process indicates a minimum recycle ratio of 9.2 at reactor temperature of 875 K for both the shift and Bosch reactors.

The question of the effect of increased hydrogen content in the shift reactor was next addressed; the idea being that perhaps the moles recycled could be sustantially decreased by "pushing" reaction F to the right in the prereactor. This hopefully would allow a larger fraction of water to be produced and consequently removed prior to processing in a Bosch recycle reactor. This could be done by feeding the inlet gases entirely to the shift reactor. Then, using a palladium-silver membrane separator, hydrogen would be recycled to the shift reactor increasing the hydrogen content. Figure 58 is a computer generated plot of the total moles recycled (hydrogen and Bosch recycle) per mole of CO_2 processed in the system versus temperature. The optimal O/H ratio (intersection point) was used in calculating the minimum recycle at each temperature. As shown, the hydrogen recycle increased the <u>total</u> moles recycled per mole of CO_2 processed. The recycle in the Bosch reactor did indeed go down but only insignificantly relative to the increased hydrogen recycle rate.

If one maintains no recycle in the shift reactor, the

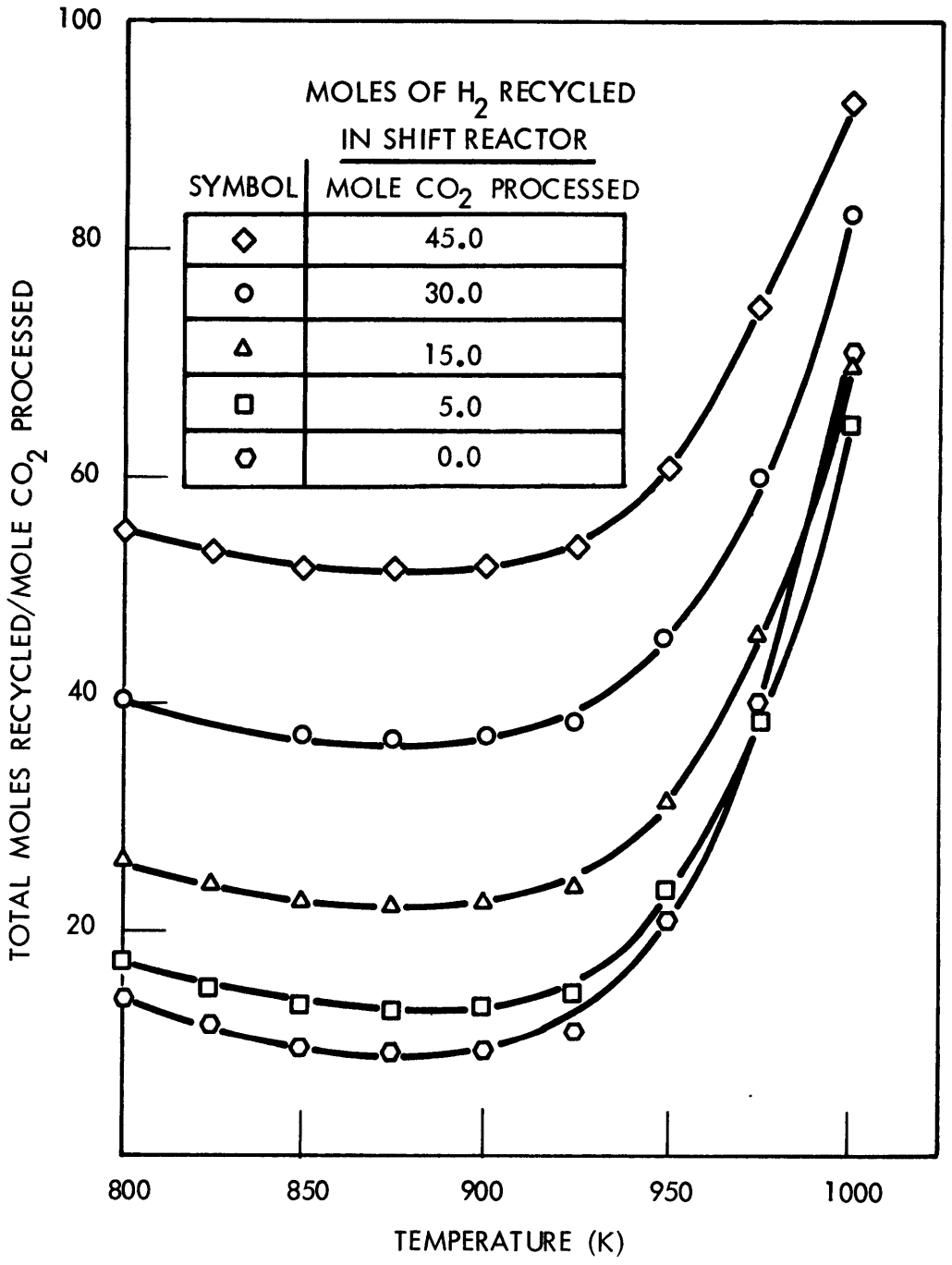

FIGURE 58

EFFECT OF HYDROGEN RECYCLE IN THE SHIFT REACTOR ON TOTAL MOLES RECYCLED

effect of decreased H_2/CO_2 feed ratio to the shift reactor can be investigated by using a palladium-silver membrane separator prior to entering the reactor system, Figure 57. Figure 59 indicates by decreasing the inlet H_2/CO_2 ratio (i.e., increasing the O/H ratio), the minimum moles recycled, again increased.

The reverse water-gas shift reaction is endothermic. The possibility therefore exists for a decrease in minimum recycle with increase in shift reactor temperature relative to Bosch reactor temperature. In Figure 59 the dotted lines shown indicate conditions under which the Bosch reactor is maintained at the temperature indicated by the intersection of the curve for H_2/CO_2 equal to two and the dotted line, while the minimum recycle is obtained by following dotted lines to the desired shift temperature. The total moles recycled is then read off the abscissa. For example, at a Bosch reactor temperature of 875 K if we increase the shift reactor temperature to 950 K (following the dotted line), the total moles recycled is seen to decrease by 3%.

The improvement in Bosch efficiency with increased shift reactor temperature is small. Also, the penalty for increased hydrogen recycle in the shift reactor was shown to be restrictive. Thus, the suggested mode of operation, based on equilibrium consideration alone, is to run both a shift and Bosch reactor at 875 K with a recycle ratio, at the optimum O/H value, of 9.2 total moles recycled per mole of CO_2 processed.

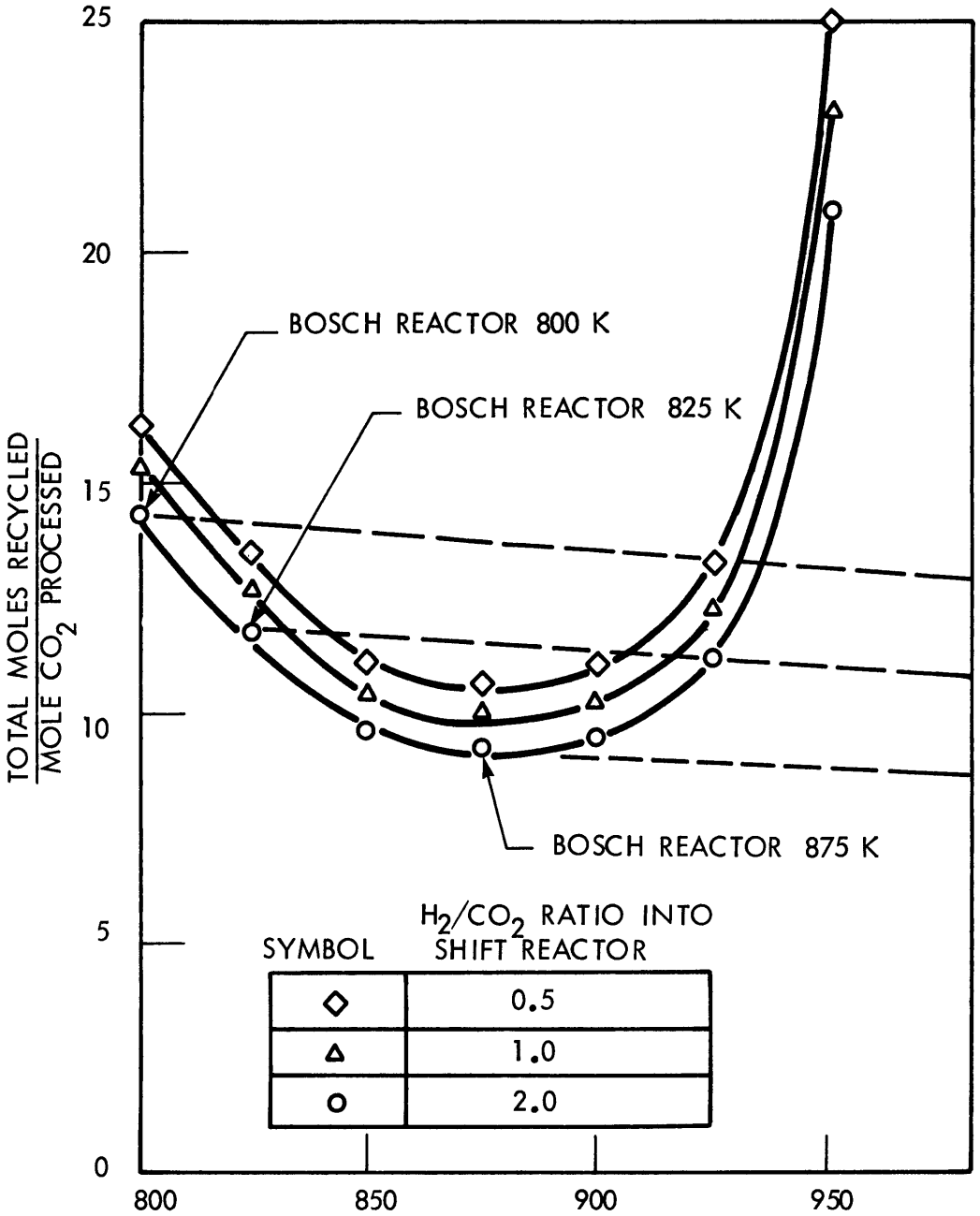

FIGURE 59

EFFECT OF INLET $H_2/CO_2 \leq 2.0$ IN THE SHIFT REACTOR ON TOTAL MOLES RECYCLED

6. Conclusions and Recommendations

6.1 Conclusions

The following conclusions were drawn from the data presented in the Results Section and represent to the best of the author's ability, the essence of these data.

6.1.1 Carbon Deposition and Methane Formation

The results of the preliminary experiments indicate that at high temperature (i.e., >930 K) and high carbon monoxide conversion (i.e., >9%), the Boudouard reaction is the primary carbon formation reaction. At low conversion, no definitive statements can be made. The inability to determine the precise mechanism for carbon deposition at low conversion can be attributed to the inherent errors involved in experimentation and data analysis.

Methane formation has been shown to be kinetically favorable at high temperature ($\geq$930 K). Once formed, methane concentration appears to remain constant.

6.1.2 Preconditioning at 800 K and 900 K

Preconditioning a steel wool catalyst by first oxidizing in carbon dioxide and water and then reducing in hydrogen has been shown to produce two distinct surface structures depending on temperature.

At 800 K, a dense irregular surface is formed around a smooth central core. This type of morphology is representa-

tive of a reduction process which is controlled by solid state diffusion.

When preconditioning is performed at 900 K, the resulting shell and core type morphology is highly porous. This type of reduction can be best represented by a model assuming a porous catalyst structure under diffusion (gas) or mixed diffusion and interfacial reaction control. The outer porous shell has been shown to consist of two distinct layers, suggesting multiple oxide formation. The solid central core appears to be regular and rather smooth in appearance.

6.1.3 Oxidation Effects on Carbon Deposition

Oxide(s) formed at 800 and 900 K were investigated to determine their effect on carbon deposition. The following results were obtained.

6.1.3.1 Effect of Magnetite (Fe_3O_4) Formation

Data have been presented which indicate Fe_3O_4 is not a catalyst for carbon deposition from reaction D or E

$$2CO \rightleftharpoons CO_2 + C \qquad (D)$$

$$CO + H_2 \rightleftharpoons H_2O + C \qquad (E)$$

The theoretically predicted alpha-iron/magnetite phase boundary has been experimentally verified. The location was determined by observing the point at which carbon deposition starts or stops. The solid phase favored during reaction was found to be controlled by adjusting the P_{H_2}/P_{H_2O} ratio (reaction N-B).

$$H_2O + 3/4Fe \rightleftarrows 1/4Fe_3O_4 + H_2 \qquad (N\text{-}B)$$

6.1.3.2 Effect of Wustite ($Fe_{1-y}O$) Formation

Wustite has been shown to inhibit carbon deposition. The theoretically predicted alpha-iron/wustite phase boundary was shown to be accurately predicted by the experimental data. Scatter observed around the phase boundary was attributed to error involved in experimental procedures and data acquisition and reduction. Multiple oxide formation was also shown to be important in predicting the system response at temperatures above 833-843 K.

Although oxide formation was shown to be critical in determining if carbon would deposit, the data indicate a critical driving force for reactions D and E is also of importance.

6.1.4 Carbide Formation and Carbon Inhibition

Carbide formation and/or carbon deposition from methane was shown to be slow at 823 K. Data indicate that methane formation does not proceed primarily through a carbide intermediate. The main methane formation reaction in a carbon, hydrogen, methane system is reaction G, catalyzed by metallic iron.

$$2H_2 + C \rightleftarrows CH_4 \qquad (G)$$

At 900 K, in a 5 component gas mixture, carbon deposition from carbon monoxide has been found to be fast relative to carbide formation. The effect of substantial carbiding on

carbon deposition has not been established. However, due to the slow rate of carbide formation from both carbon monoxide and methane, it is believed that oxide formation presents the limiting factor in efficient Bosch operation.

6.1.5 Structural Effects

A series of transmission and scanning electron micrographs have shown a rather complex series of structural changes can occur during normal Bosch operations. Micrographs have been presented which clearly show the formation of multiple oxides. Depending on temperature, the oxidation-reduction history of the catalyst will greatly effect the structure and associated porosity.

Following standard preconditioning, carbon deposition resulted in the shell or surface layer forming localized fiber bundles. These bundles or nodules were suspended from the main body by hollow, tubular shaped carbon fibers and were determined by electron diffraction analysis to be composed of iron and iron compounds. Carbon fibers were seen to use these nodules as growth centers. The fibers themselves were hollow, tubular, or circular in shape, having electron dense material along their length as well as at their tip.

In combination these various structural effects add a high degree of complexity to any analysis of the Bosch process.

6.2 Recommendations

The conclusions drawn from this investigation lead to the

following recommendations: first, if it is desirable to use steel wool as a catalyst, there is an optimum system design. This optimum design utilizes the knowledge that carbide formation is slow and will not influence process operation. However, care must be taken to avoid and/or utilize oxide formation to maximum advantage. Second, if other transition metal catalysts are investigated, the amount of water or carbon dioxide that the system can maintain before oxidation must be carefully evaluated. This is, hopefully, to avoid the oxide limitation found in this investigation. Also, the rate and conditions under which carbides formed should be carefully evaluated.

6.2.1 Optimal Design

A computer simulation of various reactor systems indicates a reverse water-gas shift prereactor in series with a recycle Bosch reactor is the optimal system design. The optimal operating conditions are 9.2 total moles recycled per mole of CO_2 processed at a temperature of 875 K in both reactors.

6.2.2 Other Catalyst Systems

The iron system has been shown to be restrictive due to oxide formation. Other transition metals such as nickel and cobalt have been known to catalyze all the reaction systems involved in the Bosch sequence but,no determination as to the behavior of their oxides is known. Garmirian and Reid (1977) have shown that oxide formation may not be a problem for these systems. That is, the nickel-nickel oxide and cobalt/cobalt

oxide sytems have equilibrium water concentrations well above that expected for the Bosch system (i.e., the graphite-gas equilibrium). Thus, these two metals are possible candidates for the Bosch process.

In all metallic catalyst systems, the various phases which form during reaction should be closely evaluated. A tractable way to accomplish this is the phase diagram type of analysis used in this investigation.

7.0 Appendix

7.1 Mathematical Model of Iron Oxide Reduction

A general treatment of the methodology used in deriving mathematical models to describe the kinetics of gas-solid reaction is presented below. The models assume, in all cases, that the combined transport and chemical reaction steps can be represented by electrical circuits. These circuits are analyzed using conventional circuit analysis, resulting in the desired mathematical representation.

The rate of removal of oxygen (gram-atoms per second) from a single iron oxide particle is equal to the molar oxygen density of the core times the rate of consumption of the core volume.

$$N_o = C_o \frac{dV}{d\theta} = C_o \, 4\pi \, x_i^2 \frac{dx_i}{d\theta} \tag{11}$$

From the stoichiometry of iron-oxide reduction:

$$\dot{N}_o = \dot{N}_A = -\dot{N}_B \tag{12}$$

where A is the reactant (i.e., hydrogen or carbon monoxide) and B is the product (i.e., water or carbon dioxide). The following are the "resistances" of importance.

7.1.1 Gas-Film Resistance

The molar flux between the bulk stream and the solid surface is given by:

$$\dot{N}_{j,film} = -\left(\frac{k_{m,j}}{R_g T}\ 4\pi\ x_o^2\right) \cdot (P_j^{(b)} - P_j^{(o)}),\ j=A,B \qquad (13_a, 13_b)$$

k_m was determined by:

$$\frac{k_m 2x_o}{D_{AB}} = 2.0 + 0.60 \left(\frac{2x_o G'_\infty}{\mu}\right)^{1/2} \left(\frac{\mu}{\rho D_{AB}}\right)^{1/3} \qquad (14)$$

The physical properties of the gas phase are a function of composition. Thus, the Reynolds and Schmidt numbers were evaluated at the film composition, taken as the arithematic mean of the bulk-phase and the surface composition.

7.1.2 Shell-Layer Resistance

The molar current through a porous layer is given by:

$$\dot{N}_j^{(t)} = -\left(\frac{4\pi x_i x_o}{x_o - x_i}\right) \frac{D_j^{eff}}{R_g T} \cdot (P_j^{(o)} - P_j^{(i)}),\ j=a,b \qquad (15_a, 15_b)$$

$$D_j^{eff} = D_j^{(P)}\ \frac{\varepsilon_{Fe}}{\tau} \qquad (16)$$

$D_j^{(P)}$ is the diffusion coefficient in a single pore, ε_{Fe} is the void fraction of the porous solid layer, and τ is a tortuosity factor depending on structure of the reduced oxide layer.

7.1.3 Interface Resistance

The rate of consumption of reactant (A) and formation of product gas (B) due to chemical reaction is proportional to

the area of the receding interface.

$$-N_o = r_o \, 4\pi \, x_i^2 \tag{17}$$

assuming a first order reversible reaction:

$$r_o = \frac{k_r^{(t)}}{R_g T} \left[P_a^{(i)} - \frac{P_b^{(i)}}{K_e} \right] \tag{18}$$

As an example we can take the case of the dense pellet model developed by Spitzer et al. (1966). Equations 13, 15, and 18 can be put in terms of oxygen removal and summed to eliminate the surface and interface partial pressures.

$$\left[\frac{R_g T}{k_{m,(A)}} \cdot \frac{1}{4\pi x_o^2} \right] \cdot (-\dot{N}_o) = P_A^{(b)} - P_A^{(o)}$$

$$\left[\frac{R_g T}{D_A^{eff}} \cdot \frac{\{x_o - x_i\}}{4\pi x_i \, x_o} \right] \cdot (-\dot{N}_o) = P_A^{(o)} - P_A^{(i)}$$

$$\left[\frac{R_g T}{k_r} \cdot \frac{1}{4\pi x_i^2} \right] \cdot (-\dot{N}_o) = P_A^{(i)} - P_B^{(i)} \; / \; K_e$$

$$\left[\frac{R_g T}{K_e D_B^{eff}} \cdot \frac{\{x_o - x_i\}}{4\pi x_i \, x_o} \right] \cdot (-N_o) = \frac{P_B^{(i)}}{K_e} - \frac{P_B^{(o)}}{K_e}$$

$$\left[\frac{R_g T}{K_e k_{m,(B)}} \cdot \frac{1}{4\pi x_o^2} \right] \cdot (-N_o) = \frac{P_B^{(o)}}{K_e} - \frac{P_B^{(b)}}{K_e}$$

$$\left(\frac{1}{\alpha 4\pi x_o^2} + \frac{x_o - x_i}{\beta 4\pi x_i x_o} + \frac{1}{k_r 4\pi x_i^2} \right) \cdot \{-\dot{N}_o\} = \frac{1}{R_g T} \left\{ P_A^{(b)} - \frac{P_B^{(b)}}{K_e} \right\} \quad (19)$$

where

$$\alpha = \frac{K_e \, k_{m,(A)} \, k_{m,(B)}}{K_e \, k_{m,(B)} + k_{m,(A)}}$$

and

$$\beta = \frac{K_e \, D_A^{eff} \, D_B^{eff}}{K_e \, D_B^{eff} \, D_A^{eff}}$$

substituting equation 11 into equation 19 results in equation 20

$$\frac{dx_i}{d\theta} = - \frac{k_{ov}}{R_g T \, C_o} \left(P_A^{(b)} - \frac{P_B^{(b)}}{K_e} \right) \quad (20)$$

The more complex electrical resistance analogies formulated by Spitzer et al. (1966) and Szekely et al. (1976), used the same basic approach. For additional details, the reader is encouraged to consult the appropriate articles.

7.2 Determination of Triangular Phase Diagrams

In this investigation the catalytic activity of iron oxides and iron carbides for carbon deposition were to be determined. This determination was to be made under actual Bosch operating conditions; the gas phase being composed of CH_4, H_2, H_2O, CO, and CO_2, while the solid phase would consist of carbon deposited on a steel wool catalyst.

A convenient way to approach this problem is to construct

an equilibrium phase diagram including all pertinent solid phases. By simultaneously adjusting the gas phase composition to thermodynamically favor carbon deposition and also to be in the phase region of interest, the catalytic activity of this particular phase could be determined. The solid phase being investigated is determined to be catalytic if a weight increase in the catalyst assembly is noticed and if the reaction effluent indicates carbon monoxide conversion. If no weight increase is observed, the particular phase of interest is assumed to be noncatalytic towards carbon deposition.

There are many different forms of equilibrium phase diagrams. In this investigation the approach developed by Cairns and Tevebaugh (1964) was adopted. Cairns and Tevebaugh derived the equilibrium phase boundary for the graphite-gas system and plotted it on a triangular diagram. These triangular phase diagrams are conveninet in that they graphically indicate the gas phase composition in percentage of O, C, and H in equilibrium with the solid phase of interest.

7.2.1 Graphite-Gas Phase Boundary

To derive the graphite-gas phase boundary one first must determine the intensive variables necessary to completely specify the system. This is accomplished through the application of Gibb's phase rule.

For the graphite-gas system:

N = number of components (CH_4, H_2, H_2O, CO, CO_2, C) = 6

π = " " phases (gas, solid) = 2

$f = 6 + \cancel{2} - \cancel{2} - R = 6 - R$

R, the number of independent reactions, can be shown to equal 3; thus, the number of intensive variables, f = 3. By specifying the pressure and O/H ratio (in the gas phase) at a given temperature, the system is completely fixed.

$$P_{Total} = P_{H_2} + P_{CH_4} + P_{H_2O} + P_{CO} + P_{CO_2} \tag{21}$$

$$O/H = \frac{P_{CO} + P_{H_2O} + 2P_{CO_2}}{2P_{H_2} + 2P_{H_2O} + 4P_{CH_4}} \tag{22}$$

$$2H_2 + C \rightleftarrows CH_4 \qquad K_a = \frac{P_{CH_4}}{P_{H_2}{}^2 \, a_c{}^1} \tag{23}$$

$$H_2 + CO_2 \rightleftarrows CO + H_2O, \qquad K_b = \frac{P_{CO}P_{H_2O}}{P_{H_2}P_{CO_2}} \tag{24}$$

$$3H_2 + CO \rightleftarrows CH_4 + H_2O, \qquad K_c = \frac{P_{CH_4}P_{H_2O}}{P_{CO}P_{H_2}{}^3} \tag{25}$$

Equations 21, 22, 23, 24, and 25 were solved by successive substitution giving a single polynomial of the form.

$$W_6P_{H_2}{}^6 + W_5P_{H_2}{}^5 + W_4P_{H_2}{}^4 + W_3P_{H_2}{}^3 + W_2P_{H_2}{}^2 + W_1P_{H_2} + W_0 = 0 \tag{26}$$

Where W_0-W_6 are expressed as functions of P_{Total}, $\sum_{i=a}^{Z} K_i$, and O/H ratio.

Using conventional iterative search techniques, such as the Newton-Raphson method, P_{H_2} was numerically determined and the procedure was reversed to obtain the remaining partial pressures.

7.2.2 Iron-Iron Oxide-Gas Phase Boundary

Manning (1976) extended the method developed by Cairns and Tevebaugh to the iron-iron oxide equilibrium. Here N = 7, π = 3, and R = 3; thus, f = 3 and again temperature, pressure, and, this time, C/H ratios were specified. The following set of equations was determined to specify completely the system at a given temperature.

$$P_{Total} = P_{H_2} + P_{CH_4} + P_{H_2O} + P_{CO} + P_{CO_2} \tag{21}$$

$$aH_2O + bFe \rightleftarrows Fe_bO_a + aH_2, \qquad K_d = \frac{P_{H_2}^{a}\, a_{Fe_bO_a}^{1}}{P_{H_2O}^{a}\, a_{Fe}^{b}} \tag{27}$$

$$aCO_2 + bFe \rightleftarrows Fe_bO_a + aCO, \qquad K_e = \frac{P_{CO}^{a}\, a_{Fe_bO_a}^{1}}{P_{CO_2}^{a}\, a_{Fe}^{b}\, 1} \tag{28}$$

$$3H_2 + CO \rightleftarrows CH_4 + H_2O, \qquad K_c = \frac{P_{CH_4} P_{H_2O}}{P_{CO} P_{H_2}^{3}} \tag{25}$$

$$C/H = \frac{P_{CO} + P_{CO_2} + P_{CH_4}}{2P_{H_2} + 2P_{H_2O} + 4P_{CH_4}} \tag{29}$$

Again, the method of successive substitutions was used to obtain a single polynomial which was solved using the Newton-Raphson iteractive search technique.

7.2.3 Iron-Iron Carbide-Gas Boundary

The final solid phases of interest were carbides. Following the same approach as discussed previously, the following equations at fixed temperature were found to completely determine the system.

$$P_{Total} = P_{H_2} + P_{H_2O} + P_{CH_4} + P_{CO} + P_{CO_2} \tag{21}$$

$$O/H = \frac{P_{CO} + 2P_{CO_2} + P_{H_2O}}{2P_{H_2} + 2P_{H_2O} + 4P_{CH_4}} \tag{22}$$

$$3Fe + CH_4 \rightleftarrows 2H_2 + Fe_3C \ , \qquad K_g = \frac{a_{Fe_3C}^{1} \, P_{H_2}^{2}}{P_{CH_4} \, a_{Fe}^{3 \ 1}} \tag{30}$$

$$CH_4 + CO_2 \rightleftarrows 2H_2 + 2CO \ , \qquad K_h = \frac{P_{H_2}^{2} \, P_{CO}^{2}}{P_{CO_2} \, P_{CH_4}} \tag{31}$$

$$4H_2 + CO_2 \rightleftarrows CH_4 + 2H_2O \ , \qquad K_I = \frac{P_{CH_4} \, P_{H_2O}^{2}}{P_{CO_2} \, P_{H_2}^{4}} \tag{32}$$

Following the same mathematical procedure as before, the solution of these equations determined the appropriate gas phase composition in equilibrium with iron and iron carbide.

The numerical solution for each of the individual phase boundaries was done by subroutine computer programs which were loaded on call to a main plotting routine as desired. The main plotting routine and support subroutines are shown at the end of this section. Figure 60 is a sample of a typical triangular phase diagram showing the various solid phase regions.

7.2.4 Determination of Reactant Gas Compositions

The inlet gas compositions were determined in a similar fashion. In order to be able to move from one phase field to the next, it was necessary to be able to fix the P_{H_2}/P_{H_2O} at a desired value as well as the temperature, pressure, and O/H or C/H ratios. Thus, the number of intensive variables (f) is seen to be:

$$f = N + 2 - \pi - R - 4$$

Assuming initially that all solid phases will catalyze all reactions which make up the Bosch reaction sequence, $\pi = 1$ (gas), $R = 2$ (reactions 24 and 25), fixing temperature, pressure, C/H or O/H and the P_{H_2}/P_{H_2O} ratio for the 5 component gas mixture will completely specify the system. A computer program is shown at the end of the section which calculates the gas composition, gives the appropriate flow settings for the feed gas delivery section, and sets the saturator bath temperature.

This approach presents a straight-forward way to obtain the desired gas compositions over the phase field of interest.

```
C     TDIA CONSTRUCTS A TRIANGLER PHASE DIAGRAM AND LABELS IT                AL 001
C     EQKS CALCULATES THE APROPRIATE EQUILBRIUM CONSTANTS, ASSUMING IDEA     AL 002
C     L GAS CONDITIONS AND UNIT FUGASITY FOR CONDENSED PHASES                AL 003
C     GRAPH CONSTRUCTS THE GRAPHITE GAS PHASE BOUNDARY                       AL 004
C     BFE3C CALCULATES THE CARBON -OXYGEN HYDROGEN-OXYGEN BOUNDARY CONDI     AL 005
C TION FOR THE FE3C-FE-GAS PHASE BOUNDARY                                    AL 006
C     FE3C CONSTRUCTS THE FE3C- FE-GAS PHASE BOUNDARY                        AL 007
C     BIHO  CALCULATES THE HYDROGEN-OXYGEN BOUNDARY CONDITION FOR THE IR     AL 008
C ON-IRON OXIDE PHASE BOUNDARY                                               AL 009
C     BICO CALCULATES THE CARBON-OXYGEN BOUNDARY CONDITION FOR THE IRON-     AL 010
C IRON OXIDE PHASE BOUNDARY                                                  AL 011
C     IRON CONSTRUCTS THE IRON-IRON OXIDE PHASE BOUNDARY                     AL 012
C     BHC CALCULATES THE HYDROGEN-CARBON BOUNDARY CONDITION FOR THE GRAP     AL 013
C HITE-GAS PHASE BOUNDARY                                                    AL 014
C     BGCO CALCULATES THE CARBON-OXYGEN BOUNDARY FOR THE GRAPHITE-GAS EQ     AL 015
C UILIBRIUM                                                                  AL 016
      EXTERNAL IEOEQ,TCT2,DA                                                 AL 017
      COMMON CO,C1,C2,C3,C4,C5,C6,EPS,IEND,XST                               AL 018
      PRES=1.                                                                AL 019
      PI=3.14159                                                             AL 020
      K=1                                                                    AL 021
      DO 10 I=1,K,1                                                          AL 022
      CALL SCALF(1.,1.,0.0,2.)                                               AL 023
      READ(2,999)TEMP                                                        AL 024
  999 FORMAT(F5.1)                                                           AL 025
         CALL    EQKS(TEMP,EQCH4,EQCO2,EQH2O,EQH2,EQCO,EQC,EQFE3,EQFE2,E     AL 026
     1QCO1,EQH21)                                                            AL 027
      CALL DATSW(7,J)                                                        AL 028
      IF(J-1)22,98,99                                                        AL 029
   22 WRITE(3,269)                                                           AL 030
  269 FORMAT('TROUBLE IN DATSW')                                             AL 031
      GO TO 99                                                               AL 032
   98 WRITE(3,97)                                                            AL 033
   97 FORMAT(4X,'KCH4',4X,'KCO2',4X,'KH2O',4X,'KH2',5X,'KCO',5X,'KC',5X,     AL 034
     1'KFE3C',3X,'KFE2C',4X,'KCO1',4X,'KH21')                                AL 035
```

```
      WRITE(3,900)EQCH4,EQCO2,EQH2O,EQH2,EQCO,EQC ,EQFE3,EQFE2,EQCO1,EQH   AL 036
     121                                                                    AL 037
  900 FORMAT(1X,10F8.3)                                                     AL 038
   99 CONTINUE                                                              AL 039
      CALL TDIA(TEMP,PRES)                                                  AL 040
      CALL BIHO(PRES,EQH2,PIH2,PIH2O)                                       AL 041
      CALL BICO(PRES, EQCO,PICO,PICO2)                                      AL 042
      CALL IRON(EQH2,EQH2O,EQCO,IEOEQ,TCT2,PIH2,PIH2O,PICO,PICO2,TEMP)      AL 043
      CALL BHC (PRES,EQCH4,PGH2,PGCH4)                                      AL 044
      CALL BGCO(PRES,EQC,PGCO,PGCO2)                                        AL 045
      CALL GRAPH(EQCO2,EQH2O,EQCH4,IEOEQ,TCT2,PGH2,PGCH4,PGCO,PGCO2,TEMP    AL 046
     1)                                                                     AL 047
      CALL BFE3C(PRES,EQFE2,EQFE3,PFCO,PFCO2,PFCH4,PFH2)                    AL 048
      CALL FE3C(EQFE3,EQCO1,EQH21,IEOEQ,TCT2,PFH2,PFCH4,PFCO,PFCO2,DA,TE    AL 049
     1MP)                                                                   AL 050
   10 CONTINUE                                                              AL 051
      CALL EXIT                                                             AL 052
      END                                                                   AL 053
```

```
      SUBROUTINE TDIA(TEMP,PRES)                                          TDIA 001
C TDIA USED TO CONSTRUCT A TRIAN(ULER PHASE DIAGRAM FOR THE IRON, IRON-O  TDIA 002
C XIDE, IRON-CARBIDE, CARBON, NICKEL-NICKEL OXIDE, COBALT-COBALT OXIDE A  TDIA 003
C ND GAS SYSTEMS                                                          TDIA 004
    1 FORMAT('HYDROGEN')                                                  TDIA 005
    2 FORMAT('OXYGEN')                                                    TDIA 006
    3 FORMAT('CARBON')                                                    TDIA 007
    4 FORMAT('UPPER CURVE*')                                              TDIA 008
    5 FORMAT('IRON-IRON OXIDE-GAS EQUILIBRIA')                            TDIA 009
    6 FORMAT('LOWER CURVE*')                                              TDIA 010
    7 FORMAT('GRAPHITE-GAS EQUILIBRIA')                                   TDIA 011
    8 FORMAT('TEMP.=', F6.2,'K')                                          TDIA 012
    9 FORMAT('PRES.=',F4.2,'ATM')                                         TDIA 013
   11 FORMAT('CO')                                                        TDIA 014
   12 FORMAT('CO2')                                                       TDIA 015
   13 FORMAT('H2O')                                                       TDIA 016
   14 FORMAT('CH4')                                                       TDIA 017
   15 FORMAT('MIDDLE CURVE ')                                             TDIA 018
   16 FORMAT('IRON-IRON CARBIDE-GAS EQUILIBRIA')                          TDIA 019
      CALL FPLOT(3,12.,2.)                                                TDIA 020
      CALL SCALF(.85,.85,0.,0.)                                           TDIA 021
      X=5.                                                                TDIA 022
      Y=5.*SQRT(3.)                                                       TDIA 023
      CALL FPLOT(2,10.,0.0)                                               TDIA 024
      CALL FPLOT(0,X,Y)                                                   TDIA 025
      CALL FPLOT(0,0.,0.)                                                 TDIA 026
      PI=3.14159                                                          TDIA 027
      D=PI/6.                                                             TDIA 028
      X=1.                                                                TDIA 029
      DO 28 I=1,9,1                                                       TDIA 030
      CALL FPLOT(0,X,0.)                                                  TDIA 031
      Z=X-(X*SIN(D))                                                      TDIA 032
      W=X*COS(D)                                                          TDIA 033
      CALL FPLOT(-3,Z,W)                                                  TDIA 034
      X=X+1.                                                              TDIA 035
```

```
      CALL FPLOT(-2,X,0.)                                          TDIA 036
   28 CONTINUE                                                     TDIA 037
      Q=1.                                                         TDIA 038
      C=X                                                          TDIA 039
      DO 29 I=1,9,1                                                TDIA 040
      Z=C-(Q*SIN(D))                                               TDIA 041
      W=Q*COS(D)                                                   TDIA 042
      CALL FPLOT(0,Z,W)                                            TDIA 043
      X=X-1.                                                       TDIA 044
      CALL FPLOT(0,X,0.)                                           TDIA 045
      CALL FPLOT(0,C,0.)                                           TDIA 046
      Q=Q+1.                                                       TDIA 047
   29 CONTINUE                                                     TDIA 048
      Q=1.                                                         TDIA 049
      DO 30 I=1,5,1                                                TDIA 050
      Z=C-(Q*SIN(D))                                               TDIA 051
      W=Q*COS(D)                                                   TDIA 052
      CALL FPLOT(3,Z,W)                                            TDIA 053
      T=Q-(Q*SIN(D))                                               TDIA 054
      G=Q*COS(D)                                                   TDIA 055
      CALL FPLOT(2,T,G)                                            TDIA 056
      Q=Q+1.                                                       TDIA 057
      IF(9.-Q)32,34,34                                             TDIA 058
   34 T=Q-(Q*SIN(D))                                               TDIA 059
      G=Q*COS(D)                                                   TDIA 060
      CALL FPLOT(3,T,G)                                            TDIA 061
      Z=C-(Q*SIN(D))                                               TDIA 062
      W=Q*COS(D)                                                   TDIA 063
      CALL FPLOT(2,Z,W)                                            TDIA 064
      Q=Q+1.                                                       TDIA 065
   30 CONTINUE                                                     TDIA 066
   32 CALL FCHAR(-.5,-.3,.1,.1,0.)                                 TDIA 067
      WRITE(7,1)                                                   TDIA 068
      CALL FCHAR(9.62,-.3,.1,.1,0.)                                TDIA 069
      WRITE(7,2)                                                   TDIA 070
```

```
CALL FCHAR(4.6,8.96 ,.1,.1,0.)                                  TDIA 071
WRITE(7,3)                                                      TDIA 072
CALL FCHAR(.6,-.55,.1,.1,.0)                                    TDIA 073
WRITE(7,4)                                                      TDIA 074
CALL FCHAR(2.,-.55,.2,.2,.0)                                    TDIA 075
WRITE(7,5)                                                      TDIA 076
CALL FCHAR(.6,-1.1,.1,.1,.0)                                    TDIA 077
WRITE(7,15)                                                     TDIA 078
CALL FCHAR(2., -1.1,.2,.2,.0)                                   TDIA 079
WRITE(7,16)                                                     TDIA 080
CALL FCHAR(.6,-1.65,.1,.1,.0)                                   TDIA 081
WRITE(7,6)                                                      TDIA 082
CALL FCHAR(2.,-1.65,.2,.2,.0)                                   TDIA 083
WRITE(7,7)                                                      TDIA 084
CALL FCHAR(8.,8.,.2,.2,.0)                                      TDIA 085
WRITE(7,8) TEMP                                                 TDIA 086
CALL FCHAR(8.,7.,.2,.2,.0)                                      TDIA 087
WRITE(7,9) PRES                                                 TDIA 088
CALL FPLOT(3,7.5,4.33)                                          TDIA 089
CALL FPLOT(2,7.5,4.33)                                          TDIA 090
CALL POINT(1)                                                   TDIA 091
CALL FCHAR(7.55,4.33,.1,.1,.0)                                  TDIA 092
WRITE(7,11)                                                     TDIA 093
CALL FPLOT(3,8.33,2.89)                                         TDIA 094
CALL FPLOT(2,8.33,2.89)                                         TDIA 095
CALL POINT(1)                                                   TDIA 096
CALL FCHAR(8.38,2.89,.1,.1,.0)                                  TDIA 097
WRITE(7,12)                                                     TDIA 098
CALL FPLOT(3,3.33,.0)                                           TDIA 099
CALL FPLOT(2,3.33,.0)                                           TDIA 100
CALL POINT(1)                                                   TDIA 101
CALL FCHAR(3.13,-.15,.1,.1,.0)                                  TDIA 102
WRITE(7,13)                                                     TDIA 103
CALL FPLOT(3,1.,1.73)                                           TDIA 104
CALL FPLOT(2,1.,1.73)                                           TDIA 105
```

```
CALL POINT(1)                                                    TDIA 106
CALL FCHAR(.61,1.73,.1,.1,.0)                                    TDIA 107
WRITE(7,14)                                                      TDIA 108
RETURN                                                           TDIA 109
END                                                              TDIA 110
```

```
      SUBROUTINE BFE3C(PRES,EQFE2,EQFE3,PFCO,PFCO2,PFCH4,PFH2)          BFE3C 001
C CALCULATES THE BOUNDARY CONDITIONS FOR *FE3C*                         BFE3C 002
      PCO=(-1.+SQRT(1.+4.*EQFE2*PRES))/(2.*EQFE2)                       BFE3C 003
      IF(PCO)3,2,2                                                      BFE3C 004
    2 PCO2=PRES-PCO                                                     BFE3C 005
      IF(PCO2)3,5,5                                                     BFE3C 006
    3 PCO=(-1.-SQRT(1.+4.*EQFE2*PRES))/(2.*EQFE2)                       BFE3C 007
      IF(PCO)4,6,6                                                      BFE3C 008
    6 PCO2=PRES-PCO                                                     BFE3C 009
      IF(PCO2)4,5,5                                                     BFE3C 010
    5 PFCO2=PCO2                                                        BFE3C 011
      PFCO=PCO                                                          BFE3C 012
      PH2=(-EQFE3+SQRT((EQFE3**2.)+4.*EQFE3*PRES))/2.                   BFE3C 013
      IF(PH2)7,8,8                                                      BFE3C 014
    8 PCH4=PRES-PH2                                                     BFE3C 015
      IF(PCH4)7,12,12                                                   BFE3C 016
    7 PH2=(-EQFE3-SQRT((EQFE3**2.)+4.*EQFE3*PRES))/2.                   BFE3C 017
      IF(PH2)10,11,11                                                   BFE3C 018
   11 PCH4=PRES-PH2                                                     BFE3C 019
      IF(PCH4)10,12,12                                                  BFE3C 020
    4 WRITE(3,13)                                                       BFE3C 021
   13 FORMAT(1X,'PROBLEM IN BFE3C, PFCO*PFCO2 SECTION')                 BFE3C 022
      GO TO 5                                                           BFE3C 023
   10 WRITE(3,14)                                                       BFE3C 024
   14 FORMAT(1X,'PROBLEM IN BFE3C, PFH2*PFCH4 SECTION')                 BFE3C 025
   12 PFH2=PH2                                                          BFE3C 026
      PFCH4=PCH4                                                        BFE3C 027
      RETURN                                                            BFE3C 028
      END                                                               BFE3C 029
```

```
      SUBROUTINE FE3C(EQFE3,EQCO1,EQH21,IEOEQ,TCT2,PFH2,PFCH4,PFCO,PFCO2  FE3C 001
     1,DA,TEMP)                                                          FE3C 002
C CONSTRUCTS THE IRON-IRON CARBIDE PHASE BOUNDARY                        FE3C 003
      EXTERNAL TCT2                                                      FE3C 004
      COMMON CO,C1,C2,C3,C4,C5,C6,EPS,IEND,XST                           FE3C 005
      PI=3.14159                                                         FE3C 006
      PRES=1.                                                            FE3C 007
      N=0                                                                FE3C 008
      Z=PI/6.                                                            FE3C 009
      PH2O=0.0                                                           FE3C 010
      PCO=0.0                                                            FE3C 011
      PCO2=0.0                                                           FE3C 012
      ATOMH=2.*PH2O+2.*PFH2+4.*PFCH4                                     FE3C 013
      ATOMC=PCO+PCO2+PFCH4                                               FE3C 014
      ATOMO=0.0                                                          FE3C 015
      ATOMT=ATOMC+ATOMH+ATOMO                                            FE3C 016
      ULH=10.-(ATOMH/(ATOMT*.1))                                         FE3C 017
      ULO=ATOMO/(ATOMT*.1)                                               FE3C 018
      ULC=ATOMC/(ATOMT*.1)                                               FE3C 019
      X1=ULH-(ULH-ULO)*SIN(Z)                                            FE3C 020
      Y1=(ULH-ULO)*COS(Z)                                                FE3C 021
      XST=PFH2*PRES                                                      FE3C 022
      PTEST=PFH2                                                         FE3C 023
      IEND=1000                                                          FE3C 024
      EPS=.001                                                           FE3C 025
      CALL FPLOT(3,X1,Y1)                                                FE3C 026
      CALL FPLOT(2,X1,Y1)                                                FE3C 027
      ROH=.01                                                            FE3C 028
   84 D=2.*ROH                                                           FE3C 029
         CALL    DA(PRES,D,EQFE3,EQCO1,EQH21,A,B,C,E,AA,BB,CC,DD,EE,G,Z,  FE3C 030
     1W,T,X,TL,FF,GG,HH )                                                FE3C 031
      CO=T*HH+TL*EE                                                      FE3C 032
      C1=HH*X+T*GG+TL*DD-A*EE                                            FE3C 033
      C2=HH*W+GG*X+FF*T+TL*CC-A*DD                                       FE3C 034
      C3=HH*Z+W*GG+X*FF+TL*BB-A*CC                                       FE3C 035
```

```
      C4=GG*Z+W*FF+TL*AA-A*BB                                                    FE3C 036
      C5=FF*Z-A*AA                                                               FE3C 037
      C6=0.0                                                                     FE3C 038
   45 CALL IEOEQ (X,F,DERF,TCT2,XST,EPS,IEND,IER)                                FE3C 039
      IF(IER-1)42,43,44                                                          FE3C 040
   43 IEND=10000                                                                 FE3C 041
      EPS=.001                                                                   FE3C 042
      GO TO 45                                                                   FE3C 043
   44 XST=XST+.01                                                                FE3C 044
      GO TO 45                                                                   FE3C 045
   42 PH2=X                                                                      FE3C 046
      PCH4=(PH2**2.)/EQFE3                                                       FE3C 047
      S=AA*(PH2**4.)+BB*(PH2**3.)+CC*(PH2**2.)+DD*(PH2)+EE                       FE3C 048
      Y=FF*(PH2**2.)+GG*(PH2)+HH                                                 FE3C 049
      PCO2=S/Y                                                                   FE3C 050
      PH2O=(PRES/D)-A*PH2-(B/EQFE3)*(PH2**2.)+(1./D)*(S/Y)                       FE3C 051
      PCO=PH2O/(G*PH2)                                                           FE3C 052
      PRES= PH2+PH2O+PCO+PCO2+PCH4                                               FE3C 053
      RCH=(PCO+PCO2+PCH4)/(2.*(PH2+PH2O)+4.*PCH4)                                FE3C 054
      CRHM=PH2/PCH4                                                              FE3C 055
      CRCC2=PCO/PCO2                                                             FE3C 056
      CRHW=PH2/PH2O                                                              FE3C 057
      CALL DATSW(8,J)                                                            FE3C 058
      IF(J-1)22,98,99                                                            FE3C 059
   22 WRITE(3,269)                                                               FE3C 060
  269 FORMAT('TROUBLE IN DATSW')                                                 FE3C 061
      GO TO 99                                                                   FE3C 062
   98 IF(N)695,695,694                                                           FE3C 063
  695 N=N+1                                                                      FE3C 064
      WRITE(3,691)                                                               FE3C 065
  691 FORMAT(///,44X,'IRON-IRON CARBIDE-GAS EQUILIBRIUM',/)                      FE3C 066
      WRITE(3,692) TEMP,PRES                                                     FE3C 067
  692 FORMAT(38X,'TEMPERATURE=',F5.1,'K',3X,'TOTAL PRESSURE=',F2.0,'ATM'         FE3C 068
     1)                                                                          FE3C 069
  694 WRITE(3,97)                                                                FE3C 070
```

```
 97 FORMAT(5X,'PH2',8X,'PH2O',7X,'PCO',8X,'PCO2',7X,'PCH4',4X,'PRESSUR   FE3C 071
   1E',5X,'O/H',9X,'C/H',4X,'PH2/PH2O',4X,'PCO/PCO2',4X,'PH2/PCH4')     FE3C 072
    WRITE(3,100)PH2,PH2O,PCO,PCO2,PCH4,PRES,ROH,RCH,CRHW,CRCC2,CRHM      FE3C 073
100 FORMAT(1X,2F10.6,1X,F10.6,;X,F10.6,F10.6,1X,F10.6,1X,F10.6,1X,F10.   FE3C 074
   16,F6.2,6X,F6.2,6X,F6.2,//)                                          FE3C 075
 99 CONTINUE                                                            FE3C 076
    IF(ABS(PRES-1.)-.01)82,82,(1                                        FE3C 077
 81 ROH=ROH+.01                                                         FE3C 078
    PRES=1.                                                             FE3C 079
    GO TO 84                                                            FE3C 080
 82 IF(PH2-PTEST)87,81,81                                               FE3C 081
 87 ROH=ROH+.05                                                         FE3C 082
    ATOMH=2.*PH2O+2.*PH2+4.*PCH4                                        FE3C 083
    Z=PI/6.                                                             FE3C 084
    ATOMC=PCO+PCO2+PCH4                                                 FE3C 085
    ATOMO=PCO+2.*PCO2+PH2O                                              FE3C 086
    ATOMT=ATOMH+ATOMO+ATOMC                                             FE3C 087
    ULH=10.-(ATOMH/(ATOMT*.1))                                          FE3C 088
    ULO=ATOMO/(ATOMT*.1)                                                FE3C 089
    ULC=ATOMC/(ATOMT*.1)                                                FE3C 090
    X2=ULH-(ULH-ULO)*SIN(Z)                                             FE3C 091
    Y2=(ULH-ULO)*COS(Z)                                                 FE3C 092
    CALL FPLOT(2,X2,Y2)                                                 FE3C 093
    PTEST=PH2                                                           FE3C 094
    PRES=1.                                                             FE3C 095
    XST=PH2*PRES                                                        FE3C 096
    IF(ROH- 6.)85,86,86                                                 FE3C 097
 85 GO TO 84                                                            FE3C 098
 86 CONTINUE                                                            FE3C 099
    PCH4=0.0                                                            FE3C 100
    PH2=0.0                                                             FE3C 101
    PH2O=0.0                                                            FE3C 102
    ATOMH=0.0                                                           FE3C 103
    ATOMC=PFCO+PFCO2+PCH4                                               FE3C 104
    ATOMO=PFCO+2.*PFCO2+PH2O                                            FE3C 105
```

```
ATOMT=ATOMC+ATOMH+ATOMO                                          FE3C 106
ULH=10.-(ATOMH/(ATOMT*.1))                                       FE3C 107
ULO=ATOMO/(ATOMT*.1)                                             FE3C 108
ULC=ATOMC/(ATOMT*.1)                                             FE3C 109
Y3=(ULH-ULO)*COS(Z)                                              FE3C 110
X3=ULH-(ULH-ULO)*SIN(Z)                                          FE3C 111
CALL FPLOT(0,X3,Y3)                                              FE3C 112
CALL FPLOT(3,.0,.0)                                              FE3C 113
RETURN                                                           FE3C 114
END                                                              FE3C 115
```

```
      SUBROUTINE BIHO(PRES,EQH2,PIH2,PIH2O)                              BIHO 001
C CALCULATES THE BOUNDARY CONDITIONS FOR THE HYDROGEN-OXYGEN SYSTEM FOR  BIHO 002
C IRON                                                                   BIHO 003
C     IF TEMP. LESS THAN 860 K 3/4FE+H2O=1/4FE3O4+H2                     BIHO 004
C     IF TEMP. GREATER THAN OR = TO 860 K FE +H2O=FEO+H2                 BIHO 005
      PH2O=PRES/(EQH2+1.)                                                BIHO 006
      IF(PH2O)400,401,401                                                BIHO 007
  401 PH2=PRES-PH2O                                                      BIHO 008
      IF(PH2)400,402,402                                                 BIHO 009
  400 WRITE(3,403)                                                       BIHO 010
  403 FORMAT(1X,'ERROR PRES OR EQH2 IN SUBROUTINE BIHO')                 BIHO 011
  402 PIH2O=PH2O                                                         BIHO 012
      PIH2=PH2                                                           BIHO 013
      RETURN                                                             BIHO 014
      END                                                                BIHO 015
```

```
      SUBROUTINE BICO(PRES,EQCO,PICO,PICO2)                              BICO 001
C CALCULATES THE BOUNDARY CONDITIONS FOR THE CARBON-OXYGEN SYSTEM FOR    BICO 002
C IRON                                                                   BICO 003
C     IF TEMP. IS GREATER THAN 860 K 3/4FE+CO2=1/4FE3O4+CO               BICO 004
C     IF TEMP IS LESS THAN OR EQUAL TO 860 K FE+CO2=FEO+CO               BICO 005
      PCO2=PRES/(EQCO+1.)                                                BICO 006
      IF(PCO2)500,501,501                                                BICO 007
  501 PCO= PRES-PCO2                                                     BICO 008
      IF(PCO)500,502,502                                                 BICO 009
  500 WRITE(3,503)                                                       BICO 010
  503 FORMAT(1X,'ERROR IN PRES OR EQCO IN SUBROUTINE BICO')              BICO 011
  502 PICO=PCO                                                           BICO 012
      PICO2=PCO2                                                         BICO 013
      RETURN                                                             BICO 014
      END                                                                BICO 015
```

```
      SUBROUTINE IRON(EQH2,EQH2O,EQCO,IEOEQ,TCT2,PIH2,PIH2O,PICO,PICO2,T   IRON 001
     1EMP)                                                                 IRON 002
C CONSTRUCTS THE IRON-IRON OXIDE PHASE BOUNDARY                            IRON 003
      EXTERNAL TCT2                                                        IRON 004
      COMMON CO,C1,C2,C3,C4,C5,C6,EPS,IEND,XST                             IRON 005
      PI=3.14159                                                           IRON 006
      N=0                                                                  IRON 007
      PTEST=.0                                                             IRON 008
      Z=PI/6.                                                              IRON 009
      PRES=1.                                                              IRON 010
      IEND=10000                                                           IRON 011
      EPS=.001                                                             IRON 012
      RO=.001                                                              IRON 013
      PCH4=0.0                                                             IRON 014
      PCO=0.0                                                              IRON 015
      PCO2=0.0                                                             IRON 016
      ATOMH=2.*PIH2O+2.*PIH2+4.*PCH4                                       IRON 017
      ATOMO=PCO+2.*PCO2+PIH2O                                              IRON 018
      ATOMC=PCO+PCO2+PCH4                                                  IRON 019
      ATOMT=ATOMH+ATOMO+ATOMC                                              IRON 020
      ULH=10.-(ATOMH/(ATOMT*.1))                                           IRON 021
      ULO=ATOMO/(ATOMT*.1)                                                 IRON 022
      ULC=ATOMC/(ATOMT*.1)                                                 IRON 023
      X3=ULH-(ULH-ULO)*SIN(Z)                                              IRON 024
      Y3=(ULH-ULO)*COS(Z)                                                  IRON 025
      CALL FPLOT(-2,X3,Y3)                                                 IRON 026
      XST=PIH2*PRES                                                        IRON 027
   93 CO=-EQH2*PRES*(EQCO+1.)                                              IRON 028
      C1=(2.*RO+1.)*(EQH2+1.)*(EQCO+1.)                                    IRON 029
      C2=(4.*RO-1.)*EQH2*EQCO*EQH2O*(EQH2*PRES)                            IRON 030
      C3=(1.-2.*RO)*(EQH2+1.)*EQH2*EQCO*EQH2O                              IRON 031
      C4=0.0                                                               IRON 032
      C5=0.0                                                               IRON 033
      C6=0.0                                                               IRON 034
      CALL IEOEQ (X,F,DERF,TCT2,XST,EPS,IEND,IER)                          IRON 035
```

```
      PH2=X                                                                 IRON 036
      PH2O=PH2/EQH2                                                         IRON 037
      ABC=(2.*RO*(PH2O+PH2))                                                IRON 038
      DEF=(1./(2.*RO)-1.)                                                   IRON 039
      GHI=(PRES*(4.*RO-1.))                                                 IRON 040
      PQR=(4.*RO*(1./(EQCO)+1.))                                            IRON 041
      PCO=(ABC*DEF+GHI)/PQR                                                 IRON 042
      PCO2=PCO/EQCO                                                         IRON 043
      PCH4=EQH2O*PCO*(PH2**3.)/(PH2O)                                       IRON 044
      P=PH2+PH2O+PCO+PCO2+PCH4                                              IRON 045
      ROH=(PCO+PH2O+2.*PCO2)/(2.*(PH2+PH2O)+4.*PCH4)                        IRON 046
      CRHM=PH2/PCH4                                                         IRON 047
      CRCC2=PCO/PCO2                                                        IRON 048
      CRHW=PH2/PH2O                                                         IRON 049
      CALL DATSW(8,J)                                                       IRON 050
      IF(J-1)22,98,99                                                       IRON 051
   22 WRITE(3,269)                                                          IRON 052
  269 FORMAT('TROUBLE IN DATSW')                                            IRON 053
      GO TO 99                                                              IRON 054
   98 IF(N)695,695,694                                                      IRON 055
  695 N=N+1                                                                 IRON 056
      WRITE(3,691)                                                          IRON 057
  691 FORMAT(///,45X,'IRON-IRON OXIDE-GAS EQUILIBRIUM',/)                   IRON 058
      WRITE(3,692) TEMP,PRES                                                IRON 059
  692 FORMAT(38X,'TEMPERATURE=',F6.1,'K',3X,'TOTAL PRESSURE=',F2.0,'ATM'    IRON 060
     1)                                                                     IRON 061
  694 WRITE(3,97)                                                           IRON 062
   97 FORMAT(5X,'PH2',8X,'PH2O',7X,'PCO',8X,'PCO2',7X,'PCH4',4X,'PRESSUR    IRON 063
     1E',5X,'O/H',9X,'C/H',4X,'PH2/PH2O',4X,'PCO/PCO2',4X,'PH2/PCH4')       IRON 064
      WRITE(3,10 )PH2,PH2O,PCO,PCO2,PCH4,P,ROH,RO,CRHW,CRCC2,CRHM           IRON 065
   10 FORMAT(1X,2F10.6,1X,F10.6,2X,F10.6,F10.6,1X,F10.6,1X,F10.6,1X,F10.    IRON 066
     16,F6.2,6X,F6.2,6X,F6.2,//)                                            IRON 067
   99 CONTINUE                                                              IRON 068
      IF (ABS(P-1.)-.01)92, 92, 91                                          IRON 069
   91 RO=RO+.01                                                             IRON 070
```

```
      GO TO 93                                                          IRON 071
   92 ATOMH=2.*PH2O+2.*PH2+4.*PCH4                                      IRON 072
      ATOMO=PCO+2.*PCO2+PH2O                                            IRON 073
      ATOMC=PCO+PCO2+PCH4                                               IRON 074
      ATOMT=ATOMH+ATOMO+ATOMC                                           IRON 075
      ULH=10.-(ATOMH/(ATOMT*.1))                                        IRON 076
      ULO=ATOMO/(ATOMT*.1)                                              IRON 077
      ULC=ATOMC/(ATOMT*.1)                                              IRON 078
      Y2=(ULH-ULO)*COS(Z)                                               IRON 079
      X2=ULH-(ULH-ULO)*SIN(Z)                                           IRON 080
      CALL FPLOT(2,X2,Y2)                                               IRON 081
      PTEST=PH2                                                         IRON 082
      PRES=1.                                                           IRON 083
      XST=PH2*PRES                                                      IRON 084
      IF(RO- 6.)94,95,95                                                IRON 085
   94 RO=RO+.05                                                         IRON 086
      GO TO 93                                                          IRON 087
   95 CONTINUE                                                          IRON 088
      PH2=0.0                                                           IRON 089
      PH2O=0.0                                                          IRON 090
      PCH4=0.0                                                          IRON 091
      ATOMH=2.*PH2O+2.*PH2+4.*PCH4                                      IRON 092
      ATOMC=PICO+PICO2+PCH4                                             IRON 093
      ATOMO=PICO+2.*PICO2+PH2O                                          IRON 094
      ATOMT=ATOMH+ATOMO+ATOMC                                           IRON 095
      ULH=10.-(ATOMH/(ATOMT*.1))                                        IRON 096
      ULO=ATOMO/(ATOMT*.1)                                              IRON 097
      ULC=ATOMC/(ATOMT*.1)                                              IRON 098
      Y1=(ULH-ULO)*COS(Z)                                               IRON 099
      X1=ULH-(ULH-ULO)*SIN(Z)                                           IRON 100
      CALL FPLOT(0,X1,Y1)                                               IRON 101
      CALL FPLOT(3,0.0,0.0)                                             IRON 102
      RETURN                                                            IRON 103
      END                                                               IRON 104
```

```
      SUBROUTINE BGCO(PRES,EQC,PGCO,PGCO2)                              BGCO 001
C CALCULATES THE BOUNDARY CONDITIONS FOR THE CARBON-OXYGEN SYSTEM FOR *G BGCO 002
C RAPH*                                                                 BGCO 003
      PCO=(-1.+SQRT(1.+4.*EQC*PRES))/(2.*EQC)                           BGCO 004
      IF(PCO)300,301,301                                                BGCO 005
  301 PCO2=PRES-PCO                                                     BGCO 006
      IF(PCO2)300,303,303                                               BGCO 007
  300 PCO=(-1.-SQRT(1.+4.*EQC*PRES))/(2.*EQC)                           BGCO 008
      IF(PCO)304,305,305                                                BGCO 009
  305 PCO2=PRES-PCO                                                     BGCO 010
      IF(PCO2)304,303,303                                               BGCO 011
  304 WRITE(3,306)                                                      BGCO 012
  306 FORMAT(1X,'WE HAVE A PROBLEM IN SUBROUTINE BGCO')                 BGCO 013
  303 PGCO=PCO                                                          BGCO 014
      PGCO2=PCO2                                                        BGCO 015
      RETURN                                                            BGCO 016
      END                                                               BGCO 017
```

```
      SUBROUTINE BHC (PRES,EQCH4,PGH2,PGCH4)                            BHC 001
C CALCULATES THE BOUNDARY CONDITIONS FOR THE CARBON-HYDROGEN SYSTEM FOR  BHC 002
C GRAPH                                                                 BHC 003
      PH2=(-1.+SQRT(1.+4.*EQCH4*PRES))/(2.*EQCH4)                       BHC 004
      IF(PH2)200,201,201                                                BHC 005
  201 PCH4=PRES-PH2                                                     BHC 006
      IF(PCH4)200,203,203                                               BHC 007
  200 PH2=(-1.-SQRT(1.+4.*EQCH4*PRES))/(2.*EQCH4)                       BHC 008
      IF(PH2)204,205,205                                                BHC 009
  205 PCH4=PRES-PH2                                                     BHC 010
      IF(PCH4)204,203,203                                               BHC 011
  204 WRITE(3,206)                                                      BHC 012
  206 FORMAT(1X,'WE HAVE A PROBLEM IN SUBROUTINE BHC')                  BHC 013
  203 PGH2=PH2                                                          BHC 014
      PGCH4=PCH4                                                        BHC 015
      RETURN                                                            BHC 016
      END                                                               BHC 017
```

```
      SUBROUTINE GRAPH(EQCO2,EQH2O,EQCH4,IEOEQ,TCT2,PGH2,PGCH4,PGCO,PGCO  GRAPH 001
     12,TEMP)                                                           GRAPH 002
C CONSTRUCTS THE GRAPHITE-GAS PHASE BOUNDARY                            GRAPH 003
      EXTERNAL TCT2                                                     GRAPH 004
      COMMON CO,C1,C2,C3,C4,C5,C6,EPS,IEND,XST                          GRAPH 005
      PI=3.14159                                                        GRAPH 006
      PRES=1.                                                           GRAPH 007
      N=0                                                               GRAPH 008
      ROH=.01                                                           GRAPH 009
      Z=PI/6.                                                           GRAPH 010
      PH2O=0.0                                                          GRAPH 011
      PCO=0.0                                                           GRAPH 012
      PCO2=0.0                                                          GRAPH 013
      ATOMH=2.*PH2O+2.*PGH2+4.*PGCH4                                    GRAPH 014
      ATOMC=PCO+PCO2+PGCH4                                              GRAPH 015
      ATOMO=0.0                                                         GRAPH 016
      ATOMT=ATOMC+ATOMH+ATOMO                                           GRAPH 017
      ULH=10.-(ATOMH/(ATOMT*.1))                                        GRAPH 018
      ULO=ATOMO/(ATOMT*.1)                                              GRAPH 019
      ULC=ATOMC/(ATOMT*.1)                                              GRAPH 020
      X1=ULH-(ULH-ULO)*SIN(Z)                                           GRAPH 021
      Y1=(ULH-ULO)*COS(Z)                                               GRAPH 022
      XST=PGH2*PRES                                                     GRAPH 023
      PTEST=PGH2                                                        GRAPH 024
      IEND=1000                                                         GRAPH 025
      EPS=.001                                                          GRAPH 026
      CALL FPLOT(3,X1,Y1)                                               GRAPH 027
      CALL FPLOT(2,X1,Y1)                                               GRAPH 028
   84 A=(-PRES*EQCH4)                                                   GRAPH 029
      B=2.*ROH                                                          GRAPH 030
      CC=1.-2.*ROH                                                      GRAPH 031
      D=1.+2.*ROH                                                       GRAPH 032
      AA=(EQCH4*D-PRES*EQH2O*CC)                                        GRAPH 033
      AB=(EQCH4**2.)*(1.+4.*ROH)+EQH2O                                  GRAPH 034
      AC=EQCH4*EQH2O*D                                                  GRAPH 035
```

```
    AD=(-EQCO2*(EQCH4**2.))/(4.*EQH2O)                                  GRAPH 036
    AE=(((-EQCH4*EQCO2)/4.)*(3.-2.*ROH)-2.*EQCH4*ROH)                   GRAPH 037
    AF=((-EQCO2*EQH2O/4.)*CC*(3.+2.*ROH)-4.*ROH*(EQCH4**2.)-2.*EQH2O*   GRAPH 038
   1ROH*D)                                                              GRAPH 039
    AG=((-EQCO2/(4.*EQCH4))*((EQH2O**2.)*(CC**2.)*D)-4.*EQCH4*EQH2O*    GRAPH 040
   1ROH*D)                                                              GRAPH 041
    C0=(A**2.)+AD*A                                                     GRAPH 042
    C1=2.*A*AA+AD*AA+A*AE                                               GRAPH 043
    C2=2.*A*AB+(AA**2.)+AD*AB+A*AE+A*AF+(EQCH4**2.)*(ROH**2.)           GRAPH 044
    C3=2.*A*AC+2.*AA*AB+AD*AC+AE+AF*AA+A*AG+2.*(ROH**2.)*EQCH4*         GRAPH 045
   1EQH2O*D+4.*(ROH**2.)*(EQCH4**3.)                                    GRAPH 046
    C4=2.*AA*AC+(AB**2.)+AC*AE+AF*AB+AG*AA+(EQH2O**2.)*(ROH**2.)*       GRAPH 047
   1(D**2.)+4.*(EQCH4**4.)*(ROH**2.)+8.*(ROH**2.)*(EQCH4**2.)*(EQH2O    GRAPH 048
   1)*D                                                                 GRAPH 049
    C5=2.*AB*AC+AF*AC+AB*AG+8.*(EQCH4**3.)*(EQH2O)*(ROH**2.)*D          GRAPH 050
   1+4.*(ROH**2.)*EQCH4*(EQH2O**2.)*(D**2.)                             GRAPH 051
    C6=AC**2.+AG*AC+4.*(ROH**2.)*(EQCH4**2.)*(EQH2O**2.)*(D**2.)        GRAPH 052
45  CALL IEOEQ (X,F,DERF,TCT2,XST,EPS,IEND,IER)                         GRAPH 053
    IF(IER-1)42,43,44                                                   GRAPH 054
43  IEND=10000                                                          GRAPH 055
    EPS=.001                                                            GRAPH 056
    GO TO 45                                                            GRAPH 057
44  XST=XST+.01                                                         GRAPH 058
    GO TO 45                                                            GRAPH 059
42  PH2=X                                                               GRAPH 060
    PCH4=(PH2**2.)*EQCH4                                                GRAPH 061
    EQ1=EQH2O*(PH2**3.)/(PCH4)                                          GRAPH 062
    PH2O=(2.-2.*(PH2+EQCH4*(PH2**2.))-2.*ROH*(PH2+2.*EQCH4*(PH2**2.     GRAPH 063
   1)))/(2.*ROH+(1./EQ1)+1.)                                            GRAPH 064
    PCO=PCH4*PH2O/(EQH2O*(PH2**3.))                                     GRAPH 065
    PCO2=PH2O*PCO/(PH2*EQCO2)                                           GRAPH 066
    PRES= PH2+PH2O+PCO+PCO2+PCH4                                        GRAPH 067
    RCH=(PCO+PCO2+PCH4)/(2.*(PH2+PH2O)+4.*PCH4)                         GRAPH 068
    CRHM=PH2/PCH4                                                       GRAPH 069
    CRCC2=PCO/PCO2                                                      GRAPH 070
```

```
      CRHW=PH2/PH2O                                                    GRAPH 071
      CALL DATSW(8,J)                                                  GRAPH 072
      IF(J-1)22,98,99                                                  GRAPH 073
   22 WRITE(3,269)                                                     GRAPH 074
  269 FORMAT('TROUBLE IN DATSW')                                       GRAPH 075
      GO TO 99                                                         GRAPH 076
   98 IF(N)695,695,694                                                 GRAPH 077
  695 N=N+1                                                            GRAPH 078
      WRITE(3,691)                                                     GRAPH 079
  691 FORMAT(///, 48X,'GRAPHITE-GAS EQUILIBRIUM',/)                    GRAPH 080
      WRITE(3,692) TEMP,PRES                                           GRAPH 081
  692 FORMAT(38X,'TEMPERATURE=',F6.1,'K',3X,'TOTAL PRESSURE=',F2.0,'ATM'  GRAPH 082
     1)                                                                GRAPH 083
  694 WRITE(3,97)                                                      GRAPH 084
   97 FORMAT(5X,'PH2',8X,'PH2O',7X,'PCO',8X,'PCO2',7X,'PCH4',4X,'PRESSUR  GRAPH 085
     1E',5X,'O/H',9X,'C/H',4X,'PH2/PH2O',4X,'PCO/PCO2',4X,'PH2/PCH4')  GRAPH 086
      WRITE(3,100)PH2,PH2O,PCO,PCO2,PCH4,PRES,ROH,RCH,CRHW,CRCC2,CRHM  GRAPH 087
  100 FORMAT(1X,2F10.6,1X,F10.6,2X,F10.6,F10.6,1X,F10.6,1X,F10.6,1X,F10.  GRAPH 088
     16,F6.2,6X,F6.2,6X,F6.2,//)                                       GRAPH 089
   99 CONTINUE                                                         GRAPH 090
      IF(ABS(PRES-1.)-.01)82,82,81                                     GRAPH 091
   81 ROH=ROH+.01                                                      GRAPH 092
      PRES=1.                                                          GRAPH 093
      GO TO 84                                                         GRAPH 094
   82 IF(PH2-PTEST)87,81,81                                            GRAPH 095
   87 ROH=ROH+.05                                                      GRAPH 096
      ATOMH=2.*PH2O+2.*PH2+4.*PCH4                                     GRAPH 097
      ATOMC=PCO+PCO2+PCH4                                              GRAPH 098
      ATOMO=PCO+2.*PCO2+PH2O                                           GRAPH 099
      ATOMT=ATOMH+ATOMO+ATOMC                                          GRAPH 100
      ULH=10.-(ATOMH/(ATOMT*.1))                                       GRAPH 101
      ULO=ATOMO/(ATOMT*.1)                                             GRAPH 102
      ULC=ATOMC/(ATOMT*.1)                                             GRAPH 103
      X2=ULH-(ULH-ULO)*SIN(Z)                                          GRAPH 104
      Y2=(ULH-ULO)*COS(Z)                                              GRAPH 105
```

```
      CALL FPLOT(2,X2,Y2)                                          GRAPH 106
      PTEST=PH2                                                    GRAPH 107
      PRES=1.                                                      GRAPH 108
      XST=PH2*PRES                                                 GRAPH 109
      IF(ROH- 6.)85,86,86                                          GRAPH 110
   85 GO TO 84                                                     GRAPH 111
   86 CONTINUE                                                     GRAPH 112
      PCH4=0.0                                                     GRAPH 113
      PH2=0.0                                                      GRAPH 114
      PH2O=0.0                                                     GRAPH 115
      ATOMH=0.0                                                    GRAPH 116
      ATOMC=PGCO+PGCO2+PCH4                                        GRAPH 117
      ATOMO=PGCO+2.*PGCO2+PH2O                                     GRAPH 118
      ATOMT=ATOMC+ATOMH+ATOMO                                      GRAPH 119
      ULH=10.-(ATOMH/(ATOMT*.1))                                   GRAPH 120
      ULO=ATOMO/(ATOMT*.1)                                         GRAPH 121
      ULC=ATOMC/(ATOMT*.1)                                         GRAPH 122
      Y3=(ULH-ULO)*COS(Z)                                          GRAPH 123
      X3=ULH-(ULH-ULO)*SIN(Z)                                      GRAPH 124
      CALL FPLOT(0,X3,Y3)                                          GRAPH 125
      CALL FPLOT(3,0.0,0.0)                                        GRAPH 126
      RETURN                                                       GRAPH 127
      END                                                          GRAPH 128
```

```
      SUBROUTINE IEOEQ (X,F,DERF,TCT2,XST,EPS,IEND,IER)                 IEOEQ 001
C NEWTON-RAPHSON ITERATIVE SEARCH TECHNIQUE FOR PH2 (X)                 IEOEQ 002
C     PREPARE ITERATION                                                 IEOEQ 003
      IER=0                                                             IEOEQ 004
      X=XST                                                             IEOEQ 005
      TOL=X                                                             IEOEQ 006
      CALL TCT2 (TOL,F,DERF)                                            IEOEQ 007
      TOLF=100.*EPS                                                     IEOEQ 008
C     START ITERATION LOOP                                              IEOEQ 009
      DO 6 I=1,IEND                                                     IEOEQ 010
      IF(F)1,7,1                                                        IEOEQ 011
C     EQUATION IS NOT SATISFIED BY X                                    IEOEQ 012
    1 IF(DERF)2,8,2                                                     IEOEQ 013
C     ITERATION IS POSSIBLE                                             IEOEQ 014
    2 DX=F/DERF                                                         IEOEQ 015
      X=X-DX                                                            IEOEQ 016
      TOL=X                                                             IEOEQ 017
      CALL TCT2 (TOL,F,DERF)                                            IEOEQ 018
C     TEST OF SATISFACTORY ACCURACY                                     IEOEQ 019
      TOL=EPS                                                           IEOEQ 020
      A=ABS(X)                                                          IEOEQ 021
      IF(A-1.)4,4,3                                                     IEOEQ 022
    3 TOL=TOL*A                                                         IEOEQ 023
    4 IF(ABS(DX)-TOL)5,5,6                                              IEOEQ 024
    5 IF(ABS(F)-TOLF)7,7,6                                              IEOEQ 025
    6 CONTINUE                                                          IEOEQ 026
C     END OF ITERATION LOOP                                             IEOEQ 027
C     NO CONVERGENCE AFTER IEND ITERATION STEPS.ERROR RETURN.           IEOEQ 028
      IER=1                                                             IEOEQ 029
    7 RETURN                                                            IEOEQ 030
C     ERROR RETURN IN CASE OF ZERO DIVISOR                              IEOEQ 031
    8 IER=2                                                             IEOEQ 032
      RETURN                                                            IEOEQ 033
      END                                                               IEOEQ 034
```

```
      SUBROUTINE TCT2 (X,F,DERF)                                          TCT2 001
C PART OF NEWTON-RAPHSON SEARCH ROUTINE                                   TCT2 002
      COMMON CO,C1,C2,C3,C4,C5,C6,EPS,IEND,XST                            TCT2 003
      PH2=X                                                               TCT2 004
      F=CO+C1*PH2+C2*(PH2**2.)+C3*(PH2**3.)+C4*(PH2**4.)+C5*(PH2**5.)+    TCT2 005
     1C6*(PH2**6.)                                                        TCT2 006
      DERF=C1+2.*C2*PH2+3.*C3*(PH2**2.)+C4*4.*(PH2**3.)+5.*C5*(PH2**4.)   TCT2 007
     1+6.*C6*(PH2**5.)                                                    TCT2 008
      RETURN                                                              TCT2 009
      END                                                                 TCT2 010
```

```
C PROGRAM TO CURVE FIT LNK DATA AND G AND H                              CURVE 001
      DIMENSION T(100),Y(100),A(5,6),YC(100),B(5)                        CURVE 002
1     FORMAT(I2,1X,I1)                                                   CURVE 003
 2    FORMAT(F11.0,5F12.4)                                               CURVE 004
3     FORMAT(1X,'LN KP=',E12.5,'/T ',E12.5,'LN(T) ',E12.5,'T ',E12.5,    CURVE 005
     1'T**2 ',E12.5,'T**3 ')                                             CURVE 006
4     FORMAT(6X,'T',11X,'YINPUT',8X,'YCALC')                             CURVE 007
5     FORMAT(1X,E12.5,2X,E12.5,2X,E12.5)                                 CURVE 008
6     FORMAT(1H1)                                                        CURVE 009
7     FORMAT(1H0)                                                        CURVE 010
 8    FORMAT(1X,'H= ',E12.5,2X,E12.5,'T ',E12.5,'T**2 ',E12.5,'T**3 '    CURVE 011
     1,E12.5,'T**4 ')                                                    CURVE 012
      DO 20 I=1,5                                                        CURVE 013
      DO 10 J=1,6                                                        CURVE 014
10    A(I,J)=0.                                                          CURVE 015
20    CONTINUE                                                           CURVE 016
      READ(2,1) N,ICODE                                                  CURVE 017
 24   IF(ICODE)26,26,25                                                  CURVE 018
 25   A(1,3)=N                                                           CURVE 019
      A(3,1)=N                                                           CURVE 020
      READ(2,2) (T(I),Y(I),I=1,N)                                        CURVE 021
      DO 30 I=1,N                                                        CURVE 022
      A(1,2)=A(1,2)+ALOG(T(I))/T(I)                                      CURVE 023
      A(1,1)=A(1,1)+1./T(I)**2                                           CURVE 024
      A(2,1)=A(1,2)                                                      CURVE 025
      A(4,1)=A(4,1)+T(I)                                                 CURVE 026
      A(1,4)=A(4,1)                                                      CURVE 027
      A(1,5)=A(1,5)+T(I)**2                                              CURVE 028
      A(5,1)=A(1,5)                                                      CURVE 029
      A(3,3)=A(1,5)                                                      CURVE 030
      A(1,6)=A(1,6)+Y(I)/T(I)                                            CURVE 031
      A(2,2)=A(2,2)+(ALOG(T(I)))**2                                      CURVE 032
      A(2,3)=A(2,3)+T(I)*ALOG(T(I))                                      CURVE 033
      A(3,2)=A(2,3)                                                      CURVE 034
      A(2,4)=A(2,4)+ALOG(T(I))*T(I)**2                                   CURVE 035
```

```
      A(4,2)=A(2,4)                                                    CURVE 036
      A(5,2)=A(5,2)+ALOG(T(I))*T(I)**3                                 CURVE 037
      A(2,5)=A(5,2)                                                    CURVE 038
      A(2,6)=Y(I)*ALOG(T(I))+A(2,5)                                    CURVE 039
      A(3,4)=A(3,4)+T(I)**3                                            CURVE 040
      A(4,3)=A(3,4)                                                    CURVE 041
      A(3,5)=A(3,5)+T(I)**4                                            CURVE 042
      A(5,3)=A(3,5)                                                    CURVE 043
      A(3,6)=A(3,6)+Y(I)*T(I)                                          CURVE 044
      A(4,4)=A(3,5)                                                    CURVE 045
      A(4,5)=A(4,5)+T(I)**5                                            CURVE 046
      A(5,4)=A(4,5)                                                    CURVE 047
      A(4,6)=A(4,6)+Y(I)*T(I)**2                                       CURVE 048
      A(5,5)=A(5,5)+T(I)**6                                            CURVE 049
30    A(5,6)=A(5,6)+Y(I)*T(I)**3                                       CURVE 050
      GO TO 40                                                         CURVE 051
26    A(1,1)=N                                                         CURVE 052
      READ(2,2) (T(I),Y(I),I=1,N)                                      CURVE 053
      DO 27 I=1,N                                                      CURVE 054
      A(1,2)=A(1,2)+T(I)                                               CURVE 055
      A(2,1)=A(1,2)                                                    CURVE 056
      A(1,3)=A(1,3)+T(I)**2                                            CURVE 057
      A(2,2)=A(1,3)                                                    CURVE 058
      A(3,1)=A(1,3)                                                    CURVE 059
      A(1,4)=A(1,4)+T(I)**3                                            CURVE 060
      A(2,3)=A(1,4)                                                    CURVE 061
      A(3,2)=A(1,4)                                                    CURVE 062
      A(4,1)=A(1,4)                                                    CURVE 063
      A(1,5)=A(1,5)+T(I)**4                                            CURVE 064
      A(2,4)=A(1,5)                                                    CURVE 065
      A(4,2)=A(1,5)                                                    CURVE 066
      A(3,3)=A(1,5)                                                    CURVE 067
      A(5,1)=A(1,5)                                                    CURVE 068
      A(1,6)=A(1,6)+Y(I)                                               CURVE 069
      A(2,5)=A(2,5)+T(I)**5                                            CURVE 070
```

```
      A(3,4)=A(2,5)                                                    CURVE 071
      A(4,3)=A(2,5)                                                    CURVE 072
      A(5,2)=A(2,5)                                                    CURVE 073
      A(2,6)=A(2,6)+Y(I)*T(I)                                          CURVE 074
      A(3,5)=A(3,5)+T(I)**6                                            CURVE 075
      A(4,4)=A(3,5)                                                    CURVE 076
      A(5,3)=A(3,5)                                                    CURVE 077
      A(3,6)=A(3,6)+Y(I)*T(I)**2                                       CURVE 078
      A(4,5)=A(4,5)+T(I)**7                                            CURVE 079
      A(5,4)=A(4,5)                                                    CURVE 080
      A(4,6)=A(4,6)+Y(I)*T(I)**3                                       CURVE 081
      A(5,5)=A(5,5)+T(I)**8                                            CURVE 082
27    A(5,6)=A(5,6)+Y(I)*T(I)**4                                       CURVE 083
40    DO 50 K=2,6                                                      CURVE 084
50    A(1,K)=A(1,K)/A(1,1)                                             CURVE 085
      DO 80 IDEX=2,5                                                   CURVE 086
      JM=IDEX-1                                                        CURVE 087
      DO 60 I=IDEX,5                                                   CURVE 088
      SUM=0.                                                           CURVE 089
      DO 55 K=1,JM                                                     CURVE 090
55    SUM=SUM+A(I,K)*A(K,IDEX)                                         CURVE 091
60    A(I,IDEX)=A(I,IDEX)-SUM                                          CURVE 092
      JP=IDEX+1                                                        CURVE 093
      IM=IDEX-1                                                        CURVE 094
      DO 70 J=JP,6                                                     CURVE 095
      SUM=0.                                                           CURVE 096
      DO 65 K=1,IM                                                     CURVE 097
65    SUM=SUM+A(IDEX,K)*A(K,J)                                         CURVE 098
70    A(IDEX,J)=(A(IDEX,J)-SUM)/A(IDEX,IDEX)                           CURVE 099
80    CONTINUE                                                         CURVE 100
      B(5)=A(5,6)                                                      CURVE 101
      DO 100 IDEX=2,5                                                  CURVE 102
      I=6-IDEX                                                         CURVE 103
      IP=I+1                                                           CURVE 104
      SUM=0.                                                           CURVE 105
```

```
      DO 90 K=IP,5                                                          CURVE 106
90    SUM=SUM+A(I,K)*B(K)                                                   CURVE 107
100   B(I)=A(I,6)-SUM                                                       CURVE 108
      WRITE(3,6)                                                            CURVE 109
      IF(ICODE)101,101,102                                                  CURVE 110
101   WRITE(3,8) (B(I),I=1,5)                                               CURVE 111
      GO TO 103                                                             CURVE 112
102   WRITE(3,3) (B(I),I=1,5)                                               CURVE 113
103   WRITE(3,7)                                                            CURVE 114
      IF(ICODE)104,104,106                                                  CURVE 115
104   DO 105 I=1,N                                                          CURVE 116
105   YC(I)=B(1)+B(2)*T(I)+B(3)*T(I)**2+B(4)*T(I)**3+B(5)*T(I)**4           CURVE 117
      GO TO 112                                                             CURVE 118
106   DO 110 I=1,N                                                          CURVE 119
110   YC(I)=B(1)/T(I)+B(2)*ALOG(T(I))+B(3)*T(I)+B(4)*T(I)**2+B(5)*T(I)      CURVE 120
     1**3                                                                   CURVE 121
112   WRITE(3,4)                                                            CURVE 122
      WRITE(3,5) (T(I),Y(I),YC(I),I=1,N)                                    CURVE 123
      READ(2,1) N,ICODE                                                     CURVE 124
      IF(ICODE-1)115,115,120                                                CURVE 125
115   DO 117 I=1,5                                                          CURVE 126
      DO 116 J=1,6                                                          CURVE 127
116   A(I,J)=0.                                                             CURVE 128
117   CONTINUE                                                              CURVE 129
      GO TO 24                                                              CURVE 130
120   CALL EXIT                                                             CURVE 131
      END                                                                   CURVE 132
```

```
      SUBROUTINE EQKS(TEMP,EQCH4,EQCO2,EQH2O,EQH2,EQCO,EQC,EQFE3,EQFE2,E   EQKS 001
     1QCO1,EQH21)                                                          EQKS 002
C CALCULATES THE APPROPRIATE  LNK. VALUES TO DELIVER TO THE PHASE BOUNDAR  EQKS 003
C Y SUBROUTINES                                                            EQKS 004
C      REACTION 1 C+2H2=CH4  EQCH4                                         EQKS 005
C      REACTION 2 H2+CO2=CO+H2O   EQCO2                                    EQKS 006
C      REACTION 3 3H2+CO=H2O+CH4  EQH2O                                    EQKS 007
C      REACTION 4 3/4FE+H2O=H2+1/4FE3O4  EQH2                              EQKS 008
C      REACTION 5 3/4FE+CO2=CO+1/4FE3O4  EQCO                              EQKS 009
C      REACTION 6  2CO=CO2+C  EQC                                          EQKS 010
C      REACTION 7* 3FE+CH4=2H2+FE3C   EQFE3                               EQKS 011
C      REACTION 8*  CO2+CH4=2H2+2CO   EQCO1                               EQKS 012
C      REACTION 9*  4H2+CO2=CH4+2H2O  EQH21                               EQKS 013
C      RANGE OF CORREL. FOR LNK BETWEEN 298-2000 K                         EQKS 014
       EKCH4=    (8372.2/(TEMP)-1.0769*ALOG(TEMP)-(.56435E-2)*TEMP+(.2904  EQKS 015
     16E-5)*(TEMP**2.)-(.52351E-9)*(TEMP**3.))                             EQKS 016
       EKCO=    (13612./(TEMP)+1.8317*(ALOG(TEMP))-(2.7584E-3)*TEMP+      EQKS 017
     2(.6536E-6)*(TEMP**2.)-(.78772E-10)*(TEMP**3.))                       EQKS 018
       EKCO2=    (47280./(TEMP)+(.1322)*(ALOG(TEMP))-(.94025E-3)*(TEMP)+  EQKS 019
     3(.45112E-6)*(TEMP**2.)-(.91901E-10)*(TEMP**3.))                      EQKS 020
       EKH2O=    (28780./(TEMP)-(.69477)*(ALOG(TEMP))-(.14283E-2)*(TEMP)+ EQKS 021
     4(.74925E-6)*(TEMP**2.)-(.13785E-9)*(TEMP**3.))                       EQKS 022
       WRITE(1,83)                                                         EQKS 023
   83 FORMAT(5X,'IF SPECIES AT EQUILIBRIUM IS THOUGHT TO BE FEO(CRYSTAL)   EQKS 024
     1 TYPE IN 1., IF FEO.9470(WUSTITE) TYPE IN 2.,'/,'IF NIO TYPE IN -1   EQKS 025
     1.')                                                                  EQKS 026
       READ(6,84) TEST                                                     EQKS 027
   84 FORMAT(7X,F4.1)                                                      EQKS 028
       IF(TEST-1.)88,85,86                                                 EQKS 029
   85 EKFEO=    ((32461./TEMP)-(.15184E+1)*(ALOG(TEMP))+(.44208E-2)*(TEMP  EQKS 030
     5)-(.17970E-5)*(TEMP**2.)+(.28776E-9)*(TEMP**3.))                     EQKS 031
       GO TO 87                                                            EQKS 032
   86 EKFEO=(.317327E05/(TEMP))-.150692E01*(ALOG(TEMP))+.383287E-2*TEMP-   EQKS 033
     1.135694E-5*(TEMP**2.)+.175926E-9*(TEMP**3.)                          EQKS 034
       WRITE(3,90)  TEST                                                   EQKS 035
```

```
90 FORMAT(5X,F4.1)                                                      EQKS 036
   GOTO 87                                                              EQKS 037
88 EKFE0=(2.9045E04/TEMP)-2.03977*ALOG(TEMP)+3.7856E-03*TEMP-1.42491E   EQKS 038
  1-06*TEMP**2+2.48586E-10*TEMP**3                                      EQKS 039
87 EKFE2=    ((98359./TEMP)-(.59363E+1)*(ALOG(TEMP))+(.13798E-1)*(TEMP  EQKS 040
  6)-(.39931E-5)*(TEMP**2.)+(.40036E-9)*(TEMP**3.))                     EQKS 041
   EKFE3=    ((133880./TEMP)-(.77989E+1)*(ALOG(TEMP))+(.20934E-1)*(TEM  EQKS 042
  7P)-(.63194E-5)*(TEMP**2.)+(.63808E-9)*(TEMP**3.))                    EQKS 043
   EKF3C=((-.27892E04/TEMP)-(.42754E-01)*(ALOG(TEMP))+(.62806E-02)*(T   EQKS 044
  1EMP)-(.42543E-05)*(TEMP**2.)+(.82417E-09)*(TEMP**3.))                EQKS 045
   EKF2C=((-.26706E04/TEMP)+(.48958)*(ALOG(TEMP))-(.37848E-02)*(TEMP)   EQKS 046
  1+(.25141E-05)*(TEMP**2.)-(.53351E-09)*(TEMP**3.))                    EQKS 047
   EQCH4=EXP(EKCH4)                                                     EQKS 048
   EQCO2=EXP((EKH2O+EKCO)-EKC(2)                                        EQKS 049
   EQH2O=EXP((EKH2O+EKCH4)-EKCO)                                        EQKS 050
   EQC=EXP(EKCO2-(2.*EKCO))                                             EQKS 051
   EQCO1=EXP(2.*EKCO-(EKCH4+EKCO2))                                     EQKS 052
   EQH21=EXP((2.*EKH2O+EKCH4)-(EKCO2))                                  EQKS 053
   IF(TEST)71,91,91                                                     EQKS 054
91 IF(TEMP-833.)70,71,71                                                EQKS 055
70 EQH2=EXP(.25*EKFE3-EKH2O)                                            EQKS 056
   EQCO=EXP((.25*EKFE3+EKCO)-EKCO2)                                     EQKS 057
   GO TO 72                                                             EQKS 058
71 EQH2=EXP(EKFE0-EKH2O)                                                EQKS 059
   EQCO=EXP((EKFE0+EKCO)-(EKCO2))                                       EQKS 060
72 IF(TEMP-600.)80,80,81                                                EQKS 061
81 EQFE2=EXP((EKCO2+EKF3C)-2.*(EKCO))                                   EQKS 062
   EQFE3=EXP(EKF3C-EKCH4)                                               EQKS 063
   GO TO 82                                                             EQKS 064
80 EQFE2=EXP((EKCO2+EKF2C)-2.*(EKCO))                                   EQKS 065
   EQFE3=EXP(EKF2C-EKCH4)                                               EQKS 066
82 CONTINUE                                                             EQKS 067
   RETURN                                                               EQKS 068
   END                                                                  EQKS 069
```

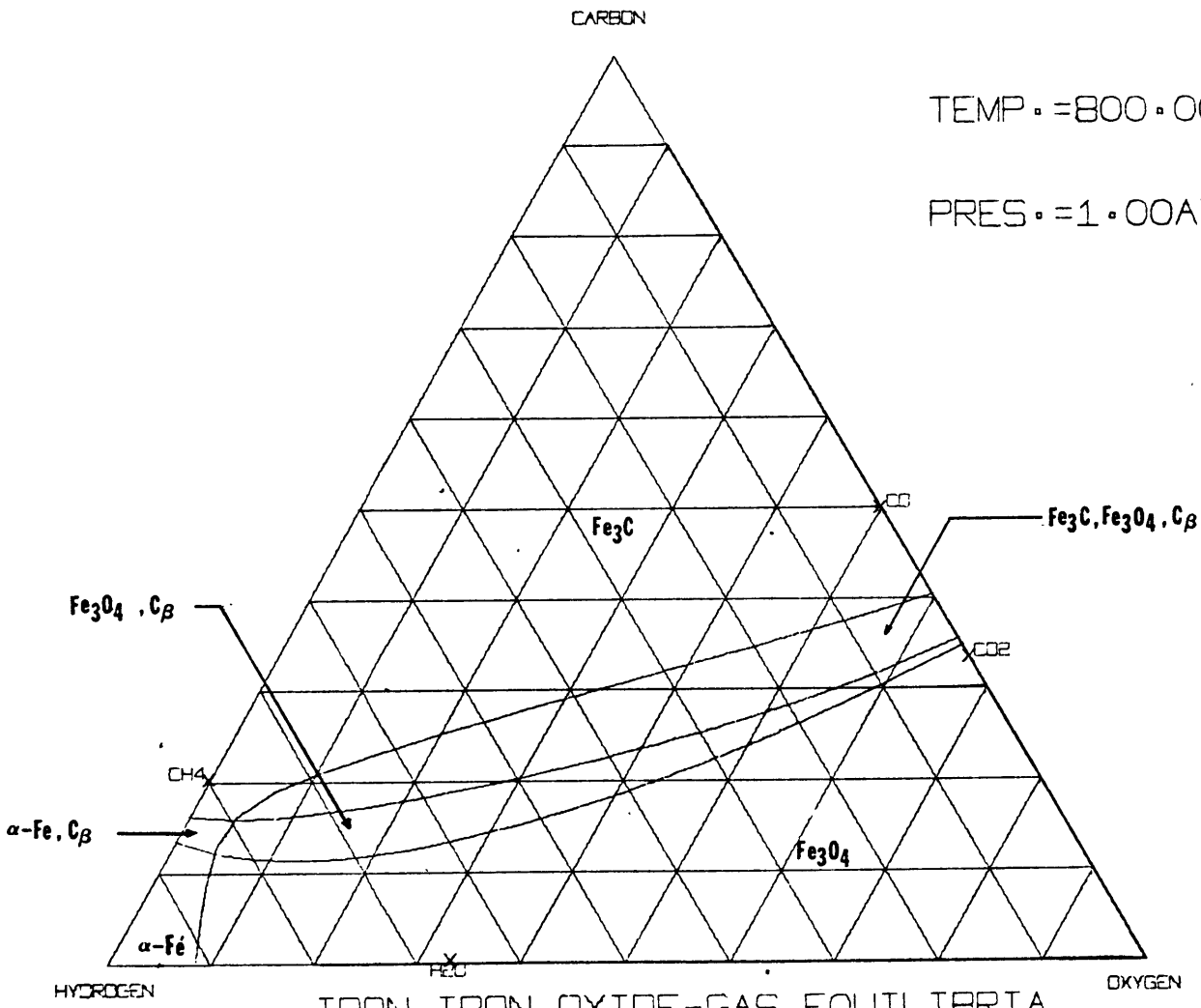

FIGURE 60: TRIANGULAR PHASE DIAGRAM AT 800 K

7.3 Mass Transfer Limitations in a Five Component Gas Mixture

The following calculations were made to determine if mass transfer limitations were present in Bosch reactor.

Representative Run, A - 25

temperature 900 K, pressure = 1 atmophere, catalyst charge = 50 8 mg

COMPONENT	EXPERIMENTAL (%)	THEORETICAL (α-Fe/$Fe_{1-y}O$, %)
H_2	0.3729	0.3879
CO	0.2708	0.2175
CO_2	0.1570	0.1825
CH_4	0.1010	0.0715
H_2O	0.0982	0.1407

Calculating Reynolds Number:

$$N_{Re_d} = d\, V\, \rho_{mix}/\mu_{mix} \tag{33}$$

$$V = 20\ cm^3/s\ (STP) \cdot \frac{900\ K}{273\ K} \cdot \frac{4}{\pi(1.9cm)^2}$$

$V = 23.25$ cm/s at 900 K (superficial velocity)

From the ideal-gas law:

$$PV_m = NR_gT$$

$$\frac{M_{wt}N}{V_m} = \rho_{mix} = \frac{M_{wt}P}{R_gT} \tag{34}$$

where

$$M_{wt} = \sum_{i=1}^{5} M_i X_i\ (exp) \tag{35}$$

$M_{wt} = 18.62$ g/g-mole (molecular weight of reactant gas)

$$\rho_{mix} = \frac{18.62 \text{ g/g-mole} \cdot 1.0 \text{ ATM}}{\frac{82.1 \text{ ATM cm}^3}{\text{g-mole K}} \cdot 900 \text{ K}}$$

$$\rho_{mix} = 2.52 \times 10^{-4} \text{ g/cm}^3 \quad \text{(gas mixture density)}$$

Viscosity of the various gases was obtained at a variety of different temperatures. Equation 36 (Reid and Sherwood, 1950) was used to bring all viscosities to 900 K. The data used and calculated is shown in Table 5.

$$\mu_{900} = \mu_T \left(\frac{T^*_{900}}{T^*_T}\right)^{1/2} \Big/ \left(\frac{\Omega_{900}}{\Omega_T}\right) \tag{36}$$

Table 5 Viscosity Data

COMPONENT	μ_T(poise) x 10^{-4}	T (K)	$\frac{\varepsilon_o}{k}$(°K)	T^*	Ω_T
H_2	1.829	874	59.7	14.64	0.79
CO	2.714	549.9	91.7	5.99	0.90
CO_2	3.300	763	195.2	3.91	0.97
CH_4	2.264	772	148.6	5.20	0.93
H_2O	1.255	373	809.1	0.46	2.37
		Results			
H_2	1.86	900 K		15.10	0.79
CO	3.76	"		9.80	0.83
CO_2	3.69	"	same	4.60	0.94
CH_4	2.56	"		6.10	0.89
H_2O	1.19	"		1.11	0.69

Assuming that the mixture viscosity can be reliably approximated by a mole-fraction average:

$$\mu_{mix} = \sum_{i=1}^{5} \mu_i X_i \tag{37}$$

$$\mu_{mix} = 3.478 \times 10^{-4} \text{ g/cm-s}$$

$$N_{Re_d} = \frac{0.075\text{cm} \cdot 23.25\text{cm/s} \cdot 2.52 \times 10^{-4}\text{g/cm}^3}{3.478 \times 10^{-4} \text{ g/s - cm}}$$

$$N_{Re_d} = 1.26$$

Using a correlation for mass transfer to and from tubes in crossflow (Zhukauskas et al., 1968):

$$N_{sh} = (0.43 + 0.50\ N_{Re}^{0.5})\ Sc^{0.38} \left[\frac{Sc_g}{Sc_w}\right]^{0.25} \tag{38}$$

$$k_{m,j} = \frac{D}{d} \cdot (0.43 + 0.50\ N_{Re}^{0.5})\ Sc^{0.38}$$

Equation 39 was used to calculate the various binary diffusion coefficients. Ω_D (collision integral) and σ (Lennard-Jones force constant) were obtained from equation 40 and 41 in conjunction with Appendix G and Table 11.1 from Reid-Sherwood.

$$D_{AB} = 0.001858\ T^{3/2}\ (\{M_A + M_B\} / M_A M_B)^{1/2} / P\sigma_{AB}^2 \Omega_D \tag{39}$$

$$\varepsilon_{\circ AB}/k\ (\{\varepsilon_{\circ A}/k\}\ \{\varepsilon_{\circ B}/k\})^{1/2} \tag{40}$$

$$\sigma_{AB} = 1/2\ (\sigma_A + \sigma_B) \tag{41}$$

Table 6 Binary Diffusion Coefficients

	D_{H_2} (cm^2/s)	D_{CO}	D_{CO_2}	D_{CH_4}
CO	4.65	-	-	-
CO_2	4.13	1.04	-	-
CH_4	4.65	1.45	1.17	-
H_2O	5.75	1.18	1.00	1.686

As an approximation the diffusion coefficients of any of the reactant gases into the mixture were represented by the equation

$$D_{Am} = \frac{(1-X_A)}{\sum_{j=B}^{N} (X_j/D_{Aj})} \qquad (42)$$

Using equation 42 and equation 38 along with the data from Table 6, the diffusion coefficients and mass transfer coefficients were calculated. The results are shown in Table 7.

Table 7 Diffusion Coefficients and Mass Transfer Coefficients in a Five Component Gas Mixture

Component	$D_{i-m}(cm^2/s)$	k_m (cm/s)
H_2	4.64	38.67
CO	1.89	21.3
CO_2	1.58	18.27
CH_4	1.96	22.67
H_2O	1.77	21.28

From run A-25, the maximum rate of carbon deposition was 1.57×10^{-6} g-moles carbon/s, assuming carbon is formed from reaction D or reaction E

$$2CO = CO_2 + C \qquad (D)$$

$$CO + H_2 = H_2O + C \qquad (E)$$

$$N = k_{CO} A \quad \Delta C$$

where

$$C = \frac{N}{V} = \frac{P}{R_g T}$$

The area of a typical preconditioned catalyst is 1912 cm^2/gm. Therefore, assuming mass transfer limitations do exist, (i.e., the surface concentration equals that of equilibrium)

$$N_{CO} = (21.30 cm/s)\ \left(\frac{1912 cm^2}{g\not{m}}\right)\ (0.508 g\not{m})\left(\frac{1}{\frac{82.1 a\not{t}m\ cm^3 \cdot 900K}{g\text{-}mole\ K}}\right) \cdot (.2708 - .2175\ a\not{t}m)$$

$$N_{CO} = 1.49 \times 10^{-2} \text{ g-moles carbon/s}$$

Mass transfer is seen not to be limiting in the case of carbon monoxide reacting to carbon.

It should be noted that because of the complexities of the Bosch reaction sequence and also the low conversion obtained, it was impossible to calculate whether product concentration was limiting or not. This is due to the fact that the rate of product formation can not be accurately calculated and thus compared to the mass transfer rate.

7.4 Computer Programs Used in Data Analysis

7.4.1 Data Reduction Logic (Computer Analysis)

The inlet and outlet gas phase compositions were determined by a modified computer program originally developed by Manning (1976). Calculations of all gas component concentrations except hydrogen were determined by using the absolute method described by Dal Nogare and Juvet (1962) in conjunction with a precision made external standard. Hydrogen was determined by using an empirical calibration curve as recommended by Purcell and Ettre (1965). A detailed description of the calculation scheme is described by Manning (1976).

The program was modified to increase accuracy and to provide a provision for drawing a triangular phase diagram. The measured inlet and outlet gas compositions were simultaneously plotted on this diagram. The diagram was used to provide a visable check to insure that the solid phase being investigated was the phase of interest.

The main program "Terri" and the associated support programs are shown at the end of this section, including a sample of the output typically obtained. Volume II of this thesis provides a history of all the data obtained both in raw and reduced form.

7.4.2 Propagation of Error Analysis

A propagation of error analysis was performed on the data reduction procedure. This maximum possible error (propagation

error) in each individual gas composition was determined using program "Error". Program Error, along with a sample of its output is presented at the end of this section.

7.4.3 Initial Conditions

As mentioned in Section 3.2.1, the starting conditions were obtained by solving the appropriate equilibrium relationships assuming that all solid phases acted as catalysts for all the reaction systems involved. Then, by setting temperature, pressure, O/H or C/H ratio, and the P_{H_2}/P_{H_2O} ratio, the composition of the gas phase could be made to fix the system in the phase field of interest. This was done by Program "Set", which follows Program "Error".

7.4.4 Optimal Reactor Design

In order to determine the optimal reactor design, it was first necessary to determine the intersection of the iron-iron oxide and graphite-gas phase boundaries (i.e., optimal O/H ratio). This was accomplished by a Newton-Raphson search technique. The Program called "Inter" is presented on conclusion of this section.

Program "Proc" used the results from Program Inter to determine the optimal reactor design. In Program Process the operator specifies Bosch temperature and pressure, shift O/H ratio, total carbon dioxide into the system, and the hydrogen and carbon dioxide directly fed to the shift reactor. Through messages sent out to the key board, the operator can specify

shift recycle and temperature. Program Proc follows Program Inter.

```
C PROGRAM TERRI USED TO PLOT DATA ON PHASE DIAGRAMS                                  TERRI 001
      EXTERNAL TABLE,DPLOT                                                           TERRI 002
      COMMON    ITIME( 95),DELP( 95),IGAS ( 95),DATA( 95,5),CAL(6),                  TERRI 003
     1CALCO(6),SUMD(6),ISAMP( 95),RCC(6),IDATE(5),HSLOP,A,B,CZERO,FEZER,             TERRI 004
     2PATM, PH2O,NIT,NSUM1,NSUM2,NSUM3,NSAMP,NRUN                                    TERRI 005
      X=1.                                                                           TERRI 006
   01 X=X-1.                                                                         TERRI 007
      CALL ID1                                                                       TERRI 008
      CALL ID2                                                                       TERRI 009
      CALL CALC                                                                      TERRI 010
      CALL DOUT1                                                                     TERRI 011
      IF(X)91,91,90                                                                  TERRI 012
   90 GO TO 01                                                                       TERRI 013
   91 CONTINUE                                                                       TERRI 014
      CALL EXIT                                                                      TERRI 015
      END                                                                            TERRI 016
```

```
      SUBROUTINE DA(PRES,D,EQFE3,EQCO1,EQH21,A,B,C,E,AA,BB,CC,DD,EE,G,Z,   DA 001
     1W,T,X,TL,FF,GG,HH )                                                 DA 002
C CALCULATES CONSTANTS NEEDED IN PRINT-OUT ROUTINES                       DA 003
      P=PRES                                                              DA 004
      A=(1.+D)/D                                                          DA 005
      B=(1.+2.*D)/D                                                       DA 006
      C=(2./D)+1.                                                         DA 007
      E=(1.-D)/D                                                          DA 008
      AA=(1./(EQFE3**2.))*(1.-2.*B-C*((D*B)**2.))                         DA 009
      BB=(2./(EQFE3))*(1.-A-B-(A*B*C)*(D**2.))                            DA 010
      CC=(2.*P*(E+B)/EQFE3)+(1.-2.*A)-(C*(D**2.))*((A**2.)-2.*B*P/(EQFE3  DA 011
     1*D))                                                                DA 012
      DD=2.*P*(E+A*(1.+C*D))                                              DA 013
      EE=2.*(P**2.)*((D-2.)/(2.*D)-C/2.)                                  DA 014
      G=EQFE3*SQRT(EQH21/EQCO1)                                           DA 015
      Z=(1./EQFE3)*(B-1.)                                                 DA 016
      W=(EQFE3*G*(A-1.)+B)/(EQFE3*G)                                      DA 017
      T=(-P)/(D*G)                                                        DA 018
      X=P*(A/(P*G)-E)                                                     DA 019
      TL=-1./(D*G)                                                        DA 020
      FF=(2.*B/EQFE3)*(1.-C*D)-(EQFE3*EQH21)*(1.+C*(D**2.))-2.*A/EQFE3    DA 021
      GG=-2.*A*C*D                                                        DA 022
      HH=2.*P*((D*C-1.)/D+A)+EQCO1/EQFE3                                  DA 023
      RETURN                                                              DA 024
      END                                                                 DA 025
```

```
      SUBROUTINE ID1                                                        ID1 001
C READS IN INITIAL IDENTIFICATION DATA                                      ID1 002
      COMMON    ITIME( 95),DELP( 95),IGAS ( 95),DATA( 95,5),CAL(6),         ID1 003
     1CALCO(6),SUMD(6),ISAMP( 95),RCC(6),IDATE(5),HSLOP,A,B,CZERO,FEZER,    ID1 004
     2PATM, PH2O,NIT,NSUM1,NSUM2,NSUM3,NSAMP,NRUN                           ID1 005
      READ (2,101)NRUN,NSAMP,PATM,PH2O,IDATE,CZERO,FEZER                    ID1 006
   02 WRITE(3,102)NRUN,IDATE                                                ID1 007
  101 FORMAT(5X,I5,5X,I5,5X,F5.2,5X,F6.3,4X,5A2,5X,2F10.3)                  ID1 008
  102 FORMAT(1H1,33X,21HDATA TAKEN DURING RUN,I4,3H ON,5A2)                 ID1 009
      WRITE(3,116)                                                          ID1 010
  116 FORMAT(1H0,  9HTIME SAMP,5X,70H DELP IGAS         H2         CO       ID1 011
     1  CH4         CO2         H2O          C    )                       ID1 012
      PATM=PATM*25.4                                                        ID1 013
      CAL(1)=25.18                                                          ID1 014
      CAL(2)=24.91                                                          ID1 015
      CAL(3)=24.97                                                          ID1 016
      CAL(4)=24.94                                                          ID1 017
      CAL(5)=PH2O*100./PATM                                                 ID1 018
      CAL(6)=100.                                                           ID1 019
      NIT=0                                                                 ID1 020
      RETURN                                                                ID1 021
      END                                                                   ID1 022
```

```
      SUBROUTINE ID2                                                    ID2 001
C READS IN RAW DATA AND LISTS IT                                        ID2 002
      COMMON    ITIME( 95),DELP( 95),IGAS ( 95),DATA( 95,5),CAL(6),     ID2 003
     1CALCO(6),SUMD(6),ISAMP( 95),RCC(6),IDATE(5),HSLOP,A,B,CZERO,FEZER, ID2 004
     2PATM, PH2O,NIT,NSUM1,NSUM2,NSUM3,NSAMP,NRUN                       ID2 005
      IH2O=PH2O                                                         ID2 006
      NSUM1=0                                                           ID2 007
      NSUM2=0                                                           ID2 008
      NSUM3=0                                                           ID2 009
      DO 05 N=1,6,1                                                     ID2 010
      SUMD(N)=0.                                                        ID2 011
   05 CONTINUE                                                          ID2 012
      DO 11 I=1,NSAMP,1                                                 ID2 013
   11 READ (2,103)ITIME(I),ISAMP(I),DELP(I),IGAS(I),(DATA(I,J),J=1,5)   ID2 014
      DO 10 I=1,NSAMP,1                                                 ID2 015
      IF(IGAS(I)-6)18,51,51                                             ID2 016
   18 WRITE(3,103)ITIME(I),ISAMP(I),DELP(I),IGAS(I),(DATA(I,J),J=1,5)   ID2 017
  103 FORMAT(2I5,5X,F5.2,I5,5F10.1)                                     ID2 018
      DO 20 K=1,5,1                                                     ID2 019
      DATA(I,K)=DATA(I,K)*PATM/(PATM+DELP(I))                           ID2 020
   20 CONTINUE                                                          ID2 021
      K=IGAS(I)                                                         ID2 022
      GO TO (30,40,50,10,10),K                                          ID2 023
   30 DO 70 J=1,4,1                                                     ID2 024
      SUMD(J)=SUMD(J)+DATA(I,J)                                         ID2 025
   70 CONTINUE                                                          ID2 026
      NSUM1=NSUM1+1                                                     ID2 027
      GO TO 10                                                          ID2 028
   40 SUMD(6)=SUMD(6)+DATA(I,1)                                         ID2 029
      NSUM2=NSUM2+1                                                     ID2 030
      GO TO 10                                                          ID2 031
   50 SUMD(5)=SUMD(5)+DATA(I,5)                                         ID2 032
      NSUM3=NSUM3+1                                                     ID2 033
      GO TO 10                                                          ID2 034
   51 K=IGAS(I)-5                                                       ID2 035
```

```
      GO TO (52,53,54,56),K                                                    ID2 036
   52 WRITE(3,106)ITIME(I),IGAS(I),(DATA(I,J),J=1,5)                           ID2 037
  106 FORMAT(1HO,I4,15X,I5,5F10.1)                                             ID2 038
      GO TO 10                                                                 ID2 039
   53 WRITE(3,107)ITIME(I),IGAS(I),DATA(I,1)                                   ID2 040
  107 FORMAT(I5,15X,I5,50X,F10.3)                                              ID2 041
      GO TO 10                                                                 ID2 042
   54 WRITE(3,106)ITIME(I),IGAS(I),DATA(I,1)                                   ID2 043
      GO TO 10                                                                 ID2 044
   56 WRITE(3,999)ITIME(I),IGAS(I)                                             ID2 045
  999 FORMAT(1HO,I4,15X,I5,' CHANGE INLET FLOW TO INERT HELIUM AT 20 CC/       ID2 046
     1SEC(STP) ')                                                              ID2 047
   10 CONTINUE                                                                 ID2 048
      RETURN                                                                   ID2 049
      END                                                                      ID2 050
```

```
      SUBROUTINE CALC                                                    CALC 001
C INITIAL CALCULATIONS TO DETERMINE CHROMATOGRAPH RESPONSE FACTORS        CALC 002
      COMMON    ITIME( 95),DELP( 95),IGAS ( 95),DATA( 95,5),CAL(6),      CALC 003
     1CALCO(6),SUMD(6),ISAMP( 95),RCC(6),IDATE(5),HSLOP,A,B,CZERO,FEZER,  CALC 004
     2PATM, PH2O,NIT,NSUM1,NSUM2,NSUM3,NSAMP,NRUN                        CALC 005
      DO 45 L=1,4,1                                                      CALC 006
      CALCO(L)=SUMD(L)*100./(NSUM1*CAL(L))                               CALC 007
   45 CONTINUE                                                           CALC 008
      IH2O=PH2O                                                          CALC 009
      IF(IH2O)22,46,47                                                   CALC 010
   22 WRITE(3,100)                                                       CALC 011
  100 FORMAT(1X,'WE HAVE A PROBLEM IN CALC')                             CALC 012
   46 CALCO(5)=CALCO(4)*0.69                                             CALC 013
      GO TO 48                                                           CALC 014
   47 CALCO(5)=SUMD(5)*100./(NSUM3*CAL(5))                               CALC 015
   48 CALCO(6)=SUMD(6)*100./(NSUM2*CAL(6))                               CALC 016
      A=SUMD(6)/NSUM2                                                    CALC 017
      B=SUMD(1)/NSUM1                                                    CALC 018
      HSLOP=(ALOG(100.)- ALOG(25.18))/(ALOG(A)-ALOG(B))                  CALC 019
      RETURN                                                             CALC 020
      END                                                                CALC 021
```

```
      SUBROUTINE DOUT1                                                    DOUT1 001
C MAIN CALCULATIONS DONE FOR DATA REDUCTION AND APPROPRIATE DATA PUT IN   DOUT1 002
C ECT FORM FOR PLOTTING ON THE PHASE DIAGRAM                              DOUT1 003
      COMMON    ITIME( 95),DELP( 95),IGAS ( 95),DATA( 95,5),CAL(6),       DOUT1 004
     1CALCO(6),SUMD(6),ISAMP( 95),RCC(6),IDATE(5),HSLOP,A,B,CZERO,FEZER,  DOUT1 005
     2PATM, PH2O,NIT,NSUM1,NSUM2,NSUM3,NSAMP,NRUN                         DOUT1 006
      ID=5                                                                DOUT1 007
      Y=7.                                                                DOUT1 008
      NCAL =0                                                             DOUT1 009
      NCAL1=0                                                             DOUT1 010
      NCAL2=0                                                             DOUT1 011
      CALL SCALF(.85,.85,0.,0. )                                          DOUT1 012
      CALL FPLOT(3,.0,.0)                                                 DOUT1 013
   71 DO 65 I=1,NSAMP,1                                                   DOUT1 014
      IF(NCAL1)22,80,81                                                   DOUT1 015
   22 WRITE(3,100)                                                        DOUT1 016
  100 FORMAT  ('WE HAVE A PROBLEM IN DOUT1')                              DOUT1 017
   80 WRITE(3,102)NRUN,IDATE                                              DOUT1 018
      WRITE(3,113)                                                        DOUT1 019
  113 FORMAT(//38H THE CALIBRATI(N GASES ARE KNOWN TO BE/21X,55HIGAS       DOUT1 020
     1     H2         CO        CH4        CO2        H2O    )           DOUT1 021
      SUM=100.-CAL(5)                                                     DOUT1 022
      WRITE(3,114)SUM,CAL(5)                                              DOUT1 023
  114 FORMAT(24X,52H1       25.17      24.94      24.97      24.94       0.00  DOUT1 024
     1       /24X,52H2      100.00       0.00       0.00       0.00       0.00  DOUT1 025
     2       /24X,36H3        0.00       0.00       0.00       ,F6.2,5X,F5.2)  DOUT1 026
      WRITE(3,115)                                                        DOUT1 027
  115 FORMAT(/54H CALIBRATION GAS SAMPLES FOR THIS RUN WERE ANALYSED AS)  DOUT1 028
      WRITE(3,116)                                                        DOUT1 029
  116 FORMAT(1H0,  9HTIME SAMP,5X,70H DELP IGAS         H2         CO       DOUT1 030
     1  CH4        CO2        H2O         C    )                         DOUT1 031
      NCAL1=NCAL1+1                                                       DOUT1 032
   81 IF(NCAL)22,82,83                                                    DOUT1 033
   82 IF(IGAS(I)-4)72,65,65                                               DOUT1 034
   83 IF(NCAL2)22,84,85                                                   DOUT1 035
```

```
 84 WRITE(3,102)NRUN,IDATE                                                DOUT1 036
102 FORMAT(1H1,33X,21HDATA TAKEN DURING RUN,I4,3H ON,5A2)                  DOUT1 037
    WRITE(3,116)                                                          DOUT1 038
    NCAL2=NCAL2+1                                                         DOUT1 039
 85 IF(IGAS(I)-4)65,86,86                                                 DOUT1 040
 86 IF(IGAS(I)-6)72,69,69                                                 DOUT1 041
 72 J=1                                                                   DOUT1 042
    DATA(I,J)=EXP(ALOG(100.)-(ALOG(A)-ALOG(DATA(I,J)))*HSLOP)             DOUT1 043
    SUM=DATA(I,J)                                                         DOUT1 044
    DO 66 J=2,5,1                                                         DOUT1 045
    DATA(I,J)=DATA(I,J)*100./CALCO(J)                                     DOUT1 046
    SUM=SUM+DATA(I,J)                                                     DOUT1 047
 66 CONTINUE                                                              DOUT1 048
    DO 67 J=1,5                                                           DOUT1 049
    DATA(I,J)=DATA(I,J)*100./SUM                                          DOUT1 050
 67 CONTINUE                                                              DOUT1 051
    INDEX=(SUM-100.)/10.                                                  DOUT1 052
    IF(INDEX)690,691,690                                                  DOUT1 053
690 WRITE(3,108)                                                          DOUT1 054
108 FORMAT(1X,100HTHE SUM OF THE FOLLOWING DATA DIFFERED FROM 100 PERC    DOUT1 055
   1ENT BY MORE THAN 10 PERCENT BEFORE JUSTIFICATION)                     DOUT1 056
691 WRITE(3,105)ITIME(I),ISAMP(I),DELP(I),IGAS(I),(DATA(I,J),J=1,5)       DOUT1 057
105 FORMAT(2I5,5X,F5.2,I5,5F10.2)                                         DOUT1 058
    PH2=DATA(I,1)                                                         DOUT1 059
    PCO=DATA(I,2)                                                         DOUT1 060
    PCH4=DATA(I,3)                                                        DOUT1 061
    PCO2=DATA(I,4)                                                        DOUT1 062
    PH2O=DATA(I,5)                                                        DOUT1 063
    IGASS=IGAS(I)                                                         DOUT1 064
    GO TO (925,925,925,926,927),IGASS                                     DOUT1 065
926 IF(NIT-2)23,24,25                                                     DOUT1 066
 23 NUM=NIT-1                                                             DOUT1 067
    GO TO 928                                                             DOUT1 068
 24 NUM=NIT                                                               DOUT1 069
    GO TO 928                                                             DOUT1 070
```

```
 25 NUM=NIT+1.                                                          DOUT1 071
    GO TO 928                                                           DOUT1 072
928 CALL DPLOT(PH2,PCO,PCH4,PCO2,PH2O,NUM)                              DOUT1 073
    GO TO 925                                                           DOUT1 074
927 IF(NIT-2)26,27,28                                                   DOUT1 075
 26 NUM=NIT                                                             DOUT1 076
    GO TO 930                                                           DOUT1 077
 27 NUM=NIT+1                                                           DOUT1 078
    GO TO 930                                                           DOUT1 079
 28 NUM=NIT+2                                                           DOUT1 080
    GO TO 930                                                           DOUT1 081
930 CALL DPLOT(PH2,PCO,PCH4,PCO2,PH2O,NUM)                              DOUT1 082
925 GO TO 65                                                            DOUT1 083
 69 K=IGAS(I)-5                                                         DOUT1 084
    GO TO (152,156,157,998) ,K                                          DOUT1 085
152 DATA(I,1)=DATA(I,1)/1.6125                                          DOUT1 086
    DATA(I,2)=DATA(I,2)/3.4250                                          DOUT1 087
    DATA(I,3)=DATA(I,3)/ 4.3125                                         DOUT1 088
    DATA(I,4)=DATA(I,4)/3.0000                                          DOUT1 089
    SUM=0.                                                              DOUT1 090
    DO 153 K=1,4                                                        DOUT1 091
153 SUM=SUM+DATA(I,K)                                                   DOUT1 092
    DATA(I,5)=SUM*DATA(I,5)/PATM                                        DOUT1 093
    SUM=SUM+DATA(I,5)                                                   DOUT1 094
    DO 154 K=1,5                                                        DOUT1 095
154 DATA(I,K)=100.*DATA(I,K)/SUM                                        DOUT1 096
    WRITE(3,109)ITIME(I),(DATA(I,K),K=1,5),SUM                          DOUT1 097
109 FORMAT(1H0,I4,21H CHANGED INLET GAS TO,F9.2,4F10.2,11X,11HTOTAL FL  DOUT1 098
   1OW ,F4.1,13H CC/SEC (STP))                                          DOUT1 099
    PH2=DATA(I,1)                                                       DOUT1 100
    PCO=DATA(I,2)                                                       DOUT1 101
    PCH4=DATA(I,3)                                                      DOUT1 102
    PCO2=DATA(I,4)                                                      DOUT1 103
    PH2O=DATA(I,5)                                                      DOUT1 104
    NIT=NIT+1                                                           DOUT1 105
```

```
      IF(NIT-3)77,77,78                                                  DOUT1 106
   78 NIT=1                                                              DOUT1 107
      GO TO 921                                                          DOUT1 108
   77 GO TO (921,922,923),NIT                                            DOUT1 109
  921 NUM=0                                                             DOUT1 110
      CALL TABLE(PH2,PCO,PCH4,PCO2,PH2O,NUM,Y,NRUN,IDATE)               DOUT1 111
      GO TO 924                                                         DOUT1 112
  922 NUM=2                                                             DOUT1 113
      CALL TABLE(PH2,PCO,PCH4,PCO2,PH2O,NUM,Y,NRUN,IDATE)               DOUT1 114
      GO TO 924                                                         DOUT1 115
  923 NUM=4                                                             DOUT1 116
      CALL TABLE(PH2,PCO,PCH4,PCO2,PH2O,NUM,Y,NRUN,IDATE)               DOUT1 117
  924 GO TO 65                                                          DOUT1 118
  156 C=DATA(I,1)-CZERO                                                 DOUT1 119
      WRITE(3,110)ITIME(I),C                                            DOUT1 120
  110 FORMAT(I5,70X,F10.3,23H GR/GMS CARBON DEPOSITED)                  DOUT1 121
      GO TO 65                                                          DOUT1 122
  157 WRITE(3,111)ITIME(I),DATA(I,1)                                    DOUT1 123
  111 FORMAT(/I5,21H REACTOR TEMPERATURE ,F4.0,19H DEGREES CENTIGRADE/) DOUT1 124
      GO TO 65                                                          DOUT1 125
  998 WRITE(3,999)ITIME(I),IGAS(I)                                      DOUT1 126
  999 FORMAT(1HO,I4,15X,I5,' CHANGE INLET FLOW TO INERT HELIUM AT 20 CC/ DOUT1 127
     1SEC(STP) ')                                                       DOUT1 128
   65 CONTINUE                                                          DOUT1 129
      NCAL =NCAL +1                                                     DOUT1 130
      IF(NCAL2)22,89,90                                                 DOUT1 131
   89 DO 55 I=1,6,1                                                     DOUT1 132
      RCC(I)=CALCO(I)/CALCO(4)                                          DOUT1 133
   55 CONTINUE                                                          DOUT1 134
      WRITE(3,104)(RCC(I),I=1,6)                                        DOUT1 135
      WRITE(3,117)PATM                                                  DOUT1 136
      WRITE(3,118)FEZER                                                 DOUT1 137
      WRITE(3,119)CZERO                                                 DOUT1 138
  117 FORMAT(1HO,26H ATMOSPHERIC PRESSURE WAS  ,F7.2,2H .)              DOUT1 139
  118 FORMAT(1HO,60H THE WEIGHT OF CATALYST INITIALLY CHARGED TO THE REA DOUT1 140
```

```
   1CTOR IS  ,F6.3,7H GRAMS.)                                                    DOUT1 141
119 FORMAT(1H0,70H THE GROSS WEIGHT OF THE CATALYST CARRIER AND SUSPEN           DOUT1 142
   1SION MECHANISM IS  ,F7.3,7H GRAMS.)                                         DOUT1 143
104 FORMAT(1H0,24HTHE RELATIVE CALIBRATION/25H AREA COEFFICENTS ARE             DOUT1 144
   1  ,6F10.6)                                                                  DOUT1 145
    GO TO 71                                                                    DOUT1 146
 90 RETURN                                                                      DOUT1 147
    END                                                                         DOUT1 148
```

```
      SUBROUTINE TABLE(PH2,PCO,PCH4,PCO2,PH2O,NUM,Y,NRUM,IDATE)          TABLE 001
C LISTS INLET AND OUTLET GAS COMPOSITIONS ON THE PHASE DIAGRAM           TABLE 002
      DIMENSION IDATE(5)                                                 TABLE 003
      INUM=NUM                                                           TABLE 004
      IF(NUM-2)3,4,4                                                     TABLE 005
    3 CALL FCHAR(-2.9,9.,.1,.1,0.0)                                      TABLE 006
      WRITE (7,5) NRUM,IDATE                                             TABLE 007
    5 FORMAT('DATE TAKEN DURING RUN',I4,'ON',5A2)                        TABLE 008
      CALL FCHAR(-2.2,8.,.1,.1,0.0)                                      TABLE 009
      WRITE(7,1)                                                         TABLE 010
    1 FORMAT('INLET GAS COMPOSITION  ')                                  TABLE 011
      CALL FCHAR(-2.3,7.5,.1,.1,0.0)                                     TABLE 012
      WRITE(7,2)                                                         TABLE 013
    2 FORMAT('H2',5X,'CO',3X,'CH4',3X,'CO2',3X,'H2O')                    TABLE 014
    4 CALL FPLOT(3,-2.5,Y)                                               TABLE 015
      CALL FPLOT(2,-2.5,Y)                                               TABLE 016
      CALL POINT(INUM)                                                   TABLE 017
      CALL FCHAR(-2.4,Y,.1,.1,0.0)                                       TABLE 018
      WRITE(7,200) PH2,PCO,PCH4,PCO2,PH2O                                TABLE 019
  200 FORMAT(F5.1,1X,F5.1,1X,F5.1,1X,F5.1,1X,F5.1)                       TABLE 020
      INUM=INUM+1                                                        TABLE 021
      Y1=Y-.5                                                            TABLE 022
      CALL FPLOT(3,-2.5,Y1)                                              TABLE 023
      CALL FPLOT(2,-2.5,Y1)                                              TABLE 024
      CALL POINT(INUM)                                                   TABLE 025
      CALL FCHAR(-2.3,Y1,.1,.1,0.0)                                      TABLE 026
      WRITE(7,300)                                                       TABLE 027
  300 FORMAT('OUTLET GAS COMP.')                                         TABLE 028
      Y=Y-1.                                                             TABLE 029
      RETURN                                                             TABLE 030
      END                                                                TABLE 031
```

```
      SUBROUTINE DPLOT(PH2,PCO,PCH4,PCO2,PH2O,NUM)                      DPLOT 001
C PLOTS INLET AND OUTLET GAS COMPOSITIONS ON THE PHASE DIAGRAM          DPLOT 002
      PI=3.14159                                                        DPLOT 003
      Z=PI/6.                                                           DPLOT 004
      ATOMH=2.*PH2O+2.*PH2+4.*PCH4                                      DPLOT 005
      ATOMC=PCO+PCO2+PCH4                                               DPLOT 006
      ATOMO=PCO+2.*PCO2+PH2O                                            DPLOT 007
      ATOMT=ATOMH+ATOMO+ATOMC                                           DPLOT 008
      ULH=10.-(ATOMH/(ATOMT*.1))                                        DPLOT 009
      ULO=ATOMO/(ATOMT*.1)                                              DPLOT 010
      ULC=ATOMC/(ATOMT*.1)                                              DPLOT 011
      X1=ULH-(ULH-ULO)*SIN(Z)                                           DPLOT 012
      Y1=(ULH-ULO)*COS(Z)                                               DPLOT 013
      CALL FPLOT(3,X1,Y1)                                               DPLOT 014
      CALL FPLOT(2,X1,Y1)                                               DPLOT 015
      CALL POINT(NUM)                                                   DPLOT 016
      RETURN                                                            DPLOT 017
      END                                                               DPLOT 018
```

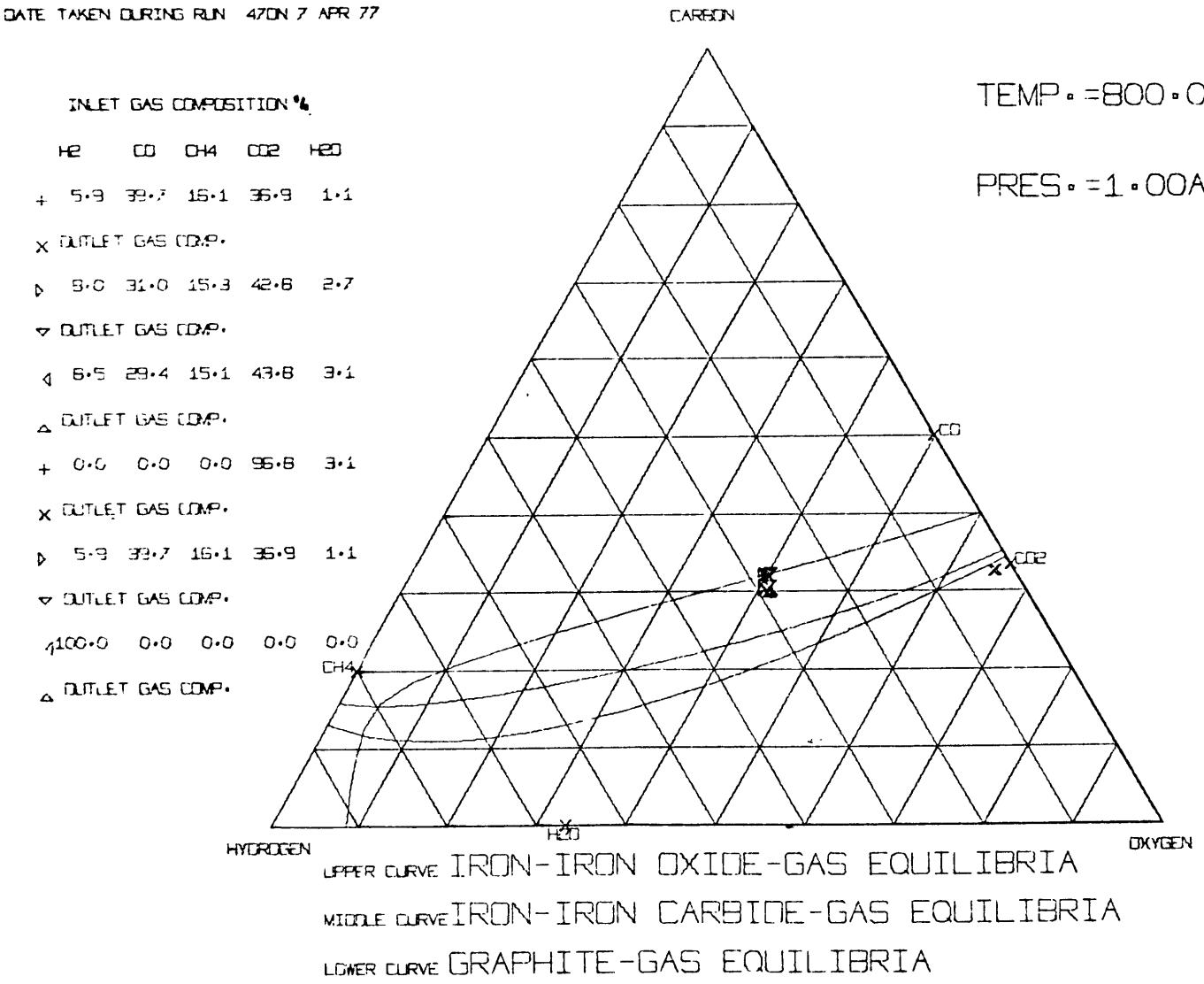

Figure 61 Example of Experimental Data as Plotted on a Triangular Phase Diagram

DATA TAKEN DURING RUN 47 ON 8 APR 77

TIME	SAMP	DELP	IGAS	H2	CO	CH4	CO2	H2O	N2	HE	C(MILLIGRAPS)
800			9	CHANGE INLET FLOW TO INERT HELIUM AT 20 CC/SEC(STP)							
930			8	527.0							
1023	1	0.00	1	3825.0	194597.0	162589.0	214608.0	0.0			
1028	2	0.00	1	3812.0	193370.0	161754.0	212472.0	0.0			
1032	3	0.00	1	3872.0	195833.0	164073.0	214550.0	0.0			
1036	4	0.00	1	3828.0	193928.0	162597.0	212021.0	0.0			
1042			7						33.269		
1045			6	1.8	26.6	13.6	21.7	9.2			
1051	5	0.00	4	779.0	312487.0	104147.0	312281.0	9708.0			
1058	6	0.00	4	789.0	309400.0	103094.0	308819.0	7207.0			
1101			7						33.296		
1116	7	-3.00	5	724.0	298610.0	104679.0	330293.0	8680.0			
1123	8	-3.50	5	729.0	294878.0	103472.0	327619.0	6786.0			
1126			7						33.355		
1143	9	0.00	4	812.0	313404.0	105212.0	315123.0	9290.0			
1148	10	0.00	4	809.0	311321.0	104648.0	311519.0	6763.0			
1152			7						33.445		
1207	11	-3.50	5	748.0	290210.0	105050.0	339968.0	9471.0			
1214	12	-3.50	5	742.0	285455.0	104140.0	337918.0	7538.0			
1218			7						33.536		
1219			9	CHANGE INLET FLOW TO INERT HELIUM AT 20 CC/SEC(STP)							
1308			7						33.524		
1318			6	2.5	20.6	12.9	24.9	21.5			
1330	13	0.00	4	1075.0	244659.0	100105.0	367833.0	17689.0			
1336	14	2.00	4	1061.0	243809.0	99746.0	363794.0	14896.0			
1340			7						33.547		
1401	15	-2.50	5	1030.0	243610.0	98931.0	375179.0	16604.0			
1408	16	-3.50	5	1008.0	240291.0	97751.0	370281.0	14395.0			
1413			7						33.558		
1448	17	0.00	4	1082.0	243834.0	99606.0	369909.0	18214.0			
1454	18	0.00	4	1054.0	242814.0	99296.0	365326.0	15923.0			
1458			7						33.565		
1510	19	-3.50	5	1019.0	242031.0	98035.0	375119.0	16652.0			
1517	20	-4.00	5	1013.0	239012.0	96753.0	370516.0	14129.0			
1521			7						33.570		
1524			9	CHANGE INLET FLOW TO INERT HELIUM AT 20 CC/SEC(STP)							
1600			7						33.573		
1611			6	2.6	19.5	12.6	25.5	24.5			
1627	21	0.00	4	1179.0	235535.0	97634.0	376478.0	19730.0			
1634	22	0.00	4	1134.0	233305.0	96683.0	371146.0	17048.0			
1638			7						33.579		
1655	23	-3.30	5	1101.0	234578.0	97098.0	382903.0	19060.0			
1702	24	-3.80	5	1072.0	231455.0	95673.0	378647.0	16426.0			
1706			7						33.579		
1728	25	0.00	4	1161.0	235762.0	97911.0	375818.0	21260.0			
1734	26	0.50	4	1139.0	234538.0	97400.0	371600.0	17894.0			
1739			7						33.579		
1755	27	-3.70	5	1093.0	234134.0	96441.0	380717.0	20158.0			
1802	28	-4.00	5	1088.0	230797.0	95240.0	375046.0	16371.0			
1806			7						33.579		
1808			6	0.0	0.0	0.0	27.5	24.5			
1829	29	0.00	3	0.0	1134.0	0.0	843407.1	18158.0			
1836	30	0.00	3	0.0	92.0	0.0	832146.1	15922.0			

Figure 62 Example of Raw Data, Run A-47

```
1840                    7                                                       33.584
1855   31     -4.20     5        0.0    22876.0        0.0   811413.1   18433.0
1902   32     -5.00     5        0.0    19630.0        0.0   804270.1   16181.0
1908                    7                                                       33.589
1910                    9 CHANGE INLET FLOW TO INERT HELIUM AT 20 CC/SEC(STP)
2034                    7                                                       33.598

2043                    6       1.8       26.6       13.6       21.7        9.2
2053   33     -0.50     4      761.0   315284.0   103308.0   317878.0   10681.0
2059   34      0.00     4      750.0   314611.0   103714.0   310405.0    8043.0
2102                    7                                                       33.586
2120   35     -3.50     5      722.0   304927.0   103068.0   327163.0    8733.0
2128   36      3.80     5      716.0   298875.0   102769.0   328014.0    6682.0
2132                    7                                                       33.598
2145   37      0.30     4      760.0   312313.0   104065.0   312637.0   10421.0
2152   38     -4.00     5      708.0   290266.0   103472.0   333706.0    8137.0
2156                    7                                                       33.644

2157                    6      32.5        0.0        0.0        0.0        0.0
2209   39      0.00     2  21938.0        0.0      732.0        0.0        0.0
2212   40      0.00     2  21695.0        0.0      600.0        0.0        0.0
2215                    7                                                       33.589
2216                    9 CHANGE INLET FLOW TO INERT HELIUM AT 20 CC/SEC(STP)
```

Figure 62 (continued)

DATA TAKEN DURING RUN 47 ON 7 APR 77

THE CALIBRATION GASES ARE KNOWN TO BE

IGAS	H2	CO	CH4	CO2	H2O
1	25.17	24.94	24.97	24.94	0.00
2	100.00	0.00	0.00	0.00	0.00
3	0.00	0.00	0.00	96.79	3.20

CALIBRATION GAS SAMPLES FOR THIS RUN WERE ANALYSED AS

TIME	SAMP	DELP	IGAS	H2	CO	CH4	CO2	H2O	N2	HE	C(MILLIGRAMS)
1023	1	0.00	1	25.10	24.90	24.92	25.05	0.00	0.00	0.00	
1028	2	0.00	1	25.19	24.90	24.94	24.95	0.00	0.00	0.00	
1032	3	0.00	1	25.19	24.91	24.99	24.89	0.00	0.00	0.00	
1036	4	0.00	1	25.21	24.91	25.01	24.84	0.00	0.00	0.00	
1829	29	0.00	3	0.00	0.14	0.00	96.51	3.34	0.00	0.00	
1836	30	0.00	3	0.00	0.01	0.00	97.00	2.98	0.00	0.00	
2209	39	0.00	2	99.88	0.00	0.11	0.00	0.00	0.00	0.00	
2212	40	0.00	2	99.90	0.00	0.09	0.00	0.00	0.00	0.00	

THE RELATIVE CALIBRATION
AREA COEFFICENTS ARE 0.017795 0.912158 0.761705 1.000000 0.622108 0.025495 0.875000

ATMOSPHERIC PRESSURE WAS 767.33 .

THE WEIGHT OF CATALYST INITIALLY CHARGED TO THE REACTOR IS 0.518 GRAMS.

THE GROSS WEIGHT OF THE CATALYST CARRIER AND SUSPENSION MECHANISM IS 32.962 GRAMS.

Figure 63 Chromatograph Response Factors for A-47

DATA TAKEN DURING RUN 47 ON 7 APR 77

TIME	SAMP	DELP	IGAS	H2	CO	CH4	CO2	H2O	N2	HE	C(MILLIGRAMS)
800			9 CHANGE INLET FLOW TO INERT HELIUM AT 20 CC/SEC(STP)								
930	REACTOR TEMPERATURE 527. DEGREES CENTIGRADE										
1042											306.999
1045	CHANGED INLET GAS TO			5.70	37.35	16.11	39.62	1.20	TOTAL FLOW 19.9 CC/SEC (STP)		
1051	5	0.00	4	7.01	39.46	15.75	35.97	1.79	0.00	0.00	
1058	6	0.00	4	7.17	39.60	15.80	36.05	1.35	0.00	0.00	
1101											333.999
1116	7	-3.00	5	6.62	37.78	15.86	38.12	1.61	0.00	0.00	
1123	8	-3.50	5	6.74	37.79	15.88	38.30	1.27	0.00	0.00	
1126											392.997
1143	9	0.00	4	7.19	39.28	15.79	36.02	1.70	0.00	0.00	
1148	10	0.00	4	7.26	39.51	15.90	36.06	1.25	0.00	0.00	
1152											483.001
1207	11	-3.50	5	6.76	36.56	15.84	39.07	1.74	0.00	0.00	
1214	12	-3.50	5	6.81	36.46	15.93	39.37	1.41	0.00	0.00	
1218											573.997
1219			9 CHANGE INLET FLOW TO INERT HELIUM AT 20 CC/SEC(STP)								
1308											561.996
1318	CHANGED INLET GAS TO			7.63	28.90	15.20	45.44	2.80	TOTAL FLOW 19.9 CC/SEC (STP)		
1330	13	0.00	4	8.98	30.67	15.02	42.06	3.25	0.00	0.00	
1336	14	2.00	4	9.00	30.94	15.16	42.11	2.77	0.00	0.00	
1340											584.999
1401	15	-2.50	5	8.67	30.53	14.84	42.89	3.05	0.00	0.00	
1408	16	-3.50	5	8.67	30.63	14.92	43.06	2.69	0.00	0.00	
1413											596.000
1448	17	0.00	4	9.01	30.50	14.92	42.21	3.34	0.00	0.00	
1454	18	0.00	4	8.94	30.77	15.07	42.24	2.95	0.00	0.00	
1458											602.996
1510	19	-3.50	5	8.63	30.45	14.77	43.05	3.07	0.00	0.00	
1517	20	-4.00	5	8.73	30.56	14.81	43.22	2.64	0.00	0.00	
1521											608.001
1524			9 CHANGE INLET FLOW TO INERT HELIUM AT 20 CC/SEC(STP)								
1600											611.000
1611	CHANGED INLET GAS TO			8.09	27.34	14.91	46.44	3.20	TOTAL FLOW 19.9 CC/SEC (STP)		
1627	21	0.00	4	9.61	29.37	14.57	42.82	3.60	0.00	0.00	
1634	22	0.00	4	9.49	29.62	14.70	42.99	3.17	0.00	0.00	
1638											616.996
1655	23	-3.30	5	9.11	29.28	14.51	43.60	3.48	0.00	0.00	
1702	24	-3.80	5	9.07	29.41	14.55	43.88	3.06	0.00	0.00	
1706											616.996
1728	25	0.00	4	9.48	29.35	14.59	42.68	3.88	0.00	0.00	
1734	26	0.50	4	9.48	29.63	14.73	42.82	3.31	0.00	0.00	
1739											616.996
1755	27	-3.70	5	9.08	29.30	14.45	43.46	3.69	0.00	0.00	
1802	28	-4.00	5	9.22	29.46	14.56	43.67	3.06	0.00	0.00	
1806											616.996
1808	CHANGED INLET GAS TO			0.00	0.00	0.00	96.79	3.20	TOTAL FLOW 10.3 CC/SEC (STP)		
1840											622.001
1855	31	-4.20	5	0.00	2.89	0.00	93.68	3.42	0.00	0.00	
1902	32	-5.00	5	0.00	2.52	0.00	94.42	3.05	0.00	0.00	
1908											626.999
1910			9 CHANGE INLET FLOW TO INERT HELIUM AT 20 CC/SEC(STP)								

Figure 64 Example of Reduced Data, Run A-47

```
2034                                                                                                636.001

2043 CHANGED INLET GAS TO      5.71      37.33      16.11      39.63      1.20          TOTAL FLOW 19.9 CC/SEC (STP)
2053   33      -0.50    4      6.81      39.45      15.48      36.28      1.95    0.00      0.00
2059   34       0.00    4      6.84      39.94      15.76      35.94      1.49    0.00      0.00
2102                                                                                                624.000
2120   35      -3.50    5      6.59      38.51      15.58      37.68      1.61    0.00      0.00
2128   36       3.80    5      6.63      38.17      15.71      38.21      1.25    0.00      0.00
2132                                                                                                636.001
2145   37       0.30    4      6.87      39.44      15.73      36.01      1.92    0.00      0.00
2152   38      -4.00    5      6.57      37.12      15.84      38.92      1.52    0.00      0.00
2156                                                                                                681.999

2157 CHANGED INLET GAS TO    100.00       0.00       0.00       0.00       0.00          TOTAL FLOW 19.6 CC/SEC (STP)
2215                                                                                                626.999
2216                  9 CHANGE INLET FLOW TO INERT HELIUM AT 20 CC/SEC(STP)
```

Figure 64 (continued)

```
********** INTERRUPT REQUEST **********
```

```
C PROGRAM ERROR USED TO DETERMINE THE ERRORS THAT OCCUR IN RAW DATA REDU
C CTION BASED ON A PROPAGATION OF ERROR ANALYSIS ON THE PRECISION GAS MI
C XTURE
      DIMENSION ITIME(008),DELP(008),IGAS (008),DATA(008,5),CAL(6),
     1CALCO(6),SUMD(6),ISAMP(008),RCC(6),IDATE(5), TE(6),  EDAT(8,5),DSM
     1D(6),DCLC(6),DCAL(6),TEST(6)
   01 READ (2,101)NRUN,NSAMP,PATM,PH2O,IDATE,CZERO,FEZER
      IF(NRUN)68,68,02
   02 WRITE(3,102)NRUN,IDATE
  101 FORMAT(5X,I5,5X,I5,5X,F5.2,5X,F6.3,4X,5A2,5X,2F10.3)
  102 FORMAT(1H1,33X,21HDATA TAKEN DURING RUN,I4,3H ON,5A2)
      WRITE(3,116)
C MAXIMUM ERROR IN BAROMETRIC PRESSURE (DPATM) AND ERROR IN PRESSURE OF
C THE SAMPLE CELL (DDELP) AND ERROR AS SPECIFIED IN THE PRECISION GAS
C MIXTURE (DCAL)
      DPATM=4.
      DDELP=1.
      DSUM=0.0
      IH2O=PH2O
      PATM=PATM*25.4
      CAL(1)=25.18
      CAL(2)=24.91
      CAL(3)=24.97
      CAL(4)=24.94
      CAL(5)=PH2O*100./PATM
      CAL(6)=100.
      NSUM1=0
      NSUM2=0
      NSUM3=0
      DO 05 N=1,6,1
      SUMD(N)=0.
      TEST(N)=0.0
      DSMD(N)=0.0
      DCAL(N)=.02
   05 CONTINUE
```

```
C START OF ANALYSIS                                                              ERROR 036
      DCAL(5)=(2.0*PH2O/PATM)+(100.*PH2O*DPATM/(PATM**2.))                       ERROR 037
      DO 11 I=1,NSAMP,1                                                          ERROR 038
   11 READ (2,103)ITIME(I),ISAMP(I),DELP(I),IGAS(I),(DATA(I,J),J=1,5)            ERROR 039
      DO 10 I=1,NSAMP,1                                                          ERROR 040
      IF(IGAS(I)-6)18,51,51                                                      ERROR 041
   18 WRITE(3,103)ITIME(I),ISAMP(I),DELP(I),IGAS(I),(DATA(I,J),J=1,5)            ERROR 042
  103 FORMAT(2I5,5X,F5.2,I5,5F10.1)                                              ERROR 043
      DO 20 K=1,5,1                                                              ERROR 044
      DATA(I,K)=DATA(I,K)*PATM/(PATM+DELP(I))                                    ERROR 045
      V=1.                                                                       ERROR 046
      IF(IGAS(I)-4)451,20,20                                                     ERROR 047
  451 EDAT(I,K)=DATA(I,K)*V*DPATM*(1./(PATM+DELP(I))+PATM/(PATM+DELP(I))         ERROR 048
     1**2.)+DATA(I,K)*V*DDELP*(PATM/(PATM+DELP(I))**2.)                          ERROR 049
   20 CONTINUE                                                                   ERROR 050
      K=IGAS(I)                                                                  ERROR 051
      GO TO (30,40,50,10,10),K                                                   ERROR 052
   30 DO 70 J=1,4,1                                                              ERROR 053
      SUMD(J)=SUMD(J)+DATA(I,J)                                                  ERROR 054
      DSMD(J)=DSMD(J)+EDAT(I,J)                                                  ERROR 055
   70 CONTINUE                                                                   ERROR 056
      NSUM1=NSUM1+1                                                              ERROR 057
      GO TO 10                                                                   ERROR 058
   40 SUMD(6)=SUMD(6)+DATA(I,1)                                                  ERROR 059
      DSMD(6)=DSMD(6)+EDAT(I,1)                                                  ERROR 060
      NSUM2=NSUM2+1                                                              ERROR 061
      GO TO 10                                                                   ERROR 062
   50 SUMD(5)=SUMD(5)+DATA(I,5)                                                  ERROR 063
      DSMD(5)=DSMD(5)+EDAT(I,5)                                                  ERROR 064
      NSUM3=NSUM3+1                                                              ERROR 065
      GO TO 10                                                                   ERROR 066
   51 K=IGAS(I)-5                                                                ERROR 067
      GO TO (52,53,54,56),K                                                      ERROR 068
   52 WRITE(3,106)ITIME(I),IGAS(I),(DATA(I,J),J=1,5)                             ERROR 069
  106 FORMAT(1H0,I4,15X,I5,5F10.1)                                               ERROR 070
```

```
      GO TO 10                                                          ERROR 071
   53 WRITE(3,107)ITIME(I),IGAS(I),DATA(I,1)                            ERROR 072
  107 FORMAT(I5,15X,I5,50X,F10.3)                                       ERROR 073
      GO TO 10                                                          ERROR 074
   54 WRITE(3,106)ITIME(I),IGAS(I),DATA(I,1)                            ERROR 075
      GO TO 10                                                          ERROR 076
   56 WRITE(3,999)ITIME(I),IGAS(I)                                      ERROR 077
   10 CONTINUE                                                          ERROR 078
      ID=0                                                              ERROR 079
      DO 45 L=1,4,1                                                     ERROR 080
      CALCO(L)=SUMD(L)*100./(NSUM1*CAL(L))                              ERROR 081
      DCLC(L)=(100.*DSMD(L)/(NSUM1*CAL(L)))+100.*SUMD(L)*DCAL(L)/(NSUM1* ERROR 082
     1CAL(L)**2.)                                                       ERROR 083
      PIT=CALCO(4)*.875                                                 ERROR 084
   45 CONTINUE                                                          ERROR 085
      IF(IH2O)68,46,47                                                  ERROR 086
   46 CALCO(5)=CALCO(4)*0.69                                            ERROR 087
      DCLC(5)=DCLC(4)*.69                                               ERROR 088
      GO TO 48                                                          ERROR 089
   47 CALCO(5)=SUMD(5)*100./(NSUM3*CAL(5))                              ERROR 090
      DCLC(5)=100.*DSMD(5)/(NSUM3*CAL(5))+100.*SUMD(5)*DCAL(5)/(NSUM3*CA ERROR 091
     1L(5)**2.)                                                         ERROR 092
   48 CALCO(6)=SUMD(6)*100./(NSUM2*CAL(6))                              ERROR 093
      DCLC(6)=100.*DSMD(6)/(NSUM2*CAL(6))+100.*SUMD(6)*DCAL(6)/(NSUM2*CA ERROR 094
     1L(6)**2.)                                                         ERROR 095
      A=SUMD(6)/NSUM2                                                   ERROR 096
      B=SUMD(1)/NSUM1                                                   ERROR 097
      C=ALOG(A)-ALOG(B)                                                 ERROR 098
      D=ALOG(100.)-ALOG(25.18)                                          ERROR 099
      HSLOP=(ALOG(100.)- ALOG(25.18))/(ALOG(A)-ALOG(B))                 ERROR 100
      DELA=DSMD(6)/NSUM2                                                ERROR 101
      DELB=DSMD(1)/NSUM1                                                ERROR 102
      DELC=DELA/(A)+(DELB/B)                                            ERROR 103
       DSLO=-(D*DELC/(C**2.))                                           ERROR 104
      NCAL =0                                                           ERROR 105
```

```
    NCAL1=0                                                                 ERROR 106
    NCAL2=0                                                                 ERROR 107
 71 DO 65 I=1,NSAMP,1                                                       ERROR 108
    IF(NCAL1)68,80,81                                                       ERROR 109
 80 WRITE(3,102)NRUN,IDATE                                                  ERROR 110
    WRITE(3,113)                                                            ERROR 111
113 FORMAT(//38H THE CALIBRATI(N GASES ARE KNOWN TO BE/21X,55HIGAS          ERROR 112
   1     H2          CO         CH4         CO2         H2O    )           ERROR 113
    SUM=100.-CAL(5)                                                         ERROR 114
    WRITE(3,114)SUM,CAL(5)                                                  ERROR 115
114 FORMAT(24X,52H1       25.17      24.94      24.97      24.94       0.00  ERROR 116
   1       /24X,52H2      100.00       0.00       0.00       0.00       0.00 ERROR 117
   2       /24X,36H3        0.00       0.00       0.00       ,F6.2,5X,F5.2) ERROR 118
    WRITE(3,115)                                                            ERROR 119
115 FORMAT(/54H CALIBRATION GAS SAMPLES FOR THIS RUN WERE ANALYSED AS)      ERROR 120
    WRITE(3,116)                                                            ERROR 121
116 FORMAT(1H0,  9HTIME SAMP,5X,  ' DELP IGAS          H2          CO       ERROR 122
   1  CH4         CO2         H2O          N2         HE         C(MILLIGRAMS)') ERROR 123
    NCAL1=NCAL1+1                                                           ERROR 124
 81 IF(NCAL)68,82,83                                                        ERROR 125
 82 IF(IGAS(I)-4)72,65,65                                                   ERROR 126
 83 IF(NCAL2)68,85,85                                                       ERROR 127
 85 NCAL2=NCAL2+1                                                           ERROR 128
    IF(IGAS(I)-4)65,86,86                                                   ERROR 129
 86 IF(IGAS(I)-6)72,69,69                                                   ERROR 130
 72 IF(ID)68,888,887                                                        ERROR 131
888 J=1                                                                     ERROR 132
    IF(IGAS(I)-3)503,512,504                                                ERROR 133
503 EDAT(I,J)=(ALOG(100.)-(ALOG(A)-ALOG(DATA(I,J)))*HSLOP)*(HSLOP*(EDA      ERROR 134
   1T(I,J)/DATA(I,J)+DELA/A)+DSLO*(ALOG(DATA(I,J))-ALOG(A)) )               ERROR 135
    GO TO 513                                                               ERROR 136
512 EDAT(I,1)=0.0                                                           ERROR 137
513 DSUM=EDAT(I,J)                                                          ERROR 138
504 DATA(I,J)=EXP(ALOG(100.)-(ALOG(A)-ALOG(DATA(I,J)))*HSLOP)               ERROR 139
    SUM=DATA(I,J)                                                           ERROR 140
```

```
      DO 66 J=2,5,1                                                    ERROR 141
      IF(IGAS(I)-4)505,510,510                                         ERROR 142
  505 EDAT(I,J)=100.*EDAT(I,J)/(CALCO(J))+(DATA(I,J)*100.*DCLC(J)/(CALCO ERROR 143
     1(J)**2.))                                                        ERROR 144
      DSUM=EDAT(I,J)+DSUM                                              ERROR 145
  510 DATA(I,J)=DATA(I,J)*100./CALCO(J)                                ERROR 146
      SUM=SUM+DATA(I,J)                                                ERROR 147
   66 CONTINUE                                                         ERROR 148
      DO 67 J=1,5                                                      ERROR 149
      IF(IGAS(I)-4)506,518,518                                         ERROR 150
  506 EDAT(I,J)=(100.*EDAT(I,J)/SUM)+(DATA(I,J)*100.*DSUM/(SUM**2.))   ERROR 151
  518 DATA(I,J)=DATA(I,J)*100./SUM                                     ERROR 152
   67 CONTINUE                                                         ERROR 153
      PN2=0.0                                                          ERROR 154
      HEL=0.0                                                          ERROR 155
      DO 777 J=1,5,1                                                   ERROR 156
      IF(EDAT(I,J)-TEST(J))777,775,775                                 ERROR 157
  775 TEST(J)=EDAT(I,J)                                                ERROR 158
      TE(J)=(EDAT(I,J)/DATA(I,J))*100.                                 ERROR 159
  777 CONTINUE                                                         ERROR 160
C ERRORS IN THE WEIGHT MEASUREMENT OF THE CATALYST ASSEMBLE            ERROR 161
      CB=.003                                                          ERROR 162
      DCZ=.003                                                         ERROR 163
      DCD=(CB+DCZ)*1000.                                               ERROR 164
      GO TO 884                                                        ERROR 165
  887 J=1                                                              ERROR 166
      DATA(I,J)=EXP(ALOG(100.)-(ALOG(A)-ALOG(DATA(I,J)))*HSLOP)        ERROR 167
      DATA(I,2)=DATA(I,2)*100./CALCO(2)                                ERROR 168
      DATA(I,3)=DATA(I,3)*100./PIT                                     ERROR 169
      SUM=DATA(I,1)+DATA(I,2)+DATA(I,3)                                ERROR 170
      DO 886 J=4,5,1                                                   ERROR 171
      DATA(I,J)=DATA(I,J)*100./CALCO(J)                                ERROR 172
      SUM=SUM+DATA(I,J)                                                ERROR 173
  886 CONTINUE                                                         ERROR 174
      HEL=100.-SUM                                                     ERROR 175
```

```
      SUM=SUM+HEL                                                       ERROR 176
      PN2=DATA(I,3)                                                     ERROR 177
      DATA(I,3)=0.0                                                     ERROR 178
  884 ERROR=ABS(SUM-100.)                                               ERROR 179
C IF THE TOTAL AREA BEFORE NORMALIZATION IS GREATER THAN 5 PERCENT THE E ERROR 180
C RROR WILL BE INDICATED ON THE OUTPUT                                  ERROR 181
      IF (ERROR-5.) 691,691,690                                         ERROR 182
  690 WRITE(3,108) ERROR                                                ERROR 183
  108 FORMAT(1X,    'THE SUM OF THE FOLLOWING DATA DIFFERED FROM 100 PERC ERROR 184
     1ENT BY',F6.2,'BEFORE JUSTIFICATION')                              ERROR 185
  691 WRITE(3,105)ITIME(I),ISAMP(I),DELP(I),IGAS(I),(DATA(I,J),J=1,5),PN ERROR 186
     12,HEL                                                             ERROR 187
  105 FORMAT(2I5,5X,F5.2,I5,7F10.2)                                     ERROR 188
      GO TO 65                                                          ERROR 189
   69 K=IGAS(I)-5                                                       ERROR 190
      GO TO (152,156,157,998),K                                         ERROR 191
  152 DATA(I,1)=DATA(I,1)/1.65                                          ERROR 192
      DATA(I,2)=DATA(I,2)/3.58                                          ERROR 193
      DATA(I,3)=DATA(I,3)/4.25                                          ERROR 194
      DATA(I,4)=DATA(I,4)/2.75                                          ERROR 195
      ID=0                                                              ERROR 196
      SUM=0.                                                            ERROR 197
      DO 153 K=1,4                                                      ERROR 198
  153 SUM=SUM+DATA(I,K)                                                 ERROR 199
      PERHC=(1.00-(DATA(I,5)/PATM))                                     ERROR 200
      SUM=SUM/PERHC                                                     ERROR 201
      DATA(I,5)=SUM*DATA(I,5)/PATM                                      ERROR 202
      DO 154 K=1,5                                                      ERROR 203
  154 DATA(I,K)=100.*DATA(I,K)/SUM                                      ERROR 204
      WRITE(3,109)ITIME(I),(DATA(I,K),K=1,5),SUM                        ERROR 205
  109 FORMAT(1H0,I4,21H CHANGED INLET GAS TO,F9.2,4F10.2,11X,11HTOTAL FL ERROR 206
     1OW ,F4.1,13H CC/SEC (STP))                                        ERROR 207
      GO TO 65                                                          ERROR 208
  998 WRITE(3,999)ITIME(I),IGAS(I)                                      ERROR 209
      ID=1                                                              ERROR 210
```

```
    GO TO 65                                                                ERROR 211
156 BC=(DATA(I,1)-CZERO)*1000.                                              ERROR 212
    WRITE(3,110)ITIME(I),BC                                                 ERROR 213
110 FORMAT(I5,95X,F10.3)                                                    ERROR 214
111 FORMAT(/I5,21H REACTOR TEMPERATURE ,F4.0,19H DEGREES CENTIGRADE/)       ERROR 215
    GO TO 65                                                                ERROR 216
157 WRITE(3,111)ITIME(I),DATA(I,1)                                          ERROR 217
 65 CONTINUE                                                                ERROR 218
    NCAL =NCAL +1                                                           ERROR 219
    IF(NCAL2)68,89,90                                                       ERROR 220
 89 DO 55 I=1,6,1                                                           ERROR 221
    PITT=PIT/CALCO(4)                                                       ERROR 222
    RCC(I)=CALCO(I)/CALCO(4)                                                ERROR 223
 55 CONTINUE                                                                ERROR 224
    WRITE(3,104)(RCC(I),I=1,6),PITT                                         ERROR 225
    WRITE(3,117)PATM                                                        ERROR 226
    WRITE(3,118)FEZER                                                       ERROR 227
    WRITE(3,119)CZERO                                                       ERROR 228
118 FORMAT(1HO,60H THE WEIGHT OF CATALYST INITIALLY CHARGED TO THE REA      ERROR 229
   1CTOR IS  ,F6.3,7H GRAMS.)                                               ERROR 230
999 FORMAT(1HO,I4,15X,I5,' CHANGE INLET FLOW TO INERT HELIUM AT 20 CC/      ERROR 231
   1SEC(STP) ')                                                             ERROR 232
119 FORMAT(1HO,70H THE GROSS WEIGHT OF THE CATALYST CARRIER AND SUSPEN      ERROR 233
   1SION MECHANISM IS  ,F7.3,7H GRAMS.)                                     ERROR 234
117 FORMAT(1HO,26H ATMOSPHERIC PRESSURE WAS  ,F7.2,2H .)                    ERROR 235
    GO TO 71                                                                ERROR 236
 90 WRITE(3,102) NRUN,IDATE                                                 ERROR 237
    WRITE(3,500)                                                            ERROR 238
500 FORMAT(//,16X,'THE FOLLOWING ERROR ANALYSIS WAS PERFORMED USING TH      ERROR 239
   1E TECHNIQUE OF PROPAGATION OF ERRORS')                                  ERROR 240
    WRITE(3,501)                                                            ERROR 241
501 FORMAT(//,28X,'H2        CO          CH4       CO2        H2O        N2  ERROR 242
   1         HE       C(MILLIGRAMS)')                                      ERROR 243
    WRITE(3,502) (TEST(J),J=1,5),DCD                                        ERROR 244
502 FORMAT(/,4X,'ABSOLUTE ERROR',4X,5F10.5,23X,F10.5)                       ERROR 245
```

```
      WRITE(3,516) (TE(J),J=1,5)                                        ERROR 246
  516 FORMAT(/,4X,'RELATIVE ERROR',4X,5F10.5)                           ERROR 247
      WRITE(3,520)                                                      ERROR 248
  520 FORMAT(5X,'(PERCENTAGE)')                                         ERROR 249
      GO TO 01                                                          ERROR 250
  104 FORMAT(1H0,24HTHE RELATIVE CALIBRATION/25H AREA COEFFICENTS ARE   ERROR 251
     1  ,7F10.6)                                                       ERROR 252
   68 CALL EXIT                                                         ERROR 253
      END                                                               ERROR 254
```

DATA TAKEN DURING RUN 47 ON 7 APR 77

TIME	SAMP	DELP	IGAS	H2	CO	CH4	CO2	H2O	N2	HE	C(MILLIGRAMS)
1023	1	0.00	1	3825.0	194597.0	162589.0	214608.0	0.0			
1028	2	0.00	1	3812.0	193370.0	161754.0	212472.0	0.0			
1032	3	0.00	1	3872.0	195833.0	164073.0	214550.0	0.0			
1036	4	0.00	1	3828.0	193928.0	162597.0	212021.0	0.0			
1829	29	0.00	3	0.0	1134.0	0.0	843407.1	18158.0			
1836	30	0.00	3	0.0	92.0	0.0	832146.1	15922.0			
2209	39	0.00	2	21938.0	0.0	732.0	0.0	0.0			
2212	40	0.00	2	21695.0	0.0	600.0	0.0	0.0			

Figure 65 Raw Data for "Error", Run A-47

DATA TAKEN DURING RUN 47 ON 7 APR 77

THE FOLLOWING ERROR ANALYSIS WAS PERFORMED USING THE TECHNIQUE OF PROPAGATION OF ERRORS

	H2	CO	CH4	CO2	H2O	N2	HE	C(MILLIGRAMS)
ABSOLUTE ERROR	0.60832	1.08676	1.09085	4.77729	0.24632			6.00000
RELATIVE ERROR (PERCENTAGE)	2.41458	4.36286	4.36046	4.92480	7.37461			

Figure 66 Example of Propagation of Error Analysis, A-47

```
C PROGRAM TO DETERMINE INITIAL START-UP CONDITIONS, GIVES THE STARTING F   SET 001
C LOW SETTINGS AND CALLS THE NEEDED PLOTTING ROUTINE                       SET 002
      DIMENSION XCOF(4),COF(4),    ROOTR(3),ROOTI(3)                       SET 003
      M=3                                                                  SET 004
      CALL  SCALF(.85,.85,0.,0.)                                           SET 005
      FLOW=20.                                                             SET 006
      NUM=1                                                                SET 007
      DO 105 L=1,NUM,1                                                     SET 008
      DO 100 I=1,6,1                                                       SET 009
      IF(I-1)8,9,8                                                         SET 010
    9 READ(2,1)RC,RO,RV,TEMP,PRES,NU,XST                                   SET 011
      GO TO 10                                                             SET 012
    8 READ(2,1)RC,RO,RV,TEMP,PRES,NU                                       SET 013
C     RC=H2O/H2                                                            SET 014
C     RO=C/H                                                               SET 015
C     RV=O/H                                                               SET 016
C     TEMP=TEMPERATURE K, PRES=PRESSURE ATMOSPHERES                        SET 017
C     XST=1   IF O/H EQUALS CONSTANT                                       SET 018
C     XST=2 IF C/H EQUALS A CONSTANT                                       SET 019
    1 FORMAT(5F10.4,I2,F10.4)                                              SET 020
   10 CALL EQKS(TEMP,EQCH4,EQCO2,EQH2O,EQH2,EQCO,EQC,EQFE3,EQFE2,E         SET 021
     1QCO1,EQH21)                                                          SET 022
      EK1=EQCO2                                                            SET 023
      EK2=1./EQCO1                                                         SET 024
      IF(I-1)4,28,29                                                       SET 025
   28 WRITE(3,18) NU                                                       SET 026
   18 FORMAT(53X,'RUN NUMBER A-',I3)                                       SET 027
      WRITE(3,19) TEMP,PRES                                                SET 028
   19 FORMAT(44X,'TEMPERATURE ',F5.0,'K',1X,',',1X,'PRESSURE ',F3.0,'ATM   SET 029
     1.',////)                                                             SET 030
   29 IF(XST-2.)5,6,4                                                      SET 031
    4 WRITE(3,7)                                                           SET 032
    7 FORMAT(1X,'PROBLEM IN RO,RV (NEG)')                                  SET 033
      GO TO 100                                                            SET 034
    5 K=3                                                                  SET 035
```

```
      C=(EK1+2.*RC)/(4.*RC*RV)                                          SET 036
      D=(RC*(1.-2.*RV)-2.*RV)/(4.*RV)                                   SET 037
      GO TO 31                                                          SET 038
    6 K=5                                                               SET 039
      C=(EK1+RC)/(RC*(4.*RO-1.))                                        SET 040
      D=-2.*RO*(RC+1.)/(4.*RO-1.)                                       SET 041
   31 E=(1.+RC+D)                                                       SET 042
      F=(1.+(EK1/RC)+C)                                                 SET 043
      G=(EK1/RC)**2.                                                    SET 044
      IF(RO-.2)800,800,801                                              SET 045
  800 IF(RV-.2)802,802,801                                              SET 046
  802 XCOF(1)=(-D*E)/((F**2.)*G*EK2)                                    SET 047
      XCOF(2)=(G*EK2+(F*D*E)-(E**2.)*C)/((F**2.)*G*EK2)                 SET 048
      XCOF(3)=-2./F                                                     SET 049
      XCOF(4)=1.                                                        SET 050
      CALL POLRT(XCOF,COF,M,ROOTR,ROOTI,IER)                            SET 051
      DO 101 MV=1,3,1                                                   SET 052
      PCO2=ROOTR(MV)                                                    SET 053
      IF(PCO2)101,102,102                                               SET 054
  102 PCO=PCO2*(EK1/RC)                                                 SET 055
      PH2=(1.-F*PCO2)/E                                                 SET 056
      IF(PH2)101,810,810                                                SET 057
  810 PCH4=EK2*((EK1/RC)**2.)*(PH2**2.)*PCO2                            SET 058
      PH2O=RC*PH2                                                       SET 059
      PT=PCO2+PCO+PCH4+PH2O+PH2                                         SET 060
      IF(ABS(PT-1.)-.01)11,11,101                                       SET 061
  101 CONTINUE                                                          SET 062
  806 WRITE(3,804)                                                      SET 063
  804 FORMAT(50X,' EQUATIONS ARE UNSTABLE')                             SET 064
      GO TO 100                                                         SET 065
  801 XCOF(1)=C/(G*EK2*E)                                               SET 066
      XCOF(2)=(D*F-C*E)/(G*EK2*E)                                       SET 067
      XCOF(3)=-1./E                                                     SET 068
      XCOF(4)=1.                                                        SET 069
      CALL POLRT(XCOF,COF,M,ROOTR,ROOTI,IER)                            SET 070
```

```
      DO 1010 NV=1,3,1                                                  SET 071
      PH2=ROOTR(NV)                                                     SET 072
      IF(PH2)1010,103,103                                               SET 073
  103 PH2O=PH2*RC                                                       SET 074
      PCO2=(1.-E*PH2)/F                                                 SET 075
      PCO=PCO2*(EK1/RC)                                                 SET 076
      PCH4=EK2*((EK1/RC)**2.)*(PH2**2.)*PCO2                            SET 077
      PT=PCO+PCO2+PCH4+PH2O+PH2                                         SET 078
      IF(ABS(PT-1.)-.01)11,11,1010                                      SET 079
 1010 CONTINUE                                                          SET 080
      GO TO 806                                                         SET 081
   11 PI=3.14157                                                        SET 082
      PW=760.*PH2O                                                      SET 083
      V=(ALOG(PW))/2.303                                                SET 084
      IF(TEMP-333.)34,34,35                                             SET 085
   34 A=8.10765                                                         SET 086
      B=1750.2860                                                       SET 087
      C=235.0                                                           SET 088
      GO TO 36                                                          SET 089
   35 A=7.96681                                                         SET 090
      B=1668.21                                                         SET 091
      C=228.                                                            SET 092
   36 SETT=(-B/(V-A))-C                                                 SET 093
      SET1=PH2*FLOW*1.65                                                SET 094
      SET2=PCO*FLOW*3.58                                                SET 095
      SET3=PCH4*FLOW*4.25                                               SET 096
      SET4=PCO2*FLOW*2.75                                               SET 097
      Z=PI/6.                                                           SET 098
      ATOMH=2.*(PH2O+PH2)+4.*PCH4                                       SET 099
      ATOMC=PCO+PCO2+PCH4                                               SET 100
      ATOMO=PCO+2.*PCO2+PH2O                                            SET 101
      ATOMT=ATOMC+ATOMH+ATOMO                                           SET 102
      ULH=10.-(ATOMH/(ATOMT*.1))                                        SET 103
      ULO=ATOMO/(ATOMT*.1)                                              SET 104
      ULC=ATOMC/(ATOMT*.1)                                              SET 105
```

```
      X1=ULH-(ULH-ULO)*SIN(Z)                                                  SET 106
      Y1=(ULH-ULO)*COS(Z)                                                      SET 107
      CALL FPLOT(-2,X1,Y1)                                                     SET 108
      CALL POINT(K)                                                            SET 109
      CALL FPLOT(3,X1,Y1)                                                      SET 110
      PERH=(ATOMH/ATOMT)*100.                                                  SET 111
       PERO=(ATOMO/ATOMT)*100.                                                 SET 112
      PERC=(ATOMC/ATOMT)*100.                                                  SET 113
      RV=ATOMO/ATOMH                                                           SET 114
      RO=ATOMC/ATOMH                                                           SET 115
      WRITE(3,26)I,RC,RO,RV                                                    SET 116
   26 FORMAT(37X,'CONDITION ',I1,',',2X,'PH2O/PH2 ',F4.2,',',2X,'C/H ',F       SET 117
     14.2,',',2X,'O/H ',F4.2)                                                  SET 118
      WRITE(3,27)                                                              SET 119
   27 FORMAT(52X,'GAS COMPOSITIONS',/)                                         SET 120
      WRITE(3,12)                                                              SET 121
   12 FORMAT(28X,'PCO2',8X,'PCO',9X,'PCH4',8X,'PH2O',8X,'PH2',8X,'PTOTAL       SET 122
     1')                                                                       SET 123
       WRITE(3,13)  PCO2,PCO,PCH4,PH2O,PH2,PT                                  SET 124
   13 FORMAT(25X,F10.6,2X,F10.6,2X,F10.6,2X,F10.6,2X,F10.6,2X,F10.6,/ )        SET 125
       WRITE(3,30) PERH,PERO,PERC                                              SET 126
   30 FORMAT(23X,'PERCENTAGE H',F5.2,10X,'PERCENTAGE O ',F6.2,10X,'PERCE       SET 127
     1NTAGE C ',F6.2,// )                                                      SET 128
      WRITE(3,32)                                                              SET 129
   32 FORMAT(54X,'FLOW SETTING')                                               SET 130
      WRITE(3,33)  SET4,SET2,SET3,SETT,SET1                                    SET 131
   33 FORMAT(25X,F10.6,2X,F10.6,2X,F10.6,2X,F10.6,2X,F10.6,////)               SET 132
      IF(I-6)100,807,807                                                       SET 133
  807 IF(XST-2.)808,809,4                                                      SET 134
C     CASE WHERE O/H IS CONSTANT                                               SET 135
  808 ATOMC=0.0                                                                SET 136
      ATOMT=ATOMC+ATOMH+ATOMO                                                  SET 137
      ULH=10.-(ATOMH/(ATOMT*.1))                                               SET 138
      ULO=ATOMO/(ATOMT*.1)                                                     SET 139
      X1=ULH-(ULH-ULO)*SIN(Z)                                                  SET 140
```

```
      Y1=(ULH-ULO)*COS(Z)                                              SET 141
      CALL FPLOT(-2,X1,Y1)                                             SET 142
      X=5.                                                             SET 143
      Y=5.*SQRT(3.)                                                    SET 144
      CALL FPLOT(-1,X,Y)                                               SET 145
       GO TO 100                                                       SET 146
C     CASE WHERE C/H IS CONSTANT                                       SET 147
  809 ATOMO=0.0                                                        SET 148
      ATOMT=ATOMC+ATOMH+ATOMO                                          SET 149
      ULH=10.-(ATOMH/(ATOMT*.1))                                       SET 150
      ULC=ATOMC/(ATOMT*.1)                                             SET 151
      X1=ULH-(ULH-ULO)*SIN(Z)                                          SET 152
      Y1=(ULH-ULO)*COS(Z)                                              SET 153
      X=10.                                                            SET 154
      Y=0.0                                                            SET 155
      CALL FPLOT(-2,X,Y)                                               SET 156
      CALL FPLOT(-1,X1,Y1)                                             SET 157
  100 CONTINUE                                                         SET 158
  105 CONTINUE                                                         SET 159
  106 CONTINUE                                                         SET 160
      CALL FPLOT(3,0.,0.)                                              SET 161
      STOP                                                             SET 162
      END                                                              SET 163
```

```
C  PROGRAM TO OBTAIN INTERSECTIOI OF GRAPHITE-GAS AND IRON-IRON-OXIDE BO   INTER 001
C UNDARY                                                                   INTER 002
      EXTERNAL TCT2                                                        INTER 003
      COMMON CO,C1,C2,C3,C4,C5,C( ,EPS,IEND,XST                            INTER 004
      IEND=1000                                                            INTER 005
      EPS=.001                                                             INTER 006
      KK=9                                                                 INTER 007
      DO 2 K=1,KK                                                          INTER 008
      READ(2,4) TEMP,PRES,ROH,PH2    ,NN                                   INTER 009
         CALL    EQKS(TEMP,EQCH4,EQCO2,EQH2O,EQH2,EQCO,EQC,EQFE3,EQFE2,E   INTER 010
     1QCO1,EQH21)                                                          INTER 011
    4 FORMAT(4F16.8,I3)                                                    INTER 012
      DO 1 N=1,NN                                                          INTER 013
      XST=PH2                                                              INTER 014
      A=(-PRES*EQCH4)                                                      INTER 015
      B=2.*ROH                                                             INTER 016
      CC=1.-2.*ROH                                                         INTER 017
      D=1.+2.*ROH                                                          INTER 018
      AA=(EQCH4*D-PRES*EQH2O*CC)                                           INTER 019
      AB=(EQCH4**2.)*(1.+4.*ROH)+EQH2O                                     INTER 020
      AC=EQCH4*EQH2O*D                                                     INTER 021
      AD=(-EQCO2*(EQCH4**2.))/(4.*EQH2O)                                   INTER 022
      AE=(((-EQCH4*EQCO2)/4.)*(3.-2.*ROH)-2.*EQCH4*ROH)                    INTER 023
      AF=((-EQCO2*EQH2O/4.)*CC*(3.+2.*ROH)-4.*ROH*(EQCH4**2.)-2.*EQH2O*    INTER 024
     1ROH*D)                                                               INTER 025
      AG=((-EQCO2/(4.*EQCH4))*((EQH2O**2.)*(CC**2.)*D)-4.*EQCH4*EQH2O*     INTER 026
     1ROH*D)                                                               INTER 027
      CO=(A**2.)+AD*A                                                      INTER 028
      C1=2.*A*AA+AD*AA+A*AE                                                INTER 029
      C2=2.*A*AB+(AA**2.)+AD*AB+AA*AE+A*AF+(EQCH4**2.)*(ROH**2.)           INTER 030
      C3=2.*A*AC+2.*AA*AB+AD*AC+AB*AE+AF*AA+A*AG+2.*(ROH**2.)*EQCH4*       INTER 031
     1EQH2O*D+4.*(ROH**2.)*(EQCH4**3.)                                     INTER 032
      C4=2.*AA*AC+(AB**2.)+AC*AE+AF*AB+AG*AA+(EQH2O**2.)*(ROH**2.)*        INTER 033
     1(D**2.)+4.*(EQCH4**4.)*(ROH**2.)+8.*(ROH**2.)*(EQCH4**2.)*(EQH2O     INTER 034
     1)*D                                                                  INTER 035
```

```
      C5=2.*AB*AC+AF*AC+AB*AG+8.*(EQCH4**3.)*(EQH2O)*(ROH**2.)*D          INTER 036
     1+4.*(ROH**2.)*EQCH4*(EQH2O**2.)*(D**2.)                            INTER 037
      C6=AC**2.+AG*AC+4.*(ROH**2.)*(EQCH4**2.)*(EQH2O**2.)*(D**2.)       INTER 038
   45 CALL IEOEQ (X,F,DERF,TCT2,XST,EPS,IEND,IER)                        INTER 039
      IF(IER-1)42,43,44                                                  INTER 040
   43 IEND=10000                                                         INTER 041
      EPS=.001                                                           INTER 042
      GO TO 45                                                           INTER 043
   44 XST=XST+.01                                                        INTER 044
      GO TO 45                                                           INTER 045
   42 PH2=X                                                              INTER 046
      PCH4=(PH2**2.)*EQCH4                                               INTER 047
      EQ1=EQH2O*(PH2**3.)/(PCH4)                                         INTER 048
      PH2O=(2.-2.*(PH2+EQCH4*(PH2**2.))-2.*ROH*(PH2+2.*EQCH4*(PH2**2.    INTER 049
     1)))/(2.*ROH+(1./EQ1)+1.)                                           INTER 050
      PCO=PCH4*PH2O/(EQH2O*(PH2**3.))                                    INTER 051
      PCO2=PH2O*PCO/(PH2*EQCO2)                                          INTER 052
      RO=(PCH4+PCO+PCO2)/(2.*(PH2+PH2O)+4.*PCH4)                         INTER 053
      C7=-EQH2*PRES*(EQCO+1.)                                            INTER 054
      C8=(2.*RO+1.)*(EQH2+1.)*(EQCO+1.)                                  INTER 055
      C9=(4.*RO-1.)*EQH2*EQCO*EQH2O*(EQH2*PRES)                          INTER 056
      C10=(1.-2.*RO)*(EQH2+1.)*EQH2*EQCO*EQH2O                           INTER 057
      PH =-(C7/C8+(C9/C8)*PH2**2.+(C10/C8)*PH2**3.)                      INTER 058
      IF(ABS(PH2-PH)-.004)3,3,1                                          INTER 059
    1 ROH=ROH+.001                                                       INTER 060
    3 WRITE(3,5)                                                         INTER 061
    5 FORMAT(3X,'TEMP',7X,'PRES',7X,'ROH',7X, 'PH2',7X,'PH2O',7X,'PCH4   INTER 062
     1',7X,'PCO',7X,'PCO2')                                              INTER 063
      WRITE(3,7)TEMP,PRES,ROH,PH       ,PH2O,PCH4,PCO,PCO2               INTER 064
    7 FORMAT(2X,F6.1,5X,F3.1,6X,F5.3,5X,F8.6,5X,F8.6,5X,F8.6,6X,F8.6,5   INTER 065
     1X,F8.6)                                                            INTER 066
    2 CONTINUE                                                           INTER 067
      STOP                                                               INTER 068
      END                                                                INTER 069
```

```
C PROGRAM FOR PROCESS-PARAMETERS STUDY,  EQUILIBRIUM ASSUMED                    PROC 001
C READING IN FIXED CONDITIONS                                                   PROC 002
      NN=9                                                                      PROC 003
      DO 1 I=1,NN                                                               PROC 004
      READ(2,2) TEMP1,PRES,ROH,CAA,CDD,HDD                                      PROC 005
    2 FORMAT(6F10.3)                                                            PROC 006
C CALL DATA SWITCH TO ALTER SHIFT REACTOR TEMPERATURE RELATIVE TO BOSCH          PROC 007
      CALL DATSW(7,J)                                                           PROC 008
      IF(J-1)16,33,26                                                           PROC 009
   33 WRITE(1,24)                                                               PROC 010
   24 FORMAT(5X,'PUNCH IN DESIRED SHIFT TEMPERATURE')                           PROC 011
      READ(6,25) TEMP                                                           PROC 012
   25 FORMAT(F6.1)                                                              PROC 013
         CALL    EQKS(TEMP,EQCH4,EQCO2,EQH2O,EQH2,EQCO,EQC,EQFE3,EQFE2,E      PROC 014
     1QCO1,EQH21)                                                               PROC 015
      GO TO 30                                                                  PROC 016
   26 TEMP=TEMP1                                                                PROC 017
         CALL    EQKS(TEMP,EQCH4,EQCO2,EQH2O,EQH2,EQCO,EQC,EQFE3,EQFE2,E      PROC 018
     1QCO1,EQH21)                                                               PROC 019
C DETERMINE EXIT COMPOSITIONS OUT OF THE SHIFT REACTOR ASSUMING T,P,CDD,        PROC 020
C HDD,ROH,CAA                                                                   PROC 021
C CALL DATA SWITCH USED TO  INITIATE SHIFT HYDROGEN RECYCLE                     PROC 022
   30 CALL DATSW(6,J)                                                           PROC 023
      IF(J-1)16,17,18                                                           PROC 024
   16 WRITE(3,20)                                                               PROC 025
   20 FORMAT(5X,'PROBLEM IN DATSW(6,J)')                                        PROC 026
      GO TO 23                                                                  PROC 027
   17 WRITE(1,21)                                                               PROC 028
   21 FORMAT(5X,'PUNCH IN HYDROGEN RECYCLE FOR SHIFT REACTOR')                  PROC 029
      READ(6,22) HS                                                             PROC 030
   22 FORMAT(F5.2)                                                              PROC 031
      HDD=HS+HDD                                                                PROC 032
       GO TO 19                                                                 PROC 033
   18 HS=0.0                                                                    PROC 034
   19 A=EQCO2-1.                                                                PROC 035
```

```
      B=EQCO2*(HDD+CDD) *(-1.)                                                  PROC 036
      C=EQCO2*HDD*CDD                                                           PROC 037
      WN=(-(B)-SQRT((B**2.)-4.*A*C))/(2.*A)                                     PROC 038
      IF(WN)3,4,4                                                               PROC 039
    4 IF(WN-1.)5,5,3                                                            PROC 040
    3 WN=(-(B)+SQRT((B**2.)-4.*A*C))/(2.*A)                                     PROC 041
      WRITE(3,6)                                                                PROC 042
    6 FORMAT(10X,'PROBLEM IN STATEMENT NUMBER 4')                               PROC 043
    5 HAA=2.*CAA                                                                PROC 044
      CCCP=CAA                                                                  PROC 045
      HMM=WN                                                                    PROC 046
      WJJ=HAA-HMM                                                               PROC 047
C READ IN THE GRAPHITE-GAS,  IRON-IRON OXIDE PHASE BOUNDARY INTERSECTION        PROC 048
      READ(2,7) PH2,PCO2,PCH4,PCO,PH2O                                          PROC 049
    7 FORMAT(5F8.6)                                                             PROC 050
      WII=WJJ                                                                   PROC 051
      TOT=WII/PH2O                                                              PROC 052
      HII=PH2*TOT                                                               PROC 053
      CII=PCO2*TOT                                                              PROC 054
      AMII=PCH4*TOT                                                             PROC 055
      COII=PCO*TOT                                                              PROC 056
      AMHH=AMII                                                                 PROC 057
      CON=WN                                                                    PROC 058
      HHH=HDD-WN+HII                                                            PROC 059
      CHH=CDD-CON+CII                                                           PROC 060
      COHH=CON+COII                                                             PROC 061
      HFF=HAA-HDD                                                               PROC 062
      CFF=CAA-CDD                                                               PROC 063
      AMHH=AMII                                                                 PROC 064
      ROHS=CDD/HDD                                                              PROC 065
      HNN=HDD-WN                                                                PROC 066
      CNN=CDD-WN                                                                PROC 067
      AMN=0.0                                                                   PROC 068
      H=HHH+CHH+COHH+HFF+CFF+AMHH                                               PROC 069
      WRITE(3,8)                                                                PROC 070
```

```
 8 FORMAT(10X,'SHIFT REACTOR')                                          PROC 071
   WRITE(3,9)                                                           PROC 072
 9 FORMAT(10X,'CO2+H2=CO+H2O',31X,'INLET',29X,'OUTLET')                 PROC 073
   WRITE(3,10)                                                          PROC 074
10 FORMAT(8X,'TEMP',6X,'PRES',7X,'O/H',4X,'RECYCLE',6X,'PH2',6X,'PCO2   PROC 075
  1'   ,7X,'PH2',6X,'PCO2',7X,'PCO',6X,'PH2O',6X,'PCH4')                PROC 076
   WRITE(3,11) TEMP,PRES,ROHS,HS,HDD,CDD,HNN,CNN,CON,WN,AMN             PROC 077
11 FORMAT(5X,11F10.5,/ )                                                PROC 078
   WRITE(3,12)                                                          PROC 079
12 FORMAT(10X,'BOSCH REACTOR')                                          PROC 080
   WRITE(3,13)                                                          PROC 081
13 FORMAT(10X,'CO2+2H2=2H2O+C',30X,'INLET',29X,'OUTLET')                PROC 082
   WRITE(3,14)                                                          PROC 083
14 FORMAT(8X,'TEMP',6X,'PRES',7X,'O/H',4X,'RECYCLE',2X,'OUTPUT FROM S   PROC 084
  1HIFT-H2O',4X,'PH2',6X,'PCO2',7X,'PCO',6X,'PH2O',6X,'PCH4')           PROC 085
   WRITE(3,15) TEMP1,PRES,ROH,H,PH2,PCO2,PCO,PH2O,PCH4                  PROC 086
15 FORMAT(5X,4F10.5,20X,5F10.5,////)                                    PROC 087
 1 CONTINUE                                                             PROC 088
23 CONTINUE                                                             PROC 089
   CALL EXIT                                                            PROC 090
   END                                                                  PROC 091
```

7.5 Nomenclature

a_j	activity of species, j
A	area, cm^2
C_j	concentration of species j, moles/cm^3
C_o	concentration of reducible oxygen in oxide, g-atoms 0/cm^3
d	diameter of steel wool fiber, cm
$D_j^{(eff)}$	effective diffusivity of species j in porous product layer, cm^2/s
$D_j^{(P)}$	diffusivity of species j in a single pore, cm^2/s
$D_{j,k}$	binary gaseous diffusion coefficient, cm^2/s
$D_{j,m}$	gas phase diffusivity of j into multi-component mixture, cm^2/s
G_∞	approach flowrate of reducing gas, moles/cm^2-s
k	Bohzmann's constant
$k_{m(j)}$	mass-transfer coefficient for species j, cm/s
k_{ov}	over-all conductance, cm/s
$k_r^{(t)}$	specific rate constant for surface reaction forming Product t, cm/s
$K_a^{(j)}$	adsorption equilibrium constant for species j, cm^3/mole
$K_e^{(t)}$	equilibrium constants for s/t equilibrium $\left.P_{H_2O}/P_{H_2}\right\|_{eq}$ or $\left.P_{CO_2}/P_{CO}\right\|_{eq}$
L	thickness of slab
M_j	molecular weight of species j, g/g-mole
M_{wt}	average molecular weight of 5 component reactant

	gas, g/g-mole
$\dot{N}_j$	molar flow of species j, moles/s
N_{Re_d}	Reynold's number based on catalyst fiber diameter, $d\ \underline{V}\ \rho / \mu$
N_{sc}	Schmidt number, $\mu/\rho\ D_{j,k}$ {subscript (f) = film {subscript (w) = wall
N_{sh}	Sherwood number, $d\ k_{m,j}\ /\ D_{j,k}$
P_j	partial pressure of species j, atm (with superscript denoting where located)
P_T	total pressure, atm
r_o	reduction rate, g-atoms O/cm^2 s
R	resistance to molar current of gas, $(\text{moles/s atm})^{-1}$ (with identifying superscripts)
R_g	gas constant, 82.1 atm cm^3/g-mole K
t	time, s
T	temperature, Kelvin unless otherwise specified
T^*	$k\ T/\varepsilon_o$
$\underline{V}$	free stream velocity, cm/s
V	volume of unreacted core, cm^3
V_m	unit volume of gas mixture
x_i	mole fraction of i in 5 component gas mixture
x_o	external radius of oxide sphere, cm
$x_i^{(t)}$	effective interface radius, distance from the origin to inner boundary of the indicated product phase t, cm
$\underline{X}$	overall conversion

Greek

β_n	defined as $\text{Cos}\beta_n = \beta_n\ (2Ds/k_{m,j}\ L)$
ε_{Fe}	void fraction in reduced iron layer
ε_o	energy-potential parameter
ρ_{mix}	density of mixture, g/cm^3
σ	Lennary-Jones force constant
θ	reaction time, s
μ_i	viscosity of component i, g/cm s
μ_{mix}	viscosity of mixture, g/cm s
Ω_D	collision integral for diffusion
Ω_T	collision integral for viscosity at temperature T

Superscripts

b	Associates principle symbol with the bulk gas phase
Fe	Associates principle symbol with the iron phase
h	Associates principle symbol with the hematite phase
m	Associates principle symbol with the magnetite phase
s	Associates principle symbol with the reactant phase in a given reduction step, s →t
t	Associates principle symbol with the product phase in a given reduction step, s→t
w	Associates principle symbol with the Wustite phase

Subscripts

A	Designates reactant gas, H_2 or CO
B	Designates product gas, H_2O or CO_2
F	Associates principle symbol with external mass-transfer resistance

I	Associates principle symbol with interface reaction
j,k	Designates chemical species j, k
S	Associates principle symbol with a shell layer reaction product -- Associates principle symbol with solid phase

7.6 Literature References

Baker, R.T.K., and P.S. Harris, "Controlled Atmosphere Electron Microscopy", J. Phys., Sect. E, Scientific Instruments, 5, 793 (1972).

Baker, R.T.K., M.A. Barber, P.S. Harris, F.S. Feates, and R.J. Waite, "Nucleation and Growth of Carbon Deposits from the Nickel Catalyzed Decomposition of Acetylene", J. Catalysis, 26, 51 (1972).

Baker, R.T.K., P.S. Harris, R.B. Thomas, and R.J. Waite, "Formation of Filamentous Carbon from Iron, Cobalt, and Chromium Catalyzed Decomposition of Acetylene", J. Catalysis, 30, 86 (1973).

Baker, R.T.K., and R.J. Waite, "Formation of Carbonaceous Deposits from the Platinum-Iron Catalyzed Decomposition of Acetylene", J. Catalysis, 37, 101 (1975).

Barkley, L.W., T.E. Corrigan, H.W. Wainwright, and A.E. Sands, "Catalytic Reverse Shift Reaction: A Kinetic Study", Ind. Eng. Chem., 44, 1066 (1952).

Boehm, H.P., "Carbon from Carbon Monoxide Disproportionation on Nickel and Iron Catalysts: Morphological Studies and Possible Growth Mechanisms", Carbon, 11, 583 (1973).

Bortolini, P., "Kinetics of the Water-Gas Conversion Reaction", Chem. Eng. Sc., 9, 135 (1958).

Browning, L.C., T.W. DeWitt, and P.H. Emmett, "Equilibria in the Systems Fe_2C-Fe-CH_4-H_2 and Fe_3C-Fe-CH_4-H_2", J. Am. Chem. Soc., 72, 4211 (1950).

Browning, L.C., and P.H. Emmett, "Equilibrium Measurements in the System C-CH_4-H_2", J. Am. Chem. Soc., 73, 581 (1951).

Cahn, R.W., "Physical Metallurgy Principles", D. Van Nostrand Co., New York (1973).

Chatterjee, B., and P.P. Das, "Nature of the Catalyst in the Decomposition of Carbon Monoxide in the Presence of Iron", Nature, 173, 1046 (1954).

Dal Nogare, S., and R.S. Juvet, "Gas-Liquid Chromatography, Theory, and Practice", Wiley, New York (1962), pp. 257-264.

Das, P.P., and B. Chatterjee, "Iron as a Catalyst in the Decomposition of Carbon Monoxide", Trans. Indian Inst. Metals, 6, 279 (1952).

Das, P.P., and B. Chatterjee, "The Nature of the Catalyst in the Decomposition of Carbon Monoxide in the Presence of Iron", Trans. Indian Inst. Metals, 7, 189 (1955).

Dietz, W.A., "Response Factors for Gas Chromatographic Analyses", J. Gas Chromatog., 5, 68 (1967).

Douglas, W.Y.M., and S.W. Churchill, "Recorrelation of Data for Convective Heat Transfer Between Gases and Single

Cylinders with Large Temperature Differences", AIChE Heat Transfer Symp., Nat'l. Meeting, Louisville, Ky., 1955, Reprint 16.

Duggin, M.J., and L.J.E. Hofer, "Nature of χ-Iron Carbide", Nature, 212, 248 (1966).

Eckert, E.R.G., and R.M. Drake, Jr., "Analysis of Heat and Mass Transfer", McGraw-Hill Book Co., New York, 1972.

Eckstrom, H.C., and W.A. Adcock, "A New Iron Carbide in Hydro-carbon Synthesis Catalysts", J. Am. Chem. Soc., 72, 1042 (1950).

Edstrom, J.O., and G. Bitsianes, Trans. Am. Inst. Mining Eng., 203, 760 (1955).

Elliott, R.P., "Constitution of Binary Alloys, First Supplement", McGraw-Hill, New York (1965).

Evans, E.L., J.M. Thomas, P.A. Thrower, and P.L. Walker, "Growth of Filamentary Carbon on Metallic Surfaces During the Pyrolysis of Methane and Acetone", Carbon, 11, 441 (1973).

Everett, M.R., "The Kinetics of Carbon Deposition Reactions in High-Temperature Gas-Cooled Reactors", D.P. Report 500, Atomic Energy Establishment, Winfrith (January 1967).

Fleureau, B., "Sur la formation de graphite par decomposition catalytique de l'oxyde de carbone", Compt. rend., 237, 330 (1953).

Garmirian, J.E. and R.C. Reid, 10.90 Project Report, Massachusetts Institute of Technology, Massachusetts (1977).

Hansen, M., editor, "Constitution of Binary Alloys", 2nd ed., McGraw-Hill, New York (1958).

Herbstein, F.H., and J.A. Snyman, "Identification of Eckstrom-Adcock Iron Carbide as Fe_7C_3", Inorg. Chem., 3, 894 (1964).

Hofer, L.J.E., E.M. Cohn, and W.C. Peebles, "The Modifications of the Carbide, Fe_2C; Their Properties and Identification", J. Am. Chem. Soc., 71, 189 (1949).

Hollis, O.L., and M.V. Hayes, "Water Analysis by Gas Chromatography Using Porous Polymer Columns", J. Gas Chromatography, 4, 235 (1966).

Holmes, R.F., E.E. Keller, and C.D. King, "A Carbon Dioxide Reduction Unit Using Bosch Reaction and Expendable Catalyst Cartridges", NASA CR-1682, (November 1970).

Jack, K.H., "Iron-Nitrogen, Iron-Carbon, and Iron-Carbon-Nitrogen Interstitial Alloys: Their Occurrence in Tempered Martenstite", Nature, No. 4002, 61 (July 13, 1946).

Jack, K.H., and S. Wild, "Nature of χ-Carbide and Its Possible Occurrence in Steels", Nature, 212, 248 (1966).

Karcher, W., and P. Glaude, "Inhibition of Carbon Deposition on Iron and Steel Surfaces", Carbon, 9, 617 (1971).

Kawasaki, E., J. Sanscraninte, T.J. Walsh, "Kinetics of

Reduction of Iron Oxide with Carbon Monoxide and Hydrogen", A.I.Ch.E. J., 8, 1, 48 (1962).

Kohn, J.A., and D.W. Eckart, "X-Ray Study of Synthetic Diamond and Associated Phases", Am. Mineralogist, 47, 1422 (1962).

Kusner, R.E., "Kinetics of the Iron Catalyzed Reverse Water-Gas Shift Reaction", Ph.D. Thesis, Case Institute of Technology, Ohio (1962).

Landler, P.F.J., and K.L. Komarek, Trans. Met. Soc., AIME, 236, 138 (1970) As referenced by Szekely, #27.

Louw, J.D., J.P. Van Den Berg, L.C. Ferreira, and J.J. Pienaar, "Appearance of FeC in a Hydrocarbon Synthesis Catalyst", J. Am. Chem. Soc., 79, 5899 (1957).

MacIver, D.S., and P.H. Emmett, "Surface Area Measurements on Carbon Black Produced by the Catalytic Decomposition of Carbon Monoxide Over Iron", J. Phys. Chem., 59, 1109 (1955).

Manning, M.P., "An Investigation of the Bosch Process", Massachusetts Institute of Technology, Sc.D. (1976).

Manning, M.P., and R.C. Reid, "Carbon Dioxide Reduction by the Bosch Process", Inter-American Congress of Chemical Engineering, Caracas, Venezuela, July 13-16, 1975.

Mars, P., "Factors Governing the Behavior of the Adiabatic Water-Gas Shift Reactor", Chem. Eng. Sci., 14, 375 (1961).

McCarthy, J.T., L.J.E. Hofer, B. Seligman, J.A. Lecky, W.C. Peebles, and R.B. Anderson, "Electron and X-Ray Diffraction Studies of Iron Fischer-Tropsch Catalysts", J. Phys. Chem., 57, 730 (1953).

McKewan, W.M., Trans. Met. Soc., AIME, 224, 2-5 (1962).

Meissner, H.P., and R.C. Reid, "The Bosch Process", Environmental Control & Life Support Systems Conference, San Francisco, California, August 14-16, 1972.

Muan, A., and E.F. Osborn, "Phase Equilibria Among Oxides in Steel Making", Addison-Wesley Publishing Co., Reading, Massachusetts (1965).

Nabi, G. and W.K. Lu, "Reduction Kinetics of Hematite to Magnetite in Hydrogen-Water Vapor Mixtures", Trans. Met. Soc., AIME, 242, 2471 (1968).

Nelson, H.R., "The Primary Oxide Film on Iron", J. Chem. Phys., 5, 252 (1937).

Podgurski, H.H., J.T.Kummer, T.W. DeWitt, and P.H. Emmett, "Preparation, Stability, and Adsorptive Properties of the Carbides of Iron", J. Am. Chem. Soc., 72, 5382 (1950).

Podolski, W.F., and Y.G. Kim, "Modeling the Water-Gas Shift Reaction", Ind. Eng. Chem. Proc. Des. Develop., 13, 415 (1974).

Purcell, J.E., and L.S. Ettre, "Analysis of Hydrogen with Thermal Conductivity Detectors", J. Gas Chromatog., 3,

69 (1965).

Ratliff, J.T., "Early Stages in the Interaction of Carbon Monoxide with Single Crystal Films", Ph.D. Thesis, Georgia Institute of Technology.

Reed-Hill, R.E., "Physical Metallurgy Principles", D. Van Nostrand Co., 2nd Ed., New York (1973).

Reid, R.C., and T.K. Sherwood, "The Principles of Gases and Liquids", McGraw-Hill, 2nd Ed. (1966).

Renshaw, G.D., C. Roscoe, and P.L. Walker, Jr., "Disproportionation of CO Over Iron and Silicon-Iron Single Crystals", J. Catalysis, 18, 164 (1970).

Robertson, S.D., "Carbon Formation from Methane Pyrolysis Over Some Transition Metal Surfaces I. Nature and Properties of the Carbon Formed", Carbon, 8, 365 (1970).

Rossini, R.D., Ed., "Selected Values of Chemical Thermodynamic Properties", Circular of the National Bureau of Standards 500 (1961).

Ruston, W.R., M. Warzee, J. Hennaut, and J. Waty, "The Solid Reaction Products of the Catalytic Decomposition of Carbon Monoxide on Iron at 550°C", Carbon, 7, (1969).

Ruston, W.R., M. Warzee, J. Hennaut, and J. Waty, "Basic Studies on the Growth of Carbon Deposition from Carbon Monoxide on a Metal Catalyst", D.P. Report 394, Atomic Energy Establishment, Winfrith (1966).

Ruthven, D.M., "A Simple Method of Calculating Mass Transfer Factors for Heterogeneous Catalytic Gas Reactors", Chem. Eng. Sci., 23, 759 (1968).

Sherwood, T.K., and R.L. Pigford, "Absorption and Extraction", McGraw-Hill, New York (1952).

Shunk, F.A., "Constitution of Binary Alloys, Second Supplement", McGraw-Hill, New York (1969).

Spitzer, R.H., F.S. Manning, and W.O. Philbrook, "Generalized Model for the Gaseous Topochemical Reduction of Porous Hematite Spheres", Trans. Met. Soc., AIME, 236, 1715 (1966).

Spitzer, R.H., F.S. Manning, and W.O. Philbrook, "Mixed-Control Reaction Kinetics in the Gaseous Reduction of Hematite", Trans. Met. Soc., AIME, 236, 726 (1966).

Stricoff, R.S., "The Reduction of Carbon Dioxide with Hydrogen Over Iron Catalysts", S.M. Thesis, Massachusetts Institute of Technology (1972).

Stull, D.R., and H. Prophet, "JANAF Thermochemical Tables", 2nd Ed., National Bureau of Standards, Washington (1971).

Szekely, J., J.W. Evans, and H.Y. Sohn, "Gas-Solid Reactions", Academic Press (1976).

Tamar, Y., Y. Nishiyama, and M. Takahashi, "The Effects of Helium Upon Carbon Deposition Onto Metal Surfaces", Carbon,

7, 209 (1969).

Tesner, P.A., E.Y. Rabinovich, I.S. Rafalkes, and E.F. Arefieva, "Formation of Carbon Fibers from Acetylene", Carbon, 8, 435 (1970).

Tevebaugh, A.D., and E.J. Cairns, "CHO Gas Phase Compositions in Equilibrium with Carbon and Carbon Deposition Boundaries at One Atmosphere", J. Chem. Eng. Data, 9, 453 (1964).

Tevebaugh, A.D., and E.J. Cairns, "Carbon Deposition Boundaries in the CHO System at Several Pressures", J. Chem. Eng. Data, 10, 359 (1965).

Todorov, R.P., D.K. Lambieu, and St. M. Mechkova, "Effect of Carbide-Forming Elements and Their Compounds on the Catalytic Action of Iron in Bell's Reaction", Kenetika i Kataliz, 15, 687 (1974).

Tsao, T., "Kinetics of Dissociation of Carbon Monoxide on α-Fe", Carnegie-Mellon University, Ph.D. (1974).

Tsay, Q.T., W.H. Ray, and Julian Szekely, "The Modeling of Hematite Reduction with Hydrogen Plus Carbon Monoxide Mixtures". Part I "The Behavior of Single Pellets", AIChE J., 22, 6, 1064 (1976). Part II, "The Direct Reduction Process in a Shaft Furance Arrangement", Ibid., 1072 (1976).

Turkdogan, E.T., and J.V. Vinters, "Catalytic Oxidation of Carbon", Carbon, 10, 97111 (1971).

Van Vlack, L.H., "Elements of Materials Science", 2nd Ed., Addison-Wesley Publishing Co., Reading, Massachusetts (1964).

Walker, P.L., Jr., J.F. Rakszawski, and G.R. Imperial, "Carbon Formation from Carbon Monoxide-Hydrogen Mixtures Over Iron Catalysts I. "Properties of Carbon Formed", J. Phys. Chem., 73, 133 (1959), II. "Rates of Carbon Formation", Ibid., 140 (1959).

Warzee, M., C. Sonnen, J. Hennaut, and W.R. Ruston, "Study of Catalytic Decomposition of Carbon Monoxide on Pure Iron, Mild Steels, and Alloyed Steels", D.P. Report 530, Atomic Energy Establishment, Winfrith (1967).

Watase, T., J. Chem. Soc. Japan, 54, 110 (1933).

West, C.A., "Precipitation from Solid Solutions of C and N in α-Iron", J. App. Phys., 20, 943 (1949).

Wert, C.A., "Diffusion Coefficient of C in α-Iron", Phys. Rev., 79, 601 (1950).

Westerman, R.V., "Mechanism and Kinetics of Iron Deterioration in Carbon Monoxide", Ph.D. Thesis, Georgia Institute of Technology (1967).

Wilson, R.B., "Fundamental Investigation of the Bosch Reaction", S.M. Thesis, Massachusetts Institute of Technology (1971).